DISSERTATION

PHYSICAL-SOCIO-ECONOMIC SYSTEMS INTEGRATION FOR COMMUNITY RESILIENCE-INFORMED DECISION-MAKING AND POLICY SELECTION

Submitted by:

Wanting (Lisa) Wang

Department of Civil and Environmental Engineering

In partial fulfillment of the requirements

For the Degree of Doctor of Philosophy

Colorado State University

Fort Collins, Colorado

Fall 2022

Doctoral Committee:

Advisor: John W. van de Lindt

Hussam Mahmoud
Yanlin Guo
Harvey Cutler

ABSTRACT

PHYSICAL-SOCIO-ECONOMIC SYSTEMS INTEGRATION FOR COMMUNITY RESILIENCE-INFORMED DECISION-MAKING AND POLICY SELECTION

Natural hazards are damaging communities with cascading catastrophic economic and social consequences at an increasing rate due to climate change and land use policies. Comprehensive community resilience assessment and improvement requires the analyst to develop a model of interacting physical infrastructure systems with socio-economic systems to measure outcomes that result from specific decisions (policies) made. There is limited research in this area currently because of the complexity associated with combining physics-based and data-driven socio-economic models. This dissertation proposes a series of multi-disciplinary community resilience assessment models (e.g., multi-disciplinary disruption assessment and multi-disciplinary recovery assessment) subjected to an illustrative natural hazard across physical infrastructure and socio-economic systems. As illustrative examples, all the proposed methodologies were applied to the Joplin, Missouri, testbed subjected to tornado hazard but are generalizable. The goal is to enable community leaders and stakeholders to better understand the community-wide impacts of a scenario beyond physical damage and further empower them to develop and support short-term and long-term policies and strategies that improve community resilience prior to events. Advancements in multi-disciplinary community resilience modeling can help accelerate the development of building codes and standards to meet the requirements of community-wide resilience goals of the broader built environment, consistent with the performance objectives of individual buildings throughout their service lives.

ACKNOWLEDGEMENTS

I would first like to express my deep appreciation to my advisor Professor John W. van de Lindt, for his guidance, support, and encouragement throughout my studies at Colorado State University. Prof. van de Lindt, you accepted me when I was during the most challenging period in my past 32 years, facing the double risk of program termination and status maintenance. Without your acceptance, I have no chance to transfer to Colorado State University to continue my Ph.D. studies, let alone get my Ph.D. degree. Without the above, how can we say possibly further have an academic career for the next chapter in my life? I am always grateful and proud to be your student. Without your guidance and support, I have no chance to collaborate with multi-disciplinary groups in economics, social science, computer science, and operations research. The extensive experience paved the way for me to obtain enough knowledge to lead/participate in cross-cutting and cutting-edge research in present-day academia. Thanks for constantly introducing me to many renowned professors and excellent researchers in conferences, workshops, and seminars, enabling me to learn to build my academic networks and leading me to step into academia gradually. I hope everyone who has a chance to read this dissertation can understand your significance and my sincere gratitude. I will never forget all these above throughout my life.

I would like to convey my gratitude to the distinguished committee members, Prof. Hussam Mahmoud, Prof. Yanlin Guo, and Prof. Harvey Cutler. Their invaluable suggestions and comments have greatly improved the quality of this dissertation. I would also like to express my sincere appreciation to other professors in the Structural Engineering Group in the CEE department. Prof. Paul Heyliger, thanks for all the courses given, which let me know the understanding level I should acquire for graduate courses beyond getting an “A”. Prof. Becki Atadero, I am grateful to be your

graduate teaching assistant, where my teaching strategies have been greatly improved. It might be also an important starting point for my teaching in my future career. Prof. Suren Chen, thanks for the invitation to visit for 2019 Thanksgiving, and Prof. Gaofeng Jia, thanks for organizing the outdoor barbeques. I am thrilled to join these events filled with fun and laughter.

I would also like to thank my former and current fellow graduate students and friends in structural engineering at Colorado State University, Omar Nofal, Milad Roohi, Jace Furley, Emad Hassan, Blythe Johnson, Mojtaba Harati, Abdelrahman Kamal, Mona Hemmati, Mohamed Abdelhafez, Kenny Bui, and all my Chinese friends, Yangyang Wu, Min Li, Qiling Zou, Guangyang Hou, Zhenqiang Wang, Chao Jiang, Kaisen Yao, Yue Dong, Ziluo Xiong, Jiate Li. You, everyone, have excellent characteristics and unique expertise I do not have but want to learn. I will always memorize our lasting friendship and your continued support. All colleagues, collaborators, and friends in other majors at Colorado State University and in all majors at the NIST Center for Risk-Based Community Resilience Planning are always appreciated, but please understand I do not have enough space to mention your names here. Life at Colorado State University enabled me to regain my conference, reshape my personality, and develop solid problem-solving skills and academic visions. It is an unforgettable experience in my life.

Most importantly, I would like to express my profound gratitude to my parents for their early family education. Their early family education helped me develop personal hobbies beneficial to my social network and professional development and develop values to shape and direct my life. I am pleased to share that Figure 4-2 in this dissertation was developed with the guidance and suggestion of my mother, Kangyun Xin. I want to put it in my dissertation, recording our collaboration. As a young structural engineer in a family of structural engineers with three

generations, I would love to always be humble and contribute more to the area throughout my life, like my grandparents and parents.

In the end, I would like to appreciate the support for my studies by the Center for Risk-based Community Resilience Center funded by the National Institute of Standards and Technology Science (NIST) under Grant No. 70NANB15H044 and 70NANB20H008. Moreover, I was honored to be a recipient of the 2020, 2021, and 2022 Jack E. Cermak Wind Engineering Graduate Fellowship, 2021 NTU Foundation Graduate Fellowship, and 2021 ASCE O.H. Ammann Research Fellowship in Structural Engineering, and would like to take this opportunity to thank the selection committee for selecting me for these prestigious awards.

DEDICATION

To my beloved parents

TABLE OF CONTENTS

LIST OF TABLES

LIST OF FIGURES

CHAPTER 1 INTRODUCTION

1.1 Background and Motivation

The performance of civil infrastructure systems supports community resilience but has been primarily controlled by probability-based limit states design over the last several decades (e.g., ASCE 7-16). In 2015, the U.S. NIST proposed a general framework to help communities develop resilience plans for building clusters (a group of buildings that support a community function such as education) and infrastructure associated with social and economic systems (NIST 2015). Since then, an increasing number of researchers have focused on physical infrastructure systems and related distributed networks to quantitatively assess community-level resilience with multi-disciplinary measurements (e.g., Doorn et al. 2019, Wei et al. 2020, Wang et al. 2021b, Roohi et al. 2020). According to McAllister (2016), engineering outcomes can be quantitatively coupled with socio-economic performance, providing more flexible and informative support for risk-informed decision-making with the public interest in mind. Advancements in multi-disciplinary community resilience modeling can help accelerate the development of building codes and standards to meet the requirements of community-wide resilience goals of the broader built environment at a higher level, consistent with performance objectives of individual buildings throughout their service lives (e.g., Ellingwood et al. 2017, Masoomi and van de Lindt 2019), which is also the focus and contribution of this dissertation. Many more multi-disciplinary community resilience approaches will be introduced below from disruption assessment and recovery assessment perspectives.

1.1.1 Multi-Disciplinary Disruption in Community Resilience

1.1.1.1 Multi-Disciplinary Disruption Assessment

The concept of community resilience refers to the cycle of a community and its capability of resisting, absorbing, adapting to, and rapidly recovering from disruptive events (NIST 2015, PPD 21). The definition of resilience was initially proposed by Holling in the 1970s, and community resilience-related research emerged over the last decade (e.g., Holling 1973; Alexander 2013; Koliou et al. 2017; McAllister 2016; Ellingwood et al. 2017). Over the last several decades, an increasing number of researchers have focused on physical infrastructure systems and their networks to assess community-level resilience and mitigate risk and resulting impacts. Researchers have performed risk assessment of physical infrastructure including buildings (e.g. McAllister 2013; Wang et al. 2018; Pilkington 2019), water systems (Guidotti et al, 2016; Masoomi and van de Lindt 2018), electric power systems (Ouyang and Duenas-Osorio 2014; Ma et al. 2020), oil and gas networks (Ouyang and Wang 2015; Ameri and van de Lindt 2019), transportation networks (Bocchini and Frangopol 2011; Yanweerasak et al. 2018; Wang and Jia 2019; Dong and Frangopol 2015; Capacci et al. 2016; Sun et al. 2020), as well as their interdependencies (Guidotti et al. 2016; Dong and Frangopol 2017; Attary et al. 2019; Zou and Chen 2019; Zou and Chen 2020; Zhang et al. 2016). Moreover, limited studies have also addressed the integration of physical infrastructure systems and socio-economic systems throughout the community (Bocchini et al. 2014; Massomi and van de Lindt 2019, Roohi et al. 2020). Ellingwood et al. (2016) developed the Centerville virtual community as a community resilience testbed and proposed a fully integrated decision framework for interacting physical, economic, and social infrastructure systems. As part of that effort, Cutler et al. (2016) integrated physical resilience metrics from natural hazard models into a dynamic CGE model using economic fundamentals. Rosenheim et al. (2019) coupled engineering-social science modeling by allocating household socio-demographic data to housing units in residential structures that were linked to critical infrastructure systems.

1.1.1.2 Multi-Disciplinary Resilience Goals

In the United States, building codes and standards (e.g., ASCE 2017) have focused on life safety goals, but the role of the individual building performance in fulfilling community resilience goals is unknown (Ellingwood et al. 2017). In order to address this grand challenge over the next decade, there is a need to link resilience design objectives with individual building performance levels (Wang et al. 2018). Physical performance of buildings has been quantitatively linked to community-wide social and economic outcomes in only one study by Roohi et al. (2020), without focusing on achieving community-level goals. Therefore, a systematic community-level analysis of linked physical, social, and economic systems is needed to de-aggregate performance targets of buildings to enable the community to achieve pre-defined socio-economic community-wide resilience goals. The performance targets can be expressed in terms of individual building fragilities to further guide the performance-based engineering design of structural components given specific design features.

Community resilience goals mainly focus on robustness and rapidity (NIST 2015). The robustness goals emphasize improvements in the performance of building components, and the rapidity goals are devoted to allocating limited resources and creating organizational guidelines to ensure community recovery is implemented effectively and efficiently (Wang et al. 2018, Wang and van de Lindt 2021). The NIST Community Resilience Planning Guide, the San Francisco Planning and Urban Research Association, and the Oregon Resilience Plan provided examples of specifying the desired time-to-recovery as performance goals for building clusters at different functional levels (NIST 2015, NIST 2020, OSSPAC 2013, Poland 2009). Schultz and Smith (2016) developed rapidity resilience objectives for housing, utility systems, and transportation individually when the community is exposed to flood events at different return periods. However, only a few studies focused on examining the achievement of robustness goals. Chang and Shinozuka (2004) set a reliability goal of 95% likelihood of being able to meet the objectives for water systems (e.g., major pump station loses function) in given seismic events. Kameshwar et al. (2019) estimated the likelihood of achieving robustness performance goals (i.e., the performance of infrastructure systems from 0% to 100%) for the coastal town of Seaside, Oregon, subjected to combined seismic and tsunami hazards. Wang et al. (2018) used the Direct Loss Ratio (DLR) and Un-Inhabitable Ratio (UIR) as the resilience goals for measuring the robustness of a residential building cluster under tornado hazards, with the damage values linked to direct loss and un-inhabitability as defined from the HAZUS-MH MR4 technical manual for consistency.

In order to measure socio-economic aspects of community resilience, researchers have proposed metrics that can be potentially considered as indicators of community resilience. Potential indicators of economic resilience include the unemployment rate, income equality (e.g., based on gender, race/ethnicity), and business diversity (e.g., ratio of large to small businesses). Social resilience metrics reflect individual human and social needs, which can be represented in population changes and the distribution of socio-demographic characteristics (e.g., age, race, education levels) over time (Burton 2015, Cutter et al. 2014), access to social services and networks, and quality of life assessments. Some metrics can reflect the multifaceted socio-economic indicators of resilience. For example, temporary and permanent population dislocation following a disaster is a complex social and economic process jointly impacted by the functionality loss of physical systems and the socio-demographic characteristics (Wang et al. 2018). The effects of population dislocation can ripple through the local economy, social institutions, and building inventory. For example, local businesses may lose both employees and customers, and therefore, decide to close permanently and relocate. As residents and businesses leave and relocate, tax revenue for local government shrinks, forcing layoffs that can induce more residents to leave (Mieler et al. 2015) as well as shrinking resources for restoring and maintaining physical infrastructure.

1.1.2 Multi-Disciplinary Recovery in Community Resilience

1.1.2.1 Building Infrastructure Recovery

Community resilience is the ability of a community to prepare for natural or human-made hazards, adapt to changing conditions, and withstand and recover rapidly from disruptions (PPD-8, PPD-21, NIST 2015). Resilience modeling and analysis can support risk-informed decisions including assisting stakeholders and decision-makers in understanding the different dimensions of the challenge, establishing short-term and long-term community goals and objectives, and executing their community planning. Community resilience assessment addresses the quantitative measures of robustness, rapidity, resourcefulness, and redundancy from a multi-dimensional perspective (Bruneau et al. 2003, Koliou et al. 2017). However, numerous studies have focused on assessing the residual functional capacity of the built environment and, in particular, lifeline systems following a disaster. Limited studies have been performed to explore the continuous recovery of building infrastructure and most model trajectories, making it difficult to model interventions at different points in time during the recovery process.

The Federal Emergency Management Agency (FEMA), which is an agency within the U.S. Department of Homeland Security, first proposed the National Disaster Recovery Framework (NDRF) in 2011 as guidance, in which they explained how government agencies, nongovernmental organizations (NGO), and the private sector could (should) organize and utilize existing resources to promote effective recovery by phase and support disaster-impacted states (FEMA 2011). In more recent years, researchers have developed comprehensive restoration models to explore the restoration process specific to critical infrastructure systems like buildings (e.g., Koliou and van de Lindt 2020, Bonstrom and Corotis 2016), electric power networks (e.g., Ouyang and Duenas-Osorio 2014), water and wastewater (e.g., Tomar et al. 2020), oil and gas (e.g., Ameri and van de Lindt 2019), and the interaction between networks of infrastructure systems (e.g., He and Cha 2018, Smith et al. 2019). When assessing the restoration time or sequences of the community involved with an interdependent network, the community topology associated with graph theory and critical paths is one of the most straightforward and efficient approaches to solve the problem (He and Cha 2018, Ramachandran et al. 2015, Masoomi and van de Lindt 2018). Moreover, some research efforts have focused on modeling housing recovery and re-occupancy of displaced households in the aftermath of a disastrous event (Zhang and Peacock 2009, Hamideh et al. 2018, Lin et al. 2019). Others were devoted to examining the effects of household dislocation on business recovery reflected in resilience metrics such as revenue recovery and customer retention (Watson et al. 2020a, Aghababaei et al. 2020).

Data-driven models have played an important role in quantifying certain aspects of community recovery. For example, some researchers have measured building recovery progress after hazard events via longitudinal field investigations (van de Lindt et al. 2020) and aerial imagery techniques (Kikitsu and Sarkar 2015, Crawford et al. 2019, Aghababaei et al. 2020). Hamideh et al. (2018) investigated the effect of damage, tenure, minority population, and income on the housing recovery trajectory using a regression model. Burton et al. (2019) considered integrating household decision-making into recovery models with real-world data collected from Los Angeles households combined with multinomial logistic regression. The results showed that the household decisions were significantly impacted by physical damage to the residential community as well as other household socio-economic characteristics such as neighborhood evacuation level, household income, and insurance coverage.

Simulation-based modeling is another process that helps researchers, engineers, and decision-makers better understand community recovery under different conditions. Such model simulation results can further help leaders and their stakeholders develop community plans to mitigate the adverse effects of hazard events and accelerate the restoration process. Solving an optimization problem for repair priority sequences or community resource allocation is one of the most common research topics examining recovery (Sun et al. 2020, Zhang et al. 2017, Nozhati et al. 2020). Hassan and Mahmoud (2020) used a Markov chain process coupled with a success tree to perform a dynamic optimization to estimate the recovery of healthcare facilities considering the availability of repair crews. González et al. (2016) developed the minimum-cost reconstruction strategy of a partially destroyed infrastructure network system with the limitation of budget, resources, and operationality.

1.1.2.2 Business Recovery

Community resilience modeling requires the analyst to model the physical infrastructure, social institutions, households, and the economy. Key to the resilience modeling process and related planning for decision support is the ability to model interdependent recovery, which includes the recovery of commercial businesses. The number of operational or recovered businesses in a hazard-affected area is one of the most important metrics towards this end (e.g., Marshall and Schrank 2014, Stevenson et al. 2018, Xiao and Van Zandt, 2012). However, business recovery following natural hazard events is a complex process (e.g., Aghababaei et al. 2021) which depends on many factors (Zhang et al.2009), such as physical property damage (Yang et al., 2016), loss of utility services (e.g., Dahlhamer and Tierney 1998), supplier disruption (e.g., Lee 2019), mitigation strategies employed by business owners such as the existence of an emergency plan (e.g., Xiao and Peacock 2014) and the use of backup technologies and resources (e.g., Cremen et al. 2020), as well as ecological and socio-economic factors (e.g., Dietch and Corey 2011, Dahlhamer and Tierney 1998).

Some businesses are highly vulnerable to physical damage to the building itself and interior contents/inventory, including retail stores, service businesses, and hotels, due to their reliance on physical premises for walk-in customers, product storage, and specialized equipment (Lee 2019). In addition, physical property damage affects the approach a business utilizes to finance its building recovery (Watson 2022, Lee 2019). Property damage can lead to a vicious cycle in business recovery (Watson, 2022), where the resulting downtime leads to lost revenue, which reduces resources needed for repair, and can also make incurring debt from recovery loans more hazardous as time increases post-disaster (Dahlhamer and Tierney 1998). Prolonged business closure is then interdependent with overall community recovery (Watson et al. 2020b, Xiao and Van Zandt, 2012). Employees lose work and dislocate due to damage to their homes, and customers go elsewhere for goods and services and may not return when the business does finally reopen (Alesch et al. 2001).

Over the past several decades, quantitative analysis of impeding factors impacting business recovery have mainly focused on empirical analysis and regression analysis (e.g., Corey and Deitch 2011), such as logistic regression (e.g., Dahlhamer and Tierney 1998, Khan and Sayem 2013, Orhan 2016, Wasileski et al. 2011) and probit regression (e.g., Lee 2019, Torres et al. 2019, McDonald et al. 2014). The data for these analyses are often based on surveys, which collect business population information on company/industry type, franchise status, and number of employees, and post-event information on business operational status, property damage dollars, financing arrangements, and government aid (e.g., Cremen et al. 2020, Lee 2019, Corey and Deitch 2011). However, despite long-term recovery of businesses after disaster events depending on both the recovery of commercial buildings as well as the recovery of households as customers and employees (Watson et al. 2020a, Xiao and Van Zandt 2012), limited previous studies performed a probabilistic quantitative analysis of commercial buildings recovery as an essential input for business recovery.

Furthermore, planning for and implementing recovery activities requires funding resources from public, private, and semi-private entities. Understanding the types and amounts of resources available to business owners is critical to identifying how alternative funding sources impact the post-event business recovery process. Given the multi-scale and the multi-agency nature of different management systems, there are many challenges associated with tracking resilience resources. Therefore, real-world funding resource data used for community resilience-related research in previous studies are relatively scarce (e.g., Karamouz et al. 2018, Salignac et al. 2019). In order to more accurately track resilience resources, an iterative combination of approaches is appropriate. A top-down analysis of federal budgets and domestic assistance acts as a scoping review of types of disaster programs, their funding mechanisms, and their eligible recipients (Watson et al., 2020b). From there, content analysis of all documents related to the identified funding streams can track the management, amount, and timing of funds from their appropriation to final disbursement (Berd and Watson 2020). Individual case studies and survey data can then illustrate how programs are translated in real-world events, which businesses receive assistance, the types of local programs implemented, and how recovery is financed at the individual business level. The collected resilience resources for case communities can be integrated as a resilience resource portfolio, including different financing resources available to business owners, and then integrated into the probabilistic recovery modeling.

1.1.2.3 Physical-Social Interdependent Recovery

Climate change and other environmental variables increasingly lead to more intense and frequent hazard events, resulting in more risk and potential demands on physical infrastructure systems (e.g., Chester et al. 2020, Ghanbari et al. 2021, Feng et al. 2022). A loss of functionality and serviceability for physical infrastructure systems can result in families becoming houseless, businesses closing, and education interruption. Multi-disciplinary and multi-dimensional community resilience assessment has emerged over the last decade, which focuses on modeling the complex interactions over physical infrastructure and other social systems (e.g., housing, business, education, and healthcare) to support planning effort and related decisions (e.g., Berkes and Ross 2013, Aldrich and Meyer 2015, Fereshtehnejad et al. 2021, Koliou et al. 2020, Aghababaei and Koliou 2022, Wang et al. 2021, Wang and van de Lindt 2022). A number of multi-disciplinary community resilience models were developed to examine the physical performance of buildings and lifeline network systems (e.g., Burton et al. 2016, Sharma and Gardoni 2021, Sanderson et al. 2022), and some included propagation to economic losses and social disruption (e.g., Sanderson et al. 2021, Kim and Marcouiller 2016). However, most community recovery models thus far were designed to examine the recovery of a single system or multiple systems either from the perspective of physical stability, such as buildings and electric power systems (e.g., Aghababaei et al. 2020, He and Cha 2018, Capacci et al. 2022, Huang et al. 2022), or from the perspective of social stability such as housing, business, and social institutions (e.g., Binder et al. 2019, Xiao and Van Zandt 2012, Hassan and Mahmoud 2021). The available literature for modeling interdependent community recovery linking physical infrastructure and social systems, is scarce due to its complexity of combining physics-based and data-driven models, but is urgently needed.

More than 90% of the total building stock in the United States is residential, with more than 124 million occupied housing units, and more than 90% of residential buildings are wood frame construction (Potter 2020, Masoomi et al. 2018, American Housing Survey 2019). Therefore, exploring the interdependent recovery across physical infrastructure and other social systems clearly starts with this building type. Understanding recovery of the most prevalent building type and their inhabitants in the U.S. will have the most significant impact to help communities guide their planning process, and maintain population stability following the hazard event. Social factors impact the ability of communities and their populations to resist and recover from disasters. Recently, social vulnerability factors or social equity metrics have been increasingly incorporated into community resilience assessment and planning (e.g., Van Zandt et al. 2012, Merrow et al. 2019, Kim and Sutley 2021, Enderami et al. 2022). For residential structures damaged by hazard events, households having different social vulnerability levels impacts their ability to efficiently access funding resources, such as insurance and loans, for financing their building repairs (e.g., Wang and van de Lindt 2021, Lin and Wang 2017). These vast disparities also inevitably occur in housing recovery trajectories for socially vulnerable populations and other households (e.g., Sutley and Hamideh 2020, Griego et al. 2020).

1.2 Research Objectives and Dissertation Outline

As the title of this dissertation indicates, the objective of this dissertation is to comprehensively combine physical infrastructure systems with socio-economic systems and model them over time to enable resilience-informed policy making and community planning. The key community resilience metrics can further inform the design guidelines of building codes and standards. Additionally, this dissertation proposes a set of policies that impact community resilience quantitatively. The goal is to enable community leaders and stakeholders to better understand the community-wide impacts of a scenario beyond physical damage and further help them develop short-term and long-term policies and strategies and therefore improve the community resilience. As an illustrative example, the proposed methodology in each of the following chapters will be applied to the Joplin testbed subjected to tornado events. The objective will be accomplished following the integrated conceptual framework shown in Figure 1-1 and the following chapters. Each chapter corresponds to the specific steps shown in the framework.

Each chapter closes with a summary of the novelty and contribution to community resilience research. However, the overarching novelty of this dissertation is as follows: (1) for the first time, validated physical infrastructure, field-study driven social science models, and data-driven economic models have been fully linked/chained to investigate pre- and post-even policies; (2) real-world validation using data over the years following a hazard event has been used to validate a system-wide recovery model for residential structure recovery; (3) the ability to investigate policies both pre- and post-event has been demonstrated at the community level; (4) the ability to calibrate a policy decision recommendation as a function of the predictive effect on core physical, social, and economic metrics has been demonstrated; and finally, (5) a new computational environment, IN-CORE, was used to complete all analyses. The NIST-funded Center for Risk-Based Community Resilience Planning, headquartered at Colorado State University in Fort Collins, Colorado, USA, developed a multi-disciplinary computational environment, the Interdependent Networked Community Resilience (IN-CORE) Modeling Environment. This open-source computational environment continuously releases a series of community-level resilience assessment modules that integrate physical infrastructure with socio-economic systems and simulate the effect of different natural hazards on communities (e.g., Wang et al. 2021b, Sanderson et al. 2021, Nofal et al. 2021, Nofal and van de Lindt 2020). All the proposed methodologies in this dissertation will be integrated into the IN-CORE computational environment and enhance the resilience assessment of the IN-CORE computational environment for public use and therefore support risk-informed, or resilience-informed, decision-making.

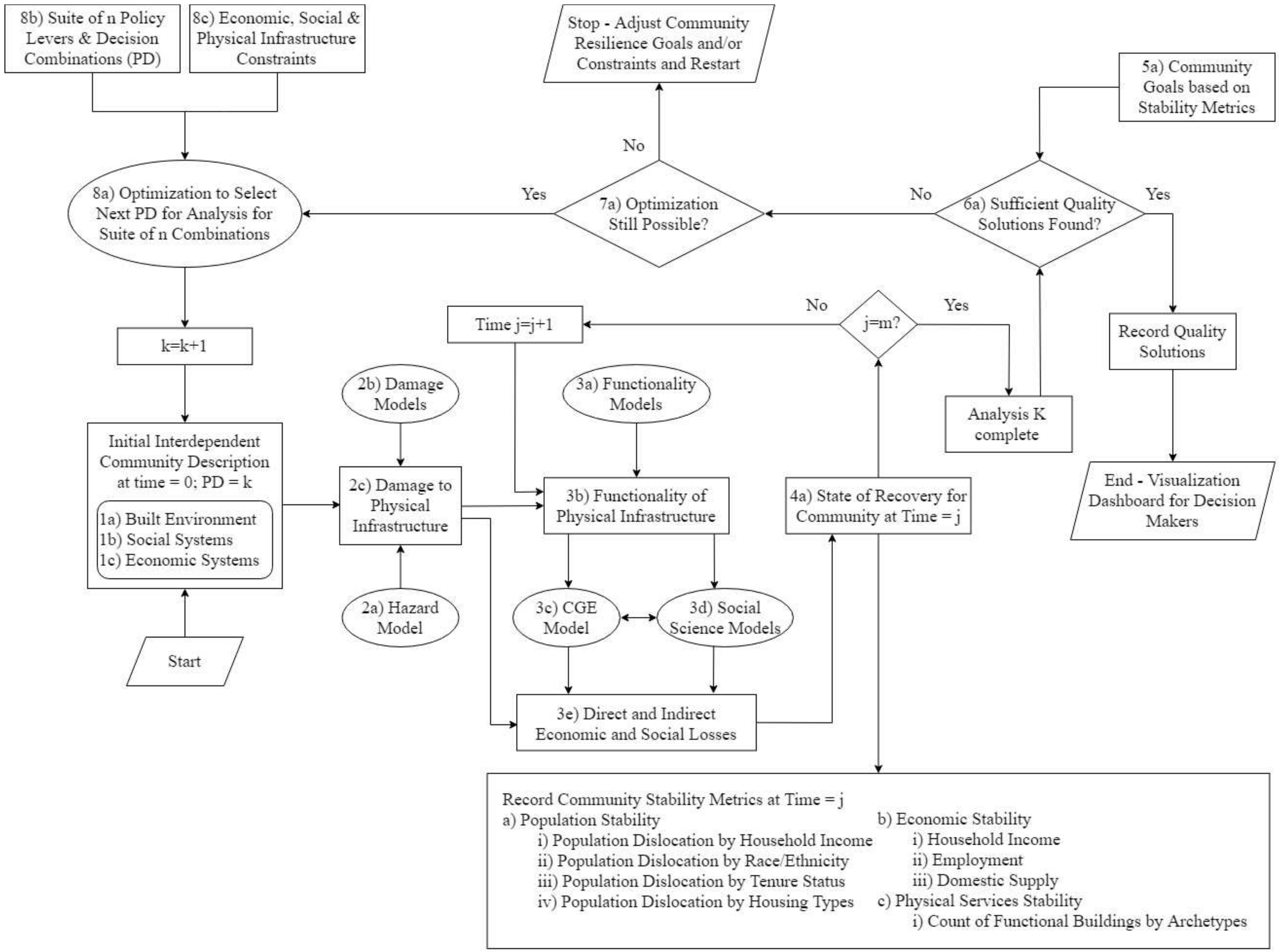

Figure 1-1. A conceptual description of the framework

Chapter 2: Multi-disciplinary disruption assessment (1a, 1b, 1c, 2a, 2b, 2c, 3a, 3b, 3c, 3d, 3e, 8b in Figure 1-1)

This chapter examines the effect of a tornado damaging physical infrastructure (buildings and electrical power network) and the effects on the population and the local economy for a real community (Wang et al. 2021b). In addition, this chapter proposes three residential building retrofit strategies as alternatives to improve community resilience and explores the effects of mitigation strategies on multi-disciplinary resilience metrics (Wang et al. 2021b).

Chapter 3: Multi-disciplinary resilience goals de-aggregation (1a, 1b, 1c, 2a, 2b, 2c, 3a, 3b, 3c, 3d, 3e, 5a, 6a in Figure 1-1)

This chapter develops multi-disciplinary community resilience goals targeted for routine levels, design levels, and extreme levels of tornado events (Wang et al. 2022c). In addition, this chapter de-aggregates performance targets for individual residential buildings and determines the percentage of buildings that should be retrofitted to achieve community-level resilience goals in terms of physical, social, and economic metrics (Wang et al. 2022c).

Chapter 4: Improved school designs and social service stability (2a, 2b, 2c, 3a, 3b, 3d, 3e in Figure 1-1)

This chapter proposes different design combinations for a reinforced masonry high school building (from each primary structural/nonstructural component to the entire building) specified for different performance levels (Wang and van de Lindt 2022). In addition, this chapter integrates the developed fragilities into a community level model with school attendance zones to investigate the effect of improving school building designs would have on maintaining school continuity (and more rapid return) for school children (Wang and van de Lindt 2022).

Chapter 5: Residential building recovery (1a, 1b, 1c, 2a, 2b, 2c, 3a, 3b, 4a in Figure 1-1)

This chapter develops a methodology based on a multi-layer Monte Carlo simulation to model a two-stage recovery process for residential buildings: functional downtime due to delays and functional downtime due to repairs (Wang and van de Lindt 2021). In addition, this chapter quantifies the disaster recovery of residential buildings impacted by pre- and post-event policies, such as building retrofits and relaxed building permits (Wang and van de Lindt 2021).

Chapter 6: Commercial building recovery (1a, 1b, 1c, 2a, 2b, 2c, 3a, 3b, 4a in Figure 1-1)

This chapter develops a resilience resource portfolio (e.g., personal savings, insurance, loans, and government grants) to support the commercial recovery and quantifies the financing delay referenced from personal surveys and the REDi framework (Wang et al. 2023). In addition, this chapter performs the commercial building recovery assessment, determines the time-stepping building recovery trajectory, and calculates recovery resilience metrics for building clusters following the tornado events (Wang et al. 2023).

Chapter 7: Physical-social interdependent recovery (1a, 1b, 1c, 2a, 2b, 2c, 3a, 3b, 3c, 3d, 3e, 4a in Figure 1-1)

This chapter develops a methodology to examine the interdependent community recovery process across physical infrastructure and social systems. In addition, this chapter examines the integrated recovery process of residential buildings and their households over the community impacted by social vulnerability factors.

Chapter 8: Summary, conclusions, and recommendations

CHAPTER 2 MULTI-DISCIPLINARY DISRUPTION ASSESSMENT

2.1 Introduction

Tornadoes occur at a high frequency in the United States compared with other natural hazards but have a relatively small footprint. A single high-intensity tornado can result in high casualty rates and catastrophic economic and social consequences, particularly for small to medium size communities. Comprehensive community resilience assessment and improvement requires the analyst to develop a model of interacting physical, social, and economic systems and to measure outcomes that result from specific decisions made. These outcomes often are in the form of metrics such as the number of people injured or the number of households and/or businesses without water, but it has been recognized that most community resilience metrics have socio-economic characteristics. In this chapter, for the first time, a fully quantitative interacting methodology is developed to examine the effect of a tornado damaging physical infrastructure (buildings and electrical power network) and the effects on the population and the local economy for a real community, as depicted in the flowchart shown in Figure 2-1. Then, three residential building retrofit strategies are considered as alternatives to improve community resilience and the metrics for the physical, economic, and social sectors are computed. An illustrative example is presented for the 2011 Joplin tornado in a new open-source Interdependent Networked Community Resilience Modeling Environment (IN-CORE), with a computable general equilibrium (CGE) economics model that computes household income, employment, and domestic supply before and after the tornado. Detailed demographic data was allocated to each structure to enable the calculation of resilience metrics related to population dislocation impacts from the tornado. The results of these analyses stemming from building damage estimation have a logical trend, but the substantial contribution of this chapter is that, for the first time, the effect of retrofit strategies for tornado loading can be quantified in terms of their effects on both social science and economic community-level metrics. This chapter presents the methodology and concept first published in Wang et al. (2021b).

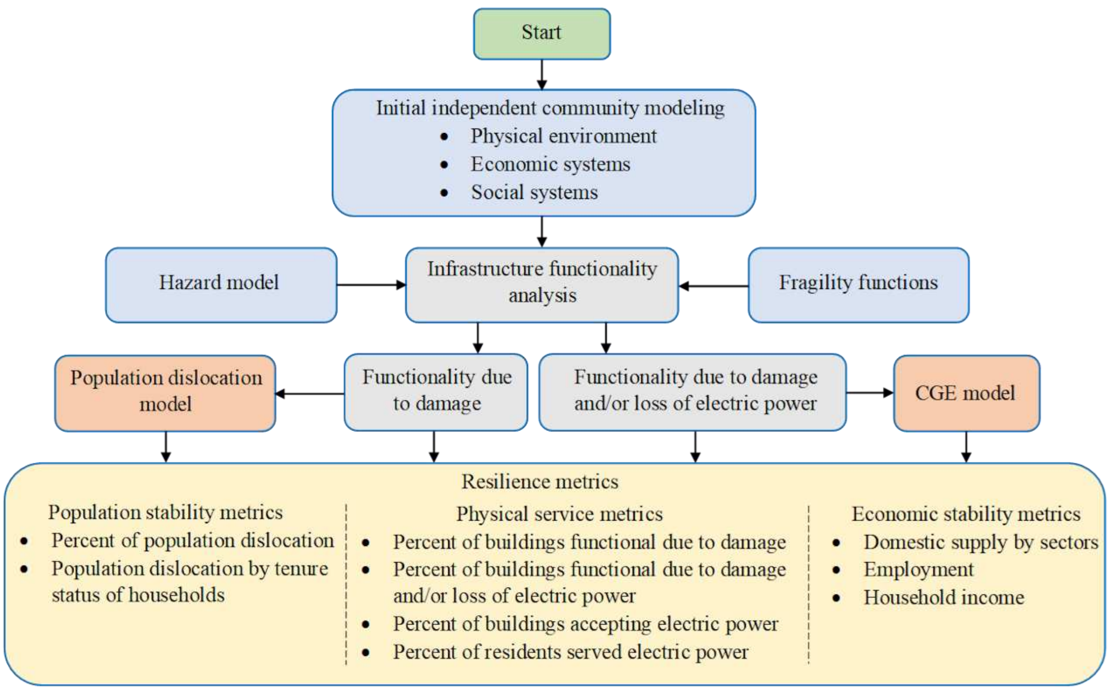

Figure 2-1. Resilience assessment methodology

2.2 Resilience Assessment Methodology

2.2.1 Damage Modeling

In order to perform a probabilistic analysis of structural components and systems subjected to natural hazards, a set of limit states must be first identified that describes specified levels of performance for the components. For fragility assessment, the limit state function, $g(x)$ for a component is written as:

$$g(x) = R - (W - D) \tag{2.1}$$

where W is the load effect, e.g. wind or acceleration for a tornado or earthquake, respectively; R is the resistance of structural components; D is dead loads of structural components. Therefore, component failure can be defined as $g(X) < 0$. The probability of each component exceeding a specified limit state (ls_i), namely slight, moderate, extensive, and complete levels, for a given intensity measure (IM) of the hazard can be calculated as follows (e.g. Memari et al. 2018; Masoomi et al. 2018):

$$F_r(x) = P[LS \geq ls_i | IM = x] \tag{2.2}$$

The fragility of components can then be assembled to the fragility at the building level, which is defined as the conditional probability of occurrence of any defined damage states of j components (i.e., the most unfavorable case).

$$F_r(x) = P[\cup_j (LS \geq ls_{ij}) | IM = x] \tag{2.3}$$

The resulting building-level fragility within Monte Carlo simulation (MCS) is commonly expressed as a lognormal cumulative distribution function (CDF) via curve fitting and controlled by two parameters: median and standard deviation, as shown in Equation (2.4) (Amini and van de Lindt 2014).

$$F_r(x) = \Phi[\frac{ln(x) - \lambda}{\xi}] \tag{2.4}$$

where x is specified intensity measure expressed as, for example, a 3-s gust wind speed (m/s or mph) for wind fragility analysis; λ and ξ are logarithmic means and standard deviations of lognormal functions at a specified damage state.

2.2.2 Functionality Assessment Model

A community is a complex system that includes assorted utility networks with a high degree of interaction. Any disruption in the networks, especially for lifeline system networks, can result in a cascading failure within the network or a loss of functionality to other dependent networks in the community. Therefore, community resilience assessment requires that the community topology be simulated with necessary dependencies and interdependencies included among networks (Masoomi and van de Lindt 2018). Referring back to Figure 2-1, the section of Infrastructure Functionality Analysis which will introduce later depicts a probabilistic analysis of interdependent networks that is required, and the relationship among intrinsic, extrinsic, and functionality failure probabilities of the infrastructure for a wind event needs to be determined. The intrinsic failure of a component is defined as the failure due to the estimated physical damage of the component under a specific hazard intensity. The extrinsic failure of a component is defined as the failure of a component based on either its own system failure or due to it interacting with other components in other networks in the community. The union of intrinsic and extrinsic failures of a component result in the functionality failure of the component (Masoomi and van de Lindt 2018), which can be written as:

$$P\left(F_{fnc}\right) = P(F_{int} \cup F_{ext}) = P(F_{bdg} \cup (F_{sub} \cup F_{pole})) \tag{2.5}$$

where F_{fnc}, F_{int}, and F_{ext} are functionality, intrinsic, and extrinsic failure events for a single component, respectively. F_{bdg}, F_{sub}, F_{pole} are building, substation, pole failure events involved with this chapter as an example.

2.2.3 CGE Model

For many years, Input-Output (I-O) economic models were the most widely used approach to determine the regional economic activity impacted by natural hazards (e.g., Rose and Liao 2005). However, I-O models adequately modeled demand-side shocks but were limited in their ability to model impacts to the supply-side such as the loss of buildings and lifeline systems (Koliou et al. 2017). In recent years, the advanced CGE model, which can address this limitation of I-O models, was extensively used to address this subject. CGE models are based on fundamental microeconomic principles and are a widely used tool in the evaluation of government policy and external societal shifts such as those arising from technological innovation (Lofgren et al. 2002; Burfisher 2017). The models are particularly useful for investigation of the dynamic behavior of an economy's private agents, public sector, and the external sector that the local economy trades with (Cutler et al. 2016). CGE models are an effective approach for regional impact analysis when the expected impacts of an external shock are complex or the external shock is assimilated from many other fields (e.g., Rose and Guha 2004; Rose and Liao 2005; Attary et al. 2020). Financial shocks, health consequences of pollution, climate change, and, as this chapter conveys, hazard events, are all capable of being integrated into a CGE model to simulate economic outcomes.

The CGE model is based on (1) utility-maximizing households that supply labor and capital, using the proceeds to pay for goods and services (both locally produced and imported) and taxes; (2) the production sector, with perfectly competitive, profit-maximizing firms using intermediate inputs, capital, land, and labor to produce goods and services for both domestic consumption and export; (3) the government sector that collects taxes and uses tax revenues in order to finance the provision of public services; and (4) exchanges between the local economy and the rest of the world. A CGE model relies on extensive data from relevant private and public sources such as the Bureau of Economic Analysis and from the U.S. Census Bureau representing the interaction of households, firms, and the relevant governmental entity into a social accounting matrix (SAM). The CGE model consists of a series of equations and is calibrated when those equations exactly reproduce that data in the SAM. The CGE model can then be used to simulate the outcomes from a wide range of exogenous shocks. See Attary et al. (2020) for a complete description of the CGE model used in this chapter.

CGE models have been used extensively at the country, state (subregion), city and small-town level to examine a myriad of issues. Robinson (1991) examines a series of closure assumptions used for a large number of country level CGE models. Ballard et al. (1985) use a CGE model for the U.S. to examine alternative tax policies. At the state level, Turner et al. (2012) construct a CGE model for Illinois to estimate Armington elasticities. Using a CGE model for Colorado, Hannum et al. (2017) examine the implied cost of carbon and Cutler et al. (2018) examine the economic impact of changes in tax policies. At the town or small city level there are numerous examples. Taylor et al. (1999) construct a small village CGE model in Mexico to examine agricultural policy. Using a CGE model for Fort Collins CO, Schwarm and Cutler (2003) examine various growth issues and Cutler and Davies (2010) examine the consequences of productivity changes. Thomson and Psaltopoulos (2007) construct a small town CGE model to examine rural economic policy. More recently, Dorosh and Thurlow (2014) examine the role of cities and towns in driving economic growth for Ethiopia and Uganda and Attary et al. (2020) used a CGE model for Joplin MO to examine the impact of recovery trajectories from the 2011 tornado. This chapter maintains that CGE models at the small city or town level have access to richer data that results in more data intensive CGE models to be created. As an example, county assessor's data can be used at the parcel level to obtain good estimates of the capital stock for commercial and residential buildings which is typically not available at the country level. Better production functions can be modeled which can allow the researcher to estimate more accurate substitutions between capital and labor. Alternative zoning regulations can be examined as well as varying property tax rates for existing buildings and new construction.

2.2.3.1 Data Collection and SAM Assembly

Figure 2-2 provides a visualization of the Joplin social accounting matrix (SAM) with short descriptions of its major components (Wang et al, 2021b). The "Input-Output" matrix comes from U.S. Bureau of Economic Analysis (BEA) national input-output coefficients that are scaled based upon the employment statistics of Jasper County, Missouri. These IO coefficients are then applied to estimates of sector spending. A limitation of the use of these input-output coefficients is that they are generalized for the Jasper County and so are not specific to the city of Joplin. The "Wage Payments by Firms" matrix is made up of worker incomes taken from Census Public Use Microdata Sample (PUMS) which are then aggregated by sector. "Wage Transfers to Households" is the process by which wage payments to labor groups are assigned to their respective household group. Household consumption of that household group is then estimated by weighting the PUMS data with American Community Survey (ACS) data on consumer spending patterns and adjusted by population. "Imports" and "Export" Matrices describe the payments made by sectors and households within Joplin to sectors from regions outside Joplin and vice versa. Within the CGE model these values are impacted by relative prices between Joplin and the Rest of World (ROW). Capital stock values are collected from the Jasper County Assessor's Office which provides market values of residential and commercial properties. These properties are assigned to Joplin spatially using a geographic information system (GIS) algorithm.

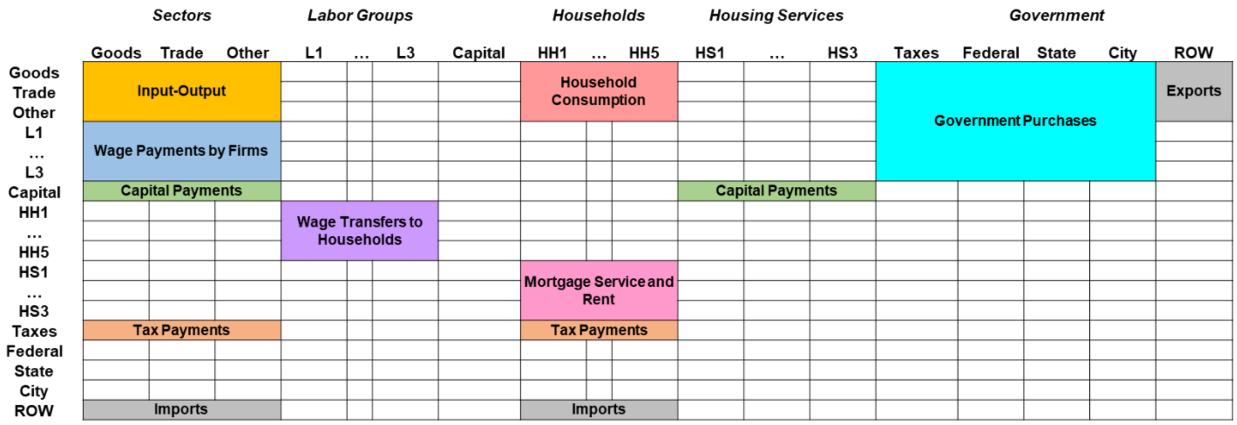

Figure 2-2. Simplified Joplin SAM Example

Capital stock shocks from tornado damage flow through the CGE models as reductions in the Capital row of the SAM. In this way, retrofit strategies that mitigate damage to homes will also then attenuate capital stock destruction of homes through the "Capital Payments" matrix (Capital row, Housing Services columns).

Within the SAM, household groups and labor groups are categorized by income. Table 2-1 describes this grouping method. Grouping labor and households this way allows for an analysis of the effects of disaster on income distributions. For example, it enables relevant insights into which economic actors are benefiting from retrofit strategies.

Table 2-1. Household and Labor Group Categorization

Household Groups		Labor Groups	
HH1	Less than $15,000	L1	Less than $15,000
HH2	$15,000 to $35,000	L2	$15,000 to $40,000
HH3	$35,000 to $70,000	L3	More than $40,000
HH4	$70,000 to $120,000	-	-
HH5	More than $120,000	-	-

The Census Longitudinal Employer-Household Dynamics (LEHD) supplies information on where people live and work at the census block level. These data permit the analyst to spatially anchor residential homes and commercial buildings in the SAM and CGE model so that a specific path of a tornado can accurately damage the infrastructure in our modeling approach for Joplin.

This data set is critical if one wants to use a CGE model to examine location specific hazard events. The limitation of the LEHD data is that the sectors workers are employed in are groups into the Goods, Trade, and Other sectors. These three sectors are aggregations of NAICS (North American Industry Classification System) sectors. Since Joplin is a relatively small community, aggregating sectors into the Goods, Trade and Other is not that critical but for larger communities there are workarounds where the two and three-digit NACIS sectors can be approximated using the LEHD data.

Combined within the SAM, the data sources described above provide a detailed picture of the Joplin economy that is comparable to privately owned economic data sources such as IMPLAN. Additionally, the data collected is free and open source except for county assessor's data. These data are frequently free but, in some cases, the data is available for a nominal fee. In this way, the methods used to organize the data can be extended to any city or county in the nation and therefore provide a consistent source of economic data.

2.2.4 Population Dislocation Algorithm

Population dislocation is defined as a household leaving their housing unit immediately after a hazard event for any period of time. Population dislocation models provide a means to study population stability within a community or region. The population dislocation model, which is integrated with hazard and building damage analysis, predicts dislocation using a logistic regression model based on household-level surveys from Hurricane Andrew in 1992, which was a significant wind event (Girard and Peacock, 1997; Peacock et al. 1997). The logistic regression equation provides a probability of dislocation based on value loss caused by building damage and the other factors, including structural types (single-family or multi-family), and neighborhood characteristics (percent minority populations). After dislocation probabilities are estimated for each damage state using the logistic regression model, the sum of the four probabilities multiplied by the four probabilities of damage states is estimated as the dislocation probability of each structure. For more details on the population dislocation algorithm and the logistic regression model, please see Rosenheim et al. (2019).

The population dislocation model depends first on the allocation of a particular housing unit and household characteristic data associated with each residential building within the community. The allocation of detailed household characteristic data provides an estimate of household characteristics such as the number of people, vacancy, and tenure within each structure. For a more detailed summary of the housing unit allocation process, please refer to Rosenheim et al. (2019).

2.3 Illustrative Example

The Enhanced Fujita 5 (EF5) tornado that struck the city of Joplin, Missouri, on May 22, 2011, was the deadliest, costliest, and most intense single tornado in US history in 60 years (FEMA 2011; Roueche and Prevatt 2013). The National Institute of Standards and Technology (NIST) conducted a comprehensive technical investigation of this devastating event which was completed in 2014 (Kuligowski et al. 2014). The structural damage of Joplin tornado was widely studied by researchers using empirical approaches and/or numerical simulation since 2011 (e.g., Prevatt et al. 2012; Roueche et al. 2015). Understanding how to conduct a community-level resilience assessment is crucial for researchers and public decision-makers to enable them to explore strategies for risk mitigation and resilience enhancement. The remainder of this chapter uses the Joplin testbed as an example to explore the effect of wind-retrofit strategies on the selected typical multi-disciplinary community resilience metrics.

In summary, the tornado was simulated to have the same wind speeds spatially as the Joplin tornado adapted from the wind field model grouped by EF Scale, which was estimated by NIST (Kuligowski et al. 2014), and resilience metrics for physical, social, and economic sectors were computed. The initial damage prediction utilized the tornado path (Kuligowski et al. 2014), tornado fragility curves representative of a 19-archetype building dataset (Memari et al. 2018), and electric power network (EPN) datasets. The functionality of the infrastructure was linked with the CGE model described above which computes household income, employment, and domestic supply. Detailed demographic data was allocated to each structure to provide resilience metrics related to population impacts such as population dislocation as a function of tenure status of households. These physical, social, and economic metrics were compared to quantify the effect of each retrofit strategy on resilience metrics at the community level. It is worth noting that studies have been performed that look at the effect of retrofitting on damage and direct losses (e.g., Prevatt et al. 2014), but no studies have looked at the effect of retrofits on both social science and economic metrics at the community level.

2.3.1 Computational Environment

In order to enhance community resilience and integrate physical, economic, and sociological sectors into a robust computational platform, the Center for Risk-Based Community Resilience Planning developed the Interdependent Networked Community Resilience Modeling Environment (IN-CORE) (van de Lindt et al. 2019). IN-CORE integrates a broad range of scientific, engineering, and socio-economic algorithms and data to enable analysts the ability to simulate the effects of different natural hazards on a community and provides a detailed assessment of the impact. IN-CORE was used in the analysis, and this example demonstrates how users can interact with the IN-CORE computational environment by conducting a multi-disciplinary resilience assessment and determine the effect of retrofit strategies for residential buildings in a tornado. All analyses and data were developed and are available on the IN-CORE web services and IN-CORE Python library (pyIncore) for researchers worldwide to expand the analysis beyond the work presented herein. In addition, this chapter is available online in a Jupyter Notebook, which allows users to reproduce this research with Python codes, data, and visualization. The interested reader is referred to https://incore.ncsa.illinois.edu/doc/incore/notebooks/Joplin_testbed/Joplin_testbed.html.

2.3.2 Community and Hazard Modeling

2.3.2.1 Community Topology

A total of 19 archetype buildings were used in this chapter to represent the Joplin community with a total of 28,152 buildings, as shown in Figure 2-3. Five typical woodframe residential buildings with different footprint areas, roof structures, and the number of stories, were used to represent all the residential buildings in the city of Joplin. More than 85% of Joplin buildings are typical woodframe residential buildings, which is typical for small to mid-size North American communities (Masoomi et al. 2018). Other building types, such as commercial buildings, school buildings, and hospitals, were also included in the spatial description of the community using the suite developed by Memari et al. (2018). The electric power network (EPN) for Joplin was included in the community model beginning with the raw data for the EPN, including substations, poles, transmission lines, and distribution lines from the Empire District Electric Company just prior to the tornado (Attary et al. 2019). The EPN damage was combined with building damage to perform building functionality analysis immediately following the tornado.

Since woodframe residential buildings account for most buildings in the city of Joplin and are the most susceptible building type for tornadoes, this chapter focuses on woodframe buildings.

The retrofit of residential structures is an essential tool to mitigate risk, thereby enhancing resilience. Table 2-2 presents three retrofit strategies used in this chapter based on different combinations of roof covering, roof sheathing nailing pattern, and roof-to-wall connection. The material for roof covering used for retrofit was planned to be either asphalt shingles or clay tiles. The shingles used were regular shingles with the upgraded shingles then being hurricane rated shingles. The roof sheathing nailing pattern was assumed to use hand-driven 8d common nails attaching roof deck sheathing panels to rafters spaced at either 150/300 mm (6/12 inch) or 150/150 mm (6/6 inch). Two different selections of roof-to-wall connections refer that the roof rafters could be connected to the top plates over the vertical studs using two H2.5 hurricane clips or two 16d toenails. The retrofit strategies and related fragilities for these woodframe residential buildings were developed by Masoomi et al. (2018) and first used in a simplified virtual community example that looked at functionality but stopped short of investigating socio-economic metrics for community resilience (Farokhnia et al. 2019). The original design combination for residential buildings in areas typically susceptible to tornadoes is the same combination as retrofit strategy 1, except wood shingles, are in place rather than asphalt shingles (Niemiec and Brown 1988).

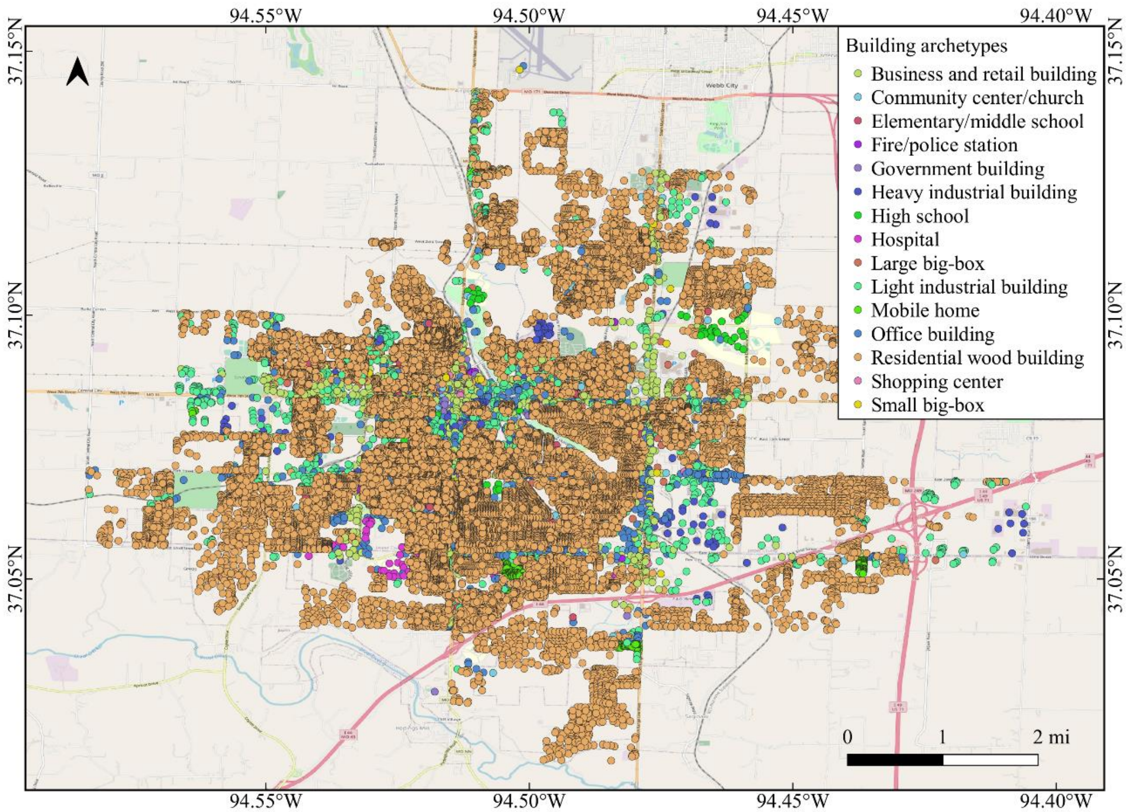

Figure 2-3. 19 archetype buildings in the city of Joplin

Table 2-2. Different types of retrofit strategy schemes for residential buildings

Structural elements	Selections	Retrofit strategy 1	Retrofit strategy 2	Retrofit strategy 3
Roof covering	Asphalt shingles	X	X	
	Clay tiles			X
Roof sheathing nailing pattern	8d C6/12	X		
	8d C6/6		X	X
Roof-to-wall connection type	Two 16d toenails	X		
	Two H2.5 clips		X	X

2.3.2.2 Socio-Economic Systems

Joplin, Missouri spans part of both Jasper and Newton County, with the majority being located in Jasper County. Based on the 2010 Decennial Census (U.S. Census Bureau 2010a, 2010b, 2010c), the city of Joplin had 23,322 housing units (11,389 owner-occupied, 9,471 renter-occupied, and 2,462 vacant). The household size was distributed from 1-person to 7-or-more persons, and the total population count of the community was 50,150, with 27,076 people living in owner-occupied housing units and 21,086 people living in renter-occupied housing units. Table 2-3 provides a summary of the allocated housing units and population characteristics. Notice that the estimated housing units was 23,261 in the building inventory, compared to 23,322 based on the 2010 Census data, an error of 0.26% (U.S. Census Bureau 2010a; 2010b; 2010c). The average household size in Joplin was estimated to be 2.31 people (lower than the state average of 2.45), with owner-occupied households being slightly larger than renter-occupied households (2.38 vs. 2.23) (U.S. Census Bureau 2010d). The average allocated household size was 2.30; 2.37 for owner-occupied housing units and 2.22 for renter-occupied housing units, an error of 0.47%. Table 2.3 verifies that the population data in the model accurately reflects Joplin's estimated household size distribution by tenure status. These allocated data are important parameters to estimate population dislocation and the residents who were served by electric power following the tornado hazard, discussed in the section of Electrical Power Network Damage later. Household size and type did not impact the CGE model which reflects the local economy.

Table 2-3. Allocated housing unit characteristics for Joplin, MO in 2010

	Owner-occupied	Renter-occupied	Housing unit count
1-person household	3,135	3,788	6,923
2-person household	4,398	2,564	6,963
3-person household	1,658	1,414	3,072
4-person household	1,255	944	2,199
5-person household	566	433	1,000
6-person household	206	194	403
7-person household	126	98	224
Group Quarters	-	-	22
Vacant	-	-	2,455
Total number	11,344	9,435	23,261
Total population	26,873	20,949	49,810

2.3.2.3 Tornado Hazard Modeling

Figure 2-4 shows the 2011 Joplin tornado path with EF zones provided in the legend (after Wang et al. 2021a). The tornado path represents the wind speed within the vortex (multi-vortex in the case of Joplin) that was estimated to have EF5 wind speeds of more than 321.9 kph (200 mph), reducing to EF4 wind speeds as the areas move outwardly perpendicular from the centerline, and eventually reaching EF1 zone (Attary et al. 2018). Obviously, this concept is not perfect, as seen clearly through inspection of Figure 2-4. It should be noted that generic tornado paths with idealized rectangular EF regions can also be used, and users can define their tornado path for the simulation (Standohar-Alfano and van de Lindt 2014). For communities that have not experienced a tornado, this idealized representation allows users to perform “what if” scenarios. Besides, different wind field models to estimate near-surface wind speed exist for the Joplin tornado, some of which are independent of the field damage assessment to the buildings and are based on tree fall patterns (Lombardo et at. 2015).

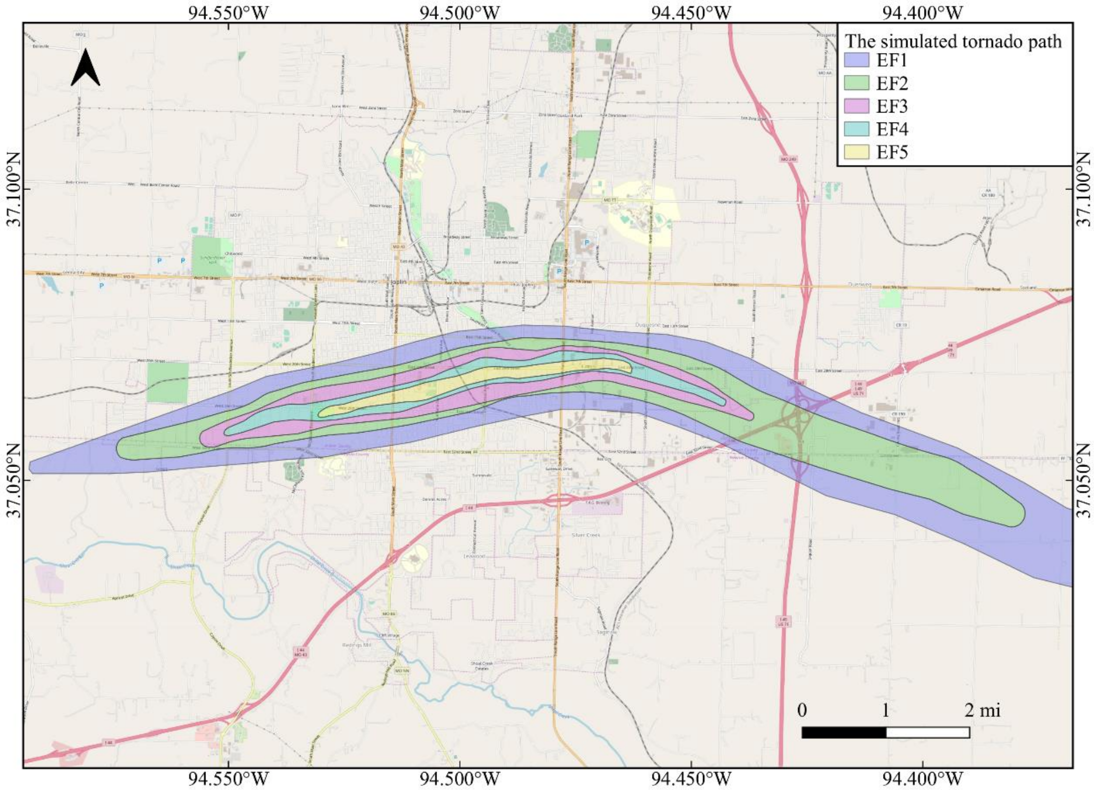

Figure 2-4. Joplin tornado path with EF zones

2.3.3 Fragility Functions

The damage fragility curves for a suite of 19 building types for four damage states are available to cover the entire range of wind speeds associated with tornadoes (Attary et al. 2018; Memari et al. 2018; Koliou et al. 2017; Masoomi et al. 2016). For details on all building fragilities, the interested reader is referred to Memari et al. (2018). Table 2-4 provides tornado fragilities for the five residential building archetypes when the three different retrofit strategies were applied which were extracted from Masoomi and van de Lindt (2018). Referring back to Equation (2.4), λ and ξ shown in Table 2-4 are two parameters that control tornado fragility curves. These parameters could determine the vulnerability of buildings subjected to a tornado. Generally, the higher λ is, and the buildings are more robust to resist the hazard, and ξ shows the dispersion of the distribution considering uncertainties to obtain the fragilities. Note that the numbers with and without parentheses of each cell shown in Table 2-4 are the logarithmic mean and standard deviation of the tornado fragilities in U.S. customary units (mph) and metric units (m/s), respectively. For each residential building archetype, this required a full structural analysis at each wind speed to calculate the resistance when implementing different retrofit strategies. A reduction is damage occurs, but each retrofit has other implications such as cost and disruption to households.

Table 2-4. Lognormal tornado fragilities of residential buildings with three retrofit strategies

Damage state (DS)	Retrofit strategies #	Archetype 1		Archetype 2		Archetype 3		Archetype 4		Archetype 5	
		λ	ξ	λ	ξ	λ	ξ	λ	ξ	λ	ξ
DS1	1	3.68 (4.49)	0.13 (0.13)	3.60 (4.41)	0.13 (0.13)	3.61 (4.42)	0.13 (0.13)	3.73 (4.54)	0.13 (0.13)	3.75 (4.56)	0.13 (0.13)
	2	3.68 (4.49)	0.14 (0.14)	3.60 (4.41)	0.13 (0.13)	3.61 (4.42)	0.13 (0.13)	3.73 (4.54)	0.13 (0.13)	3.75 (4.56)	0.13 (0.13)
	3	3.93 (4.74)	0.12 (0.12)	3.87 (4.68)	0.12 (0.12)	3.89 (4.70)	0.12 (0.12)	3.95 (4.76)	0.12 (0.12)	3.95 (4.76)	0.12 (0.12)
DS2	1	3.56 (4.37)	0.14 (0.14)	3.53 (4.34)	0.13 (0.13)	3.51 (4.32)	0.13 (0.13)	3.65 (4.46)	0.13 (0.13)	3.65 (4.46)	0.13 (0.13)
	2	3.85 (4.66)	0.12 (0.12)	3.76 (4.57)	0.12 (0.12)	3.77 (4.58)	0.12 (0.12)	3.87 (4.68)	0.12 (0.12)	3.88 (4.69)	0.12 (0.12)
	3	3.99 (4.80)	0.11 (0.11)	3.96 (4.77)	0.11 (0.11)	3.96 (4.77)	0.11 (0.11)	4.03 (4.84)	0.10 (0.10)	4.02 (4.83)	0.11 (0.11)
DS3	1	3.63 (4.44)	0.13 (0.13)	3.59 (4.40)	0.13 (0.13)	3.57 (4.38)	0.13 (0.13)	3.71 (4.52)	0.13 (0.13)	3.70 (4.51)	0.13 (0.13)
	2	3.98 (4.79)	0.11 (0.11)	3.91 (4.72)	0.11 (0.11)	3.92 (4.73)	0.11 (0.11)	4.00 (4.81)	0.11 (0.11)	3.98 (4.79)	0.11 (0.11)
	3	4.08 (4.88)	0.10 (0.10)	4.04 (4.85)	0.10 (0.10)	4.04 (4.85)	0.11 (0.11)	4.12 (4.93)	0.10 (0.10)	4.11 (4.92)	0.10 (0.10)
DS4	1	3.68 (4.49)	0.14 (0.14)	3.68 (4.49)	0.13 (0.13)	3.74 (4.55)	0.12 (0.12)	3.76 (4.57)	0.13 (0.13)	3.64 (4.45)	0.15 (0.15)
	2	4.16 (4.97)	0.13 (0.13)	4.17 (4.98)	0.12 (0.12)	4.23 (5.04)	0.12 (0.12)	4.28 (5.09)	0.12 (0.12)	4.06 (4.87)	0.14 (0.14)
	3	4.29 (5.10)	0.12 (0.12)	4.26 (5.07)	0.11 (0.11)	4.31 (5.12)	0.12 (0.12)	4.36 (5.17)	0.12 (0.12)	4.24 (5.05)	0.13 (0.13)

2.3.4 Infrastructure Functionality Analysis

2.3.4.1 Functionality Due to Building Damage

Using the tornado fragilities described earlier, and wind speed at the location of each structure, the probability of exceeding each damage state can be computed using MCS. Recall that the damage states are slight, moderate, extensive, and complete, and were calculated for each building in the community to estimate the structural damage spatially. It is important to mention that the damage states for residential, commercial, school buildings and others were defined based on the component-based approach also used in "HAZUS MH 2.1" (FEMA 2012; Masoomi et al. 2018; Koliou et al. 2017; Masoomi and van de Lindt 2016), but are not HAZUS fragilities. In this chapter, the criterion for loss of building functionality as a result of damage within a single MCS iteration was defined as exceeding DS2. If more than 50% of the simulations exceeded DS2, the building was deemed not to be functional for interfacing to the CGE model. Figure 2-5 shows the criterion as mentioned for a typical residential building (archetype 4), as an example. It was assumed buildings were still safe and operational when buildings were in damage state 1 following the tornado, and there was only minor damage to building components such as the roof covering, which could be covered with a tarp to prevent excessive rainwater intrusion. The functionality criterion could be different in terms of a particular structural failure (or other) in buildings whenever the damage exceeds DS1.

The 2011 Joplin tornado path estimate with specified EF zones is deterministic in this chapter, the number of buildings falling within the tornado path by building archetypes can be determined, as illustrated in Table 2-5. For example, there are 2,626, 1,387, 1,703, 807, 556 T1 woodframe residential buildings with one story, gable roof, and small rectangular plan, falling in EF1, EF2, EF3, EF4, EF5 zones, respectively. It is well known that tornadoes impact a relatively small geographical area within a community. As a result, buildings outside the tornado path are structurally safe, and the failure probabilities of these buildings are assigned to be approximately zero. Buildings located within the tornado path were damaged at different levels with the failure probability between 0 and 1. In general, the closer to the tornado centerline with higher wind speeds, the higher the probability of buildings in damage. For example, there is a T1 woodframe residential building whose failure probability is 0.999, 0.856, and 0.579 for retrofit strategy #1, #2, and #3, respectively. The results revealed that the building was the most vulnerable if using retrofit strategy #1, and the most robust if using retrofit strategy #3. Other economic factors, such as limited budget, were beyond the scope of this chapter.

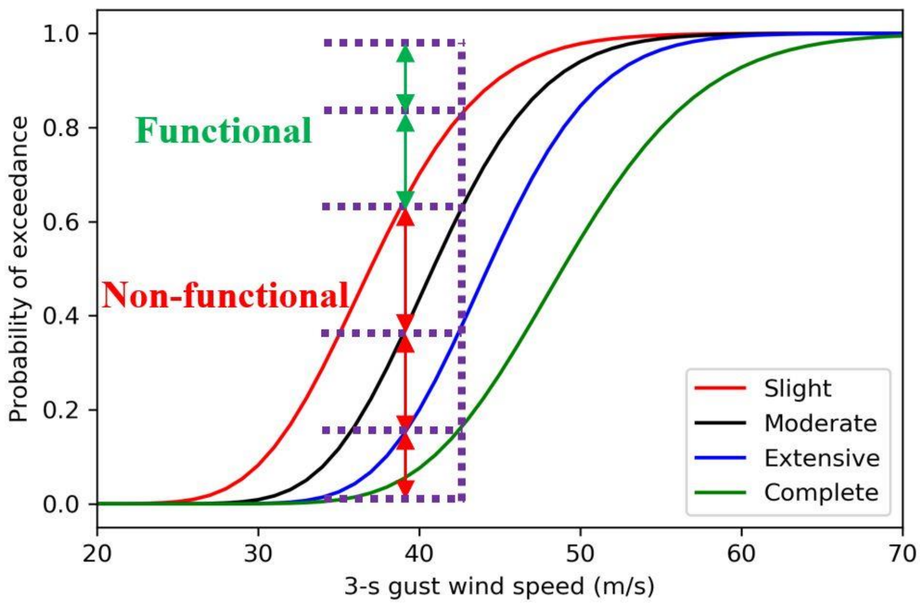

Figure 2-5. The criterion for loss of building functionality because of damage

Table 2-5. Buildings located in the simulated tornado path

Archetypes	Building description	Joplin buildings	EF1	EF2	EF3	EF4	EF5
T1	Residential wood building, small rectangular plan, gable roof, 1 story	24,757	2,626	1,387	1,703	807	556
T5	Residential wood building, large rectangular plan, gable roof, 2 stories	146	4	21	31	5	15
T6	Business and retail building (strip small)	736	45	32	37	37	35
T7	Light industrial building	963	46	39	27	21	13
T8	Heavy industrial building	155	14	2	2	0	2
T9	Elementary/middle school (unreinforced masonry)	39	6	0	1	2	3
T10	High school (reinforced masonry)	50	0	0	2	1	2
T11	Fire/police station	8	0	1	0	0	0
T12	Hospital	41	5	2	5	7	3
T13	Community center/church	88	7	5	4	3	2
T14	Government building	28	3	3	1	0	0
T15	Large big-box	21	1	1	0	2	1
T16	Small big-box	30	1	2	1	0	1
T17	Mobile home	379	12	0	0	0	0
T18	Shopping center	10	0	0	0	0	1
T19	Office building	701	84	16	21	74	41
Total number		28,152	2,854	1,511	1,835	959	675

2.3.4.2 Electrical Power Network Damage

Attary et al. (2019) applied a cellular automata (CA) algorithm, together with transmission and distribution line locations within an electrical power network, to determine service areas for the substations. Based on that work and combining it with raw 2010 data collected from the Empire District Electric Company, the authors included four more substations to cover all the buildings shown in the Joplin map, beyond the immediately impacted tornado path. This was necessary to model the building functionality, described later, which includes a loss of electrical power. There are 18 substations (transmission substations and distribution substations) and 23,857 distribution poles modeled in this chapter. Fragility parameters for the community electric power network used in this chapter were based on the work performed by Masoomi et al. (2018) and Unnikrishnan and van de Lindt (2016). The number of distribution poles in each EF region of the tornado was determined as 1,470, 800, 685, 436, and 369 in the EF1 through EF5 regions, respectively.

The failure probabilities of the substations (SS9, SS10, SS11) located in EF-5, EF-3, and EF-1 were (near) 1, 0.997, and 0.758, respectively. The EPN damage was also identified whenever the state of the electric power facility within MCS exceeded the moderate level (see Figure 2-5). In this chapter, there is no retrofit being analyzed for the electric power network. An interdependency table between all buildings and their electrical substation dependency was created to identify buildings located in each of the service areas for the substations (see Figure 2-6). Another dependency was modeled by setting up an interdependency table between each building and poles, with the closest poles to the building being linked using what is called the nearest neighbor relationship geographically. The closest poles to buildings were considered to be utility poles in the front of the house or the backyard.

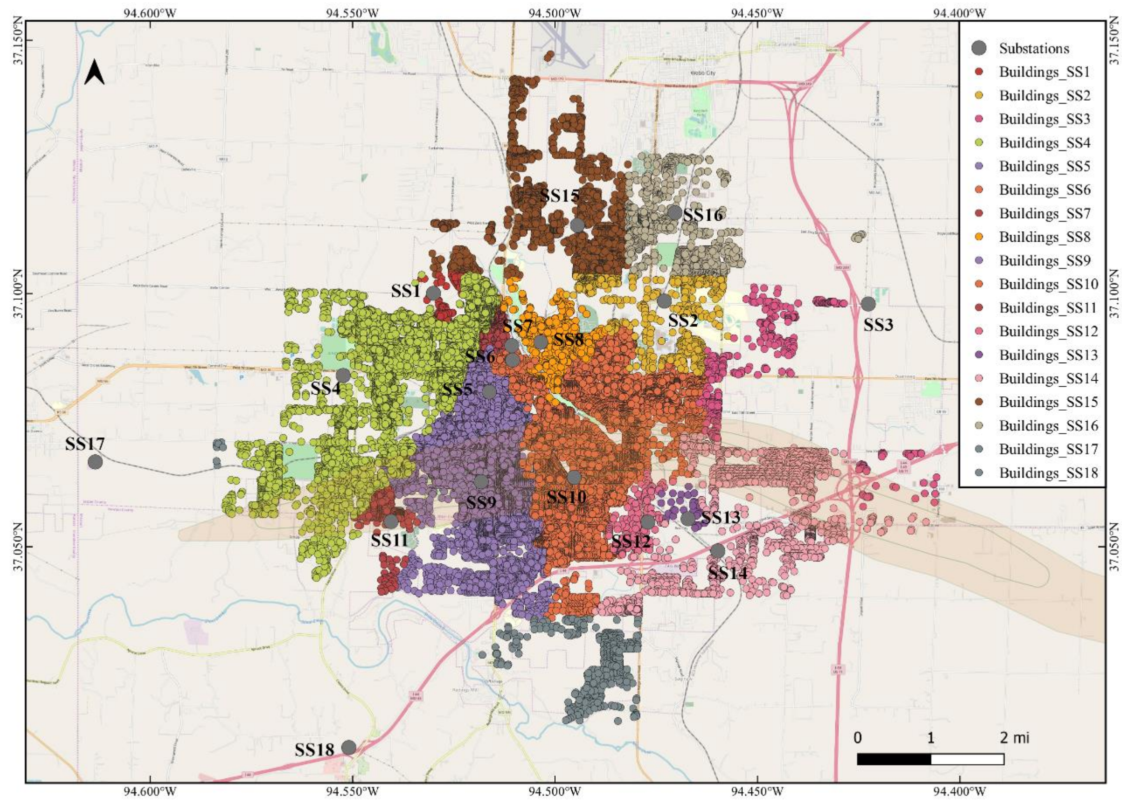

Figure 2-6. Buildings situated in the service areas of substations

2.3.4.3 Functionality Due to Building Damage and/or Loss of Electric Power

After finding the damage level for each community component (buildings, electrical substations, and distribution poles) based on their fragility curves, their intrinsic failure status was expressed in a binary format as either failed (0) or not failed (1) estimated by whether or not it exceeds DS2 for each run of the MCS. Then the functionality status of all the buildings was updated by considering their dependencies with the corresponding electric power facilities. Buildings were only considered functional when the building itself, the substation transmitting the electric power, and the closest pole were all functional (accounting for network connectivity). Each component generated enough MCS samples randomly with their functionality status determined. Both the functionality probability of each building and the percentage of building functional and nonfunctional could be calculated using the updated functionality status of all the buildings within the MCS. More detailed results determined from infrastructure functionality analysis will be summarized and introduced later in the section of physical service resilience metrics results.

2.3.5 Physical Service Metrics Results

In this chapter, the functionality of the electric power network plays an essential role in the functionality of buildings. The equation to determine the loss of physical service metrics (P_{ps}) after the tornado hazard is shown below:

$$P_{ps} = \iint L(F_{fnc}(DS)) \cdot p[DS|IM] \cdot p[IM] dDS \cdot dIM \quad (2.6)$$

where *DS* indicates the damage state, $p[\cdot|\cdot]$ denotes the probability of a random variable conditioned on the other random variable, $L(\cdot)$ represents the loss of physical service metrics based on the functionality events, and *IM* is the intensity measure which is wind speed for tornadoes.

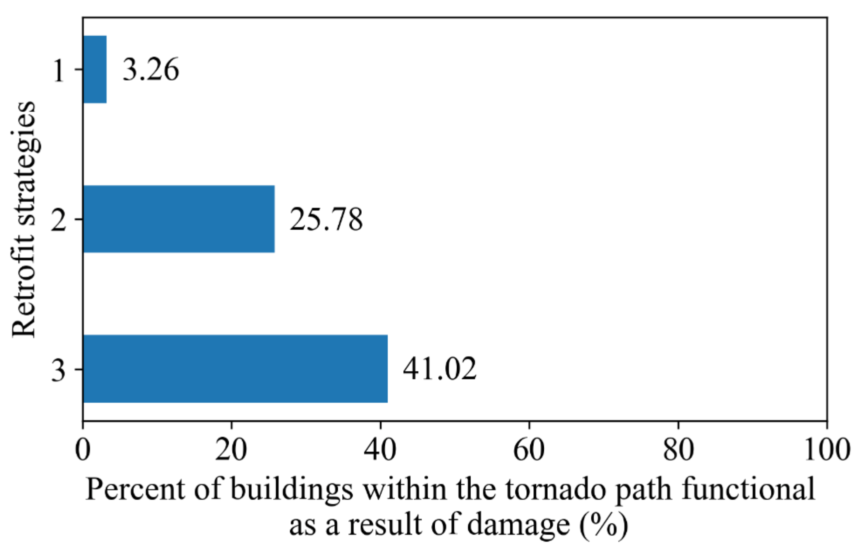

(a)

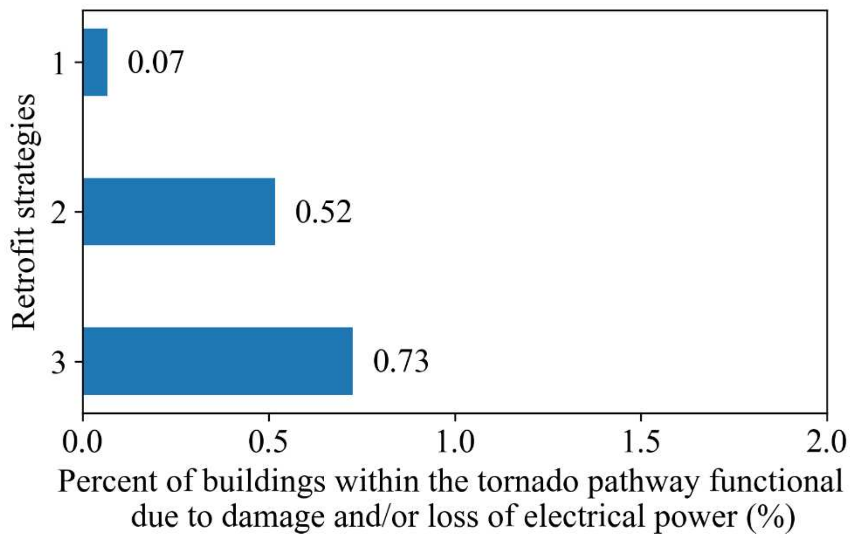

Retrofit strategies
1
2
3
0.07
0.52
0.73
0.0
0.5
1.0
1.5
2.0
Percent of buildings within the tornado pathway functional due to damage and/or loss of electrical power (%)

(b)

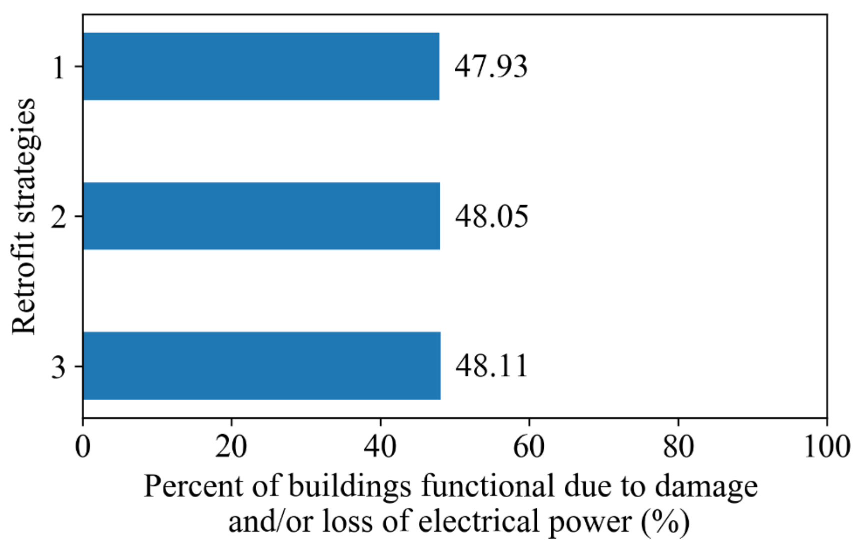

Retrofit strategies
1
2
3
47.93
48.05
48.11
0
20
40
60
80
100
Percent of buildings functional due to damage and/or loss of electrical power (%)

(c)

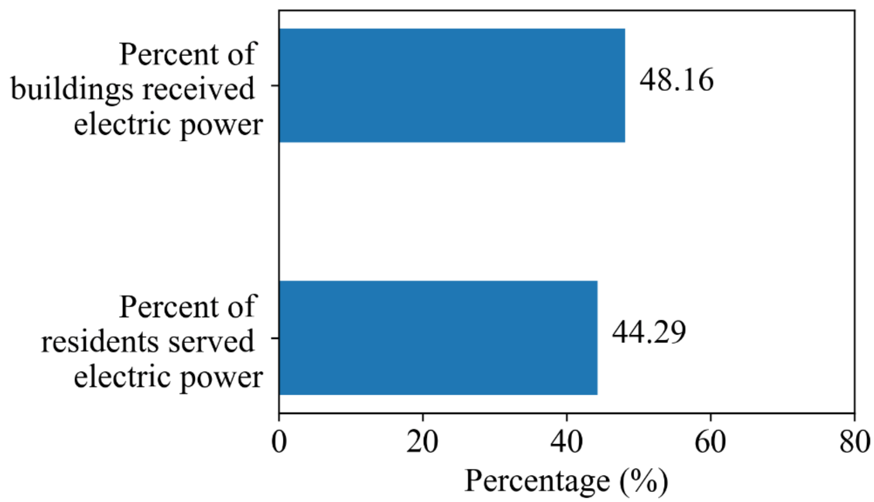

(d)

Figure 2-7. Physical service resilience metrics: (a) percent of buildings within the tornado path functional as a result of damage (%); (b) percent of buildings within the tornado pathway functional due to damage and/or loss of electrical power (%); (c) percent of buildings functional due to damage and/or loss of electric power; (d) percent of buildings receiving electric power and percent of residents served electric power

Figure 2-7 presents four representative physical service resilience metric results determined from infrastructure functionality analysis: (1) the percentage of buildings falling within the tornado path that are not functional as a result of building damage, (2) the percentage of buildings falling within the tornado path that are not functional due to building damage and/or loss of electrical power, (3) the percentage of buildings receiving electric power, and (4) percentage of residents being served electric power. The percentages in the horizontal bars of Figure 2-7(a) were the averages for the number of buildings within the tornado path that are functional divided by the total number of buildings (7,834) considered to be in the tornado path. The improvement in retrofit strategies had a significant positive effect on improving the performance of residential buildings in this Joplin tornado simulation. The difference in remaining functionality from 3.26% to 41.02% comparing retrofit strategies 1 and 3 is stark. The reason that such a large change occurs is that the edges of the tornado where EF0 and EF1 damage would normally occur and no longer an issue, and even a large portion of the EF2 damage becomes EF1 damage making it still function, e.g. often tarped and the household remains. Loss of functionality is defined as more than a 50% chance of exceeding damage state 2. Damage state 2 occurs in these lower EF regions so the effect of basic retrofits is significant. For more details on the concept of narrowing the damage path of a tornado through retrofit, the reader is referred to van de Lindt et al (2013).

The number of buildings in the path linked to SS9, SS10, and SS11 was 3,634, 2,453, and 274, which means more than 81% buildings in the path had the possibility of losing electric power regardless of whether the buildings themselves were physically damaged or not (see Figure 2-6). As a result, there was a minor difference in the percentage of buildings deemed functional due to physical damage and/or loss of electrical power with the utility of different retrofit strategies as shown in Figure 2-7(b) and 2-7(c). Despite this, there were still some changes in the probability of buildings remaining functional, which were mostly located in the EF1 region of the tornado. If considering the loss of electric power as well as building damage as the functionality criterion, the functionality of buildings does not have an evident difference between the different retrofit strategies. This is primarily because the EPN losses in wind events are often total or near total for a community.

It is noticeable that only 48.2% of buildings and 44.3% of residents could receive electric power, which means more than half of buildings and residents experienced power outage following the tornado event due to downed power poles or damage to substations. The housing unit allocation process (Rosenheim et al. 2019) was applied, and the number of people per household as a typical household characteristic was predicted. As a result, the percent of residents served electric power can be determined by the number of people residing in the residential buildings that experienced electric power loss divided by the total population of 49,810 (see Table 2-3). It should be emphasized that the buildings illustrated in Figure 2-7(d) include all archetypes such as residential, commercial, and industrial buildings within Joplin, but residents served electric power focuses on the housing units living in the residential buildings and does not include other building types.

Based on the field investigation after the 2011 Joplin tornado, Kuligowski et al. (2014) determined that over 7,400 residential buildings and 500 non-residential buildings were damaged to some degree and approximately 43% of residential buildings were considered destroyed (i.e., structures with damage classification of heavy or demolished). The devastating tornado also battered the electric power network and resulted in approximately 20,000 Empire District Electric (EDE) customers losing power during or immediately after the storm. Specific tornado impacts included two step–down substations damaged but repairable, one substation completely destroyed, and approximately 4,000 distribution poles and transmission towers damaged. In summary, all the simulations described above quantitatively estimate the physical service resilience metrics related to building damage, EPN damage, and electric loss after the tornado, and the analytical results are close to the actual field investigation data collected after 2011 Joplin tornado.

2.3.6 Economic Stability Metrics Results

In this chapter, the CGE model discussed earlier was developed for Joplin and served as the economic impact model. The model was used to quantitatively evaluate how the community economy responded to damages created by the tornado hazard. Capital stock reductions were accounted for through the connection between the engineering outputs (lack of building functionality) and the CGE model. The outputs calculated from infrastructure functionality analysis were building functionality probabilities. It is important to note that building functionality probability herein represents the probability of each building in the community being functional only due to building damage without considering electric power loss, which is consistent as the case shown in Figure 2-7(a). Building level capital stock impacts were weighted based upon the building functionality probabilities multiplied by the value of the buildings. Next, the building-level impacts were aggregated to the corresponding sectors and implemented as external shocks to these sectors within the model. The shocks took the form of percentage reductions in the capital stock of the associated residential, commercial, or industrial sectors and then were applied to the CGE model. Incorporating the output from the engineering models into external shocks enabled the CGE model to estimate employment effects, domestic supply by sectors, as well as the level and distribution of household incomes in order to explore the varying impacts of natural disasters on a regional economy (Cutler et al. 2016; Attary et al. 2020).

Table 2-6 indicates the direct and indirect economic loss following the tornado described in the chapter with the three different retrofit strategies implemented. For each retrofit strategy, which applies modified fragility curves, the building functionality analysis was performed, and the economic impacts were simulated. Recall that retrofit strategy 3 has the design combination of clay tiles as roof covering, roof sheathing nailing pattern scheduled for 8d C6/6, and two H2.5 clips used for the roof-to-wall connection. The loss of total household income was reduced from $60.5 million to $38.3 million when using retrofit strategy 3. Although it is important to consider the budget of each retrofit strategy, the methodology in this chapter presents the approach to quantify the effect of these physical modifications to residential buildings on economic losses for employment, domestic supply, and household income. Costing and optimization is beyond the scope of this chapter, but it is important should eventually be pursued. Additionally, it is acknowledged that government agencies, nongovernmental organizations (NGOs) like the American Red Cross and local churches, businesses, and individual contributors provide resources after disasters, which will contribute to the stability of the local economy. However, all aids and funds are commonly provided during the recovery over time rather than immediately after the hazard event. The significant impact of the funds or donations on the community economy is not considered in this chapter, but will need to be considered when recovery is modeled (see Chapter 5 and Chapter 6).

The key results of the CGE analysis largely concern the impact of the event on the distribution of household income. Middle-income households (HH4) were the hardest hit by the tornado and were the largest benefactors from retrofits in terms of their incomes. This is due to the location of these homes from the LEHD data relative to the path of the simulated tornado. Low-income households (HH1 to HH2) were not as negatively impacted by the disaster but saw virtually no benefit from retrofit strategies as these households are heavily comprised of renters. This result is consistent with the impact to rental property domestic supply (HS3), which experienced only minor disruption relative to homeowner residential property domestic supply (HS1 to HS2).

A particularly interesting result is that across all three cases, household income increases for HH5. Wage income falls for this group, but capital income increased by enough to more than offset the wage income losses. This occurs because HH5 households own most of the physical capital for commercial properties. When the tornado hit, many commercial buildings became nonfunctional, but it increased the rate of return on the commercial properties that were not damaged. The resulting increase in capital income for HH5 was larger than the wage losses for HH5 so total household income increased for this group. For household groups HH2, HH3 and HH4, these groups own a much smaller share of commercial property, so their wage income losses were larger in absolute value than their capital income increases. For HH1, this group was mostly dependent on government transfers, so even though their wage income fell, the government transfers dominated for this group, albeit by a small amount.

Although commercial sectors (Goods, Trade, and Other) do not directly benefit from retrofit strategies as the retrofits were only applied to residential homes, the indirect effects led to substantial negation of unemployment. This reduction in unemployment appears to be consistently applied as we increase the retrofit strategy from left to right. However, the magnitude of the employment loss to the Trade sector is far greater than Goods and Other relative to their total employment sizes. For instance, the Trade and Goods sector each respectively hold approximately one-quarter of total employment and yet twice the number of workers in the Trade sector went unemployed following the tornado (at every level of retrofit strategy).

Table 2-6. Economic resilience metrics difference

	Retrofit strategy 1	Retrofit strategy 2	Retrofit strategy 3
Employment (unit: person)			
Goods	-358.074	-270.761	-212.817
Trade	-742.131	-562.955	-443.312
Other	-1765.100	-1332.170	-1042.180
Federal	-4.710	-3.586	-2.818
State	-13.392	-10.193	-8.046
City	-58.505	-44.546	-35.144
Total	-2941.9	-2224.2	-1744.3
Domestic Supply Residential (unit: millions of $)			
HS1	-61.095	-45.638	-35.469
HS2	-67.325	-49.572	-36.768
HS3	-7.713	-6.623	-6.059
Total	-136.1	-101.8	-78.3
Domestic Supply Commercial (unit: millions of $)			
Goods	-49.254	-41.540	-36.411
Trade	-42.299	-33.169	-26.923
Other	-111.074	-85.447	-68.200
Total	-202.6	-160.2	-131.5
Household Income (unit: millions of $)			
HH1	0.072	0.046	0.018
HH2	-0.991	-0.760	-0.805
HH3	-24.430	-18.240	-14.643
HH4	-100.042	-76.532	-59.645
HH5	64.934	47.926	36.741
Total	-60.5	-47.6	-38.3

2.3.7 Population Stability Metrics Results

The population dislocation model was implemented to predict the population dislocation metrics under different natural hazards. It is noteworthy that this chapter modifies the population dislocation model to reflect the unique nature of tornado paths. Since the building damage fragilities have four categories, a building with no damage has a ~100% chance of insignificant damage and a ~0% chance of other damage levels. These structures were located across the community away from the tornado path. The authors assumed that these households would not be dislocated due to damage to their structure.

In order to determine if a household dislocates, a random value was uniformly sampled between 0 and 1: if this value was lower than the probability of dislocation, then the household was set to dislocate. Tables 2-7 and 2-8 indicate the housing units and population predicted to dislocate as a function of housing unit characteristics. The numbers of housing units predicted to dislocate were 5,567, 4,249, and 3,814 if residential buildings employ retrofit strategy #1, #2, and #3, respectively. The total population dislocated decreases by 2,701 people (11,698 to 8,997) for retrofit strategy 2 and by 944 people (8,997 to 8,053) for retrofit strategy 3. Disaggregating the dislocation statistics by housing unit characteristics reveals that the retrofit strategies reduce dislocation by 25.4% for renter-occupied households and 23.2% for owner-occupied households. Additionally, the data is disaggregated by group quarters and vacancy types, and the retrofit strategies have no impact on nursing facilities.

Table 2-7. Housing unit dislocation within tornado path by housing unit characteristics and retrofit strategy

Housing Unit Characteristics	Retrofit strategy 1	Retrofit strategy 2	Retrofit strategy 3	Total housing units
Owner-occupied	2,737 (78.5%)	2,145 (61.5%)	1,929 (55.3%)	3,487 (100%)
Renter-occupied	2,326 (76.2%)	1,732 (56.8%)	1,550 (50.8%)	3,052 (100%)
Nursing Facilities	2 (40.0%)	2 (40.0%)	2 (40.0%)	5 (100%)
Other Group Quarters	1 (100.0%)	0 (0.0%)	0 (0.0%)	1 (100%)
Vacant for Rent	184 (75.4%)	144 (59.0%)	131 (53.7%)	244 (100%)
Vacant for Sale	129 (75.9%)	100 (58.8%)	86 (50.6%)	170 (100%)
Vacant Other	188 (77.7%)	126 (52.1%)	116 (47.9%)	242 (100%)
In total	5,567 (77.3%)	4,249 (59.0%)	3,814 (53.0%)	7,201 (100%)

Table 2-8. Population dislocation within tornado path by housing unit characteristics and retrofit strategy

Housing Unit Characteristics	Retrofit strategy 1	Retrofit strategy 2	Retrofit strategy 3	Total population
Owner-occupied	6,349 (78.5%)	4,992 (61.7%)	4,468 (55.2%)	8,093 (100%)
Renter-occupied	5,204 (76.1%)	3,878 (56.7%)	3,458 (50.6%)	6,837 (100%)
Nursing Facilities	127 (34.1%)	127 (34.1%)	127 (34.1%)	372 (100%)
Other Group Quarters	18 (100.0%)	0 (0.0%)	0 (0.0%)	18 (100%)
In total	11,698 (76.4%)	8,997 (58.7%)	8,053 (52.6%)	15,320 (100%)

2.4 Summary and Conclusions

The use of risk-informed decision-making tools, which can be used by community decision and policy-makers, is vital to planning and improving the resilience of a community at risk to natural hazards. In this chapter, the results of an analyses procedure to propagate damage to buildings and the electrical power network models from a simulated tornado to the impact on physical, social, and economic metrics at the community level was presented. A new open-source computational environment, IN-CORE, was used to develop and link all models in this chapter. Initially, the building and EPN spatial damage results were computed with the use of the tornado hazard model, fragility functions, and the datasets for the physical infrastructure. With the help of the geographical dependency model developed in this chapter between buildings and the electric power network, building functionality results, and the corresponding physical stability metrics were determined. Second, the authors linked the functionality of the infrastructure with a CGE model via the shock of the capital stock reduction and computed typical economic metrics for the post-disaster community. Finally, a population dislocation model driven by building damage provides resilience metrics related to social science and explores population dislocation as a function of household tenure status.

While the method provides benefits there are clearly limitations in accuracy of the physical and economic models, uncertainty in the population dislocation models resulting from real-world data and regressions. The authors recognize these challenges and thus as much uncertainty through the use of fragility functions is included by using MCS. However, the mean values are then used to propagate into the CGE and population dislocation models for this chapter. In future work it may be possible to embed the CGE and population dislocation models within the MCS loop to better reflect the uncertainty in those models also.

The following can be concluded based on the analyses presented in the chapter:

1) The percentage of buildings in the path estimated functional as a result of physical damage was 3.26%, 25.78%, and 41.02% when using retrofit strategy #1, #2, and #3 for residential buildings. More than 81% of buildings in the tornado path had a strong possibility of losing electric power. There was a negligible difference in the percentage of buildings deemed functional if combined physical damage with loss of electrical power in different retrofit strategies. Only 48.16% of buildings and 44.29% of residents could receive electric power following the simulated tornado due to the breakdown of the electric power network. It should be noted that these simulated values are in line with past estimates of the 2011 event.

2) The CGE model was used to quantitatively evaluate how the community economy changed due to external shocks resulting from tornado hazards. Capital stock reductions were the connection linking the building damage with the CGE model. For example, the total annual household income for HH3 was estimated decrease by $24.43 million, $18.24 million, and $14.64 million for the community after the tornado if using retrofit strategy #1, #2, and #3, respectively. The more advanced retrofit strategy could enable structures to become more robust to the hazard, which lead to lower economic losses. Future work may also consider the potential budget estimation for different retrofit strategies and determine their cascade effects on the local economy.

3) The population dislocation model, also driven by the building damage results, was used to predict the probability of dislocation immediately following the event. The numbers of housing units predicted to dislocate were 5,567, 4,249, and 3,814 when residential buildings were retrofitted by the approaches of #1, #2, and #3, respectively. Retrofit strategy #3 most significantly improved the performance of residential buildings, and then reduced the population dislocated.

The results of these analyses stemming from building damage estimation have a logical trend, but the substantial contribution of this chapter is that, for the first time, the effect of retrofit strategies for tornado loading can be quantified in terms of their effect on socio-economic metrics. The ability to quantify these effects to examine different retrofits (or policies) at the community level can help support community resilience planning.

CHAPTER 3 MULTI-DISCIPLINARY RESILIENCE GOALS DEAGGREGATION

3.1 Introduction

The retrofit of woodframe residential buildings is a relatively effective strategy to mitigate damage caused by windstorms. However, little is known about the effect of modifying building performance for intense events such as a tornado, and the subsequent social and economic impacts that result at the community level following an event. This chapter presents a methodology that enables a community to select residential building performance levels representative of either retrofitting or adopting a new design code that computes target community metrics for the effects on the economy and population. Although not a full risk analysis, a series of generic tornado scenarios for different Enhanced Fujita (EF) ratings are simulated. Building functionality, employment, domestic supply, household income, and housing unit and population dislocation are used as physical and socio-economic resilience metrics in the context of a disaster. This is the first study in the literature where structural performance goals selected for buildings (or any physical system) are based on the ability to achieve both social and economic goals at the community scale. This is accomplished by chaining the performance of the built environment to a CGE model for economic metrics (i.e., household income, employment, domestic supply) and an existing population dislocation algorithm for sociological metrics (i.e., household/population dislocation) as a function of building damage and detailed socio-demographic U.S. census-based data, and ultimately determining the de-aggregated performance targets for individual buildings to meet a specified goal. The proposed methodology provides a structured but flexible approach to support resilience decision-making by helping stakeholders develop integrative implementation strategies to improve their resilience. Note that the proposed multi-disciplinary methodology builds on and integrates previous work (see Chapter 2). The method is demonstrated for Joplin, MO. All analyses and data have been developed and made available on the open-source IN-CORE modeling environment. This chapter presents the methodology and concept first published in Wang et al. (2022c).

3.2 De-aggregation of Community Resilience Goals

Figure 3-1 summarizes the methodology used in this chapter to develop individual residential building performance targets to achieve community-level resilience goals in terms of physical, social, and economic metrics. The approach starts by articulating community resilience goals such as *less than an x% increase in unemployment immediately after an EF-3 tornado occurring anywhere in the community*. The preliminary design for individual residential buildings shown in Figure 3-1 refers to structural combinations such as roof covering and is controlled by fragility functions. Please refer to the section on Wind Design to Achieve Community Resilience for more details about the design. Figure 3-2 depicts the sequencing of analyses for a given community and its physical, social, and economic attributes), damage and functionality models, CGE model, and the population dislocation algorithm, which is introduced in later subsections of this chapter, to evaluate the hazard impacts and support community resilience planning. The percentage of residential buildings that were assigned the specified retrofit were analyzed using values ranging from 0% to 100%, in intervals of 10%, for the community. The objective is to determine the percentage of buildings that should be retrofitted such that the community-wide building performance metrics and socio-economic metrics calculated in the resilience analysis meet the community resilience goals. Note that community resilience goals would typically be community defined and could be adjusted based on community-specific needs, but illustrative values are utilized in this chapter.

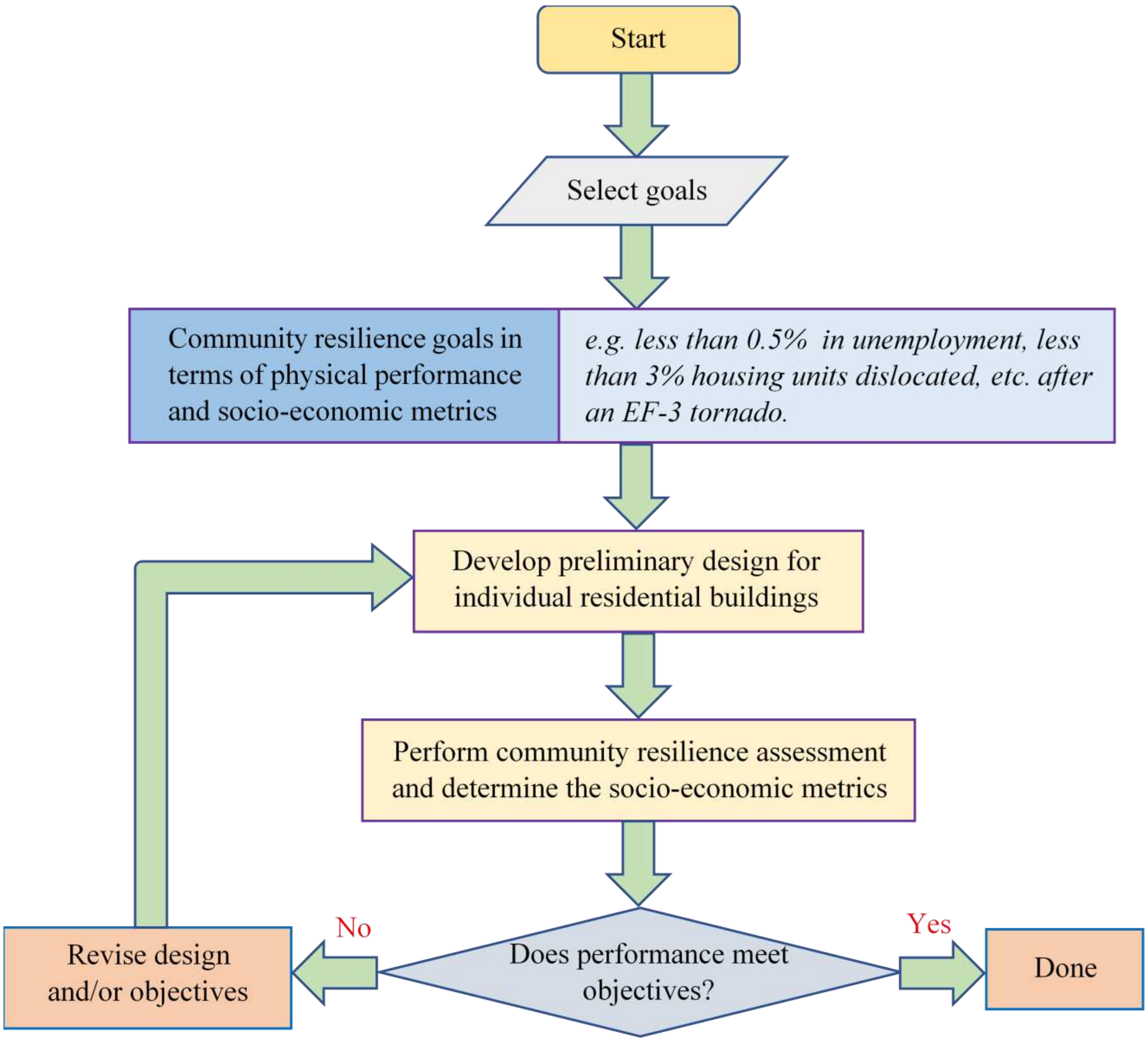

Figure 3-1. The methodology of the de-aggregation of community-level resilience goals

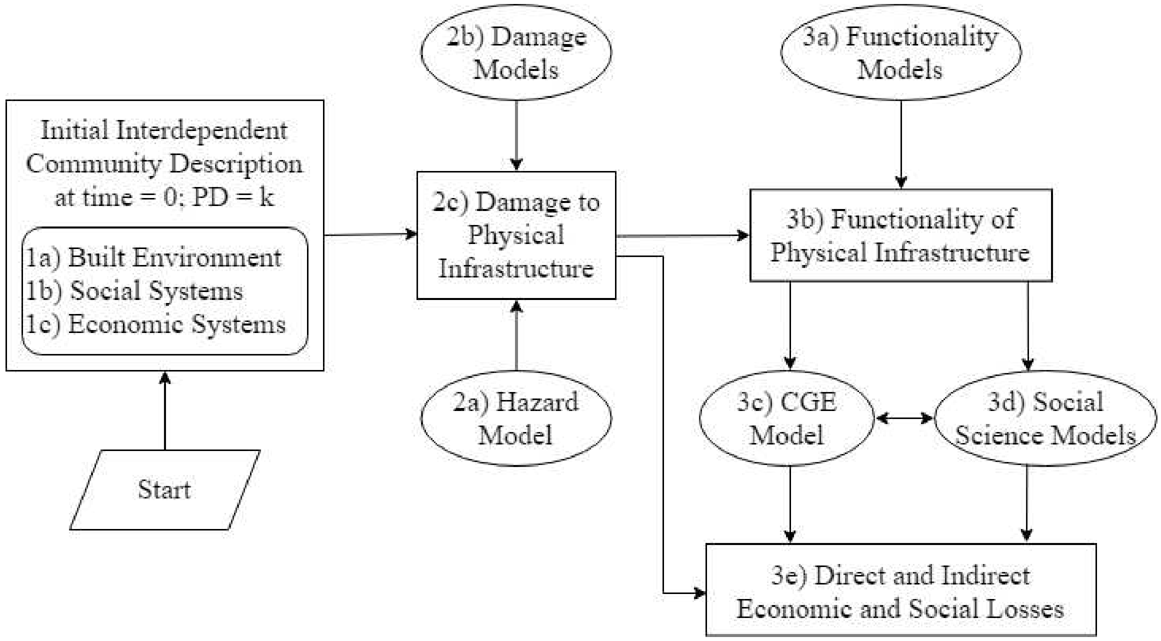

Figure 3-2. The sequence of analyses for community resilience assessment and metrics excepted from Figure 1-1

3.2.1 Damage and Functionality Model

Equation (3.1) determines the building damage probability (P_{damage}) using fragility functions for each building, which can be grouped by each building archetype, and have been fit to lognormal cumulative distribution functions (CDF) controlled by two parameters (median, λ, and standard deviation, ξ). The fragility functions (Fr_{DS}) represent the probability of exceeding damage state i (i.e., slight, moderate, extensive, complete) for each building as a function of the intensity measure (e.g., 3-s gust wind speed, spectral acceleration). For each MCS realization of a tornado event, a uniformly distributed random variable, R_j, between 0 and 1, is generated and compared to the building damage probabilities corresponding to the four damage states. As shown in Equation (3.2), if the realization experiences a *moderate* damage state or greater, the building is assumed to lose functionality in this chapter, consistent throughout the dissertation. The moderate damage state in tornado damage assessment means the building has moderate damage to window/doors and roof covering, but the building itself can be occupied and repaired (Memari et al. 2018). For business, it would not be possible to have an operational business in the moderate damage state, thus the building would be deemed nonfunctional in the CGE analysis. The building functionality status ($I^k_{fun,j}$) of Equation (3.2) is either functional (1) or non-functional (0) for each realization. The index *j* is representative of each realization of the MCS (*j* = *1* to *N*) for each building *k*. Subsequently, the building functionality probability (P_{fun}) can be approximated using Equation (3.3).

$$P^k_{Damage,i} = Fr^k_{DSi}(IM = x) \tag{3.1}$$

$$I^k_{fun,j} = \begin{cases} 1 & R_j > Fr_{DS2} \\ 0 & R_j \leq Fr_{DS2} \end{cases} \tag{3.2}$$

$$P^k_{fun} \approx \frac{N^k_{fun}}{N} = \frac{\sum_{j=1}^{N}(I^k_{fun,j}=1)}{N} \tag{3.3}$$

After the MCS building damage analysis, the results are passed to the CGE economic analysis, where the building is considered nonfunctional if the probability of being in or exceeding DS2 (moderate damage) is greater than 0.5. The CGE is only run once after the structural analysis and this full sequence shown in Figure 3-1 is completed for each tornado scenario to develop a suite of scenarios.

3.2.2 CGE Model

The design or retrofit of infrastructure systems can be quantitively related to community-level economic resilience metrics through a dynamic economic impact model. In this chapter, the CGE model served as the economic impact model to quantitatively evaluate the varying impacts of natural disasters on the local economy. The implementation of the CGE model in this chapter is consistent with Chapter 2.

3.2.2.1 Linking the Building Functionality Model and the CGE Model

Capital stock within a community is the key variable of interest linking the functionality model to the CGE model. The market values of commercial and residential buildings were aggregated into a Goods, Trade, and Other commercial sectors, and three housing services sectors (HS1, HS2, HS3). The Goods, Trade, and Other are themselves aggregations of the NAICS (North American Industry Classification System) sectors. Goods represent large manufacturing industries, Trade is mostly retail, and Other is a combination of industries including services, health and finance. This chapter focuses on residential buildings, where HS1 is lower-value homes, HS2 is higher-value homes, and HS3 is rented residential buildings.

Tornado damage to buildings, and their reduced functionality, is modeled as negative "shocks" in the CGE model. These shocks are the connection point between engineering outputs and the CGE model. Equation (3.4) calculates the sector shocks (γ_s) as a percentage of capital stock remaining, where *C* represents the capital stock of each building *k* attributed to each sector *s*.

$$\gamma_s = \frac{\sum_{k=1}^{n} C_s^k \times P_{fun,s}^k}{\sum_{k=1}^{n} C_s^k} \tag{3.4}$$

Incorporating the output from the engineering models into external shocks enables the CGE model to estimate a range of post-hazard economic losses such as employment effects and domestic supply by sectors (Cutler et al. 2016). Furthermore, retrofit strategies that mitigate damage to residential properties will attenuate the shock to capital stock in the housing services sector and thus tend to reduce overall economic loss.

3.3.3 Population Dislocation Algorithm

The population dislocation algorithm in this chapter is consistent with Chapter 2 but introduces more about the theoretical explanation. Equation (3.5) uses a logistic regression model with five constants, c_1 to c_5, to estimate population dislocation probabilities (P_{dis}) for each damage state i based on property value loss (*ploss*) and building types (single-family or multi-family, *dsf*) for each building, k, and neighborhood characteristics (percent of black, *pblack,* and Hispanic populations, *phisp*) by each census group, m. The variable *dsf* is set to 1 if the number of estimated housing units was 1. The variable is 0 if the number of estimated housing units is greater than 1. The logistic regression constants were not changed for this specific community, but the variables such as the percent of the black and Hispanic population were updated based on the Census Bureau's data. Equation (3.6) sums the dislocation probabilities for each damage state ($P_{dis,i,m}^{k}$). Damage state 1 (slight or no damage) is evaluated separately from damage states 2 to 4, consistent with the building functionality evaluations, to determine the dislocation probability of each building k in each census group m ($P_{dis,\mathrm{m}}^{k}$). For each MCS realization, the population dislocation algorithm can help predict whether the households leave their housing unit immediately after a hazard event..

$$P_{dis,i,m}^{k} = \frac{1}{1+e^{-(c_1+c_2 ploss_{i,m}^{k}+c_3 dsf_{m}^{k}+c_4 pblack_m+c_5 phisp_m)}} \tag{3.5}$$

$$P_{dis,m}^{k} = P_{dis,1,m}^{k} \times P_{damage,1}^{k} + \sum_{i=2}^{4} P_{dis,i,m}^{k} \times (\, P_{damage,i}^{k} - P_{damage,i-1}^{k}) \tag{3.6}$$

3.3 Illustrative Example

In this chapter simulated tornado wind fields defined as a peak three-second gust were used. Joplin was selected as the testbed to perform resilience assessments for tornado-induced events due to its history with a large double vortex EF5 tornado in May of 2011. The purpose of the illustrative example was to determine the minimum percentage of woodframe residential buildings that need to be retrofitted for the community to meet their resilience goals. These community-level resilience goals were defined in terms of building functionality, social, and economic metrics, using the proposed methodology. All analyses and data were performed and are available in the open-source IN-CORE modeling environment. Please refer to Wang et al. (2021a) for more details regarding the manual, datasets, and example notebooks for the IN-CORE modeling environment and visit http://resilience.colostate.edu/in_core/. Note that this example focuses on the resilience assessment at the community level specific to tornado events since tornadoes only strike a small footprint area within a community. The resilience model and the retrofit can be applied to a large urban area for other natural hazards such as earthquake events (e.g., Roohi et al. 2020).

3.3.1 Community Description

Joplin is a typical small to medium size community, located in southwest Missouri in the United States and spanning Jasper and Newton counties. In this illustrative example, a total of 19 archetype buildings (e.g., residential, business, healthcare, education) were used to represent the buildings within the community, consistent throughout the dissertation. The electric power network is generally regarded as the most impacted infrastructure system by tornado (and most wind) events and was therefore also included herein to examine the dependency between the building infrastructure and electric power network. Transmission/distribution substations and wood poles are the two types of vulnerable components included in the electric power network. Other networks such as water, transportation, and telecommunication networks were not considered in this chapter, but could be modeled in future work as needed. It is acknowledged that the functionality of other network systems depends on the reliability of the electric power network (e.g., Unnikrishnan and van de Lindt 2016, Zou and Chen 2019). For example, water towers are vulnerable in that they need to be supplied with electric power (Masoomi and van de Lindt 2018), so may only last several days following a tornado if backup generators for pumps are not available/supplied. Additionally, damaged and/or fallen trees/poles can block the roads following tornadoes and cause adverse impacts on the transportation networks (e.g., Hou and Chen 2020, Hou et al. 2019).

Table 3-1 provides a summary of the built environment and social systems for the testbed and example in this chapter. The number of buildings and the number of housing units in Joplin is 28,152 and 23,261 (Note: multi-family will have multiple households in one building), respectively, and the building dataset was developed circa 2010 before the 2011 Joplin tornado. Note that non-residential buildings include 13 building types herein such as commercial buildings and social institutions, e.g., schools. The housing unit estimation was determined based on the 2010 Decennial Census data and an existing housing unit allocation algorithm (see Rosenheim et al. 2019 for details). The allocated housing units are also designated by race/ethnicity and household income, in addition to tenure status, as shown in Table 3-1. The number of workers employed in Joplin in 2010 was 39,831, and the total domestic supply was US$3.04 billion. Please refer to Chapter 2 for more details on the building inventory, electric power network, housing unit characteristics, and economy in Joplin.

Table 3-1. Built environment and human social system for Joplin testbed

Building environment				*Human social system*			
Buildings		Electric power network		Housing units		Population	
Residential	24,903	Substations	18	Owner-occupied	11,344	Owner-occupied	26,873
Non-residential	3,249	Poles	23,857	Renter-occupied	9,435	Renter-occupied	20,949
Total	28,152			Vacant	2,455	In total	49,810
				Group quarters	22		
				In total	23,261		

Initial capital stock values come from the Newton and Jasper County Assessor's offices that encompass Joplin. It is important to note that the building level county assessor's data and the building level archetype data used in the functionality model are from different sources. Fortunately, both datasets had detailed geographic coordinate location information for every building. Therefore, in order to connect individual building level archetypes and functionality to economic sectors, the building level sector information from the county assessor's office was merged with the archetype datasets using a GIS spatial join algorithm. Building level data are then aggregated to the sector level.

3.3.2 Generic Tornado Models

A series of generic tornadoes based on the gradient technique (Standohar-Alfano and van de Lindt 2015) were used as the hazard models impacting the community, resulting in physical damage to buildings and the electric power network, and propagating economic losses, household disruption, and population dislocation. Tornados with different EF ratings (EF0 - EF5) are associated with different ranges of wind speeds. Figure 3-3 shows the geometry of the gradient model for an EF2, EF3, and EF4 single tornado, respectively, where the width of the applied tornadoes is equal to the average of the historical tornado data for the EF rating (Attary et al. 2018). The start points, end points, and the directions of all tornado scenarios were assigned randomly within the community boundaries. The NIST Community Resilience Planning Guide (NCRPG) encourages communities to use routine levels (i.e., hazard events that are more frequent with less consequential events that should not cause significant damage), design levels (i.e., hazard events used to design structures), and extreme levels (i.e., beyond design levels and likely to cause extensive damage) to address a range of potential damage and consequences (NIST 2020, Wang et al. 2022c). This chapter examines the community resilience impacted by 100 random tornadoes for each different intensity level (i.e., EF2, EF3, EF4) individually in line with the concept encouraged in the NCRPG. It is worth noting that most tornadoes travel in paths from the southwest towards the northeast

(Suckling and Ashley 2006). Additionally, it is important to mention that the building inventory was developed for Joplin exclusive of other nearby homes outside of the Joplin boundaries. Thus, some of the tornado scenarios might damage buildings outside of Joplin in the simulation but they are not included in the determination of physical damage and the associated socio-economic losses in this chapter.

The methodology presented herein is felt to be general and can be implemented for any hazard type. The socio-economic goals defined for the community, partially or wholly, do rely on a hazard-specific analysis. For example, earthquake events commonly impact the entire community, whereas a tornado directly impacts a relatively small geographic footprint within a community, but the impact can extend to the entire community in terms of social and economic impacts. Additionally, building functionality is highly related to tornado intensity, tornado path/width, and housing density (urban or rural).

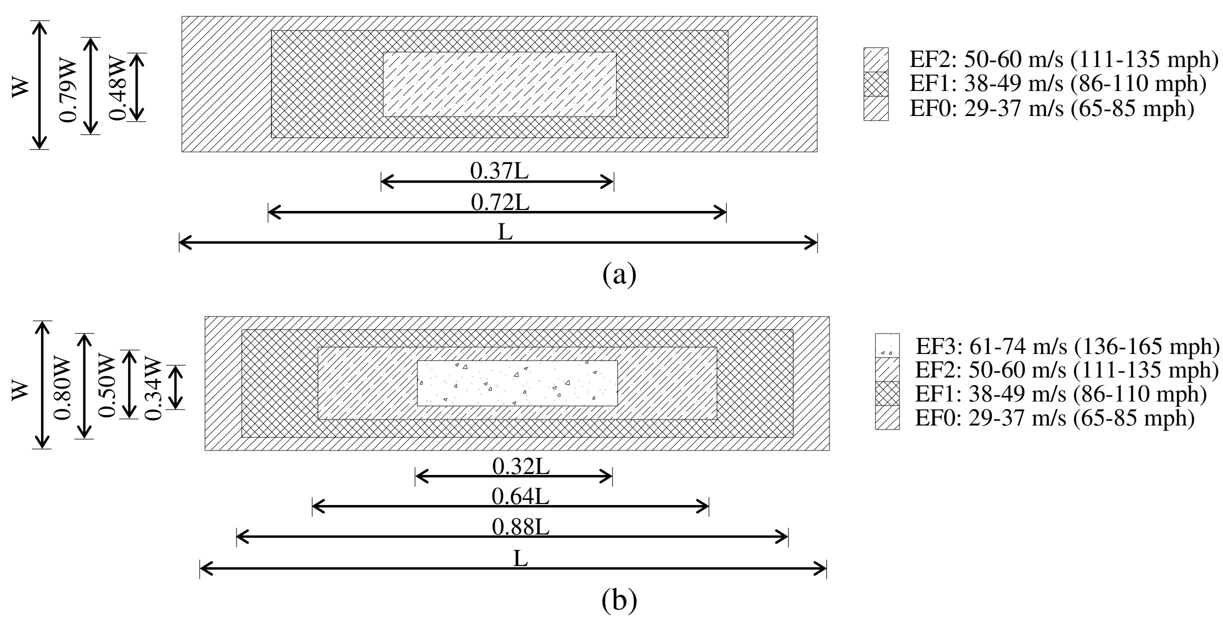

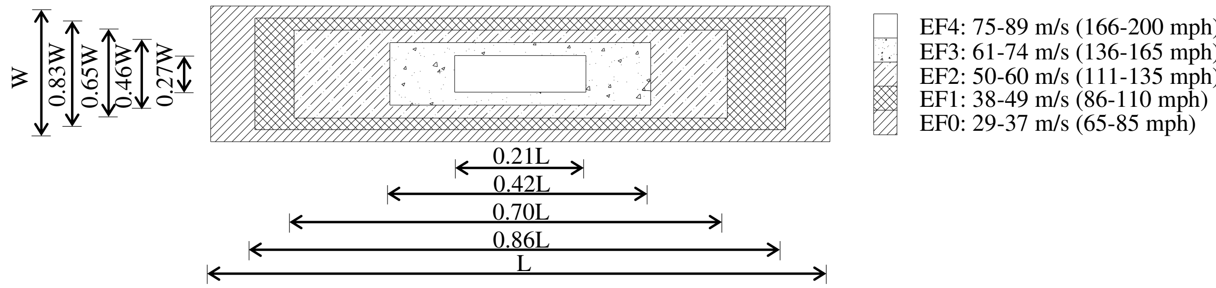

(c)

Figure 3-3. The geometry of generic tornado models for different EF ratings: (a) EF2; (b) EF3; (c) EF4

3.3.3 Multi-Disciplinary Community Resilience Goals

In this chapter, core resilience metrics inform three community stability areas, namely physical services stability, economic stability, and population stability. Physical services stability was estimated by determining building functionality two different ways: with and without the impact of the reliability of the electric power network. Percent changes in employment, domestic supply (e.g., food, care, security), and household income were used to jointly reflect the activity of the local economy. Population stability was calculated as the percent change in households being dislocated by housing unit (or population) following a disruptive event. Three community resilience goals (Goal A, Goal B, and Goal C) were targeted as routine level (EF2), design level (EF3), and extreme level (EF4) tornado events, respectively, as indicated in Table 3-2. The community resilience goals may be viewed as being modest, but reasonable because tornadoes typically strike a portion of the entire community, sometimes 5% to 10%. All residential and commercial buildings outside the tornado path were not physically damaged but may still lose electric power. Therefore, two types of physical service metrics related to building functionality were proposed herein: considering the dependency between buildings and the electric power network or neglecting the dependency of buildings on electric power.

It is important to mention that each community is unique with its own characteristics, and each will have its own specific resilience goals and potential solutions. In this chapter, having clearly defined resilience goals in terms of core metrics is intended to demonstrate how a community can change a physical design of a component within their infrastructure (buildings in this case) to affect change in their physical service, population, and economic stability areas if a natural hazard was to strike. For example, keeping the percentage of households dislocated below 5% is one of the social resilience goals identified for tornados at the extreme hazard level.

Table 3-2. Community resilience goals based on core metrics

Community goals	Tornado intensity (NCRPG hazard level)	Physical service metrics		Population stability metrics		Economic stability metrics		
		% buildings remaining functional (due to damage)	% buildings remaining functional (due to damage + electrical power)	% households dislocated (unit: households)	% population dislocated (unit: people)	% change in employment	% change in domestic supply	% change in mean household income
Goal A	EF2 (Routine)	98%	95%	1%	1%	0.2	0.5	0.2
Goal B	EF3 (Design)	96%	89%	3%	3%	0.5	1.0	0.5
Goal C	EF4 (Extreme)	94%	83%	5%	5%	0.8	1.5	0.8

3.3.4 Building Design to Achieve Community Resilience

Tornadoes are low-probability high-consequence events that often result in significant physical damage and socio-economic impacts but have not been considered in the structural design codes and standards (e.g., ASCE 7-16) so far. That will change soon since tornadoes are planned to be included for Risk Category 3 and 4 buildings (e.g., hospitals, emergency operations centers, etc.) beginning in 2022. Some challenges such as pressure deficit, vertical components of the tornadic winds, and windborne debris in tornadoes made it difficult to rationalize a design process for most buildings (e.g., Haan et al. 2010, van de Lindt et al. 2013, Masoomi and van de Lindt 2017). In this chapter, basic construction improvements were modeled using modified fragilities for individual building performance. Table 3-3 presents building fragility functions for typical and retrofitted residential buildings with a different structural combination of roof coverings, roof sheathing nailing patterns, and roof-to-wall connection types (Wang et al. 2021b). The typical design would have regular asphalt shingles, 8d common nails spaced at 150/300 mm (6/12 inch) attaching roof sheathing panels to trusses, and two 16d toenails to connect the roof rafters over the vertical studs. The retrofit design used regular asphalt shingles, roof sheathing nails spaced at 150/150 mm (6/6 inch) and two H2.5 hurricane clips as roof-to-wall connections. A series of cases was examined, ranging from 10% of residential buildings in a community being retrofitted to 100%, to select how many residential buildings would need to be retrofitted to achieve the desired community resilience goals. Several of these scenarios are illustrated in Figure 3-4. The damage fragility curves for a suite of 19 building archetypes incorporating 13 non-residential building types, each having four damage states (i.e., slight, moderate, extensive, and complete), are available to cover the entire range of wind speeds.

Table 3-3. Lognormal parameters for residential woodframe building fragilities

Building type	Building description	Damage states	Original fragility functions (m/s)		Retrofit design in terms of fragilities (m/s)	
			λ	ξ	λ	ξ
T1	Residential wood building, small rectangular plan, gable roof, 1 story	DS1	3.68	0.13	3.68	0.14
		DS2	3.56	0.14	3.85	0.12
		DS3	3.63	0.13	3.98	0.11
		DS4	3.68	0.14	4.16	0.13
T2	Residential wood building, small square plan, gable roof, 2 stories	DS1	3.60	0.13	3.60	0.13
		DS2	3.53	0.13	3.76	0.12
		DS3	3.59	0.13	3.91	0.11
		DS4	3.68	0.13	4.17	0.12
T3	Residential wood building, medium rectangular plan, gable roof, 1 story	DS1	3.61	0.13	3.61	0.13
		DS2	3.51	0.13	3.77	0.12
		DS3	3.57	0.13	3.92	0.11
		DS4	3.74	0.12	4.23	0.12
T4	Residential wood building, medium rectangular plan, hip roof, 2 stories	DS1	3.73	0.13	3.73	0.13
		DS2	3.65	0.13	3.87	0.12
		DS3	3.71	0.13	4.00	0.11
		DS4	3.76	0.13	4.28	0.12
T5	Residential wood building, large rectangular plan, gable roof, 2 stories	DS1	3.75	0.13	3.75	0.13
		DS2	3.65	0.13	3.88	0.12
		DS3	3.70	0.13	3.98	0.11
		DS4	3.64	0.15	4.06	0.14

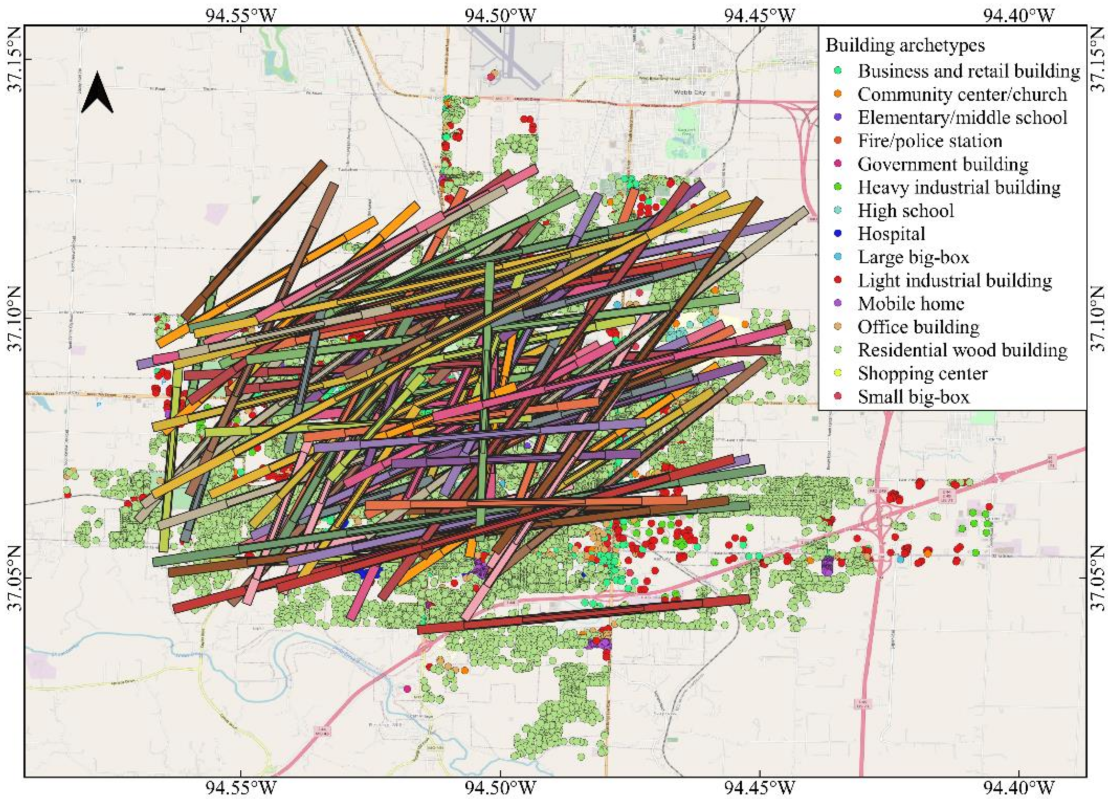

Figure 3-4. Generic tornado models of 100 EF2 scenarios overlapped with the built environment

3.3.5 Community Resilience Metrics

After combining the fragility functions for retrofitted residential buildings and the original fragility functions for other buildings in the community model, the community assessment was performed by chaining the algorithms as described earlier. Resilience metrics in terms of physical services, economic activity, and population stability were examined to explore the effect of wind mitigation retrofits on community resilience enhancement, i.e., to link resilience goals at the community level with the selection of a mitigation policy for building retrofit. Table 3-4 and Table 3-5 indicate some key findings for these core community resilience metrics in terms of the physical, economic, and social stability areas. The full suite of results for buildings retrofitted at each of the different percentages for the building stock under different scenarios are not shown herein for brevity. As an example, when the community was impacted by the idealized EF4 tornados, the number of non-functional buildings and the number of housing units dislocated can be reduced by 11.7% (1,187 to 1,048) and 11.0% (847 to 754), respectively, when 40% of residential buildings are retrofitted. The percentages shown in Table 3-4 are defined as the change in the metrics being measured (e.g., household dislocation) out of the total value that can be measured for that metric (e.g., households) for the community. Figure 3-5 illustrates the histograms of typical metrics in terms of physical services stability and population stability from one hundred (100) EF2 tornado scenarios as an example. The reason for a few extreme values at the left end in the histograms is that the socio-economic losses caused by the tornado event are also highly related to the attributes of the area hit by the tornado, such as population density. In more rural areas, both population and building density is lower, and tornadoes striking these areas impact the local economy and cause household dislocation at a smaller scale compared to dense urban areas.

Workers employed at damaged or non-functional commercial buildings may face work interruption or job loss, leading to reduced household income and consumption expenditures. As part of the CGE simulation of this event, these values are calculated and represented in Table 3-5. Table 3-5 conveys that retrofitting played a significant role in mitigating economic impacts to domestic supply, especially employment and household income. From the lowest to highest retrofit application (from 0% to 100%) for EF2 and EF3, a more than 36% reduction (from $3.9 million to $2.5 million) in household income loss, and a 53.8% reduction (from 78 to 36) in employment loss, is observed.

Table 3-4. Community resilience metrics for physical and social systems that benefit from residential building retrofits (Mean values)

Residential building retrofits	Physical service metrics		Population stability metrics	
	The number of buildings non-functional (due to damage)	The number of buildings non-functional (due to damage + electrical power)	Housing unit dislocation (unit: housing units)	Population dislocation (unit: people)
EF2				
0%	315 (1.1%)	981 (3.5%)	231 (1.0%)	478 (1.0%)
40%	251 (0.9%)	971 (3.5%)	197 (0.9%)	409 (0.8%)
70%	200 (0.7%)	963 (3.4%)	169 (0.7%)	350 (0.7%)
100%	150 (0.5%)	955 (3.4%)	142 (0.6%)	295 (0.6%)
EF3				
0%	703 (2.5%)	1,387 (4.9%)	501 (2.2%)	1,021 (2.1%)
40%	601 (2.1%)	1,377 (4.9%)	436 (1.9%)	894 (1.8%)
70%	523 (1.9%)	1,368 (4.9%)	388 (1.7%)	796 (1.6%)
100%	443 (1.6%)	1,360 (4.8%)	339 (1.5%)	692 (1.4%)
EF4				
0%	1,187 (4.2%)	2,583 (9.2%)	847 (3.6%)	1,711 (3.4%)
40%	1,048 (3.7%)	2,570 (9.1%)	754 (3.2%)	1,532 (3.1%)
70%	939 (3.3%)	2,558 (9.1%)	685 (2.9%)	1,392 (2.8%)
100%	828 (2.9%)	2,547 (9.1%)	613 (2.7%)	1,231 (2.5%)

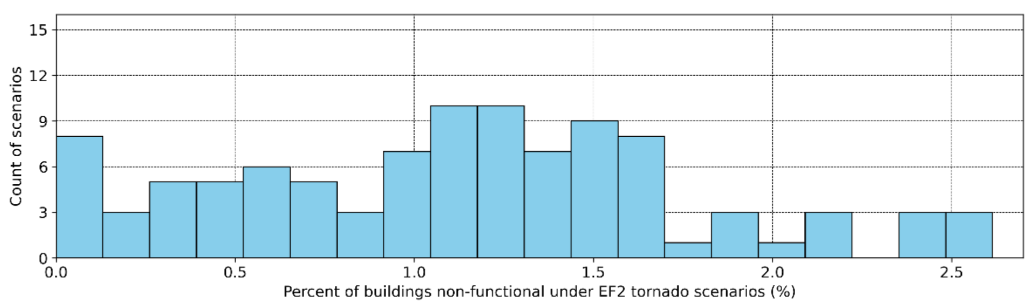

(a)

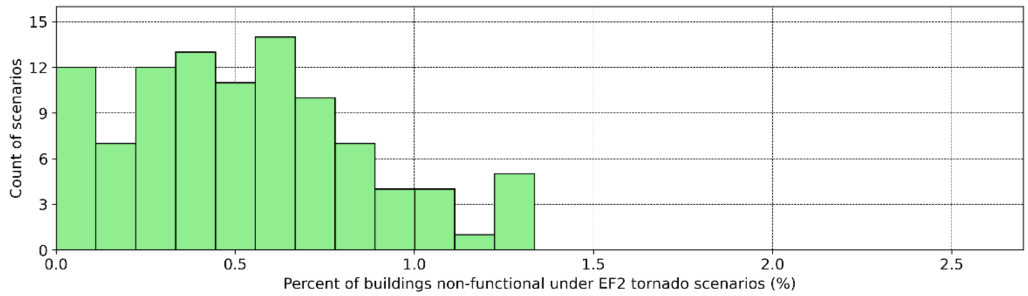

(b)

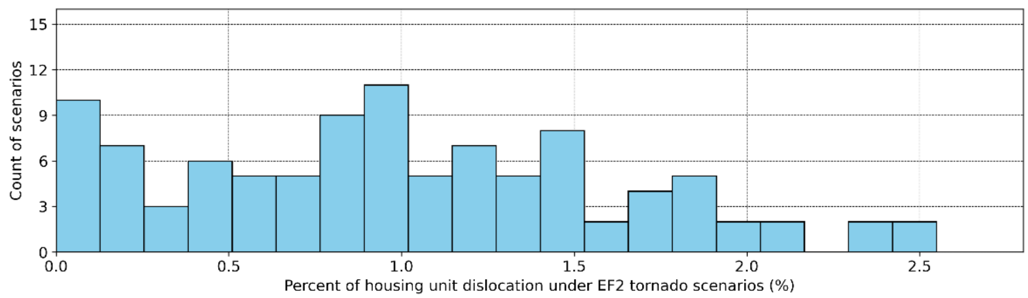

(c)

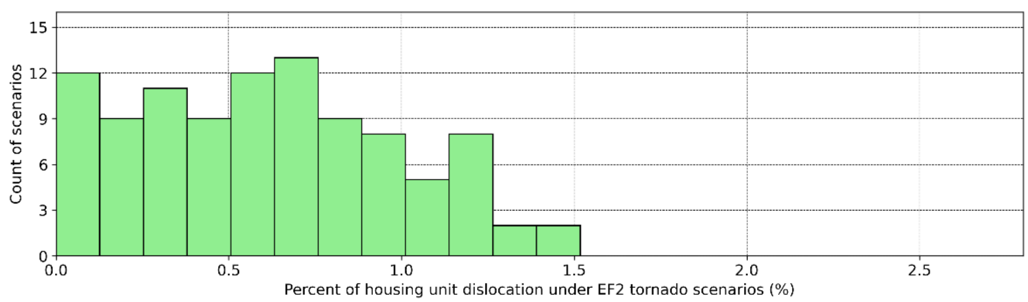

(d)

Figure 3-5. Statistics of resilience metrics in terms of physical service and population stability: (a) building functionality without retrofit; (b) building functionality with 100% residential retrofit; (c) housing unit dislocation without retrofit; (d) housing unit dislocation with 100% residential retrofit

Table 3-5. Economic stability metrics given different levels of residential building retrofits and tornado scenarios (Mean values)

Residential building retrofits	Economic stability metrics		
	Employment loss (unit: person)	Domestic supply loss (unit: millions of $)	Household income loss (unit: millions of $)
EF2			
0%	78 (0.2%)	10.4 (0.3%)	2.0 (0.2%)
40%	62 (0.2%)	8.4 (0.3%)	1.6 (0.1%)
70%	49 (0.1%)	6.9 (0.2%)	1.3 (0.1%)
100%	36 (0.1%)	5.3 (0.2%)	0.9 (0.1%)
EF3			
0%	160 (0.4%)	22.0 (0.7%)	3.9 (0.3%)
40%	136 (0.4%)	19.2 (0.6%)	3.3 (0.3%)
70%	118 (0.3%)	17.0 (0.6%)	2.9 (0.3%)
100%	99 (0.3%)	14.7 (0.5%)	2.5 (0.2%)
EF4			
0%	270 (0.7%)	36.8 (1.2%)	6.7 (0.6%)
40%	236 (0.6%)	32.7 (1.1%)	5.9 (0.5%)
70%	211 (0.5%)	29.6 (1.0%)	5.3 (0.5%)
100%	182 (0.5%)	26.2 (0.9%)	4.6 (0.4%)

The minimum percentage of residential buildings retrofitted to achieve the community-level resilience goals can be determined for each tornado scenario (e.g., average of EF rating tornado striking anywhere in the community), as illustrated in Table 3-6 and Table 3-7. Note that the column fields shown in Table 3-6 and Table 3-7 are consistent with those representing each metric in Table 3-3. In order to meet all the multi-disciplinary community resilience goals for EF2 tornadoes (see Goal A in Table 3-3), the metrics for household dislocation controlled the retrofit level and at least 34.2% of residential buildings would need to be retrofitted. However, the employment metrics control the retrofit level for the EF3 and EF4 tornado scenarios. The fundamental contribution of this analysis methodology is the ability to essentially de-aggregate the community-level resilience goals in terms of physical, social, and economic metrics into building retrofit requirements. The goals themselves are flexible and can be adjusted by the analyst on a case-by-case basis. Additionally, it would also be possible to quantify the impact of a change in building code for new construction following a tornado or with some modification to the methodology and examine the effect of implementing new building code requirements over time as a community grows.

Table 3-6. Percentage of residential buildings requiring retrofit to achieve community resilience goals

Community goals	Physical service metrics		Population stability metrics	
	% buildings remaining functional (due to damage)	% buildings remaining functional (due to damage + electrical power)	% households dislocated (unit: households)	% population dislocated (unit: people)
Goal A	3.4%	12.0%	34.2%	33.3%
Goal B	8.0%	6.0%	17.5%	14.0%
Goal C	15.1%	16.0%	19.8%	15.4%

Table 3-7. Percentage of residential buildings requiring retrofit to achieve community resilience goals

Community goals	Economic stability metrics		
	% change in employment	% change in domestic supply	% change in mean household income
Goal A	28.7%	13.1%	19.4%
Goal B	21.5%	18.7%	11.6%
Goal C	29.0%	29.0%	18.0%

3.4 Summary and Conclusions

Community resilience assessments help the community determine what is needed to improve their performance, and long-term benefits relative to the 'do nothing' case. This chapter presents a methodology to determine building retrofit targets to achieve community-level physical, social, and economic resilience goals, in support of community resilience decision-making. A series of tornado scenarios at different intensity levels were simulated and applied to an illustrative community testbed. A set of core resilience metrics includes the percent of buildings that are analytically predicted to remain functional, the percent of households/population dislocated, and the percent change in the local economy (i.e., employment, domestic supply, household income). The mitigation focuses on residential buildings, and the objective is to determine the minimum percentage of residential buildings across a community that need to be retrofitted in order to achieve the multi-disciplinary community resilience goals. Based on the work presented herein, and recognizing that uncertainty in the results is not addressed, the following preliminary conclusions can be drawn:

- The percent of loss of functionality to buildings and the percent of household dislocation, as the key resilience metric in the chapter, may be reduced by approximately 11% when 40% of residential buildings are randomly retrofitted throughout the community for the assigned EF4 tornado scenario. For the EF2 and EF3 tornado scenarios, 40% of residential building retrofit may help mitigate the housing unit dislocation by approximately 14%.
- Building retrofits can play a significant role in reducing capital stock damage and further mitigating economic loss to domestic supply, employment, and household income. From the lowest (0%) to highest (100%) retrofit application for residential buildings for the EF2 and EF3 tornado scenarios, there would be more than a 35% reduction in unemployment, and more than a 50% reduction in household income loss.
- To meet all the multi-disciplinary resilience goals for tornadoes in the routine level intensity (EF2) defined in this chapter, the household dislocation metric controlled the retrofit level and at least 34.2% of residential buildings would need to be retrofitted. For the tornadoes at the design level hazard intensity (EF3) and extreme level hazard intensity (EF4), the employment metric controlled the retrofit level. The resilience goals are flexible and can be quantitively adjusted for different levels based on community input and the unique needs of a community. Clearly different multi-disciplinary metrics may control the

retrofit requirements for different hazard intensities but are also specific to the resilience goals selected. This further underscores the need to consider goals across different community stability areas.

The chapter did not address budget constraints of the community and costs to retrofit, which would further limit selections of different retrofit strategies for different households. Note that communities have access to many funding sources outside of their own tax dollars for mitigation programs. The Federal Emergency Management Agency (FEMA) Building Resilient Infrastructure and Communities (BRIC) and Department of Housing and Urban Development (HUD) Community Development Block Grant–Disaster Recovery (CDBG-DR) programs are two examples. The residential buildings were assumed to be retrofitted randomly without the consideration of the community retrofit priorities for residential buildings or individual capacity (e.g., high-income owners versus low-income renters). Addressing the limitations above is beyond the scope of this chapter but future studies may include a risk-based cost-benefit analysis for the wind mitigation retrofits and the impact of insurance incentives and other policies, such as insurance companies offering a discount in annual insurance premiums for homeowners to encourage them to retrofit their houses.

In summary, the ability to de-aggregate community resilience goals to individual building performance targets can help accelerate the development of resilience-based building codes and standards that satisfy community-wide resilience goals of the broader built environment. The ability to achieve community-level resilience goals in terms of socio-economic metrics can provide community decision-making support for stakeholders and planners.

CHAPTER 4 IMPROVED SCHOOL DESIGNS AND SOCIAL SERVICE STABILITY

4.1 Introduction

Tornadoes are low-probability, high-consequence events that significantly threaten life safety and cause adverse impacts to communities including the local economy (e.g., van de Lindt et al. 2013, Roueche and Prevatt 2013, Wang et al. 2021b, Wang et al. 2022c). Over the last several decades, an average of more than 1,000 tornadoes were reported annually in the United States and have averaged almost 100 tornado-related deaths and $1.5 billion in direct property damage losses per year (e.g., Masoomi and van de Lindt 2018, Wang and van de Lindt 2021, Haan et al. 2008, Jain et al. 2020). Despite causing significant direct losses, as well as social disruption, building codes and standards have not previously included tornado hazards in their scope until the release of American Society of Civil Engineers (ASCE) Standard 7-22 with some limited exceptions such as storm shelters and nuclear facilities (Wang et al. 2022c, ASCE 2017, ASCE 2021). Tornado-resilient design has been considered economically unfeasible for most buildings in the United States (e.g., Haan et al. 2008, Jain et al. 2020, Roueche et al. 2017). Further, some challenges such as atmospheric pressure drop (APD) and a vertical uplift component make tornado wind fields different from straight-line wind (e.g., van de Lindt et al. 2013, Haan et al. 2010, Masoomi and van de Lindt 2017), both of which are challenging to address numerically in design. In recent years, fundamental differences between tornado wind and straight-line wind led researchers to explore tornado physical characteristics and to simulate tornado effects on buildings more accurately. Van de Lindt et al. (2013) and later Masoomi and van de Lindt (2016) used tornado pressure adjustments following Haan et al. (2010) to adjust straight-line wind loads to account for tornado effects. Researchers performed extensive experimental studies and examined the relationship between the APD and tornado-induced internal pressure responses (e.g., Sabareesh et al. 2019, Wang et al. 2018). Incorporating comprehensive research on tornado characteristics introduced in the past literature, ASCE 7-22 now includes a separate chapter focusing on tornado loads and provides the determination of tornado loads on Risk Category III and IV buildings (e.g., schools, hospitals, emergency operations centers) and incorporation of those loads into the design process for these types of buildings. Furthermore, when considering the effect of tornado hazard events on the community resilience rather than single buildings to support decision making, stakeholders and policymakers can identify hazard levels that target the performance of infrastructure systems over the community domain..

Overall, school buildings/educational facilities incorporate classroom buildings, athletic facilities, and related facilities to provide educational services to students. Schools are typically designed as Risk Category III buildings (ASCE 2017), and the importance of education systems has been recognized to maintain social services stability in community resilience (e.g., Hassan and Mahmoud 2020). Many school buildings in the United States were built before the 1970s and constructed of loadbearing masonry walls and steel joists (FEMA 2009). Tornadoes have destroyed or severely damaged a significant number of schools, causing millions of dollars in damage per event over the past decades, but perhaps more importantly the disruption to small and medium cities and communities. For example, when a tornado struck in Oologah, Oklahoma, U.S., in April 1991, significant tornado damage occurred at the Oologah School Complex. The new athletic building was heavily damaged, including the entire roof and the north side was destroyed entirely. Total damage, including contents due to the Oologah tornado, eventually totaled U.S. \$10.6 million (Ballard 1993). In the 2011 Joplin tornado, two primary schools with over 2700 students were significantly damaged. The high school was built in 1968, and the damage to the high school was extensive, particularly in high bay areas like the gymnasium and the auditorium. Exterior walls collapsed in the courtyard facing single-story classrooms, and the exterior walls of the center section of the school were shredded with wind-borne debris. The performance of the other middle school from the tornadic winds has been similar (Coulbourne and Miller 2012). While the economic loss due to damage may be significant, it is overshadowed by the impact on education and the need to maintain social stability, a key stability area in community resilience (Ellingwood et al. 2019). There is no limitation for communities interested in improving the design of their critical facilities, including social institutions such as schools, to perform better in a tornado event.

This chapter develops new school building archetypes and presents an illustrative examination of the effect of improved designs to allow more children to maintain continuous education following tornado events. The novelty of this work is (1) the development of new fragility functions for school building archetypes that can be used in community resilience studies, and (2) the illustration of the direct dependency of a core resilience metric used in community resilience planning, i.e., number of children remaining in schools. The design of the school for different design wind speed levels were conducted for each primary structural/non-structural component (e.g., roof structures, load-bearing walls) to the entire building. The improved designs and resulting fragilities used statistics provided by the original collaborator of ASCE 7-22 for the new tornado chapter. These are intended to support community resilience decision-making with K12 educational continuity and inform design guidelines for new/existing school buildings in communities. This chapter presents the methodology and concept first published in Wang and van de Lindt (2022).

Figure 4-1 shows the methodology proposed in this chapter to examine the effect of improved residential designs and school designs on maintaining educational continuity and avoiding dislocation for K12 school children. The combination of fragility functions, hazard models, and building damage models is designed to determine the probability of exceeding each damage state (i.e., slight, moderate, extensive, complete) for residential and school buildings. Then, MCS was used to generate sufficient randomized samples (N = 100 in this chapter) and determine the building-level residential and school functionality status within the hazard-impacted areas due to building damage in each MCS realization. If the realization experiences a moderate damage state or greater, the building is assumed to lose functionality. In tornado damage assessment, the moderate damage state refers to the building having moderate damage to window/doors and roof covering, but the building itself can (potentially) be occupied and repaired (Memari et al. 2018). The household allocation algorithm developed by Rosenheim et al. (2019) was implemented to allocate household information (e.g., household size, household income) to the residential buildings (Rosenheim 2021) surrounding the schools in the city/community model. The published records of school attendance zones provided by the U.S. National Center for Education Statistics (NCES) and School Attendance Boundary Survey (SABS) help determine the spatial dependency between residential buildings and their dependent K12 schools. After synthesizing the algorithms and the associated data inputs, the proposed methodology aims to explore the total number of children in households located within tornado paths in the four different cases: case 1: having both functional housing and schools; case 2: having functional schools but without housing; case 3: having functional housing but without schools; case 4: having neither housing nor schools.

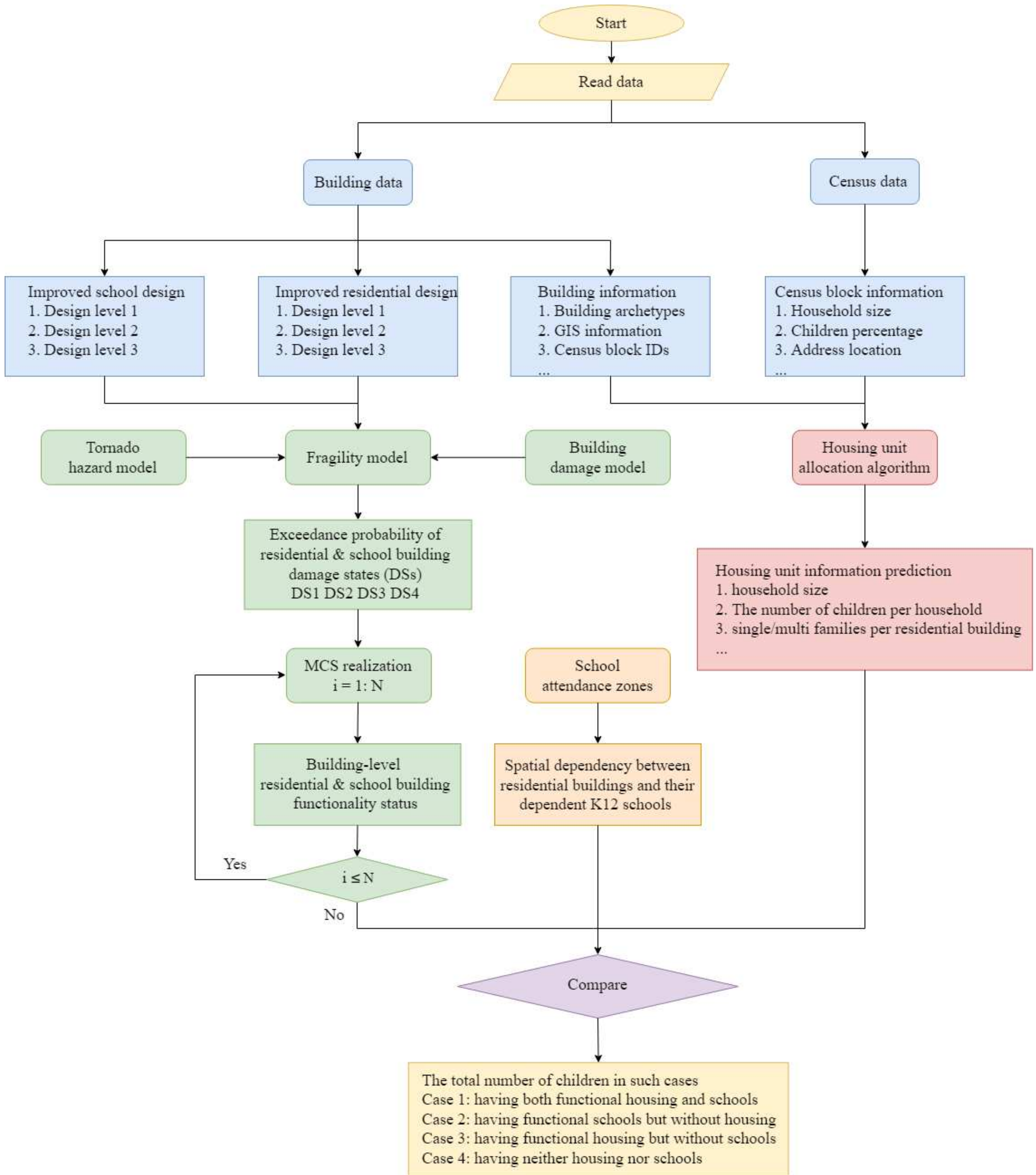

Figure 4-1. The methodology to examine the effect of improved building designs on maintaining educational continuity and avoiding dislocation for K12 school children

4.2 Improved School Building Archetype

In order to quantify the impact of improved school building designs on the measurement of social resilience metrics related to K12 school children in community resilience assessment, a suite of improved fragilities for a reinforced masonry school building archetype based on ASCE 7-22 tornado loading are described herein.

4.2.1 Fragility Methodology

ASCE 7-22 wind loads require that velocity pressure (q_z), as a function of basic wind speed (V) associated with velocity pressure exposure coefficient (K_z), topographic factor (K_{zt}), wind directionality factor (K_d), and ground elevation factor (K_e), can be determined by Equation (4.1). If following the directional procedure introduced in Chapter 27, Equation (4.2) shows the methodology to calculate design wind pressures involved with external pressure coefficient (GC_p) and internal pressure coefficient (GC_{pi}) for the main wind force resisting system (MWFRS) for buildings of all heights. Equation (4.3) illustrates design wind pressures for component and cladding (C&C) elements constructed in low-rise buildings with a height less than 18.3 m (60 ft). Please refer to Masoomi and van de Lindt (2016) for a more detailed explanations regarding wind load parameters.

$$\begin{cases} q_z = 0.00256 K_z K_{zt} K_d K_e V^2 \ \ (lb/ft^2); \ \ V \ in \ mph \\ q_z = 0.613 K_z K_{zt} K_d K_e V^2 \ \ (N/m^2); \qquad V \ in \ m/s \end{cases} \tag{4.1}$$

$$p = qGC_p - q_i(GC_{pi}) \ \ (lb/ft^2) \ \ (N/m^2) \tag{4.2}$$

$$p = q_h(GC_p - GC_{pi}) \ \ (lb/ft^2) \ \ (N/m^2) \tag{4.3}$$

Tornadoes are a type of windstorm, but they have significantly different characteristics than other windstorms. For example, tornadic winds have significant vertical components, and the atmospheric pressure changes rapidly to induce loads. Therefore, tornado loads are treated separately from straight-line wind loads in the latest loading standard in the U.S.; ASCE 7-22. Equation (4.4) to Equation (4.6) present the approach in ASCE 7-22 to determine tornado velocity pressures at height z above ground (q_{zT}), design tornado pressures for the MWFRS buildings within different exposure of all heights, and design tornado pressures on C&C elements in low-rise buildings individually.

$$\begin{cases} q_{zT} = 0.00256 K_{zTor} K_e V_T^2 \;\; (lb/ft^2); \;\; V_T \; in \; mph \\ q_{zT} = 0.613 K_{zTor} K_e V_T^2 \;\; (N/m^2); \qquad V_T \; in \; m/s \end{cases} \tag{4.4}$$

$$p_T = q G_T K_{dT} K_{vT} C_p - q_i (GC_{piT}) \tag{4.5}$$

$$p_T = q_{hT} [G_T K_{dT} K_{vT} C_p - \left(GC_{piT}\right)] \tag{4.6}$$

where K_{zTor} is the tornado velocity pressure exposure coefficient, q is external pressure evaluation, q_i is internal pressure evaluation, and q_{hT} is tornado velocity pressure evaluated at mean roof height h. G_T is the tornado gust-effect factor, K_{dT} is the tornado directionality factor, K_{vT} is the tornado pressure coefficient adjustment factor, C_p is the external pressure coefficient, and GC_{piT} is the tornado internal pressure coefficient.

Tornado speeds acting over the building can change very rapidly, particularly for large buildings. The variations in tornado speed as a function of building size are used in the determination of K_{dT}. Unlike straight-line winds along the horizontal direction, the vertical component of the wind changes the aerodynamics of wind flow around the building, resulting in increased uplift on the building, particularly for the roof. Therefore, K_{vT} is used to simulate this effect. Effects of exposure on tornado characteristics are challenging to measure near the surface with observational techniques such as radar. The latest design code does not define tornado exposure due to the complexity of tornadoes and the challenge of creating realistic terrain environments in scaled experiments. For non-tornadic winds, internal pressures are caused solely by external wind-induced pressures through openings in the building envelope. In tornadoes, a second mechanism also affects internal pressures, namely the atmospheric pressure change (APC). The atmospheric pressure at the center of the tornado is much lower than ambient values. As the core of the tornado moves near or over a building, the atmospheric pressure outside the building drops rapidly, resulting in a differential static pressure between the exterior and interior of the building, which effectively behaves as positive internal pressure. For enclosed buildings, the internal pressure coefficient is GC_{piT} = +0.55 and -0.18 for tornado pressures compared to GC_{pi} = +0.18 for straight-line wind pressures driven by the contribution of APC (ASCE 2021). For both the MWFRS and C&C load cases, the direct wind-induced pressures are computed assuming the C_p derived from boundary layer wind tunnel tests are also valid for tornadic winds (e.g., Kopp and Wu 2020, Roueche et al. 2020). Table 4-1 summarizes the nominal values of tornado load parameters for ASCE 7-22 loading, and their statistics referenced from past literature.

Table 4-1. Statistics of tornado load parameters

Parameters	Descriptions	Nominal	Mean	CoV	Distribution	References
Tornado load parameters						
K_{zTor}	0-61.0 m (0-200 ft)	1.00	1.00	0.20	Normal	Levitan et al. 2021
G_T	-	0.85	0.80	0.10	Normal	
K_{dT}	MWFRS	0.80	0.66	0.28	Beta (0,1)	
	C&C	0.75				
K_{vT}	MWFRS	1.10	1.04	0.08	Normal	
	Wall	1.00				
	All other cases	1.00				
GC_{piT}	Enclosed buildings	0.55	0.17	1.00	Exponential	
	Partially enclosed buildings	0.55	0.46	0.33	Normal	
C_p	Wall	0.80	0.69	0.15	Normal	Masoomi and van de Lindt 2016
	Roof	-0.90	-0.81			
GC_p	Parapet	1.50	1.43	0.18		
	Window	-0.81	-0.77	0.12		
	Door	-0.86	-0.81	0.12		
	Roof cover zone 1’	-0.90	-0.86	0.12	Normal	Masoomi and van de Lindt 2016, FM Global 2002a
	Roof cover zone 1	-1.70	-1.62	0.12		
	Roof cover zone 2	-2.30	-2.19	0.12		
	Roof cover zone 3	-3.20	-3.04	0.12		

Fragility models provide the probability of exceeding damage states for each building or structural component as a function of an intensity measure (e.g., 3-sec gust wind speed). The fragility model is commonly fit to a lognormal cumulative distribution function (CDF) controlled by logarithmic mean (λ) and standard deviation (ξ). Please refer to Ellingwood et al. (2004) and Wang et al. (2021b) for details on the development of fragility curves for structural components and systems subjected to natural hazards such as wind and earthquake. However, if considering the development of tornado fragility curves using the latest loading standard, some adjustments are needed to the past approach by Memari et al. (2018), who had developed a suite of tornado archetypes for use in community and urban resilience modeling. Tornado pressures can be determined using Equations (4.3) and (4.4). But if tornado speeds are less than 26.8 m/s (60 mph) or satisfy other conditions to make tornado design inapplicable (ASCE 2021), basic wind pressures following Equations (4.1) and (4.2) are utilized. As mentioned earlier, MCS was applied in this chapter to determine the exceedance probability at each intensity measure (i.e., 3-sec gust wind speeds). The failure of windows or doors during a realization accounted for the building condition, which was then varied from enclosed to partially enclosed and coefficients adjusted for each MCS realization.

4.2.2 Details of the Archetype Design: a Reinforced Masonry School Building

Three new variations of the school building archetype were designed for use in this chapter based on a design peak 3-sec gust wind speeds of 51.4 m/s (115 mph), 55.9 m/s (125 mph), and 62.6 m/s (140 mph) to control the tornado design for use in community resilience modeling. Thus, three different improved designs are produced using different components (i.e., windows and doors, roof covers, roof structures, and masonry walls) for the reinforced masonry school building with each intended to achieve a different performance level in a simulated tornado. In this chapter, design level 1 represents the benchmark for typical school buildings in a community designed for a tornado in the Midwest. Design level 2 is the advanced design level compared with Design level 1. Design level 3 is the highest design level used to improve school building performance in community resilience modeling and, therefore, maximize school continuity for school children following tornado events. Please refer to Section 4.3 for more details about the illustrative example of community resilience when applying different school designs.

The archetype was based on a real building. Xenia Senior High School was a two-story reinforced masonry building located in north Xenia, Ohio in the U.S. The school consisted of the original main building and three additions (i.e., the addition A, B, and C). The addition A had hollow-core precast concrete roof planks and loadbearing masonry walls. The addition B was constructed of open-web steel joists, 50 mm (2-in) gypsum roof decks, and lightweight steel frames. The addition C included the structural system of concrete double-tee roof beams and precast concrete frames. In addition to regular classrooms, Xenia Senior High School had a girls' gymnasium, a boys' gymnasium, and an auditorium (FEMA 2009). In the past, Xenia Senior High School was used to represent a typical school archetype in resilience assessment by the authors and others and was assumed to be a single-story reinforced masonry building as well as three long-span rooms, i.e., two gymnasiums and one auditorium, with a total footprint area of about 23,226 m^2 (250,000 ft^2) (Masoomi and van de Lindt 2016, Memari et al. 2018). Please refer to Figure 3 in Masoomi and van de Lindt (2016) about the detailed layout of the Xenia Senior High School and a simplified sketch is provided in Figure 4-2. Table 4-2 provides the assumed high school building construction details, including structural and non-structural components for each room.

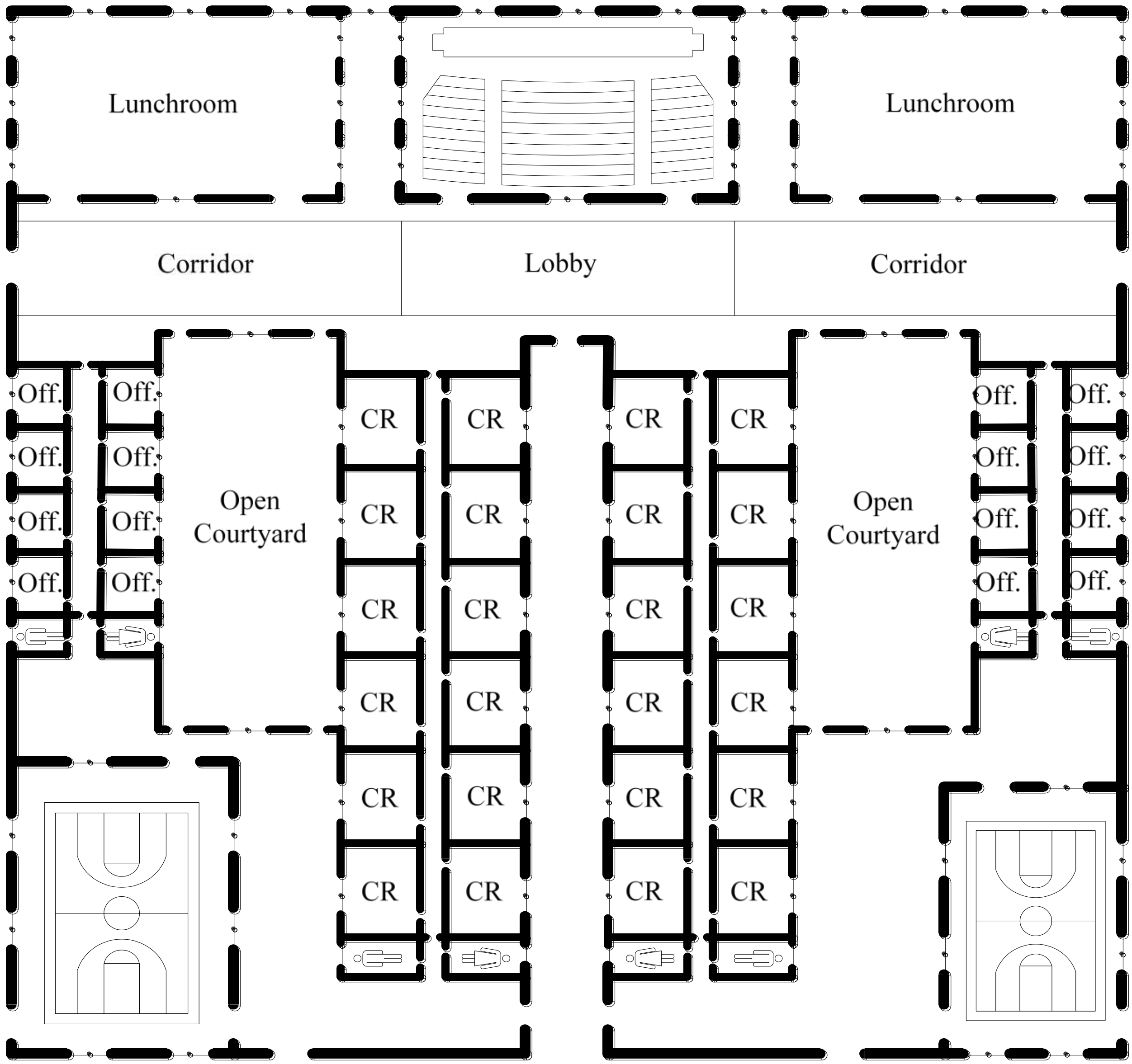

Figure 4-2. A simplified sketch of the school building

Table 4-2. High school building construction details

Buildings	Dimensions	Windows/Doors	Roof cover	Precast concrete roof system		Walls
				Beams	Strand pattern	
Main	Walls height = 4.3 m (14 ft) Parapets height = 0.9 m (3 ft) 152 m × 152 m × 4 m (500 ft × 500 ft × 14 ft)	Annealed glass, 4.7 mm (3/16 in.), 1.9 sq m (20 sq ft) / Glass entry doors	Built-up roof covers	Hollow-Core 4HC8	58-S	8' CMU
Classroom	(14 m × 11 m × 4 m) 45 ft × 35 ft × 14 ft					
Girls' gym	39 m × 24.5 m × 8 m (128 ft × 80 ft × 26 ft)			Single Tee 8ST36	128-D1	12' CMU
Boys' gym	43 m × 30.5 m × 9 m (140 ft × 100 ft × 30 ft)			Single Tee 10ST48	188-D1	12' CMU
Auditorium	44 m × 27.5 m × 9 m (144 ft × 90 ft × 30 ft)			Single Tee 10ST48	148-D1	12' CMU

Xenia Senior High School, which had a student population of 1450, was struck by an F5 tornado on April 3, 1974. The tornado touched down southwest of Xenia and destroyed the entire school building. The exterior walls collapsed, and all windows were shattered on the west and south sides. This extreme tornado tore off the lightweight roof on top of the main building, and the roofs collapsed over the three long spans rooms (FEMA 2009). In order to develop fragilities for the three different designs of the school building in improved designs, damage states for a typical school building are defined as shown in Table 4-3, consistent with Masoomi and van de Lindt (2016). The damage states are controlled by the performance of windows and doors, roof covers, roof structures, parapets, and load-bearing/non-load bearing walls. If any of the damage indicators in each damage state occur, the school building is considered in that damage state.

Table 4-3. Damage states for school buildings

Damage state (DS)	Window/door failures	Roof cover failure	Parapet failure	Non-load bearing wall failure	Roof structural failure	Load-bearing wall failure
0	No	≤2%	No	No	No	No
1	1 or 2	>2% and ≤15%	No	No	No	No
2	>2 and ≤25%	>15% and ≤50%	No	No	No	No
3	>25%	>50%	Yes	Yes	No	No
4	Typically > 25%	Typically > 50%	Typically Yes	Typically Yes	Yes	Yes

Table 4-4 presents the resistance statistics and the failure modes of the school building components for the original design, which represented the design of a 1970s school (Masoomi and van de Lindt 2016). The subsequent subsections will introduce the original design and the proposed improved resilient designs for each structural/non-structural component. Dead load statistics for structural components such as roof beams and masonry walls must be included in the numerical model, as illustrated in Table 4-5. The weight of other light non-structural components such as windows and doors were felt to be negligible and not included. Both the resistance statistics and dead load statistics are then used and combined within the model with the calculated load pressure statistics to perform reliability analysis and determine the fragility functions for the components and for the entire building.

Table 4-4. Resistance statistics of structural/non-structural components

Element type	Description	Mean	CoV	Failure mode	References
Windows	Annealed glass	1.92 kPa (40 psf)	0.20	Pressure	FEMA 2021
Doors	Entry doors	2.39 kPa (50 psf)			
BUR roof cover	Flashing resistance	328.36 N/m (22.5 plf)	0.30	Pressure	FEMA 2021
	Peeling resistance	2.39 kPa (50 psf)	0.15		
	Bubbling resistance	7.18 kPa (150 psf)	0.15		
Beams	Hollow-core, 4HC8	19.66 kN/m (174 plf)	0.10	Negative bending	Masoomi and van de Lindt 2016
	Single-tee, 8ST36	221.56 kN/m (1961 plf)			
	Single-tee, 10ST48	275.23 kN/m (2436 plf)			
Bolts #5	8'' CMU, fully grouted	49.73 kN (11.18 kip)	0.10	Break out	Cui 2007
	8'' CMU, partially grouted	32.65 kN (7.34 kip)	0.12		
	12'' CMU, fully grouted	51.38 kN (11.55 kip)	0.15		
	12'' CMU, partially grouted	40.52 kN (9.11 kip)	0.10		
CMU Walls	Fully grouted, M/S, PCL	2.0 MPa (289.6 psi)	0.11	Flexure-unreinforced	Kim and Bennett 2002
	Partially grouted, M/S, PCL	1.47 MPa (213.0 psi)	0.31		
	Ungrouted, M/S, PCL	1.29 MPa (186.5 psi)	0.48		
	Ungrouted, N, PCL	0.69 MPa (100.5 psi)	0.45		
	Ungrouted, N, MC	0.36 MPa (52.7 psi)	0.45		

Table 4-5. Dead load statistics of typical structural components

Element type		Description	Mean	CoV	CDF	References
Original design						
Beams	Hollow-core	4HC8+2	4.73 kN/m (324 plf)	0.1	Normal	Ellingwood et al. 2004, PCI 1971
	Single-tee	8ST36+2	11.59 kN/m (794 plf)			
		10ST48+2	11.54 kN/m (1065 plf)			
Walls	8' CMU	-	2.30 kPa (48 psf)	0.1	Normal	Masoomi and van de Lindt 2016
	12' CMU	-	3.54 kPa (74 psf)			
Improved resilient design						
Beams	Double-tee	8DT24+2	9.02 kN/m (618 plf)	0.1	Normal	Ellingwood et al. 2004, PCI 2017
		10DT24+2	10.48 kN/m (718 plf)			
		8DT32+2	11.54 kN/m (791 plf)			
Walls	8' CMU	Solid grouted, normal weight	4.02 kPa (84 psf)	0.1	Normal	Taly 2010
	12' CMU	Solid grouted, normal weight	6.37 kPa (133 psf)			

4.2.2.1 Doors and windows

The original design of windows was assumed to use standard annealed glass without any special treatment processes such as heat strengthened glass and laminated glass. The thickness of 4.76 mm (3/16 in) met the minimum glass thicknesses coded in ASTM E1300 (ASTM 2003). Table 4-6 illustrates the window designs specifically for different performance levels, corresponding to the "Design level" in column 1 and wind speed in column 2 (Minor and Norville 1998, Li and Ellingwood 2006, Hawley 2020). For glass breakage due to tornado pressure, the nominal resistance value for annealed glass was assumed to have the same resistance under uniform wind pressure, which can be determined by the glass strengths in terms of a 60 second duration uniform load multiplied by a factor of 1.2 (Minor and Norville 1998), and the coefficient of variation in resistance was assumed to be 0.25 (Li and van de Lindt 2006). A Weibull distribution conventionally measures the statistical failure (e.g., the pressure strength) of brittle materials such as glass (Li and Ellingwood 2006, Abiassi 1981, Dalgliesh and Taylor 1990, Gavanski and Kopp 2011) and was used in this chapter for consistency.

The number of doors and windows for the high school was assumed to be 20 and 120, respectively, consistent with Masoomi and van de Lindt (2016). Figure 4-3 shows the resulting fragility curves for the windows and doors designed with the combination of impact glass windows and entry doors using ASCE 7-22 tornado loads. As shown in Figure 4-3, it can be observed that in order to keep an enclosed building condition (Enc), windows and doors can resist tornado loads of 49.0 m/s (109.5 mph), 57.0 m/s (127.4 mph), and 75.7 mph (169.3 mph) with a 50% probability to reach the three damage states (i.e., DS1, DS2, DS3). The other fragility curves shown as dashed lines in Figure 4-3 were developed for impact glass windows and entry doors, maintaining a partially (Par) enclosed building condition. Projectiles/debris is neglected which is common during tornadoes. Unlike straight-line winds, wind speeds acting on a building during a tornado can vary significantly over the building (presented as the tornado directionality factor, K_{dT}, recall the description and load statistics of K_{dT} in section 2.1), and the generated tornado pressures significantly differ for each realization within the MCS, resulting in fragility curves significantly flatter than the hurricane fragilities presented in Masoomi and van de Lindt (2016).

Table 4-6. Window design for different performance levels

Design Level	Design Wind speed	Window design			
		Description	Resistance		
			Mean	CoV	CDF
Level 1	51.4 m/s (115 mph)	Annealed glass, 3/16 in.	1.7 kPa (36 psf)	0.25	Weibull
Level 2	55.9 m/s (125 mph)	Annealed glass, 1/4 in.	2.2 kPa (45 psf)	0.25	
Level 3	62.6 m/s (140 mph)	Impact glass	2.9 kPa (60 psf)	0.25	

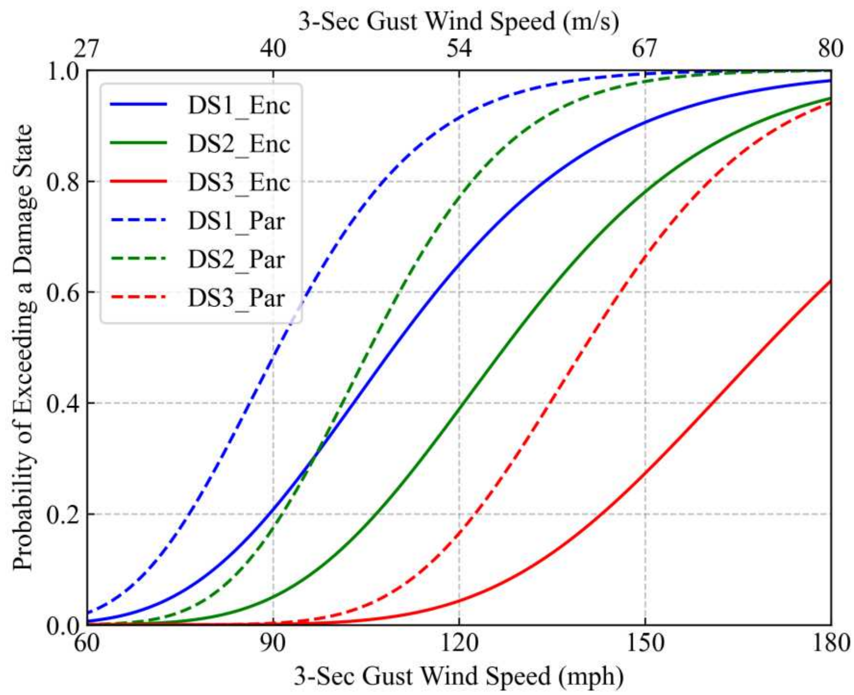

Figure 4-3. Windows and doors fragility curves using Design level 3

4.2.2.2 Roof cover

The perimeters, especially the corners of the roof cover, are exposed to higher uplift wind pressures in design codes and during field studies (Hawley 2020). The higher pressures in these areas are because the wind speed increases at the building edge as the wind flows over the structure (FM Global 2002a). For low-slope roofs such as flat roofs and gable roofs, the roof can be divided into four zones (i.e., zone 1, zone 1', zone 2, zone 3) as a function of the mean roof height roof, as shown in Figure 4-4(a) (ASCE 2021). Built-up roof (BUR) covers and single-ply membrane

(SPM) covers are two standard roof cover systems used for flat roofs. For both roof cover systems, the failure of the perimeter flashing initiates the wind-induced failure. A typical 0.3 m (1 ft) wide flashing was identified in the simulation. When the flashing fails due to wind uplift pressures, the wind can peel the roof cover membrane at the newly exposed edge, and the peeling failure can expand towards the internal area of the roof field, as illustrated in Figure 4-4(b). Another failure mode after the initiation of the flashing is bubbling, where the roof cover is separated from the structural roof due to wind suctions (FEMA 2021). Table 4-7 presents the roof cover designs proposed in this chapter (Masoomi and van de Lindt 2016, FEMA 2021, FM Global 2022b). The roof cover resistances for the different materials and designs are based on engineering judgment and survey data (FEMA 2021, FM Global 2002b). Figure 4-5 presents the resulting roof cover component fragilities for Design level 3.

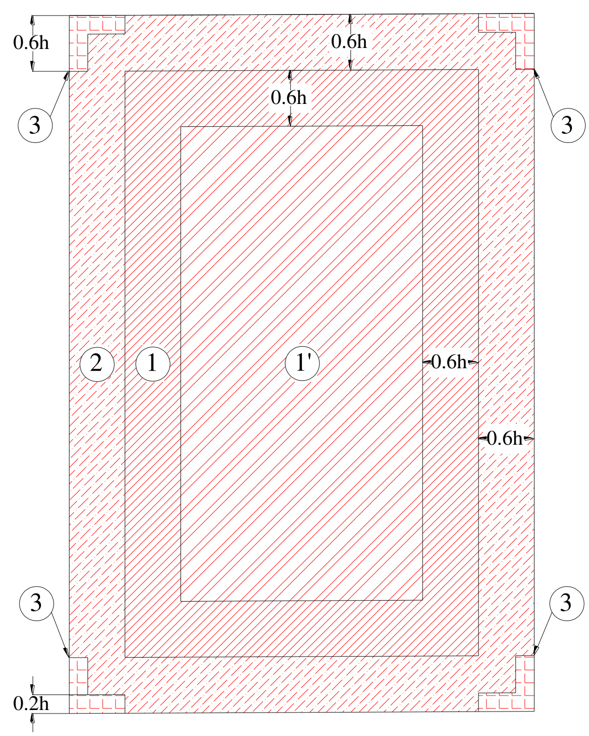

(a)

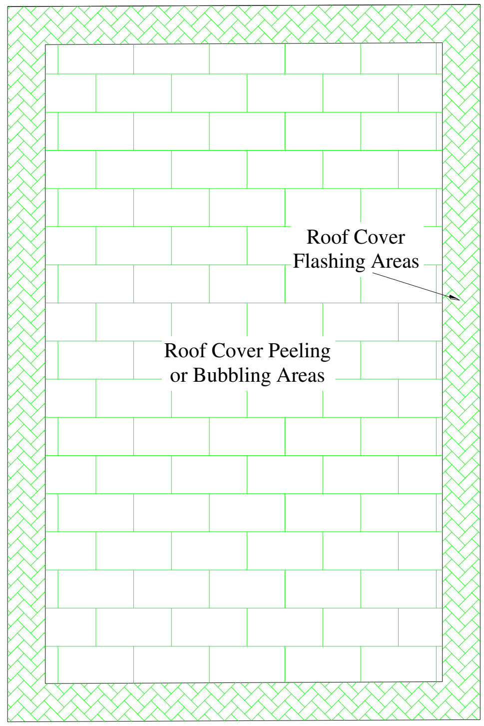

(b)

Figure 4-4. Roof cover failure: (a) different zones to determine wind pressures; (b) roof cover areas for different failure modes

Table 4-7. Roof cover design for different performance levels

Design Level	Roof cover design							
	Description	Flashing resistance		Peeling resistance		Bubbling resistance		CDF
		Mean	CoV	Mean	CoV	Mean	CoV	
Level 1	SPM cover (adhesive)	2.2 kPa (45 psf)	0.30	1.9 kPa (40 psf)	0.15	4.3 kPa (90 psf)	0.15	Normal
Level 2	SPM cover (fasteners)	2.2 kPa (45 psf)	0.30	1.9 kPa (40 psf)	0.15	5.7 kPa (120 psf)	0.15	
Level 3	BUR cover	2.2 kPa (45 psf)	0.30	2.4 kPa (50 psf)	0.15	7.2 kPa (150 psf)	0.15	

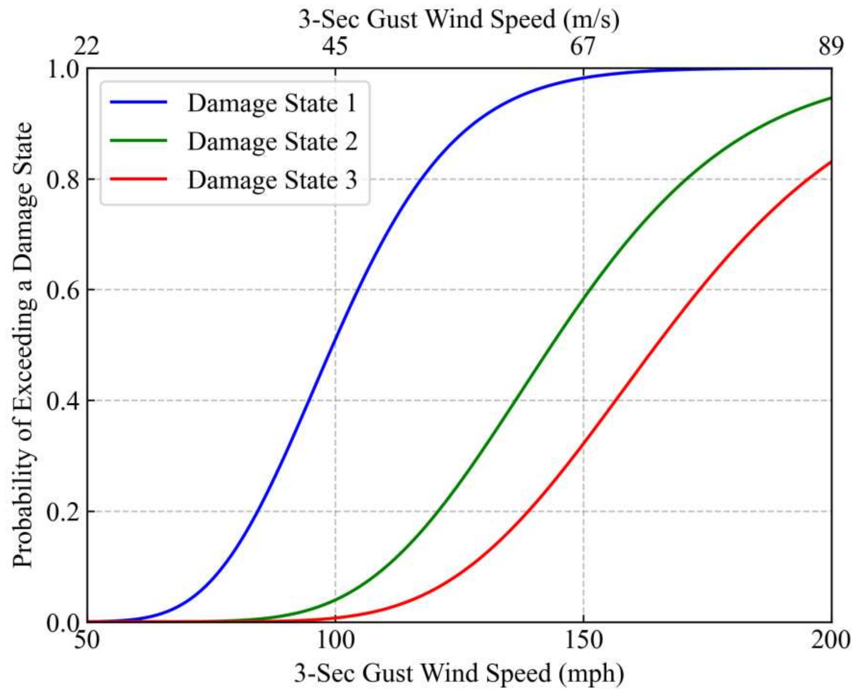

Figure 4-5. Fragility curves of roof covers in the main building using Design level 3

4.2.2.3 Structural roof system

Precast concrete hollow-core beams and precast concrete single tee beams were used for the roof systems in the original design of the main building and the other three long-span rooms, respectively. The section properties of the concrete beams and the design of the strand patterns bonded inside followed the requirements coded in the PCI 1st edition design handbook published in the 1970s (PCI 1971), and all the beams were simply supported in the original design. Overall, precast concrete beams were conventionally designed for positive bending failure due to gravity loads and other loads such as rain loads. In addition, uplift loads due to wind suction can be completely, at least largely, offset by gravity loads except for extreme wind events (e.g., Kuligowski et al. 2014). In this chapter, negative bending at the mid-span was used to control the failure of the roof beams to examine the structural performance of the roof beams impacted by uplift tornado loads. The negative moment resistance was determined by traditional design procedures of prestressed concrete beams designed with minimum reinforcement at the negative moment section. The tensile breakout of roof-to-wall connections is another failure of the roof beams considered in this chapter. If bolts were not reasonably designed to connect the roof beams and masonry walls, the roof beams could move laterally or collapse in the tornado before the negative bending failure occurred. Thus, the union of the roof beam failure and the connection failure was regarded as the structural roof failure.

Over the past few decades, single tee beams have been gradually replaced by double tee beams due to their heavy self-weight dead loads. Table 4-8 indicates the three design levels proposed using double tee roof beams designed for three long-span rooms and roof-to-wall connections spaced differently based on structural calculation and PCI (2017), ACI (2019). In this chapter, all structural roof designs proposed are adequate to resist the tornado in routine levels (50-60 m/s, 111-135 mph) and design levels (61-74 m/s, 135-165 mph). Structural failure for this type of roof is only likely to occur under tornadoes at in extreme levels (75-89 m/s, 166-200 mph), which is when uplift loads are at least greater than gravity loads for roof beams. Figure 4-6 illustrates structural roof fragility curves using the highest design level for roof beams and connections. When the 3-sec gust wind speed equals 89 m/s (200 mph), in order to ensure an enclosed building condition, the failure probabilities of the structural roof and the roof-to-wall connections under tornado loads are 12.9% and 8.6%, respectively. It can be implied that the connection failure is the most likely failure mode for the roof structure.

Table 4-8. Structural roof design for different performance levels

Design Level	Roof design					
	Beams	Negative moment resistance			Failure modes	Roof-to-wall connections
		Mean	CoV	CDF		
Level 1	8DT24+2	131.4 kN m (1163.0 kip in)	0.06	Normal	Negative moment	#5 60 in o.c.
Level 2	10DT24+2	146.6 kN m (1297.9 kip in)	0.07			#5 48 in o.c.
Level 3	8DT32+2	248.7 kN m (2201.5 kip in)	0.07			#5 36 in o.c.

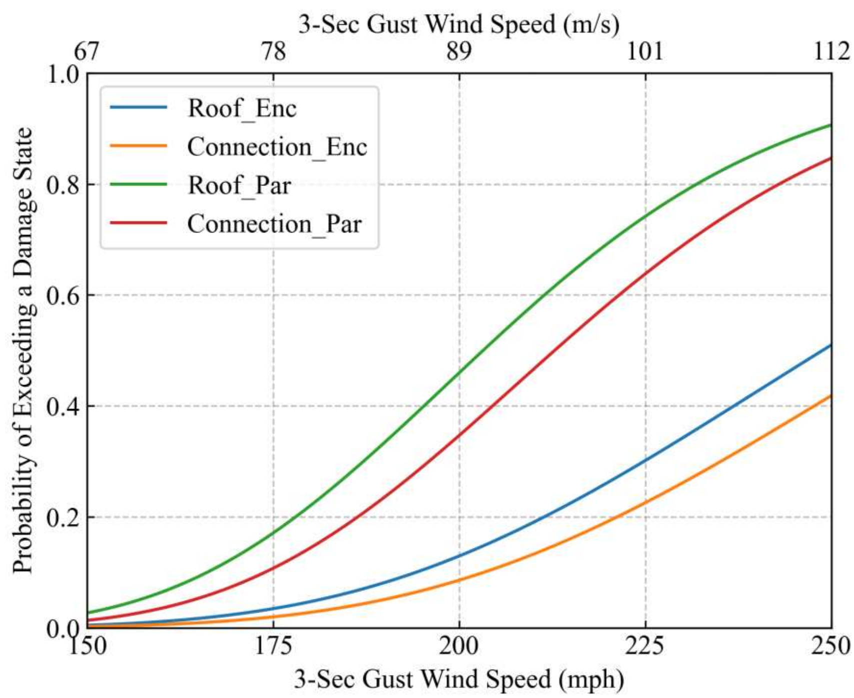

Figure 4-6. Structural roof fragility curves using Design level 3

4.2.2.4 Reinforced masonry walls

Flexure failures were commonly associated with masonry walls subject to out-of-plane loading during severe winds. Lack of horizontal and vertical reinforcement makes these walls susceptible to excessive in-plane load, where shear failures may occur (Al-Menyawi 2001). This chapter does not consider shear failures associated with in-plane loading of masonry shear walls because the new designs consist of reinforcement. The building was assumed to have unreinforced masonry walls of 0.2 m (8 in) CMU for the main building and 0.3 m (12 in) CMU for the other three long-span rooms. Traditional structural analysis of a 0.3 m (1 ft) strip of wall in terms of flexure-unreinforced failure was performed to examine the performance of unreinforced masonry walls within different masonry and mortar types to resist wind loads. The improved designs utilized reinforced masonry walls and defined three design levels that meet the standards coded in TMS 402 (TMS 2016), as illustrated in Table 4-9 (TMS 2016, Bournonville et al. 2004, Aryana 2006). The yielding of vertical reinforced bars controls the failure of reinforced masonry walls such that inspectors can identify structural defects in a timely manner when performing regular inspections. When designing the load-bearing wall, the bending moment generated from lateral wind loads and eccentric loads transferred from roof beams were determined.

Figure 4-7 shows fragility curves for the load-bearing walls of the boy's gym for all three design levels. From the dash lines shown in Figure 4-7, it can be observed that in order to keep a partially enclosed condition for the tornado hazard, the 3-sec gust wind speeds lead to the load-bearing wall failure with a 50% probability within Design level 1, Design level 2, and Design level 3 are 57.2 m/s (128.0 mph), 59.2 m/s (132.5 mph), and 68.8 m/s (154.0 mph), respectively. Based on the results, it can provide an approximate verification that three design levels of load-bearing masonry walls were proposed within a peak 3-sec gust wind speeds of 51.4 m/s (115 mph), 55.9 m/s (125 mph), and 62.6 m/s (140 mph) as design inputs to control the wind design.

Table 4-9. Wall design for different performance levels

Design	Wall design							
	Grade 60 rebars	Yield strength			Mortar types	Concrete masonry unit compressive strength		
		Mean	CoV	CDF		Mean	CoV	CDF
Level 1	#6 48 in o.c.	475.0 MPa (68.9 ksi)	0.07	Normal	M or S	34.1 MPa (4,950 psi)	0.15	Normal
Level 2	#5 32 in o.c.	475.0 MPa (68.9 ksi)	0.07		M or S	34.1 MPa (4,950 psi)	0.15	
Level 3	#4 16 in o.c.	480.6 MPa (69.7 ksi)	0.08		N	42.7 MPa (6,200 psi)	0.15	

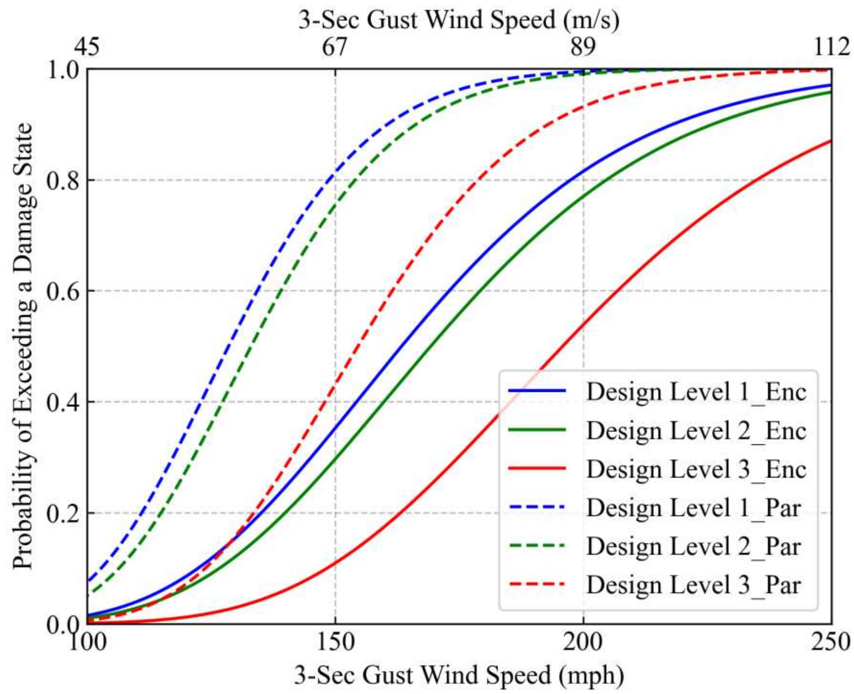

Figure 4-7. Fragility curves of load-bearing wall in the boys' gym

4.2.2.5 School building fragilities (full system)

After determining the individual component fragilities, the damage of each structural and non-structural component can be assembled to assess the damage of the entire high school building in each MCS realization, and fragility curves for the entire school building can be determined. It should be emphasized that only failure of either load-bearing walls or structural roofs leads to the building being in damage state 4. Figure 4-8 and Figure 4-9 show the fragility curves of the entire high school building using Design level 2 and Design level 3, respectively. It is worth reiterating that windows or doors may be damaged or undamaged in each MCS realization, which then determines whether the entire building has pressures consistent with an enclosed or partially enclosed building condition. Therefore, the fragility curves for the school building do not have two sets of curves (i.e., enclosed and partially enclosed) like those for components presented earlier. Overall, as shown in Figure 4-8 and Figure 4-9, the fragility curves for all damage states move to the right to a certain extent due to the advanced design application of higher-strength components. Table 4-10 presents the tornado fragility parameters for the school building using three different design levels. Note that λ and ξ summarized in Table 4-10 are logarithmic mean and standard deviation of lognormal cumulative distribution functions (as mentioned earlier) within the dual units of mph and m/s (shown in the parenthesis) individually.

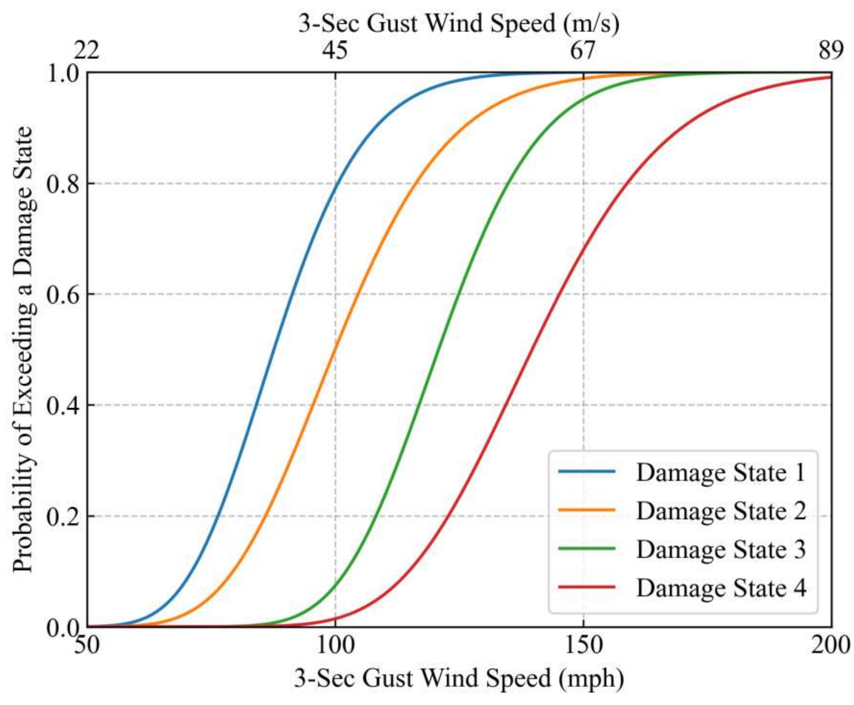

Figure 4-8. School fragility curves using Design level 2

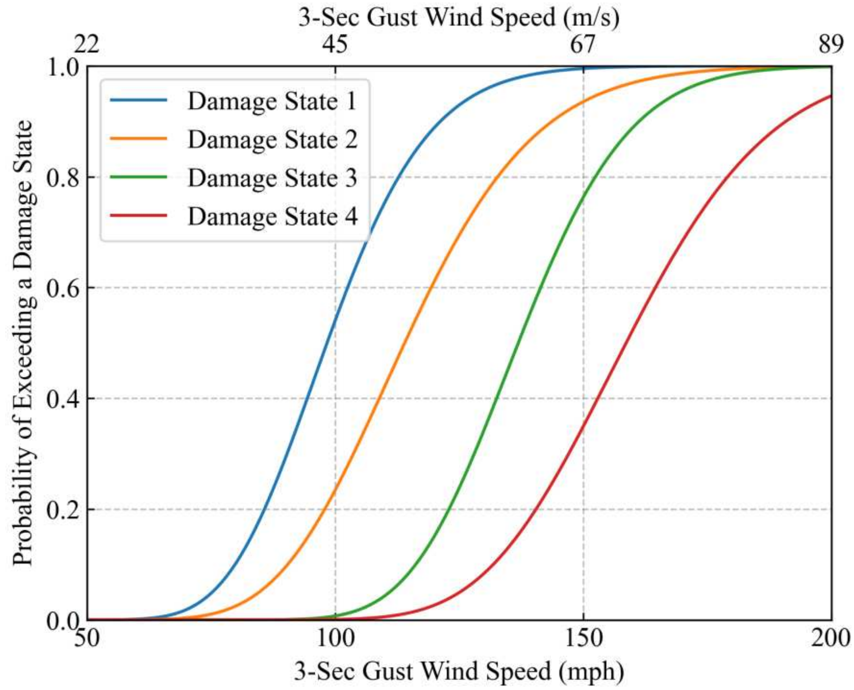

Figure 4-9. School fragility curves using Design level 3

Table 4-10. Tornado fragility parameters for the school building in different design levels

Damage states	Design level 1 Units: mph (m/s)		Design level 2 Units: mph (m/s)		Design level 3 Units: mph (m/s)	
	λ	ξ	λ	ξ	λ	ξ
DS1	4.41 (3.60)	0.17 (0.17)	4.47 (3.66)	0.16 (0.16)	4.59 (3.78)	0.16 (0.16)
DS2	4.51 (3.70)	0.19 (0.19)	4.61 (3.80)	0.18 (0.18)	4.74 (3.93)	0.18 (0.18)
DS3	4.72 (3.91)	0.14 (0.14)	4.79 (3.98)	0.13 (0.13)	4.92 (4.11)	0.13 (0.13)
DS4	4.92 (4.11)	0.15 (0.15)	4.94 (4.13)	0.15 (0.15)	5.07 (4.26)	0.14 (0.14)

4.3 Illustrative Example

A multidisciplinary perspective applied to the built environment, social, and economic systems on community resilience studies to natural hazards such as hurricanes, tornadoes, earthquakes, and floods is prevalent in recent years (e.g., Wang et al. 2021b, Koliou et al. 2020, Nofal and van de Lindt 2020, Nofal et al. 2021, Roohi et al. 2020, Bocchini et al. 2014, Li et al. 2020, Sediek et al. 2022). In order to apply the tornado-induced school building designs mentioned earlier and examine a core community resilience metric, this chapter demonstrates the use of the improved school fragilities and (subsequently developed) improved residential fragilities to examine key metrics such as dislocation of households, inability to attend school, and the combination of these two conditions for residents of a community. This illustrative example specifically examines households with children in the U.S. city of Joplin, Missouri, incorporating interdependency between residential buildings, households, and availability of school services when subjected to tornado hazards.

The retrofitted residential buildings used in this example have different design combinations in structural configurations, including roof covers, roof sheathing nailing patterns, and roof-to-wall connections (see Wang et al. 2021b for details). Table 4-11 and Table 4-12 present the details of the retrofitted designs and their fragilities for residential buildings surrounding the school buildings throughout Joplin. The building dataset in the Joplin testbed has 23,605 residential buildings with archetypes assigned based on their footprint areas and the number of stories. The NCES and SABS provides school attendance zones for more than 70,000 schools in over 12,000 school districts throughout the U.S. Based on the records for the 2015-2016 school year, the Joplin community has 11 elementary schools, three middle schools, and one high school, as illustrated in Table 4-13. The overlay of the Joplin testbed building datasets and the Joplin school attendance zones provides information on the spatial dependency between Joplin residential buildings and their dependent schools, as shown in Figure 4-10, with almost 95% of residential buildings in the Joplin testbed are covered in the Joplin school attendance zones. After allocating the household information to the residential buildings, the housing units tracked by Housing Unique Identifiers (HUIDs) can link to the residential buildings tracked by Globally Unique Identifiers (GUIDs), where the data format of the interdependency among housing units, residential buildings, and their school attendance zones is shown in Table 4-14. This chapter uses the predicted household size multiplied by 19%, an approximate percentage of children from 5 to 19 years in the total population (US Census Bureau 2019), to estimate the number of children per household and distributes them throughout the residential buildings based on the allocation methodology (Rosenheim et al. 2019, Rosenheim 2021).

Because 90% of historical tornadoes recorded are EF2 ratings or less (e.g., Haan et al. 2008, Roueche et al. 2017), this illustrative example applies 100 EF2 idealized generic tornado scenarios using the gradient technique (Standohar-Alfano and van de Lindt 2015) developed geographically in the random length and direction (Wang et al. 2022c) which strike the Joplin testbed. For each tornado scenario, both school buildings and residential buildings were designed in three different levels separately. Since school buildings in any community are relatively scattered and scarce compared with residential buildings, there are a number of tornado scenarios that may not even strike a school building. Only eighteen tornado scenarios hit the elementary schools, five tornado scenarios struck the middle schools, and none of the tornado scenarios impacted the high school in the simulation. In reality, Joplin was impacted by an EF5 tornado which destroyed the high school in 2011. The analytical results of tornado scenarios were averaged and classified into two categories for all tornado scenarios and only tornado scenarios striking school buildings separately to better discern the results, and presented in Table 4-15 and Table 4-16.

Table 4-11. Retrofit strategies of residential buildings in different design levels

Structural elements	Description	Design level 1	Design level 2	Design level 3
Roof covering	Asphalt shingles	X	X	-
	Clay tiles	-	-	X
Roof sheathing nailing pattern	8d C6/12	X	-	-
	8d C6/6	-	X	X
Roof-to-wall connection type	Two 16d toenails	X	-	-
	Two H2.5 clips	-	X	X

Table 4-12. Tornado fragility parameters for residential buildings in different design levels

Damage states	Design level 1 Units: mph (m/s)		Design level 2 Units: mph (m/s)		Design level 3 Units: mph (m/s)	
	λ	ξ	λ	ξ	λ	ξ
Archetype 1						
DS1	4.49 (3.68)	0.13 (0.13)	4.49 (3.68)	0.14 (0.14)	4.74 (3.93)	0.12 (0.12)
DS2	4.37 (3.56)	0.14 (0.14)	4.66 (3.85)	0.12 (0.12)	4.80 (3.99)	0.11 (0.11)
DS3	4.44 (3.63)	0.13 (0.13)	4.79 (3.98)	0.11 (0.11)	4.88 (4.08)	0.10 (0.10)
DS4	4.49 (3.68)	0.14 (0.14)	4.97 (4.16)	0.13 (0.13)	5.10 (4.29)	0.12 (0.12)
Archetype 5						
DS1	4.56 (3.75)	0.13 (0.13)	4.56 (3.75)	0.13 (0.13)	4.76 (3.95)	0.12 (0.12)
DS2	4.46 (3.65)	0.13 (0.13)	4.69 (3.88)	0.12 (0.12)	4.83 (4.02)	0.11 (0.11)
DS3	4.51 (3.70)	0.13 (0.13)	4.79 (3.98)	0.11 (0.11)	4.92 (4.11)	0.10 (0.10)
DS4	4.45 (3.64)	0.15 (0.15)	4.87 (4.06)	0.14 (0.14)	5.05 (4.24)	0.13 (0.13)

Table 4-13. K-12 schools in Joplin

School types	Joplin Schools	NCES school identification code
Elementary school	Cecil Floyd Elementary School	291635002432
	Columbia Elementary School	291635000772
	Eastmorland Elementary School	291635000775
	Irving Elementary School	291635003240
	Jefferson Elementary School	291635000779
	Kelsey Norman Elementary School	291635000780
	McKinley Elementary School	291635000783
	Royal Heights Elementary School	291635000788
	Soaring Heights Elementary School	291635000773
	Stapleton Elementary School	291635000791
	West Central Elementary School	291635000793
Middle school	East Middle School	291635002431
	North Middle School	291635002430
	South Middle School	291635002429
High school	Joplin High School	291635000787

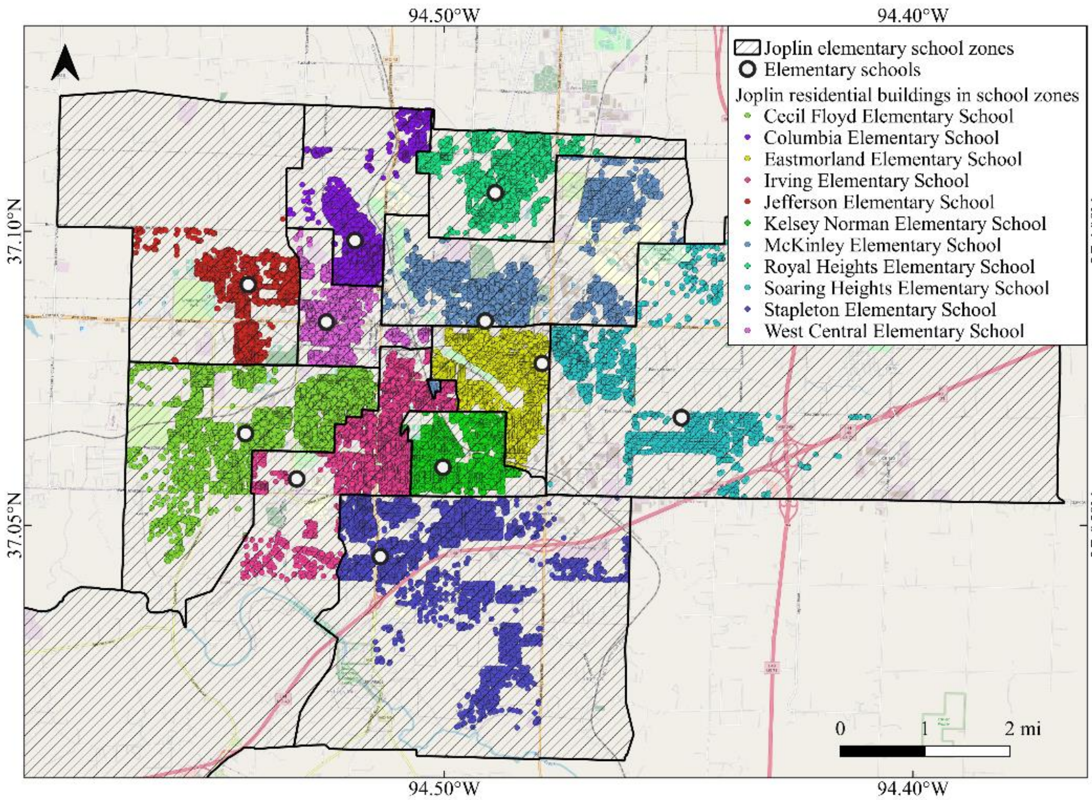
94.50°W
94.40°W
Joplin elementary school zones
Elementary schools
Joplin residential buildings in school zones
Cecil Floyd Elementary School
Columbia Elementary School
Eastmorland Elementary School
Irving Elementary School
Jefferson Elementary School
Kelsey Norman Elementary School
McKinley Elementary School
Royal Heights Elementary School
Soaring Heights Elementary School
Stapleton Elementary School
West Central Elementary School
37.10°N
37.05°N
0
1
2 mi

(a)

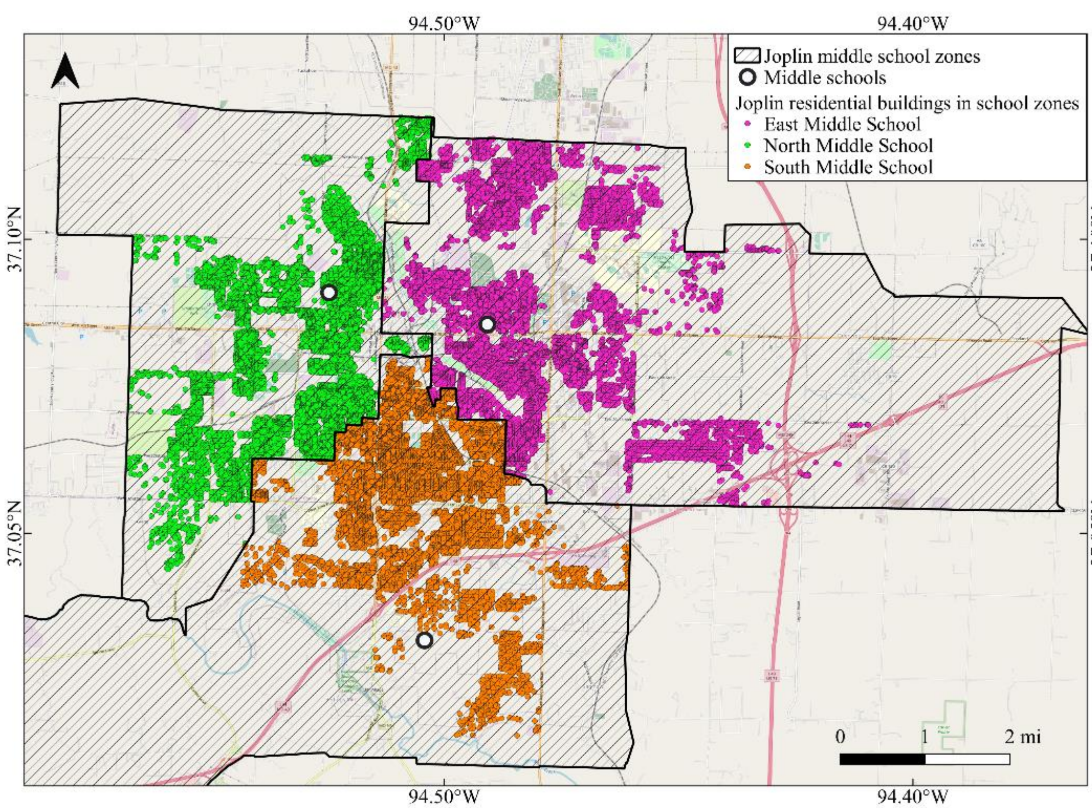
94.50°W
94.40°W
Joplin middle school zones
Middle schools
Joplin residential buildings in school zones
East Middle School
North Middle School
South Middle School
37.10°N
37.05°N
0
1
2 mi

(b)

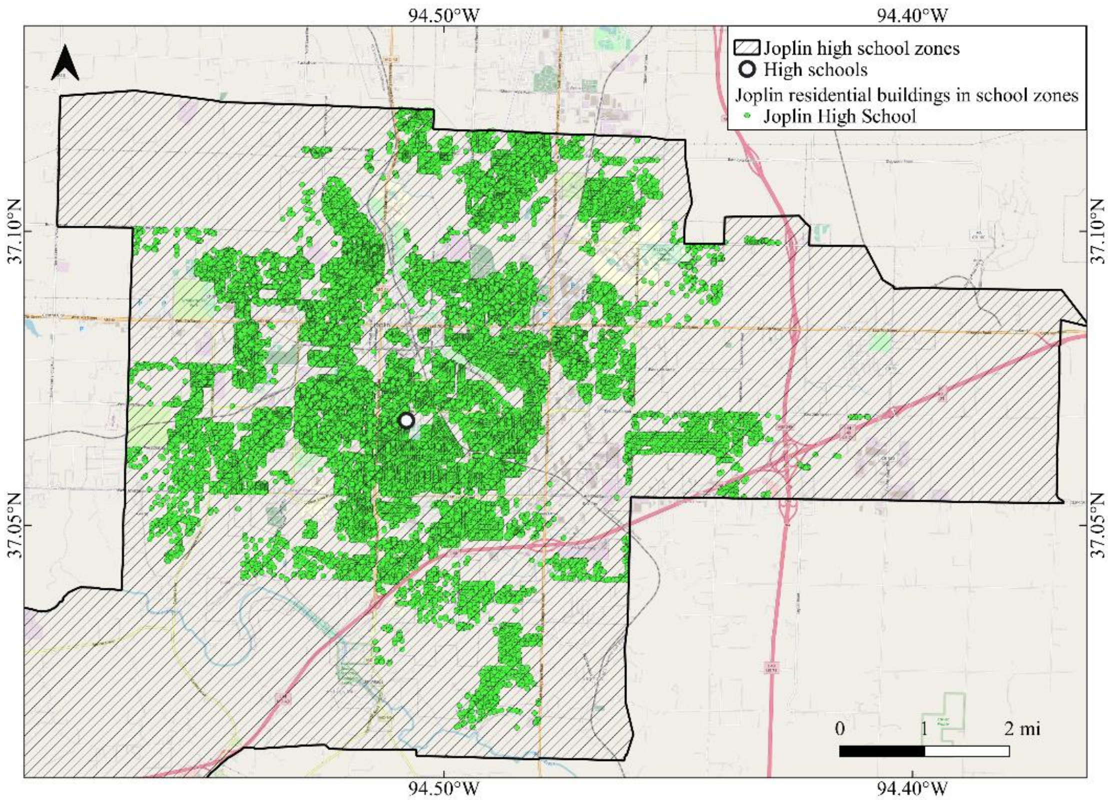

(c)

Figure 4-10. Joplin buildings associated with school attendance zones: (a) elementary schools; (b) middle schools; (c) high schools

Table 4-14. Data format example of interdependency among households, residential, and school attendance zones

GUID	HUID	Household size	NCES school identification code		
			Elementary school	Middle school	High school
GUID1	HUID1	4	291635000788	291635002431	291635000787
GUID2	HUID2	5	291635000787	291635002430	291635000787
GUID3	HUID3	2	291635000783	291635002431	291635000787
GUID4	HUID4	1	291635002432	291635002430	291635000787
GUID5	HUID5	3	291635003240	291635002429	291635000787
…	…	…	…	…	…

Since each household has its dependent elementary school and middle school, Table 4-15 and Table 4-16 present the impact of the functionality of residential buildings along with elementary schools and middle schools, respectively, on school children. Overall, if averaging the analytical results over all tornado scenarios, the number of children in all four cases are close no matter whether considering their dependent elementary school or middle school. The percentage of children who resided in residential buildings within tornado paths having both functional housing and a functional school building (Case 1) can be improved from around 25% to 85% when using Design level 3. The percentage of children losing both facilities (Case 4) are reduced from less than 5% to less than 1%. The low values and high values for coefficients of variation (CoV) for Case 3 and Case 4 when averaging the analytical results of all tornado scenarios occur because most tornado scenarios do not strike the school buildings, and therefore the number of non-functional schools in these scenarios are zero. It is important to keep in mind that an EF2 tornado, while much more common than EF4 or EF5 tornadoes, are also significantly narrower, e.g., several hundred meters rather than more than a kilometer wide.

However, if only averaging the analytical results of tornado scenarios striking elementary schools and middle schools, respectively, the number of children affected in the four cases have a relatively large difference. When combining the analytical results of Case 1 and Case 2 without considering the functionality of residential buildings, it can be observed that due to the improved school building design, the percentage of children having a functional elementary school is improved from 80.1% (20.6%+59.5%) to 92.2% (79.3%+12.9%) as shown in Table 4-15. The percentage of children having middle schools is increased from 60.7% (14.3% + 46.4%) to 80.9% (68.4%+12.5%) shown in Table 4-16. Similarly, combing the analytical results of Case 1 and Case 3 without considering the functionality of school buildings can conclude that the retrofitted residential buildings in higher design levels help more children maintain their housing after tornado events.

Table 4-15. The impact of functionality of residential and elementary schools in different improved designs on school children

Cases	Residential	Elementary Schools	Households with children residing in residential buildings within tornado paths			
			All tornado scenarios included (100 scenarios)		Tornado scenarios striking elementary school buildings (18 scenarios)	
			Mean	CoV	Mean	CoV
Design level 1						
Case 1	X	X	34.3 (24.2%)	0.74	43.1 (20.6%)	0.42
Case 2	-	X	99.9 (70.6%)	0.65	124.2 (59.5%)	0.47
Case 3	X	-	1.5 (1.1%)	3.28	8.3 (4.0%)	1.06
Case 4	-	-	6.0 (4.2%)	3.33	33.2 (15.9%)	1.08
In total			141.6 (100.0%)	0.63	208.8 (100.0%)	0.32
Design level 2						
Case 1	X	X	92.4 (65.3%)	0.64	119.4 (57.2%)	0.42
Case 2	-	X	43.3 (30.6%)	0.74	56.4 (27.0%)	0.55
Case 3	X	-	3.5 (2.5%)	3.62	19.6 (9.4%)	1.24
Case 4	-	-	2.4 (1.7%)	3.97	13.5 (6.5%)	1.42
In total			141.6 (100.0%)	0.63	208.8 (100.0%)	0.32
Design level 3						
Case 1	X	X	119.5 (84.4%)	0.63	165.6 (79.3%)	0.37
Case 2	-	X	19.1 (13.5%)	0.83	26.9 (12.9%)	0.57
Case 3	X	-	2.3 (1.6%)	5.35	13.0 (6.2%)	2.08
Case 4	-	-	0.6 (0.4%)	6.30	3.3 (1.6%)	2.52
In total			141.6 (100.0%)	0.63	208.8 (100.0%)	0.32

Table 4-16. The impact of functionality of residential and middle schools in different improved designs on school children

Cases	Residential	Middle Schools	Households with children residing in residential buildings within tornado paths			
			All tornado scenarios included (100 scenarios)		Tornado scenarios striking middle school buildings (5 scenarios)	
			Mean	CoV	Mean	CoV
Design level 1						
Case 1	X	X	34.9 (24.6%)	0.75	28.4 (14.3%)	0.69
Case 2	-	X	102.8 (72.6%)	0.67	92.2 (46.4%)	0.67
Case 3	X	-	0.9 (0.6%)	5.89	17.0 (8.6%)	0.89
Case 4	-	-	3.1 (2.2%)	5.78	61.2 (30.8%)	0.85
In total			141.6 (100.0%)	0.63	198.8 (100.0%)	0.17
Design level 2						
Case 1	X	X	94.0 (66.4%)	0.65	88.6 (44.6%)	0.59
Case 2	-	X	44.3 (31.3%)	0.75	45.0 (22.6%)	0.76
Case 3	X	-	1.9 (1.3%)	6.31	38.9 (19.6%)	1.02
Case 4	-	-	1.3 (0.9%)	6.49	26.3 (13.2%)	1.08
In total			141.6 (100.0%)	0.63	198.8 (100.0%)	0.17
Design level 3						
Case 1	X	X	120.4 (85.0%)	0.64	136.0 (68.4%)	0.43
Case 2	-	X	19.3 (13.6%)	0.85	24.8 (12.5%)	0.74
Case 3	X	-	1.5 (1.1%)	8.29	30.2 (15.2%)	1.58
Case 4	-	-	0.6 (0.4%)	8.58	7.7 (3.9%)	1.65
In total			141.6 (100.0%)	0.63	198.8 (100.0%)	0.17

4.4 Summary and Conclusions

The resilience of communities/cities relies heavily on social institutions such as schools to maintain population stability. This chapter investigated the effect a building retrofit program would have on maintaining school continuity, avoiding dislocation for school children, or the combination thereof. To do this, several improved design levels of a reinforced masonry school building were designed, and fragilities representative of archetypes for use in community resilience modeling were developed. This was done using the new tornado methodology in ASCE 7-22 (ASCE 2021). The ability to quantify the impact of improved design of buildings critical to the functionality and recovery of a community is necessary for planning and measuring resilience. Based on the work presented herein, the following conclusions can be drawn:

- Tornadic winds vary in both direction and speed over the building, resulting in the generated tornadic wind pressures having a significant difference in each MCS realization, making the fragility curves relatively flat compared to straight line winds.
- Similar wind speeds result in a likely decrease of approximately one to two damage state levels when comparing Design level 1 (representing code level) versus Design level 3 (representing an improved design). The improvement of the building performance could help significantly mitigate the damage of school buildings following moderate tornado events.
- The improved school building design and improved residential building design enable buildings to be less damaged as expected, but the impact on reducing dislocation in moderate tornadoes (EF2) and maintaining educational continuity is significant.

The tornado fragility analysis via MCS can determine the probability of exceeding the specified damage states for the school building using 3-sec gust wind speed as an intensity measure. However, the process cannot incorporate the effect of footprint areas of the buildings on the tornado speed as introduced in ASCE 7-22. Addressing the above limitation is beyond the scope of this chapter.

In summary, use of these new archetypes within community/city resilience modeling can provide communities the impetus to strengthen their school design for new/existing buildings. The fragility curves representing new archetypes provide the response of school buildings, which play an essential role in providing the social services, in resilience assessment subjected to tornado loads. This was done following the methodology in the latest U.S. standard which is the first in the world to include tornado loads. Although schools are critical, additional archetypes need to be investigated for improvement in the community resilience tornado literature for modeling.

CHAPTER 5 RESIDENTIAL BUILDING RECOVERY

5.1 Introduction

Understanding the process of community recovery impacted by various post-disaster decisions such as dynamic policies that can effectively guide the recovery process and expedite recovery, thereby establishing a more resilient community if a hazard event were to occur. This chapter proposes a methodology based on a multi-layer MCS to model a two-stage recovery process for residential buildings: functional downtime due to delay and functional downtime due to repair. The delay portion of the model was modified based on the REDi framework and models the impeding factors that delay repairs such as post-disaster inspection, insurance claims, and building permits. Household income was examined to estimate the financing delay depending on different funding resources such as insurance and loans available to households at different income levels. The repair portion of the model followed the FEMA P-58 approach (which was originally for post-earthquake analysis) and was controlled by fragility functions. This chapter also investigates a series of policies to examine an illustrative example, namely the 2011 Joplin tornado. The ability to model hypothetical policy scenarios for residential recovery of a community will enable decision-makers to better understand collective community-wide impacts of their actions and policies, thereby improving community resilience planning.

A few studies have estimated residential and business downtime due to a variety of delays before the initiation of building repairs. Lin and Wang (2017) utilized a discrete/continuous-time Markov Chain and transition probability matrix to predict the recovery trajectory involved with delay across the domain of a community for earthquake hazards using a building portfolio approach that clustered buildings by type. Iuliis et al. (2019) applied a fuzzy logic hierarchical scheme to evaluate the delay time considering repair sequences and repair crews for a residential building. Aghababaei et al. (2020) adjusted the REDi framework and used real-world Small Business Administration (SBA) loans and permitting time data to determine the delay time, filling the gap between the analytical and empirical fragilities.

Moreover, policies are essential to effectively influence the speed and quality of the recovery process when they are developed related to public resources with potential causes of delays considered (Ingram et al. 2006, Joshi and Aoki 2014, Sutley and Hamideh 2018, Richmond 2019). For example, recovery fund policies from the Federal Emergency Management Agency (FEMA) restricted any money used to repair damages caused by deferred maintenance (Sapat and Esnard 2016). Hirayama (2000) examined the temporary and permanent housing recovery policy implemented in Kobe, a city heavily damaged by the Great Hanshin Earthquake in 1995 and identified a significant gap in housing recovery for the urban area after the earthquake due to socio-economic and spatial polarization. Drennan et al. (2016) confirmed the effectiveness of intergovernmental policy and funding arrangements on reinforcing the management of natural disasters through case studies of two of the most expensive and deadly natural disasters in Australia.

The work presented in this chapter differs from past studies in that no studies to date have performed a quantitative probabilistic analysis to determine the community recovery when impacted by policy changes implemented by either federal, state, or local governments. Another significant contribution of the work is, for the first time, a methodology that provides recovery modeling as a time-stepping algorithm (e.g., monthly, quarterly, yearly) is presented with full propagation of uncertainties, thereby allowing investigation of changes in policies at different points in time during the recovery process. Finally, the methodology presented herein applies an existing housing unit allocation algorithm (Rosenheim 2020) that allows the analyst to include detailed household characteristics and to track how the recovery of housing impacts the people living in each building. This last feature allows the prediction of delays based on the household income allocated to each housing unit based on race, ethnicity, and household size at the census block level as well as census tract level income distributions. Figure 5-1 shows the schematic description of community resilience following a disruptive hazard event in terms of robustness (system-level residual functional capacity to withstand an extreme event) and rapidity (the time required to recover the desired functionality). Where *Q(t)* is the functionality performance, which is measured as a dimensionless function of time, t_r is the recovery time for the system to be fully restored, and t_o is the time of occurrence of disasters (Bruneau et al. 2003, Koliou et al. 2017). Resilience (*R*) was defined mathematically by Bruneau et al. (2003), illustrated in Equation (5.1), and can also be shown as the area under the curve between t_o and t_r in Figure 5-1. This chapter presents the methodology and concept first published in Wang and van de Lindt (2021).

$$R = \int_{t_o}^{t_o+t_r} Q(t)dt \tag{5.1}$$

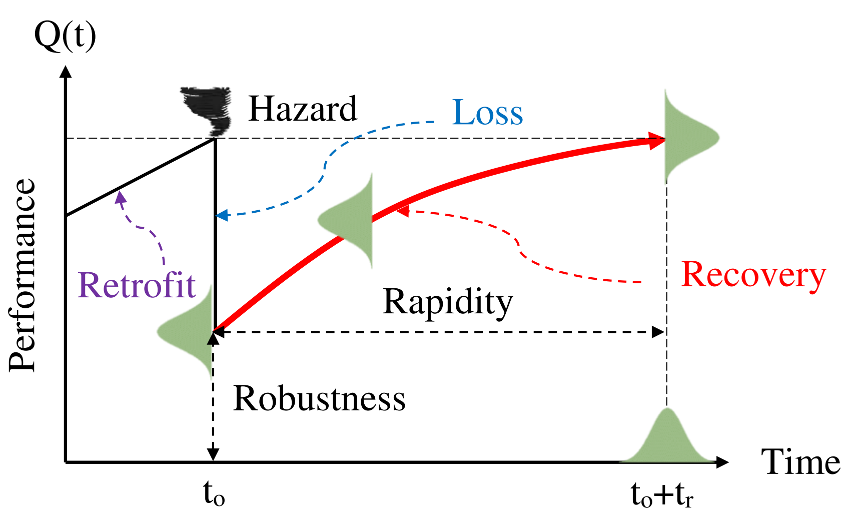

Figure 5-1. The schematic description of community resilience

5.2 Probabilistic Residential Recovery Modeling

Figure 5-2 shows a schematic of the residential recovery modeling methodology proposed in this chapter. Total recovery time for a damaged building induced by a hazard event is not limited to the time required to simply repair a building. Recovery modeling in this chapter is considered a two-step recovery: downtime due to delays and downtime due to repairs. The recovery modeling overall was a probabilistic quantitative analysis which uses multi-layer MCS. The first layer of MCS included N1 scenarios to probabilistically estimate the delay time, which is directly related to building damage from the hazard. For each realization of delay time within the MCS, N2 realizations of repair time were generated and then combined with this delay time realization to form the multi-layer MCS. The delay assessment methodology was developed based on the approach in the REDi framework (Almufti and Willford 2013). It should be mentioned that the REDi framework was initially designed for loss assessment of post-earthquake events, but the methodology developed in this chapter modified the framework to generalize it for all events, with an illustrative example for wind-induced events presented later in this chapter. The functions comprehensively incorporate the delay variables resulting from typical impeding factors, which include issues such as post-disaster inspection, securing engineer/contractor, financial assistance, and a building permit. The financing delay is assumed to be directly related to the financial resources available to a household. Thus the methodology proposes to use annual household income as a socio-demographic characteristic indicator to predict the funding options for households to finance their residential building repairs. Repair time was estimated by fragility functions, and recovery time was the combination of delay time plus repair time. Weibull distributions can be used to fit the MCS results for delay time and recovery time for each building. It was assumed that no households would out-migrate but rather stay in the community to complete the repairs following a hazard event. Relaxing and addressing this assumption is beyond the scope of the current paper, but its importance is duly noted and will be addressed in future work.

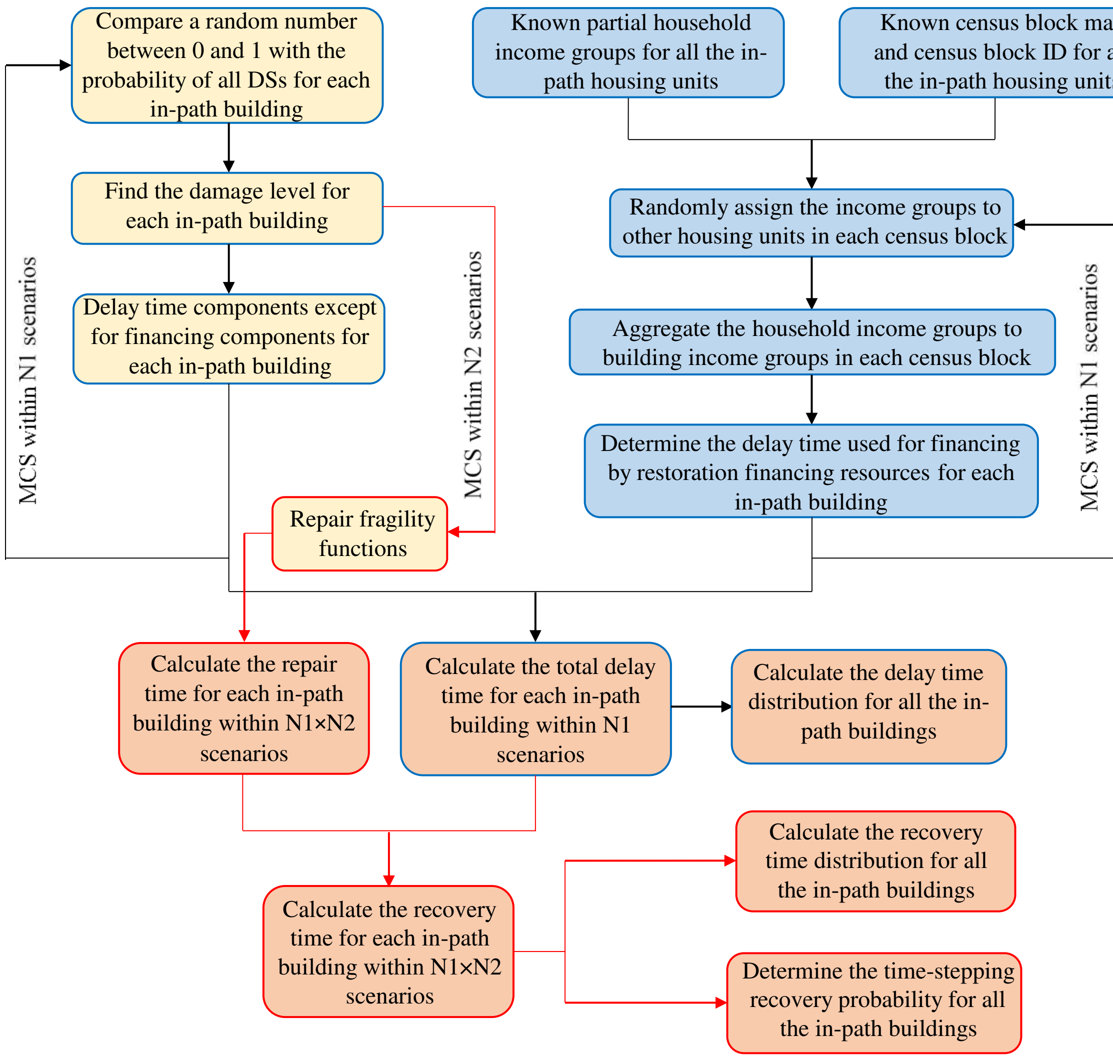

Figure 5-2. Flowchart of the residential recovery modeling following a hazard event

5.2.1 Delay Time Assessment

Several delays inevitably occur before the initiation of building repairs, which will increase the time needed for damaged buildings to reach the next (and eventually complete) recovery state. Equation (5.2) shows the delay variables considered in this chapter, where i is an index for each realization within the MCS, j is a specific building in the community; T_{Delay} is the modeled delay time, and T_{INSP}, T_{ENGM}, T_{FINA}, T_{CONM}, T_{PERM} are the times for the post-event inspection, to contact engineers, to secure funding, to secure contractors, and procure construction permitting, respectively.

$$T_{Delay,\,ij} = T_{INSP,\,ij} + max\,\{T_{ENGM,\,ij},\, T_{FINA,\,ij},\, T_{CONM,\,ij}\} + T_{PERM,\,ij} \tag{5.2}$$

This chapter assumes the following sequence of events associated with modeled delay time. First, a building inspector performs a thorough visual inspection of the damaged buildings in order to assess the extent of the damage and protect the safety of the building occupants. The building owner is then told to obtain a structural building inspection if the structural integrity of the building is in question. In addition, the jurisdiction, tenants, or insurance companies have a right to request an inspection if they deem the event may have caused damage to a building. Upon receiving the inspection report, the homeowner will typically approach a professional contractor to prepare for the repair and, if applicable by jurisdiction, identify an engineer or equivalent to review/redesign and provide drawings for the building. Simultaneously, the financial loss estimate for the building may be provided by the insurance inspection report and/or the contractor, and the owner must proceed to secure any funding resources needed. Delays during this period need to be combined, and the time required for each component cannot simply be added since some tasks are usually performed in parallel. The duration used for the engineer to review/redesign may depend on the structural damage level and may also be related to the height and footprint area of the building. Finally, if the building exhibits structural damage and then structural repairs are needed, a permit needs to be approved by the local building jurisdiction.

The duration of most of the delay variables is correlated well with the extent of the damage. Unlike most of the delay variables, financing delays rely on the household's capability to access government funding, the bank, insurance payments, and charitable organizations. Note that Federal, other state governments, and nongovernmental organizations (NGOs) like the American

Red Cross and local churches are not considered in this chapter due to the uncertainty of their assistance for each event. Instead, financial resources, including insurance, loans, and savings, are considered herein. More than 85% of homeowners have homeowner insurance in the United States, which typically covers wind damage (Croll 2021). The Small Business Administration (SBA), which is a United States government agency that provides support and loans to entrepreneurs and small businesses, has invested a large sum of money in disaster loans to repair or replace damaged components. In theory, businesses and homeowners can borrow within limits, which depends on their qualifications. Additionally, owners may qualify for private loans from banks if they meet specific minimum requirements. The personal loan amount is related to financial impact factors such as property value, credit report, and market conditions. However, specific populations, such as homeowners with low incomes and minorities, historically have less access to such public assistance (Peacock et al. 1997). For these households, any savings or family assistance may become the only option for financing repair.

The impeding factor functions are quantitatively described in the format of lognormal cumulative distribution functions with a high degree of uncertainty, as illustrated in Table 5-1 and Equation (5.3) (Almufti and Willford 2013). Note that β is the standard deviation of the lognormal function, and the columns of the median (θ_1) and coefficient of variation (CoV) shown in Table 5-1 were referenced from the REDi framework, while the modified median (θ_2) values are defined in this chapter to represent shortened delay time impacted by different policies, which will be expanded on later in the policy lever section. It is assumed that the coefficients of variation for the delay time remain the same with or without the impact of post-disaster policies. The variable of $T_{n,\,ij}$ shown in Equation (5.3), is consistent with the delay variables such as post-event inspection defined in Equation (5.2). It is worth noting that these delay time estimates may be merely applicable to the buildings located in the United States since other countries may have different emergency response plans. Lin and Wang (2017) combined delay time components with specific conditions of buildings damaged at different levels (see Table 5-1). The estimated delay time is directly related to the initial building damage level in this chapter, which is modeled using fragilities for each building, as illustrated conceptually in Figure 5-3.

$$F_R\left(T_{n,ij}\right) = \Phi\left[\frac{ln(T_{n,ij}) - ln\ (\theta)}{\beta}\right] \tag{5.3}$$

Table 5-1. Statistics of delay time associated with building damage (unit: weeks)

Sequence	Delay time impeding factor	Building damage conditions	Median (θ_1)	Modified median (θ_2)	Coefficient of variation (CoV)
Delay Phase 1	Inspection ($T_{\mathrm{INSP, ij}}$)	Slight	0	0	-
		Above slight	0.5	0.1	1.08
Delay Phase 2	Engineering mobilization & review/redesign ($T_{\mathrm{ENGM, ij}}$)	Slight	6	-	0.07
		Moderate/extensive	12	-	0.03
		Complete	50	-	0.01
	Financing ($T_{\mathrm{FINA, ij}}$)	Insurance	6	3	0.19
		Private loans	15	7.5	0.05
		SBA-backed loans	48	24	0.01
		Savings/others	48	24	0.01
	Contractor mobilization ($T_{\mathrm{CONM, ij}}$)	Slight	7	1	0.09
		Above slight	19	11	0.02
Delay Phase 3	Permitting ($T_{\mathrm{PERM, ij}}$)	Slight	1	0	0.86
		Above slight	8	0	0.04

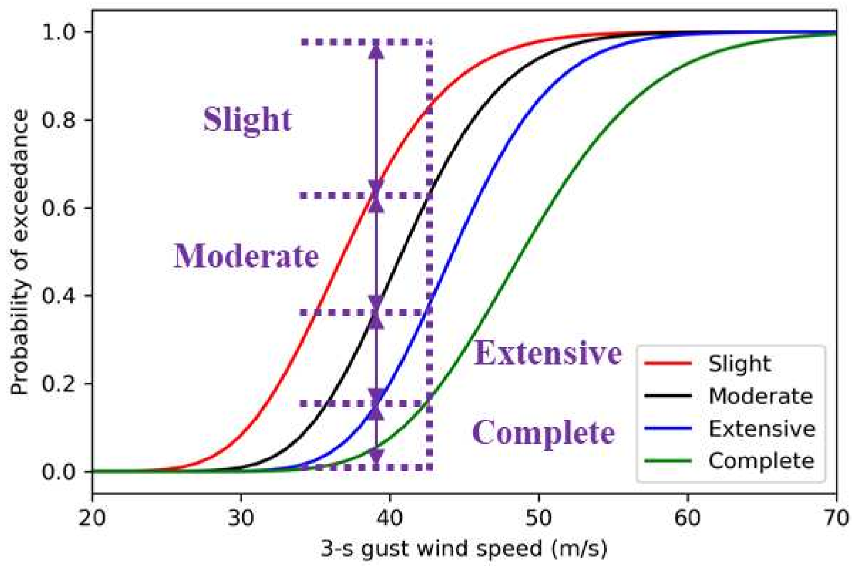

Figure 5-3. Fragility curve of a woodframe residential building subjected to a hazard (tornado)

For residential buildings, a household's income has been considered a socio-demographic indicator that can describe how households can access different financial resources (Carvalho et al. 2016). Equation (5.4) presents an estimation of the time used for financing delays, where *n* refers to four specific funding options considered herein, including homeowners insurance, SBA-backed loans, private loans, and savings/others. The indices *i* and *j* are still representative of each realization in the MCS and building identification itself, respectively; $P[T_{n,ij}]$ is the probability of the households to access one of the financial options as discussed, and $T_{n,ij}$ is the estimated time derived from cumulative lognormal functions. It is assumed in the model that each household does not assess two or more financial resources, and the probability of different household groups to approach a single financial resource is different.

$$T_{FINA,ij} = \sum_{n=1}^{4} P[T_{n,ij}] \cdot T_{n,ij} \tag{5.4}$$

The income distributions at the census tract level can be derived from the dataset developed by the American Community Survey (ACS), which is a continuous survey led by the U.S. Census

Bureau. However, issues such as missing data are unavoidable due to a lack of response by households or incomplete reports provided by the household. Therefore, when the household income information cannot be fully measured/estimated by household surveys or the specific algorithm, it is necessary to predict (extrapolate) the missing data in order to estimate financing delay times for all housing units affected by the hazard exposure. This chapter proposes what is believed to be a feasible and relatively straightforward predictive approach to use a Gaussian model to predict missing data combined with the existing procured income data. The approach incorporated housing unit de-aggregation from the census block level, as shown in Equation (5.5), where $I_{phh,imk}$ is the predicted household income and $I_{hh,mk}$ is the known household income of the k^{th} housing unit in the m^{th} census block for the i^{th} realization of the MCS. The first level of the Gaussian function is used to obtain the statistics of the household income distribution at the census block level using all the known U.S. Census household income data. The second level of the Gaussian function is then used to predict the missing household income for specific households using the determined Gaussian distribution census block in which the household with missing census data is located. This step uses MCS to make the prediction probabilistic. The motivation for this process is that, currently, census block level is the minimum geographic unit publicly reported by U.S. Census Bureau in order to maintain individual privacy.

$$I_{phh,imk} = \begin{cases} I_{hh,mk} & I \in I_{hh,mk} \\ \Phi\left(\Phi^{-1}\left(I_{hh,mk}\right)\right) & I \notin I_{hh,mk} \end{cases} \tag{5.5}$$

5.2.2 Repair Time Assessment

To this point in the , the methodology has been presented in a general sense for any hazard event. Although any repair fragilities could be implemented in the step described in this section, the authors move to a hazard-specific explanation, namely tornado hazard, to enable clarity for the example presented later. In this chapter, repair time was developed following the steps of combining isolated component damage fragility and consequence functions (i.e., repair estimates) introduced in the FEMA P-58 (FEMA 2012) methodology and then assembling the repair fragility functions from building component levels to system levels (Koliou and van de Lindt 2020). Table 5-2 presents tornado repair fragility functions of residential buildings for different damage states to reach full functionality (Q=100%), and Table 5-3 demonstrates the defined damage combination and functionality level for woodframe residential buildings. Please refer to Koliou and van de Lindt (2020) for details on the definitions of performance level and operational status for all building archetypes in detail. Figure 5-4 depicts the approach estimating the repair time for each building within MCS. For each realization of the MCS, a random number between 0 and 1 was generated and then combined with the initial damage state for the building to assess the required repair time. Note that the fragilities only refer to the building repair time due to damage without considering external parameters such as crew availability, which means the time used for delay and repair in this chapter does not overlap.

Table 5-2. Repair fragilities for woodframe residential buildings (days)

Damage states	Mean of the natural logarithm (μ)	Standard deviation (σ)
DS1	3.09	0.51
DS2	3.52	0.55
DS3	4.62	0.55
DS4	5.19	0.52

Table 5-3. Damage combination and functionality level for woodframe residential buildings

Functionality Q (%)	Damage combination	Description of damage combination			
		Roof cover failure	Window/door failures	Roof sheathing failure	Roof truss failure
100	-	-	-	-	-
75	DS1	>2% and ≤15%	1	No	No
50	DS2	>15% and ≤50%	2 or 3	1-3 panels	No
25	DS3	>50%	>3	>3 panels and ≤35% by area	No
<25	DS4	Typically>50%	Typically>3	>35% by area	Yes

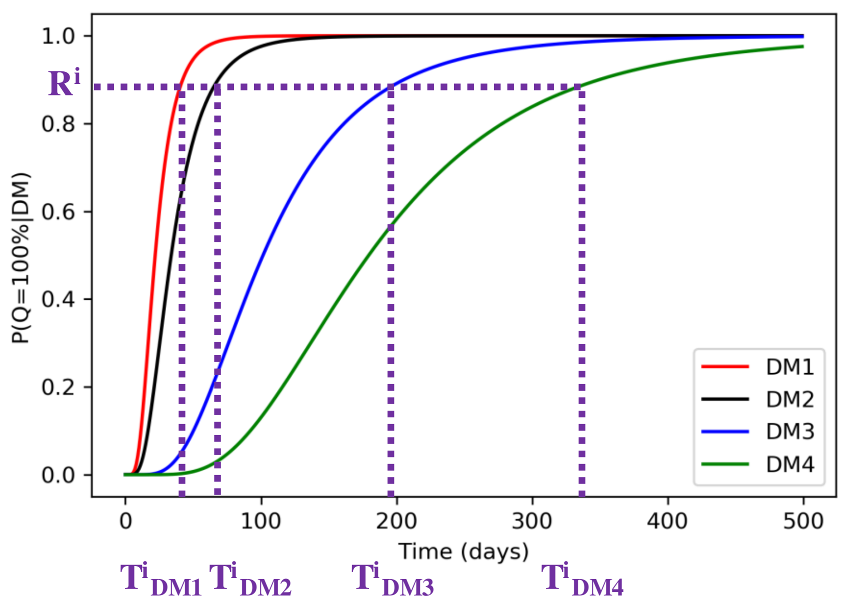

Figure 5-4. Repair fragility curves within a single MCS scenario

5.2.3 Recovery Time Assessment

Following the immediate damage, the total time required for each building to be fully restored can be determined by combining delay time and repair time. It is assumed that the two stages of building recovery (delay and repair) are statistically independent, but it is noted that correlation could be included using a copula approach if evidence of correlation becomes known. The recovery results can be presented as histograms for a single building, a single sector (i.e., household, business, healthcare, education), and even the entire community. A three-parameter Weibull distribution was used to fit the recovery time statistics for each building for modeling efficiency.

In order to track the community recovery performance, a building recovery over time, the model steps through time by quarter, as shown in Equation (5.6) and Equation (5.7), where $B_{rj}^{i}(t)$ is the building recovery performance indicator of the j^{th} building at the r^{th} quarter in the i^{th} realization. $R_r(t)$ is the time by quarter (90 days, 180 days, etc.) and $R_{j,th}^{i}$ is the calculated recovery time of buildings as thresholds. $RP_{rj}(t)$ is the quarterly recovery probability continuously increasing over the analysis period based on MCS. For each time step, the probability that each building is fully recovered and therefore the percentage of residential buildings that are fully restored can be calculated.

$$B_{rj}^{i}(t) = \begin{cases} 1 & R_r(t) \geq R_{j,th}^{i} \\ 0 & R_r(t) < R_{j,th}^{i} \end{cases}, i \in 1,2,\dots,n \tag{5.6}$$

$$RP_{rj}(t) = \frac{\sum_{i=1}^{n} B_{rj}^{i}(t)}{n}, i \in 1,2,\dots,n \tag{5.7}$$

5.3 Policy Levers

Post-disaster policies (policies that take effect in the event of a disaster) aim to create strategic plans to help expertly guide the completion of repair across the community. These policies can be related to delay time variables for completing building restoration or refer to the assessment of available resources available to a household (Sutley and Hamideh 2018). In general, flexibility in existing policies and programs is more critical than implementing rigid policies to effect recovery following a natural or human-induced disaster (Richmond 2019). Excessive government involvement might result in increased costs and interruption in the recovery process. After the 2011 Joplin tornado occurred, city and state officials published a series of policies. The policies, which included decisions such as relaxing regulations and avoiding micromanagement, were implemented to facilitate the recovery. Regulatory relief allowed local businesses to maintain operations, and quickly recovered the Joplin Public Schools and let them re-open on time for the next academic year (Smith and Sutter 2013) with some relocation. This chapter proposed a series of policies referring to the real environment after the 2011 Joplin tornado, expanded the proposed methodology, and quantitively measured how the community recovery was impacted by these policies. Table 5-4 provides selected policies that positively impact community recovery and shows examples of their combinations as potential policy cases for a community.

Recall the relationship between delay time and building damage conditions shown in Table 5-1. Building retrofits improve the performance of buildings and reduce damage for buildings within the tornado path (Amini and van de Lindt 2014), and therefore delay times such as for inspection, and contractor mobilization will be shorter since damage is less significant. In general, where damage is reduced for some portion of the buildings, both delay time and repair time are shortened accordingly. In this chapter, woodframe residential building retrofits are reflected in the different construction product combinations such as roof covering, roof sheathing nailing patterns, and roof-to-wall connections. See Wang et al. (2021b) for a description of wind retrofit strategies on residential buildings. In this chapter, the construction product combination of asphalt shingles, 8d nails with 150mm (6 in) edge nail spacing and 300mm (12 in) field nail spacing for roof sheathing, and two 16d toenails for the wall to roof truss connection was considered to be the base case without any retrofits. The retrofit case consisted of clay tiles, 8d nails with 150mm (6 in) edge and field spacing for the roof sheathing, and two H2.5 hurricane clips connecting the roof truss and wall. Additionally, if the city or county can relax building permit requirements for wood frame residential buildings, the recovery process can be moderately expedited. It is assumed that the city can choose to relax certain regulations and allow homeowners to schedule repairs without obtaining a permit. Another approach is to hire extra building inspectors, which allows time reduction for home inspectors when there is a demand surge after a hazard event. A typical inspection of a house under 95 sq. meters (1000 sq. ft) takes 2 to 3 hours, so one inspector can perform three to five per day. For contractor mobilization, the bidding process for procurement takes typically 30 days for heavily damaged buildings since the losses are significant and competitive bids need to be sought. Provided that the bidding is waived by the insurance company (or other) for procurement, only the procurement and management of items (e.g., labor, equipment, material) and their delivery to the site is needed. This is felt to be a relatively practical approach that may help reduce recovery time. Upon receiving claims from homeowners following a tornado (or any event), an insurer decides whether to accept or deny the claim. Having financing in place shortens the time needed to begin the next delay phase, thus the duration to obtain financial assistance was assumed to be cut in half to model when financing is in place in this chapter. Currently, the cost of different policy combinations and the budget limits for government investments are not considered and are beyond the scope of this chapter. Some other useful policies which cannot be directly related to the delay variables introduced in the REDi framework, such as the use of social media, were not considered herein, since quantitative effects for these are not yet available.

Table 5-4. Policies and their combinations as policy cases that can facilitate community recovery progress

Index	Policy	Case 1	Case 2	Case 3	Case 4	Case 5	Case 6	Reference
1	Building retrofits		X				X	Sutley and Hamideh (2018)
2	Relax building permits issuance			X		X	X	Sutley and Hamideh (2018)
3	Hire extra building inspectors			X		X	X	Smith and Sutter (2013)
4	Waive bidding rules for procurement			X		X	X	Smith and Sutter (2013)
5	Have financing in place				X	X	X	Lindell and Prater (2003)

5.4 Illustrative Example and Validation

Tornadoes, which are low-probability high-consequence natural hazard events, result in numerous damage and casualties associated with high socio-economic and environmental costs through an entire community (Simmons et al. 2013, Standohar-Alfano and van de Lindt 2015, Masoomi and van de Lindt 2018, Changnon 2009). Over the last two decades, tornadoes have caused almost 1,500 fatalities, 20,000 injuries, and $30.3 billion property damage loss in the U.S. according to the National Weather Service (NOAA 2020). The 2011 Joplin tornado was a devastating EF5 multiple-vortex tornado and ranked as the deadliest and costliest single tornado in U.S. history. A comprehensive field investigation was performed to make recommendations for other communities related to tornadoes (Kuligowski et al. 2014), and a number of researchers performed analyses related to this event (e.g., Attary et al. 2018, Prevatt et al. 2012, Roueche and Prevatt 2013).

As a small to medium size community in the United States, Joplin in the Midwest state of Missouri, was selected to illustrate and validate the proposed approach for a two-step recovery model for residential buildings that is able to step through time thereby allowing the analyst to explore the impact of policy levers on community recovery with the goal of eventually providing the results to support decision making for stakeholders and community planners. Wang et al. (2021b) performed a functionality analysis using the Joplin testbed to consider the interdependency between buildings and electric power networks and examined the effect of wind events on a basic set of physical and socio-economic resilience metrics. The detailed building dataset and the simulated EF5 tornado hazard used herein were not illustrated again, and the interested reader, is referred to Wang et al. (2021b). Note that a reproduceable Jupyter Notebook, including all the data, analyses, and visualization described in Wang et al. (2021a) is available online at https://incore.ncsa.illinois.edu. It is known that tornadoes have small footprints and, although a very large tornado, the Joplin tornado only hit a small geographical area of Joplin and many buildings fell outside the path of the tornado remaining undamaged. Woodframe residential buildings are the most vulnerable building sector to wind events and therefore, the recovery modeling of residential buildings located within the tornado path is the focus herein.

5.4.1 Probabilistic Initial Building Damage

Tornado fragilities together with the simulated wind speeds at each location, were combined to estimate the building damage for each building across the community (see Figure 5-3). Please refer to Masoomi et al. (2018) regarding tornado fragilities for five residential building archetypes and their descriptions (e.g., the number of stories, building sizes/area). Figure 5-3 shows the fragility functions of a typical woodframe residential building (archetype 4) as an example. Table 5-5 indicates building spatial damage results in a typical single realization within MCS. Note that of damage levels, as indicated in Table 5-5 are, 1 is slight, 2 is moderate, 3 is extensive, and 4 is complete. It can be observed from Table 5-5 that more than 85% of residential buildings within the tornado path were initially damaged at the complete level in this single realization. For each realization, probabilistic initial building damage results were then used to estimate the delay time and repair time.

Table 5-5. A typical scenario of initial building damage

Building specific conditions	Building count
Slight	174 (3.3%)
Moderate	181 (3.4%)
Extensive	234 (4.4%)
Complete	4,738 (88.9%)
Grand total	5,327 (100%)

5.4.2 Financial Resources for Repair

Low-income and ethnic minority families are more vulnerable to the risks of disasters and struggle most to recover. One of the reasons is that low-income households are more likely to reside in neighborhoods that are more susceptible to environmental shocks, and they do not have many choices to relocate to safer areas (Krause and Reeves 2007). However, this is less true for tornadoes than many hazards. For particular socio-economic groups described above that have a lower probability of being able to access some funding sources such as insurance and loans, savings and other community-level resources may be options to perform repairs/reconstruction. In this chapter, five household groups are differentiated by annual household income as shown in Table 5-6 to span the wealth distribution across the community. It is assumed that households belonging to income groups over HH3 are homeowners. HH1 is mostly a group for renters, and HH2 has a balance of low-income homeowners and renters. In Missouri, about 90% of homeowners are insured (Insurance Agency Plano 2014), and the number of people with renter's insurance is far less 27 percent (Joplin Globe 2011). In general, for homeowners with an annual income of over US$30,000, an increase in household income of US$11,000 increases the likelihood of insurance purchases by approximately one percent (Landry et al. 2021). Overall, insurance is the dominant resource for households impacted by wind damage, while SBA-backed loans and private loans are also important resources for low-income households to consider. The reason is that homeowners (and renters) insurance can be quite a burden for low-income families if not required, and the premiums may account for too significant percentage of their monthly household income. In theory, SBA-backed loans are preferable compared to private loans since they have lower interest even though the processing time might be longer. Unfortunately, SBA loans go to those who would have qualified for commercial loans, not the households in the greatest need because the ability to repay is always a crucial issue. Therefore, the probability of low-income households receiving SBA loans is limited as well (Lindell and Prater 2003).

Table 5-6 shows the deterministic household restoration financial resource distribution based on information from the literature described above. The percentages shown in Table 5-6 are the probabilities of households funding their repairs through the different financial resources. For example, households with an annual income below $15,000 will only have a low probability of obtaining funding supported by insurance and SBA-backed loans. In order to survive and recover from the disaster, this group of households more likely depends on their savings or other means such as family/friends. Conversely, households with an annual income of over $100,000 will have homeowner's insurance.

Table 5-6. Household restoration financial resource distribution

Household income group	Insurance	SBA-backed loans	Private loan	Savings/others
HH1 (less than $15,000)	30%	5%	0%	65%
HH2 ($15,000 to $24,999)	50%	5%	5%	40%
HH3 ($25,000 to $74,999)	80%	10%	10%	0%
HH4 ($75,000 to $99,999)	85%	15%	0%	0%
HH5 (more than $100,000)	100%	0%	0%	0%

5.4.3 Housing Unit De-aggregation at the Census Block Level

In order to employ annual household income as an indicator to determine household financial resources during the recovery process, household income group information needs to be collected or determined first. This information was determined through data merging at the housing unit level based on the ACS (2012) 5-year survey. The household income came from a combination of tables B19001 and B19101. This variable was designed to provide income comparable to income distributions by race/ethnicity associated. The allocation of income to a physical location does not represent the actual income for the household. Please refer to Rosenheim (2020) for the detailed household income dataset created by the housing unit allocation algorithm. The building dataset was developed for Joplin circa 2010 prior to the tornado, thus allowing some level of validation ten years later. There are 7,201 housing units contained in 5,327 buildings in the path of the Joplin tornado for Joplin based on the 2010 Decennial Census.

After completing the household income prediction by applying the housing unit allocation algorithm, there are still 10.5% of housing units with missing household income information (see Table 5-7). The reason for missing values for household income might be that the household has income, but the characteristics (race/ethnicity) did not match between the 2010 Census and the 2012 ACS at the census tract scale. Future research is required to reduce the number of missing values, especially for minority households. It is important to mention that 656 housing units are vacant, and 6 housing units are group quarters such as nursing homes, but the household income prediction from the housing unit allocation algorithm does not consider such cases, introducing error into the approach.

Table 5-7. Housing unit inventory within the tornado path

	Owner-occupied	Renter-occupied	Housing unit count	Household income missing
1-person household	1,035	1,177	2,212	147 (6.6%)
2-person household	1,135	842	2,177	293 (13.5%)
3-person household	483	487	970	146 (15.1%)
4-person household	371	325	696	97 (13.9%)
5-person household	160	138	298	43 (14.4%)
6-person household	66	56	122	22 (18.0%)
7-person household	37	27	64	9 (14.1%)
Group Quarters	-	-	6	-
Vacant	-	-	656	-
Total housing units	3,487	3,052	7,201	757 (10.5%)

Census geographic entities cover the entire United States, with the smallest being census blocks (e.g., 15-digit ID 290970108003013), which aggregate into census block groups (e.g., 12-digit ID 290970108003) and then census tracts (e.g., 11-digit ID 29097010800). Figure 5-5 shows geographic maps for Jasper County and Newton County in Missouri at different census levels. Residential buildings located in the tornado path were distributed across 10 census tracts, 28 census block groups, and 437 census blocks, respectively. Thus far, the census block is the smallest geographic unit published by the U.S. Census Bureau in order to maintain data confidentiality. Therefore, housing units were de-aggregated to the census block level in order to predict the missing income data accurately. Housing unit details and buildings with single or multiple dwellings were tracked by unique identifiers (Housing unit ID and Globally Unique Identifier (GUID) respectively) (e.g., B290970108003013H001 and 146afdcb-271f-4b7d-85ad-66b9296aefc3).

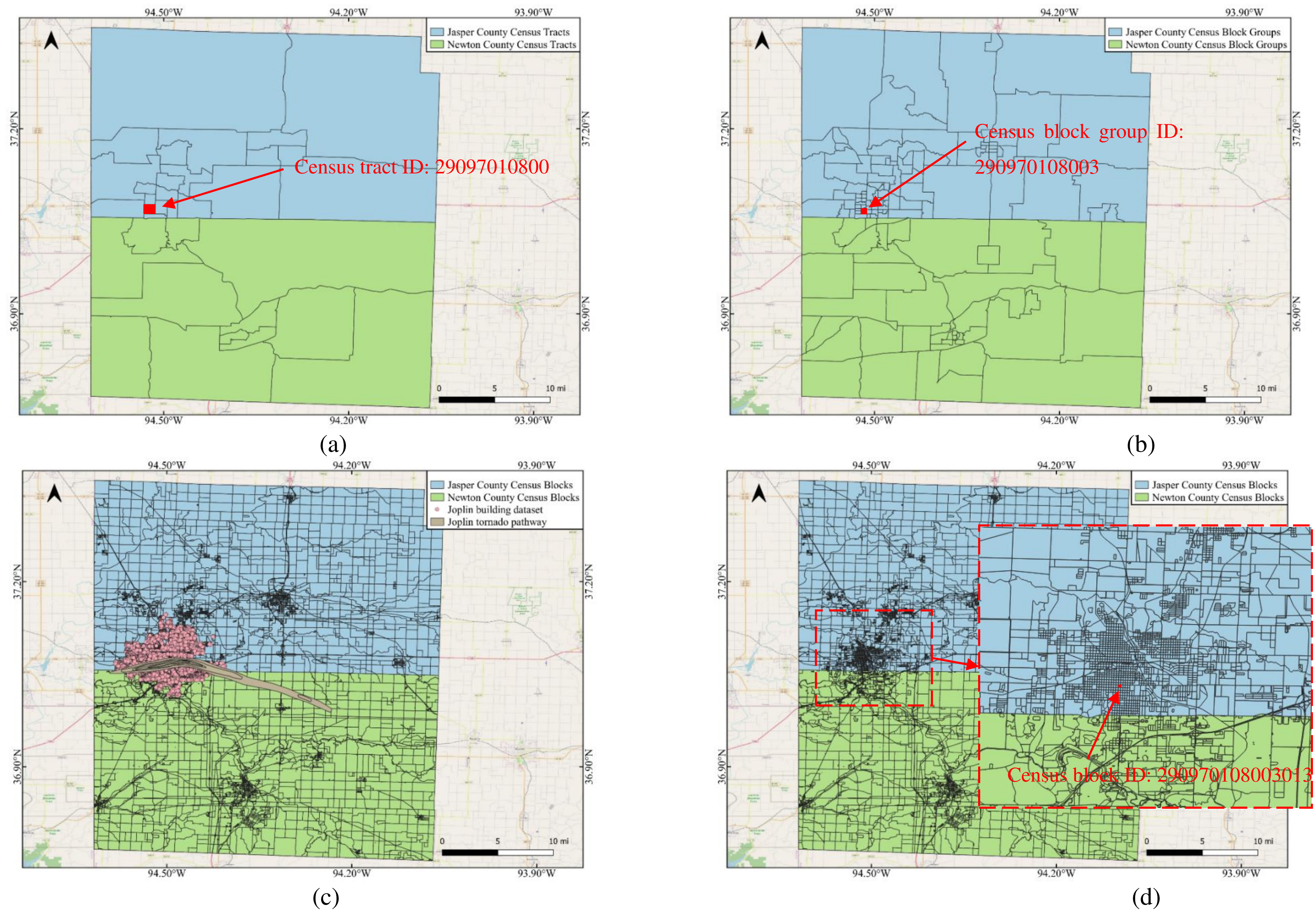

Figure 5-5. Geographic maps for Jasper County and Newton County in MO at different census levels: (a) census tracts; (b) census block groups; (c) census blocks as well as Joplin buildings and tornado pathway; (d) census blocks

Table 5-8 illustrates an example of the socio-demographic data for housing units in a typical census block, as highlighted in Figure 5-5(d). The information on ownership and the number of people predicted by the household allocation algorithm illustrates that all the 16 housing units resided in this census block were allocated as neither vacant nor as group quarters. Still, two of them are missing income group data. Therefore, it is necessary to predict the missing data at the minimum geographic unit by assuming that housing units in a census block can be sampled from the statistics of the block (recall Equation (5.5)). For each realization of the MCS, known income groups assigned to each house remained the same to ensure recovery was tracked for each allocated household. The recovery modeling performed in this chapter conducted the analysis at the building level, while the allocation of income groups described their income distribution at the household level. For multi-family buildings, the income groups were aggregated from household levels to building levels by selecting the housing unit having the highest annual income group. It is assumed that housing units with the highest estimated income group had the best restoration financial resources, which could be used to recover the multiple dwelling unit.

Table 5-8. The socio-demographic data of housing units in a typical census block

Housing unit IDs	Globally unique identifiers	Number of people	Owner ship	Household income group	Census block ID	Census block group ID
B290970108 003013H001	146afdcb-271f-4b7d-85ad-66b9296aefc3	3	2	HH3		
B290970108 003013H002	d88d7424-ee89-4788-9e05-df4c119f3ad0	2	2	HH3		
B290970108 003013H003	aad8e322-f2c8-4d9a-94ca-c301f93f20a3	7	1	HH3		
B290970108 003013H004	6d492f9a-0f48-437c-b00a-2e7866a86a68	3	1	HH5		
B290970108 003013H005	1db6a71e-8480-458b-aafd-1c9bb5a31fd1	1	2	HH1		
B290970108 003013H006	d88d7424-ee89-4788-9e05-df4c119f3ad0	3	2	HH3		
B290970108 003013H007	00205cab-e68f-42c9-a89a-4a47889795c1	2	2	-		
B290970108 003013H008	75236b8e-56a2-49be-bfc9-b499aa5dd446	5	2	HH3	290970 108003 013	290970 108003
B290970108 003013H009	75236b8e-56a2-49be-bfc9-b499aa5dd446	6	2	HH3		
B290970108 003013H010	1db6a71e-8480-458b-aafd-1c9bb5a31fd1	1	2	HH3		
B290970108 003013H011	683cf9a0-fe39-4376-abe2-380101b98327	2	2	HH3		
B290970108 003013H012	53c0bb86-8444-456f-94a0-587ad04287d9	1	2	HH1		
B290970108 003013H013	a55bce1a-e0e1-4ce1-ba7b-4b4a0afb8dfb	4	1	HH2		
B290970108 003013H014	6d492f9a-0f48-437c-b00a-2e7866a86a68	3	1	-		
B290970108 003013H015	aad8e322-f2c8-4d9a-94ca-c301f93f20a3	3	2	HH3		
B290970108 003013H016	cc60e8bf-a4f3-4e4f-bb46-b5a1ca340365	4	2	HH3		

Note: 1 is owner-occupied and 2 is renter-occupied in the column of ownership. The household income group column corresponds to the wealth distribution shown in Table 5-6.

5.4.4 Recovery Modeling Results

The probabilistic residential recovery modeling described throughout this chapter was implemented for each of the policy cases described earlier. Figure 5-6 and Figure 5-7 show delay time results and recovery time results for two typical residential buildings at different damage levels under Case 1, respectively. The results of MCS realizations are shown in histograms as well as the fitted Weibull distribution curves and parameters. Recall that recovery time, which means the total time needed for buildings to be fully restored, consists of two independent steps: delay time and repair time. It is evident that delay time dominated throughout the recovery process for residential structures, but this is likely not the case for other types of buildings where repairs take much longer, e.g., hospitals, schools, office buildings. For example, the mean recovery time for a typical building shown in Figure 5-6 was 97.2 weeks and the mean delay time accounted for 62.6 weeks. Households need at least several months to as much as two years before initiating the repair process to schedule inspection, contact engineers and contractors, and so forth. Additionally, since both delay time and repair time are directly related to initial building damage levels, buildings damaged at a higher level will, on average, take more time to achieve full recovery (see Figure 5-6 and Figure 5-7). Note that the recovery time of each building was calculated and tracked, and that only two typical residential building recovery distributions were shown herein for brevity. It is worth noting that the ability to utilize MCS and produce statistical distributions for each building within a community enables full uncertainty propagation into the broader community models.

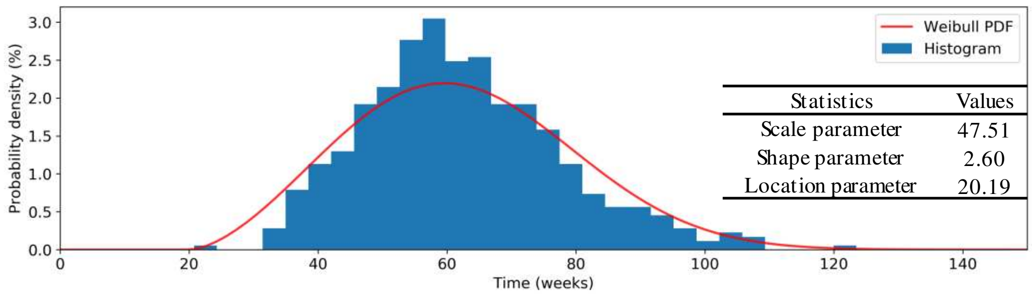

(a)

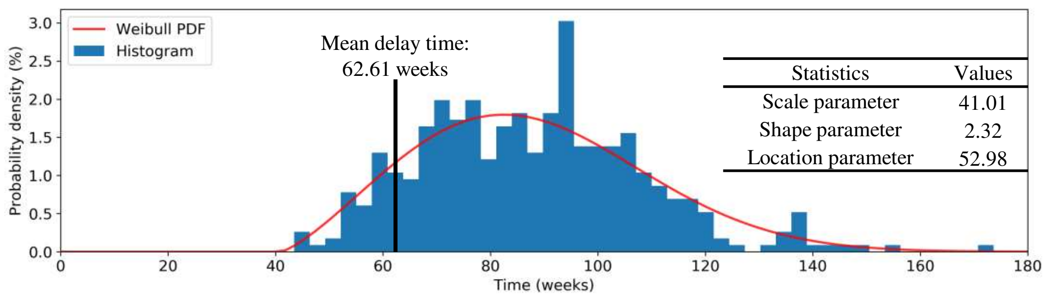

(b)

Figure 5-6. A typical residential building in the mean damage level of 3.998: (a) delay time results; (b) recovery time results

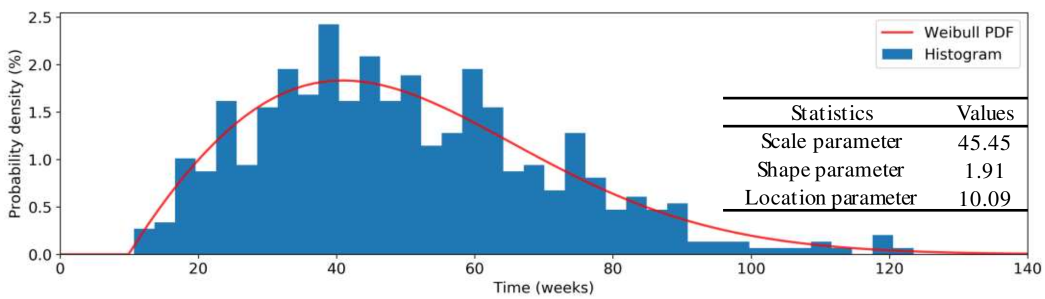

(a)

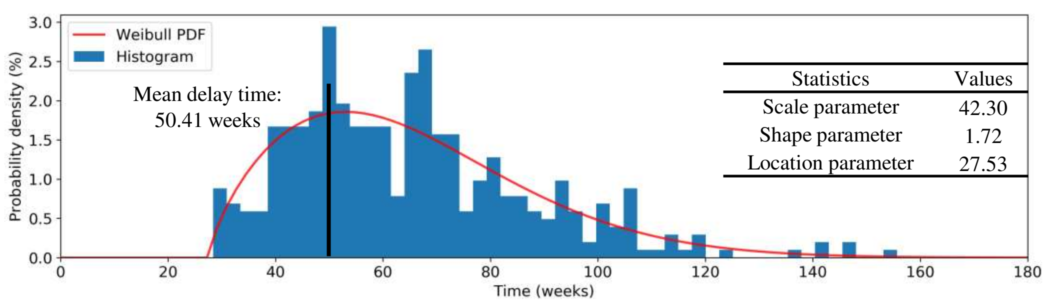

(b)

Figure 5-7. A typical residential building in the mean damage level of 2.744: (a) delay time results; (b) recovery time results

Figure 5-8 shows the building recovery when different policy cases (combinations) are implemented community wide. The time shown in Figure 5-8 is the mean recovery time, mean delay time, and mean repair time of all the in-path residential buildings in a single realization. All the other realizations within the MCS have similar results for these parameters. Since Case 2 and Case 6 considered the policy of building retrofits, the repair time in these cases was shortened from 27 weeks to approximately 14 weeks, on average. Note that building retrofits were assumed to be implemented to all buildings right now, which not realistic for a community. Additionally, all the policy cases decreased recovery time. Overall, Case 6, incorporating all the proposed policies, enabled recovery 2.4 times faster (i.e., 88.4 weeks reduced to 36.6 weeks) than the base case of no new policies or mitigations/retrofitting. If only examining the impact of a single policy, mandatory retrofits requested by Case 2 facilitated the recovery by 1.7 times than the base case. Other cases related to the relaxation of regulations (e.g., bidding, inspection) and having financing in place are also shown slightly to speed up the recovery. However, the resulting decrease in the time resulting from delay variables did not offset the time required for engineers to review and redesign due to the damage. Thus, Case 3, Case 4, and Case 5 also shortened the recovery time, but the effects were not noticeable.

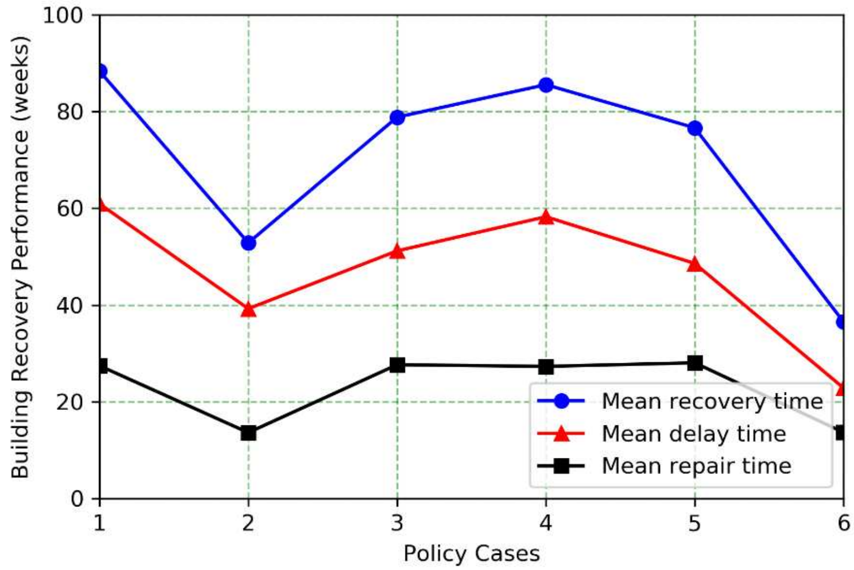

Figure 5-8. Building recovery performance impacted by different policy cases

Quarterly building recovery at a community level under the six policy cases was calculated and compared. Figure 5-9 illustrates the building post-disaster recovery probability at a community level for Case 6 as an example. After 90 days following the tornado, almost all the residential buildings that were within the EF 2 and higher wind regions still had a probability of less than 0.2 for completion of recovery, and only a few buildings in the EF1 region had a possibility of getting back to normal. For Case 6, which included all the proposed policies and mitigation strategies, the percentage of buildings 100% recovered was 51.5%, 85.4%, and 98.6% after 1.5 years, 3 years, and 4 years, respectively. However, if only Case 1 is considered, the percentage of buildings achieving recovery in these same time periods was only 0.3%, 29.47%, and 88.49%.

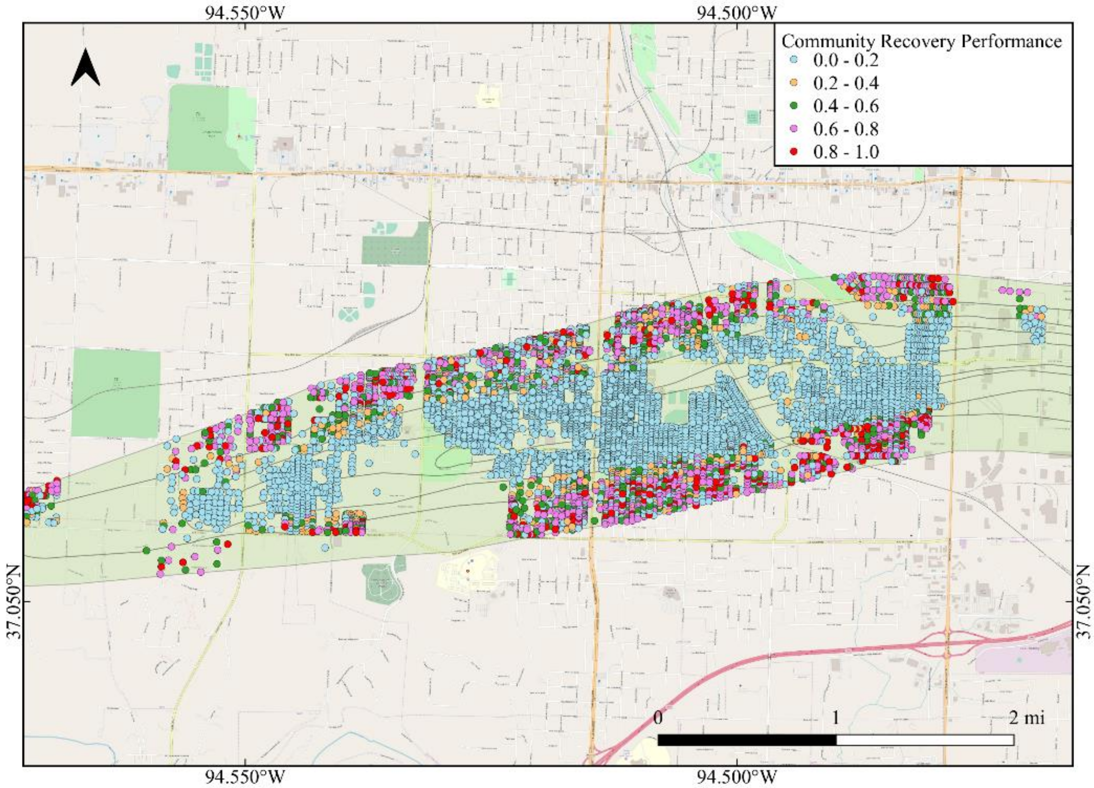
94.550°W
94.500°W
Community Recovery Performance
0.0 - 0.2
0.2 - 0.4
0.4 - 0.6
0.6 - 0.8
0.8 - 1.0
37.050°N
0
1
2 mi

(a)

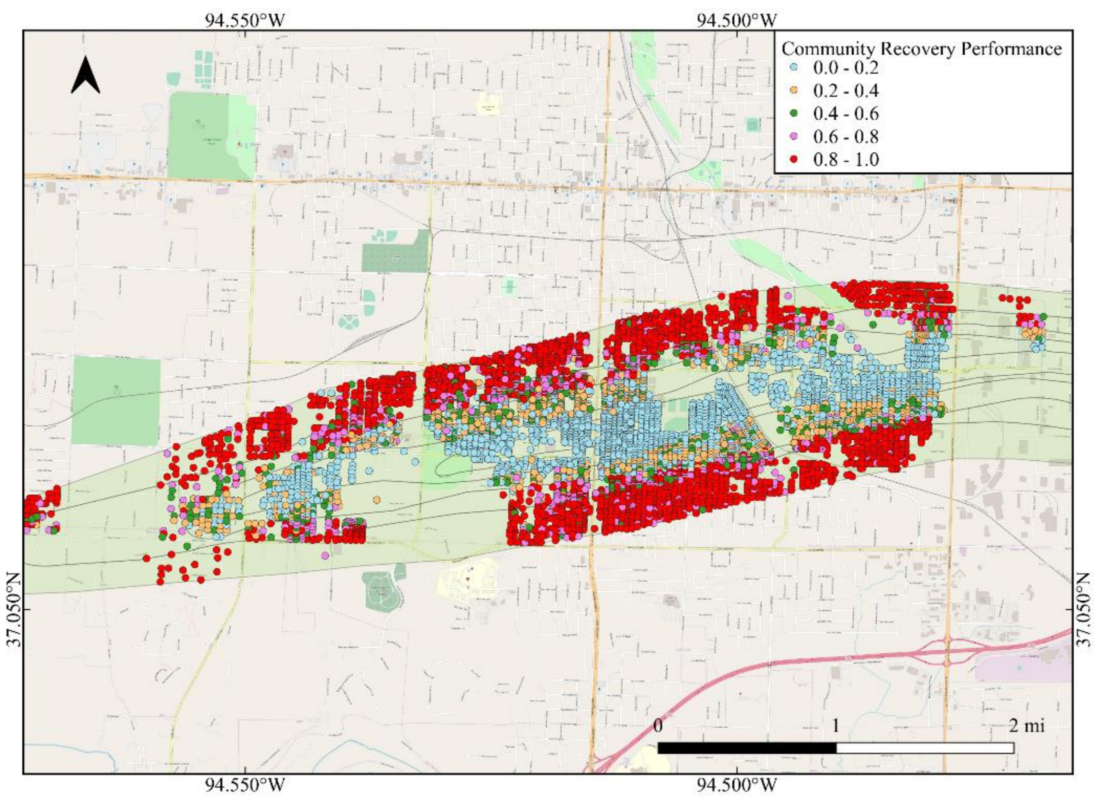
94.550°W
94.500°W
Community Recovery Performance
0.0 - 0.2
0.2 - 0.4
0.4 - 0.6
0.6 - 0.8
0.8 - 1.0
37.050°N
0
1
2 mi

(b)

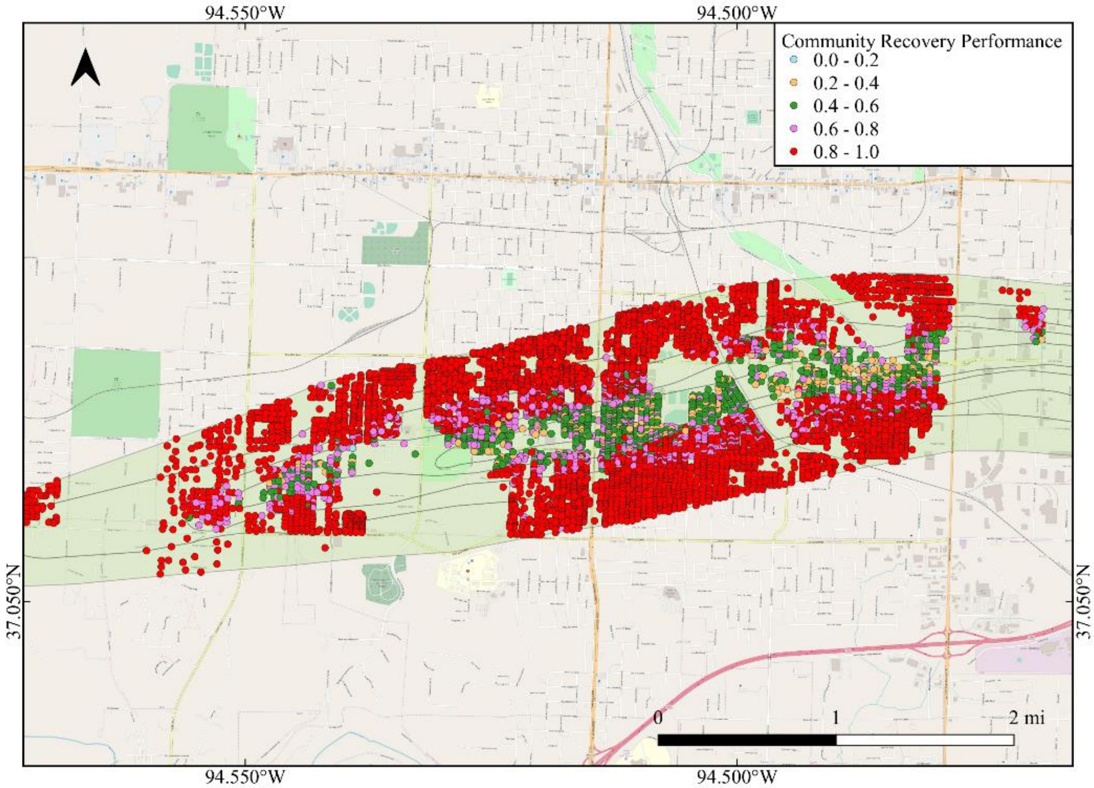

(c)

Figure 5-9. Time-stepping building recovery performance probability under Case 6: (a) time = 1 quarter; (b) time = 2 quarters; (c) time = 6 quarters

In addition to the community-level recovery presented in Figure 5-9, the probability of the mean building recovery times, defined as the average of the percentage of buildings fully recovered, as shown in Equation (5.8). Figure 5-10 illustrates the probability for the mean building recovery times for several of the cases explored in this chapter. The significant difference among cases was the probability at the short-term and intermediate recovery stages. The probabilities of mean building recovery times were 0.09, 0.58, 0.16, and 0.74 in the first year after the tornado and were increased to 0.73, 0.91, 0.84, and 0.95 in the second year under Case 1, Case 2, Case 5, and Case 6, respectively. It is worth mentioning that the restoration curves for Case 3 and Case 4 were close that of Case 1 and were not included in the plot to provide clarity.

$$RP_{r\_mean}(t) = \frac{\sum_{j=1}^{N} RP_{rj}(t)}{N} \tag{5.8}$$

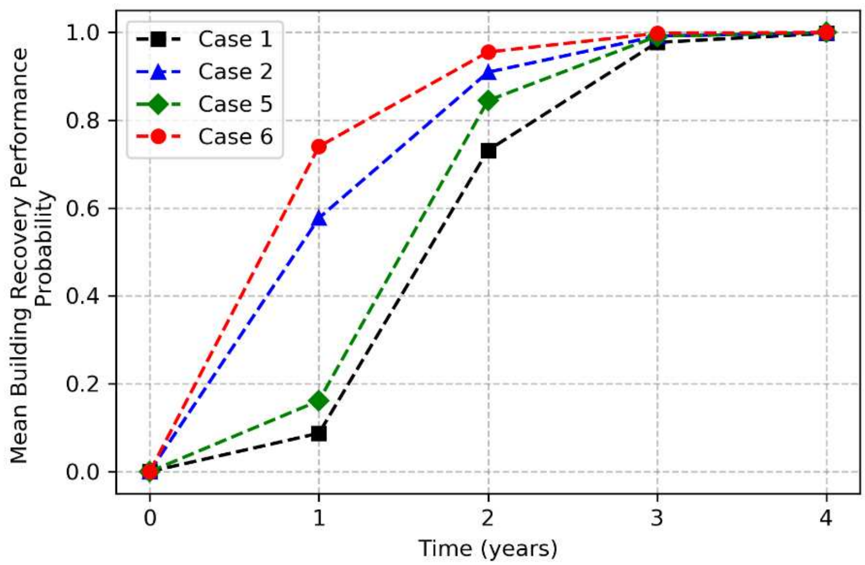

Figure 5-10. Time-stepping building recovery trajectory impacted by different policy cases

5.4.5 Validation and Discussions

As described in the paper developed by Pilkington et al. (2020), researchers used spatial videos along with a Global Positioning System (GPS) receiver to perform a longitudinal field study in the city of Joplin after the 2011 tornado. The damaged buildings were scored based on their recovery states following the defined description in detail, and then Aghababaei et al. (2020) converted the scores to the corresponding functionality levels (i.e., DM1, DM2, DM3, DM4) introduced in Koliou and van de Lindt (2020). Figure 5-11(a) overlays the simulated dataset of 5,327 residential buildings from the Joplin testbed example and the field investigation dataset of 1,874 residential buildings. The red dots shown in Figure 5-11(a) are the overlapping points on top of the green dots, which were tracked by GPS coordinate. This chapter used the longitudinal field study results of these 1,874 residential buildings, which are presented in the bar chart in Figure 5-11(b), in order to validate the analytical results determined from the proposed probabilistic residential recovery modeling. Note that more buildings were included in the longitudinal study over five years, with some of them being commercial, industrial, schools, and hospitals rather than residential buildings involved in this chapter.

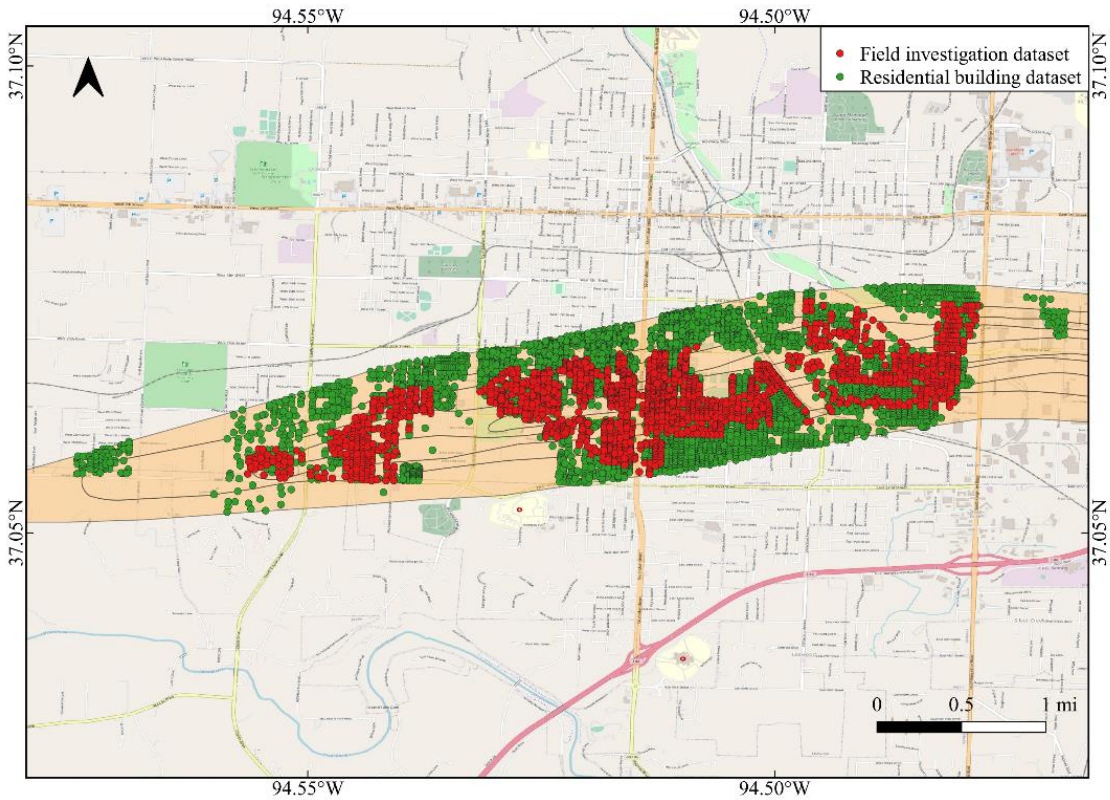

(a)

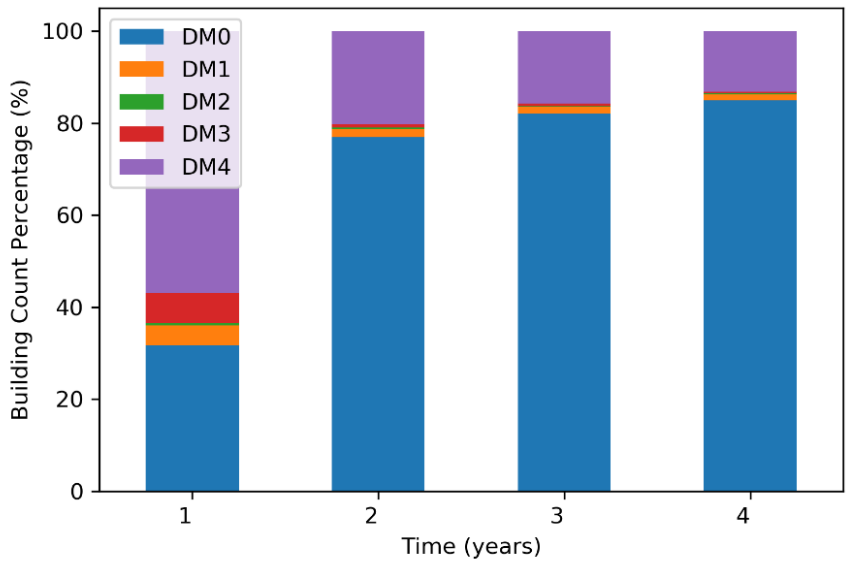

(b)

Figure 5-11. Field investigation data: (a) the overlay between field investigation dataset and the simulated residential building dataset; (b) functionality levels of residential buildings over the time from the field investigation

The analytical results of the same 1,874 residential buildings were extracted and compared with the empirical results for validation. After the Joplin tornado, city and state officials organized and facilitated the recovery process by temporarily relaxing regulations, hiring extra building inspectors, waiving procurement and bidding rules, and resisting the temptation to micromanage. Many different organizations, including the Red Cross, businesses such as Home Depot and Walmart, and individual contributors provided relief and supplies as needed and raised donations in the recovery after disasters (Smith and Sutter 2013). Therefore, this chapter used the time-stepping results under Case 5 for comparison to (approximately help) validate the methodology. Figure 5-12 shows the analytical and empirical results on the same plot. The green line (squares) and yellow line (diamonds) refer to the average of the percentage of residential buildings that are fully recovered, which is the same metric shown in Figure 5-10 using analytical results of partial buildings after the MCS. The difference is that the results for the yellow line assumed that all vacant units (see Table 5-7) were not repaired after the tornado, but the green line assumed all buildings would recover regardless of vacancy status. The pink line (triangles) shows the percentage of residential buildings that were fully recovered from any damage state at the specified time based on empirical results. It is evident that the analytical results and empirical results in the second year were close enough. As to the percentage in the first year, the empirical results were found to be higher than the analysis. Since the empirical results were derived from the analysis based on spatial videos, the damage or failure of some components like drywall inside the structures may not have been identified, so it is clear some level of uncertainty exists in the empirical analysis also. Recall that the analytical results shown in Figure 5-8, the mean delay time under Case 5 was 48.6 weeks, which was almost one year and the mean recovery time was 76.6 weeks. The residential buildings used for validation were mostly located in the higher-speed wind regions such as EF3, EF4, and EF5 regions (see Figure 5-11(a)). The modeling (analytical) results in the third year and fourth year were higher than observed (empirical) because population dislocation and/or outmigration was not considered in this chapter, and thus all the households were assumed to stay in the city and proceed to repair their damaged homes. However, this assumption is not accurate and would require inclusion of data-driven modeling methods to resolve. Specifically, some households will choose to outmigrate, or rebuild elsewhere, or simply abandon their property.

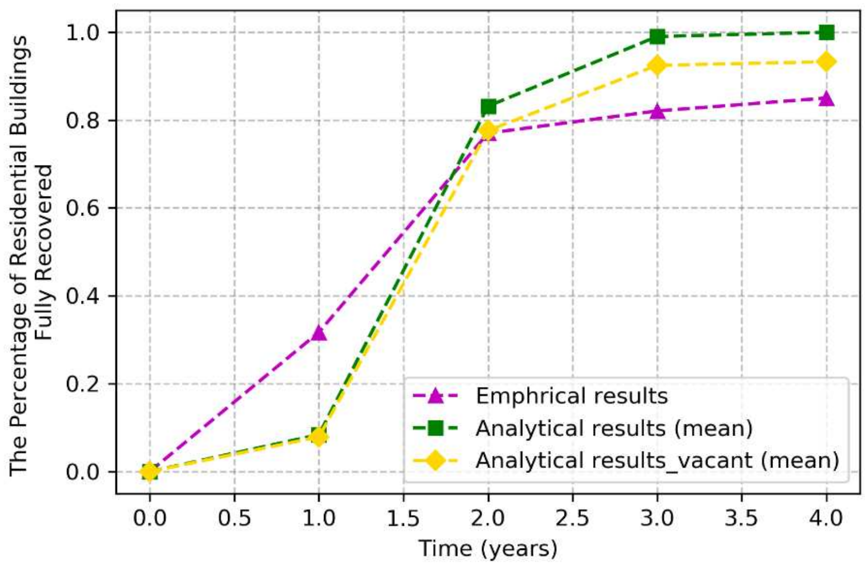

Figure 5-12. The difference between analytical results and empirical (observed) results

5.5 Summary and Conclusions

Post-disaster recovery planning can help decision-makers mitigate risk and facilitate the recovery process for their communities, and thus enhance community resilience. However, limited studies have performed an only qualitative analysis to evaluate the rapidity of community recovery impacted by dynamic policies. This chapter considered typical delay variables as well as repair fragilities for residential buildings for wind events. A time-stepping methodology to model residential building recovery was proposed and approximately validated based on existing longitudinal field investigation data. The recovery statistics were tracked for each building through the entire process from initial damage to full restoration. Based on the work described herein, the following conclusions can be reached:

- Delay time dominated throughout the recovery modeling process. For a typical building located in the EF5 region of the simulated Joplin tornado, the mean delay time was 62.6

weeks, which accounted for 64.4% of the mean recovery time totaling 97.2 weeks. This ratio of times may differ for other types of buildings.

- All the proposed policy cases affected the delay process to different extents. Based on the typical results of MCS in a single realization as an example, when considering the effect of building retrofits, the repair time was shortened from 27 weeks to 14 weeks, and the overall recovery process was expedited by 1.7 times. Case 6 involved all the proposed policies and mitigation strategies, enabled the recovery process to occur 2.4 times faster than the base case. Other cases related to the relaxation of regulations and financial support assessment were also shown slightly to speed up the recovery, but the results were not as significant.
- The percentage of buildings in the study area achieving full recovery after one and a half years, three years, and four years was 0.3%, 29.47%, and 88.49% accordingly under Case 1, which was improved to 51.49%, 85.41%, and 98.61% with the implementation of Case 6.

It is also important to point out the limitations of the methodology proposed in this chapter. First, the changes in the median for each component of the delay time for the policies were assumed and could be further improved upon with data. Second, no cost constraints or costing was assumed, which would lead to optimization as a logical approach to determine which policies provide more benefits for their cost. Third, for the retrofit, only some small or moderate portion of the community would likely adopt retrofits, so assuming all residential buildings retrofit represents an upper bound for that policy. Additionally, the methodology focused on the recovery of residential buildings themselves and did not examine the effect of the restoration of utilities such as electric power networks on the post-disaster recovery process. This will influence the delay and other timing, but the percent change in the recovery would be minor. For example, following the Joplin tornado, electrical power was restored for buildings capable of receiving power in less than a month. Nevertheless, the utility restoration delays can coincide with the delay variables considered in this chapter and will impede the implementation of policies. The methodology proposed in this chapter is based on the assumptions that residents do not out-migrate after the hazard, and the recovery of multiple dwelling units rely on the housing unit with the highest household income within the units. Addressing the limitations and assumptions described above is beyond the scope of this chapter. The methodology can be used as a basis for estimating downtime in countries/regions outside the United States, but the users should be cautioned and ensure that FEMA P-58 and the impeding factors which delay for repairs are applicable in that country/region or adjust these accordingly.

In summary, short-term post-disaster activities, like the proposed policies, can effectively guide and facilitate the recovery process. The resilience-based analysis methodology presented in this chapter can support decision making and community planning for stakeholders by being included in a broader community-level model for decision-making. The methodology, while demonstrated for tornado hazard, should be extensible to most hazards provided household income has an effect of delay time for that hazard.

CHAPTER 6 COMMERCIAL BUILDING RECOVERY

6.1 Introduction

Commercial businesses in an area affected by a natural hazard can have significant interruption and disruption because of damage and impeding factors including financing delays. The recovery of commercial buildings is a necessary but not solely sufficient condition for owners to re-open their businesses. At the community-level modeling scale for planning, the ability to model commercial recovery across the entire community, including short-term business operation disruption, is critical to understanding the interdependent recovery across engineering, economics, and social science. This chapter proposes a probabilistic commercial building recovery model to predict the recovery of commercial buildings over time following a hazard event and considers two critical types of downtime: impeding factors such as financing delays and the repair process.
A typical resilience resource portfolio for business owners was developed using survey data from Galveston Texas following Hurricane Ike in 2008 for a case community and quantitatively incorporated into the proposed probabilistic commercial building recovery model. The expected financing methodologies for business owners to repair their commercial buildings were identified based on the resilience resource portfolio and the estimated financial loss for damaged commercial buildings. The proposed financing methodologies enabled the probabilistic commercial building recovery model to directly link one of the significant delay impeding factors, financing delay, to commercial building damage states with other impeding factors resulting in delay, as explained later.

The methodology presented in this chapter develops a probabilistic commercial building recovery model to enable business recovery modeling to be integrated into a broader community resilience model and follows the methodology presented in Wang et al. (2023). The novelty of this work is (1) the development of a commercial building recovery model with the ability to fully propagate uncertainty for business recovery modeling; (2) the integration of post-disaster funding resources into a quantitative probabilistic analysis for community resilience assessment to track commercial building recovery. The ability to model commercial building recovery will inform decision-makers of the entire recovery process for upcoming business recovery and community resilience metrics related to physical services stability, thereby improving community resilience planning.

6.2 Commercial Building Recovery Model

Table 6-1 shows the building portfolio developed for wind-induced events (Memari et al. 2018), and buildings can be grouped by residential, commercial, etc, according to their occupancy classifications. This chapter focuses on the recovery of commercial buildings. Figure 6-1 shows the conceptual framework of the commercial building recovery model proposed in this chapter. The preliminary step to implementing the commercial building recovery model is to first produce the building damage results determined from fragility-driven damage models and MCS (Wang et al. 2021b, Wang et al. 2022c, Pang and Wang 2021). The methodology uses idealized tornado models (Standohar-Alfano and van de Lindt 2015, Attary et al. 2018) developed based on the gradient technique from historical tornado reports as hazard models but is not provided herein for brevity. However, it should be noted that the hazard models can be expanded to a general sense for any hazard events (Wang and van de Lindt 2021, Lin and Wang 2017).

Table 6-1. Building portfolio designed for wind-induced events

Archetypes	Building description	Occupancy classification
T1	Residential wood building, small rectangular plan, gable roof, 1 story	Residential
T2	Residential wood building, small square plan, gable roof, 2 stories	Residential
T3	Residential wood building, medium rectangular plan, gable roof, 1 story	Residential
T4	Residential wood building, medium rectangular plan, hip roof, 2 stories	Residential
T5	Residential wood building, large rectangular plan, gable roof, 2 stories	Residential
T6	Business and retail building (strip mall)	Commercial
T7	Light industrial building	Commercial
T8	Heavy industrial building	Commercial
T9	Elementary/middle school (unreinforced masonry)	Social Institutions
T10	High school (reinforced masonry)	Social Institutions
T11	Fire/police station	Social Institutions
T12	Hospital	Social Institutions
T13	Community center/church	Social Institutions
T14	Government building	Social Institutions
T15	Large big-box	Commercial
T16	Small big-box	Commercial
T17	Mobile home	Residential
T18	Shopping center	Commercial
T19	Office building	Commercial

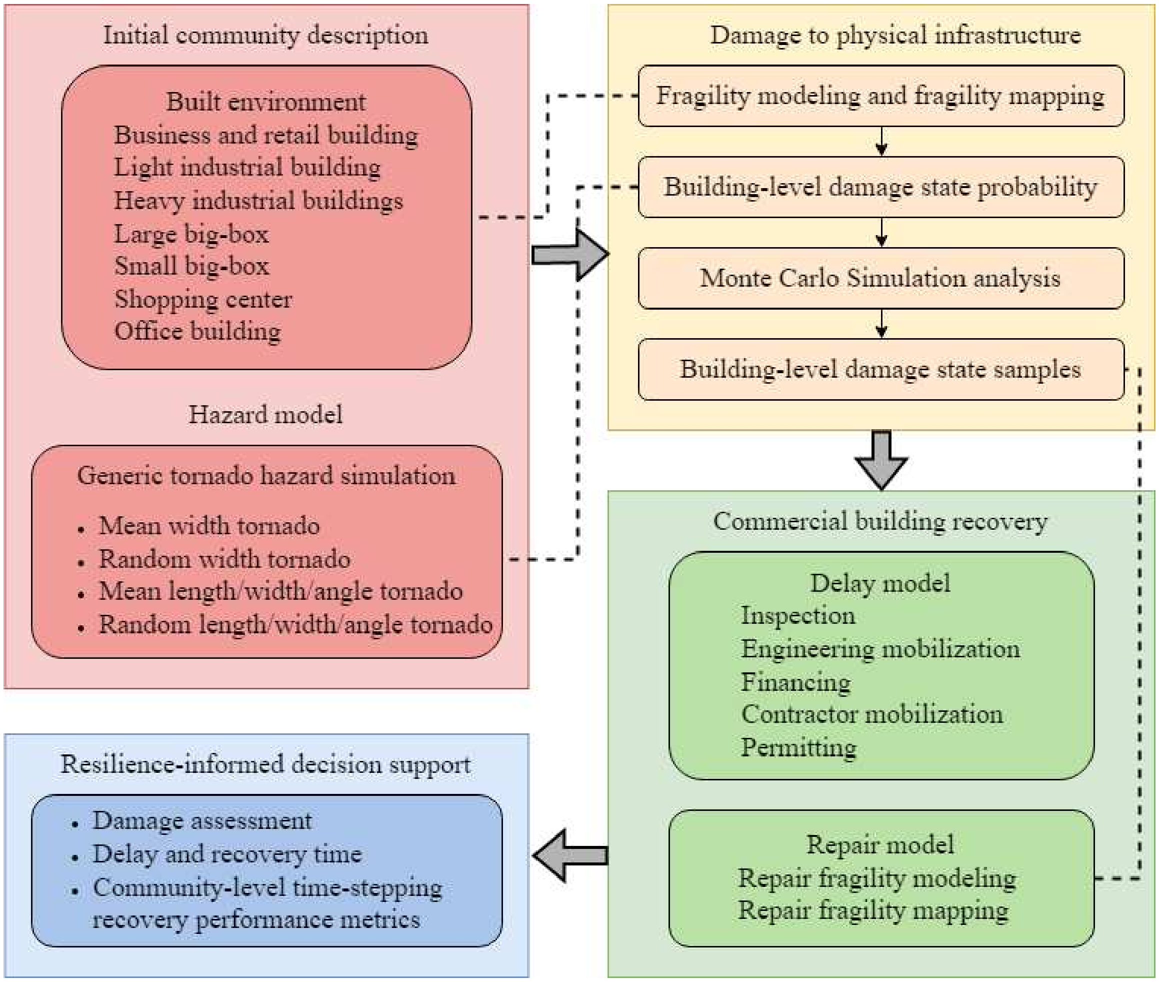

Figure 6-1. A conceptual framework of the commercial building recovery model

6.2.1 Delay Module

Several delays can occur and impede the ability to initiate repairs. This commercial building recovery model considered typical impeding factors, which include inspection, engineering mobilization, financing, contractor mobilization, and permitting following the methodology of the REDi framework (Almufti and Willford 2013), consistent with Chapter 5. The impeding factors calculated based on earthquake events and then expanded to any hazard events are presented in the form of lognormal cumulative distribution functions and have a relatively high degree of uncertainty, as illustrated in Table 6-2. Note that delay impeding factors were assumed to follow the delay phases introduced by Lin and Wang (2017). Please refer to Wang and van de Lindt (2021) to see more details about the description of each impeding factor and the approach to assembling all impeding factors and determining the modeled delay time. Unlike other impeding factors such as inspection and permitting, which are directly related to building-specific conditions after an event (Lin and Wang 2017), financing delay depends on the funding resource that the owners of each building can procure. For residential structures damaged by hazard events, households can claim the insurance depending on the hazard and their homeowner's policy/coverage, apply for all public/private loans, or even spend their savings for building repairs (see Chapter 5). Funding resources for the repair of commercial buildings such as strip malls and shopping centers fall in broadly similar categories: personal savings, insurance, Small Business Administration (SBA) loans and other recovery programs play an essential role that cannot be neglected.

Commercial property insurance is a crucial coverage for business owners, which can pay repair or replacement costs for buildings as well as for damage to the contents inside, such as furnishings, equipment, and machinery, if business properties are damaged or destroyed due to fire, wind, hailstorm, and other covered events (e.g., Vaughan and Vaughan 2007). Shopping centers, strip malls, office buildings, and manufacturing properties are typical business properties requiring commercial property insurance to protect the buildings and contents (General liability 2021a, General liability 2021b, General liability 2021c). Entrepreneurs may choose to finance recovery activities from personal savings before receiving the approval of insurance claims (Morrish and Jones 2020) or when the losses from damage do not meet the insurance deductible.

Several Federal programs can support business recovery, as well. The Small Business Association (SBA), a United States government agency and the largest Federal provider of business disaster assistance, provides debt financing to small businesses and private nonprofit organizations to 1) repair or replace damaged components via the physical disaster loan program or 2) cover working capital or normal expenses through the economic injury disaster loan (EIDL) program (e.g., Lindsay 2010, SBA 2021a, Wang and van de Lindt 2021, Lee 2019, Ravid et al. 2021, SBA 2021b). The U.S. Department of Housing and Urban Development (HUD) Community Development Block Grant–Disaster Recovery (CDBG-DR) funds, supported by the U.S. Congress, have been another way for businesses to recover from major disasters, such as floods and tornadoes over the past decades. Congress has typically allocated CDBG funds specifically for long-term business recovery, such as business-recovery loans, infrastructure improvements, and small-firm attraction/retention grants, to encourage renters/owners to stay in a particular area (e.g., Gotham 2014). The U.S. Economic Development Administration (EDA) revolving loan funds (RLFs) can also be established after disasters through the Economic Adjustment Assistance programs to provide businesses with gap financing (e.g., Chell 1992, Revolving Loan Fund Program 2021). From the private side, local community banks may also provide gap financing or bridge loans, commonly structured as a short-term interest-free loan and designed to service loans to affected credit-worthy small businesses essentially providing them the necessary cash flow for repair and re-investment expenses (e.g., Weaver and Vozikis 2010). Local government grant programs through chambers of commerce and economic development organizations also exist to help small businesses and nonprofits as needed (Ferrier 2020). Hundreds of thousands of dollars are often donated through the American Red Cross and local churches to help local businesses affected by disaster events (Farrow 2012). Note that donations and other approaches such as corporate assistance and borrowing money from family/friends were aggregated into “other funding resources” in the commercial building recovery modeling and not proposed separately due to their relative uncertainty for each affected business.

Table 6-2. Statistics of delay time associated with building damage (unit: weeks)

Sequence	Delay time impeding factor	Building specific conditions	Median	Standard deviation	Distribution
Delay Phase 1	Inspection	Slight	0	0	Lognormal
		Above slight	0.5	0.54	Lognormal
Delay Phase 2	Engineering mobilization & review/redesign	Slight	6	0.40	Lognormal
		Moderate/extensive	12	0.40	Lognormal
		Complete	50	0.32	Lognormal
	Financing	Personal savings/business revenue	1	0.54	Lognormal
		Commercial property insurance	6	1.11	Lognormal
		U.S. SBA Physical Disaster Loans	28.1	20.9	Normal
		U.S. SBA EIDL	19.3	9.7	Normal
		U.S. EDA Revolving Loan Fund	163.6	34.4	Normal
		U.S. HUD CDBG-DR Loan	146.9	2.7 within 2 months	Normal
		Local recovery program	33.7	8.0 within 6 months	Normal
		Bank bridge loans	7.7	4.0 within 3 months	Normal
		Other	48	0.65	Lognormal
	Contractor mobilization	Slight	7	0.60	Lognormal
		Above slight	19	0.38	Lognormal
Delay Phase 3	Permitting	Slight	1	0.86	Lognormal
		Above slight	8	0.32	Lognormal

In order to quantitatively simulate financing resources and financing delays following hazard events, this chapter developed a resilience resource portfolio based on real-world data collected in Galveston after Hurricane Ike. Surveys to disaster-affected businesses were performed to document the business recovery process and the resources available (Watson, 2014). Owners and managers of individual businesses were asked to put percentages by resources categories to show how they funded their recovery expenses (each survey response should add up to 100%). These responses were summarized across the sample to show how businesses financed their recovery overall across the community (see Table 6-3). Interviews with public officials and business organizations were conducted in Galveston as well as text analysis of program documents, including the Catalog of Federal Domestic Assistance, two Galveston newspapers, documents disseminated by the aid programs including loan application materials and marketing notices, and reports from the Government Accountability Office, the Congressional Research Service, and the Office of the Inspector General. This data was synthesized to determine the number of businesses supported by each program, the average days to fund disbursement, and the total funding size for each program, as illustrated in Table 6-4. The average days of financing delay that was determined for all programs in Table 6-4 then replaced the original values shown in the REDi framework (see Table 6-2). The standard deviations of the financial delay time for government grants from Watson et al. (2019) was applied in the present analysis. All the other financial delay statistics (i.e., personal savings/business revenue, commercial property insurance, and others) were jointly referenced by Almufti and Willford (2013), Lin and Wang (2017), and Wang and van de Lindt (2021).

This chapter assumed the statistical distributions could generalize actual conditions for financing delays during the commercial building recovery process in a typical community impacted by a natural hazard. It should be noted that these funding distributions were averaged and applied to the business population as a whole, rather than broken into subgroups by sector or size of the business. However, research has shown that businesses are more likely to apply for, be approved for, and use funds in their recovery across these characteristics (Dahlhamer 1994; Josephson and Marshall 2016; Watson, 2021). Though these differences are in part captured through the different commercial building types, there is an opportunity for future research to more directly integrate differences in funding composition with commercial building types and characteristics of the businesses occupying those structures.

Table 6-3. Recovery financing for all business after Hurricane Ike (Watson, 2014)

Index	Funding resources	Percentage of surveyed businesses utilizing resource	Percentage of overall recovery financed			
			Mean	Standard deviation	min	max
1	Business revenue	47%	24.9%	37%	0%	100%
2	Personal savings	44%	23.3%	37%	0%	100%
3	Commercial property insurance	29%	20.2%	35%	0%	100%
4	SBA loans	18%	9.1%	23%	0%	100%
5	Credit card	24%	6.2%	14%	0%	60%
6	Donations	11%	3.0%	15%	0%	100%
7	Other	9%	2.4%	9%	0%	40%
8	Local recovery program	13%	1.9%	5%	0%	20%
9	Local bank bridge loan program	4%	1.8%	9%	0%	60%
10	Grants	4%	1.8%	11%	0%	70%
11	Commercial bank loans	9%	1.7%	8%	0%	50%
12	Friends or family	7%	1.6%	6%	0%	30%
13	Corporate Assistance	2%	0.7%	5%	0%	31%
14	U.S. HUD CDBG-DR Loan	2%	0.2%	1%	0%	10%
15	Crowdfunding	0%	0.0%	0%	0%	0%
16	U.S. EDA Revolving Loan Fund	0%	0.0%	0%	0%	0%

Table 6-4. Surveys of business recovery programs after Hurricane Ike (Watson et al., 2019)

Index	Business recovery programs	Average days to funding	Size of fund	Loan Amount	N
1	U.S. SBA Physical Disaster Loans	216	$72.35 million	Max $2 million	499
2	U.S. SBA EIDL	135	$1.7 million	Max $2 million	20
3	U.S. EDA Revolving Loan Fund	1,145	$10 million	$30,000-$150,000 (Max $350,000)	10
4	U.S. HUD CDBG-DR Loan	1,028	$2.5 million	Average $35,000 (Max $50,000)	63
5	Local Recovery Program	236	$300,000-$400,000	$10,000-40,000	7
6	Bank Bridge Loans	54	$40 million	Varied	100+

It is important to mention that the methodology developed in this chapter considers that each business/firm can accept funding from more than one financial resource. Table 6-5 displays the resilience resources portfolio used in the commercial building recovery model, which can inform how businesses fund their recovery from all available approaches (e.g., personal savings, insurance, government grants) when they suffer damage/disruption from a hazard event. The percentage of recovery financed by personal savings/business revenue, reimbursed by commercial property insurance, and funded by commercial bank/bridge loans, are consistent with the values summarized from the Galveston survey (see Table 6-3). The percentage of financing support paid by credit cards, accepted from donations, support from friends/family/corporate assistance, and other approaches shown in Table 6-3 were aggregated to “other approaches” illustrated in Table 6-5. The percentage of recovery financed by each government program for business recovery was developed based on the proportion of the total fund size that businesses/firms received from different resources, as shown in Table 6-4. It was assumed that the uncertainty of the percentage of restoration financial resources fit a normal distribution. It was also assumed that all the types of commercial buildings have the same opportunity to access different financial resources.

Table 6-5. Resilience resource portfolio for commercial building recovery

Index	Business Recovery Programs	Percentage of restoration financial resources		
		Mean	Standard deviation	Distribution
1	Personal savings/Business revenue	48.2%	37%	Normal
2	Commercial property Insurance	20.2%	35%	
3	U.S. SBA Physical Disaster Loans	11.8%	23%	
4	U.S. SBA EIDL	0.3%	23%	
5	U.S. EDA Revolving Loan Fund	1.6%	0%	
6	U.S. HUD CDBG-DR Loan	0.4%	1%	
7	Local Recovery Program	0.1%	5%	
8	Bank Loan	3.5%	9%	
9	Other	13.9%	15%	

The time to access financing is considered the most uncertain impeding factor (Almufti and Willford 2013). Based on the REDi framework, the time associated with the longest delay should be the impeding factor if multiple funding sources are used. For example, if the regular operating budget of the facility is sufficient to cover the financial costs, and the estimated financial costs are less than the insurance deductible, then the impeding factor for personal savings is used. If available funds are sufficient to cover the insurance deductible, then the impeding factor for insurance can be used. If the insurance cannot solely cover the financial losses, and funding needs to be sought from other approaches such as bank loans and SBA-backed loans, then the impeding factor for other approaches should be used. Additionally, the REDi framework did not consider government grants as possible funding sources. Based on the statistical results determined from personal surveys (see Table 6-5), the percentage of recovery financed through government grants accounts for 2% of the total, which, though small, cannot be neglected since this may vary depending on event. If considering the longest delay time following the REDi framework, the estimated delay time to obtain approval of the U.S. EDA Revolving Loan Fund is 163.6 weeks, but this program's fund size only accounts for 1.5%. Thus, the authors felt it to be unreasonable to consider the longest delay time as the unique criterion to control the impeding factor if incorporating various government grants as funding resources for businesses. Defining the estimated financial costs and then choosing the expected method of financing for businesses after natural hazard events is a more appropriate, though challenging, approach.

This methodology in this chapter proposes to select the expected method of financing for commercial buildings based on their building-specific conditions (i.e., damage states in slight, moderate, extensive, and complete levels) following damage from a natural hazard, as illustrated in Table 6-6. Please refer to Memari et al. (2018) for the description of different damage states corresponding to different types of commercial buildings. The financial costs under different damage states were estimated by the building replacement cost multiplied by the loss ratio affected by tornado hazards (in this chapter). The building replacement cost considers both the cost of structural component damage and the value of interior damaged components, including nonstructural components and building contents (Koliou and van de Lindt 2020, Pilkington et al. 2020). The loss ratio is defined as the value of the loss divided by the insured value of the building. The definition of loss ratio has been comprehensively applied to visualize and compare the building losses (e.g., single-family residential buildings) under different natural hazards such as hurricanes, tornadoes, floods, and rainfall from the last several decades (e.g., Pant and Cha 2019, FEMA 2012, Vickery et al. 2006, Friedland and Levitan 2011, Li et al. 2012, Wang et al. 2018). The loss ratio associated with tornado-induced damage states for commercial buildings used in this chapter follows the work by Pilkington et al. (2020). Note that if this estimated loss ratio was greater than 50%, the building was considered a total loss that needed to be rebuilt entirely, consistent with the insurance industry.

Table 6-6. Available method of financing for commercial buildings based on damage state

Damage states	Funding resources		
	Personal savings/ Business revenue	Commercial property Insurance	Government grants/Others
Slight	Yes	-	-
Moderate	Yes	Yes	-
Extensive	Yes	Yes	Yes
Complete	Yes	Yes	Yes

In reality, for financial costs at different damage levels, building owners may choose the expected method of financing differently. Table 6-7 presents the damage state description of a typical commercial building, light industrial building (T7 presented in Table 6-1), as an example (Memari et al. 2018). Most insurance policies for commercial buildings typically require a deductible of 5% to 10% of the building value at a minimum (Almufti and Willford 2013), which is significantly greater than the financial costs for the slight damage. Therefore, building owners would likely spend their savings to perform slight repairs to, for example, their roof covering or other construction materials and/or replacing broken windows. Building owners may claim insurance and be reimburse from their insurance companies if their commercial buildings have roof covering failures over a relatively large area and/or the exterior walls are damaged from flying debris which is the description of moderate damage. In such cases, building owners may still need to use their savings to pay for the insurance deductible and coinsurance depending on the deductible requirements and/or coinsurance clauses written in their commercial property insurance policy. When extreme damage occurs, such as exterior wall collapse, termed extensive or complete damage, the loss ratio exceeds 0.5. Although building owners may have property insurance coverage based on the value of their buildings and contents inside, they still need to access financial resources such as government grants (e.g., SBA-backed loans, but they are limited to $2M for business) to finance their post-disaster events. For example, if the loss analysis reveals significant structural damage to many components, this may require an engineer to completely redesign the building, which may not be paid by the insurance reimbursement. At this level of damage, the financing delay time is calculated by combining the percentage of all types of government grants, bridge loans, and other approaches and their specified delay time considering uncertainty.

Table 6-7. Damage state description for light industrial buildings

Damage states	Roof covering	Window/door	Exterior wall	Garage door	Roof structure
Slight	>2% and ⩽15%	1 or 2	>2% and ⩽ 25%	No	No
Moderate	>15% and ⩽ 50%	>1 or 2 and ⩽ 25%	>25% and ⩽ 50%	Yes	No
Extensive	>50%	>25%	>50% and ⩽ 75%	Typically yes	No
Complete	Typically >50%	Typically >25%	>75%	Typically yes	Yes

6.2.2 Repair and Recovery Module

The repair time was developed based on the repair estimates following isolated component damage introduced in the FEMA P-58 methodology, presented as the repair fragility functions assembling from building component levels to system levels. Table 6-8 presents tornado repair fragility functions of commercial buildings damaged at different damage states (i.e., slight to complete, presented as DS1-DS4) as mentioned earlier to reach full functionality (Koliou and van de Lindt 2020).

Table 6-8. Repair fragility function parameters for commercial buildings

Archetypes	Building description	DS1		DS2		DS3		DS4	
		λ	ξ	λ	ξ	λ	ξ	λ	ξ
T6	Business and retail building (strip mall)	2.18	0.66	3.78	0.61	4.51	0.55	5.05	0.6
T7	Light industrial building	2.15	0.58	3.28	0.54	4.69	0.51	5.55	0.53
T8	Heavy industrial building	2.11	0.53	3.25	0.51	4.52	0.55	5.55	0.53
T15	Large big-box	2.28	0.51	3.62	0.51	4.49	0.55	5.23	0.52
T16	Small big-box	2.28	0.51	3.62	0.51	4.49	0.55	5.23	0.52
T18	Shopping center	2.15	0.49	3.83	0.55	4.57	0.55	5.18	0.55
T19	Office building	1.45	0.55	3.74	0.52	4.8	0.52	5.32	0.55

Units: ln (days) (e^{λ} = days).

The recovery module can be combined to represent the two stages, namely delay and repair, and was consistent with the methodology for residential structures explained in Chapter 5. Figure 6-2 explains the integration of the delay and repair modules through the multi-layer MCS implemented in the model. Boxes on the right side shown in Figure 6-2 shows an example of analytical results after running the commercial building recovery model impacted by an EF5 tornado event. The first layer of the MCS within N_1 realizations is associated with the delay module. In each MCS realization of this layer, the delay time of assembling all impeding factors needed for each commercial building can be determined. Then, the repair time of each commercial building damaged from any estimated damage states to fully restored can be computed within N_2 realizations, which is the second layer of MCS. Therefore, the methodology proposed in this chapter can predict the recovery time for each commercial building and then commercial building recovery performance probability over the entire community N1×N2 times in the simulation.

6.3 Illustrative Example

As low-probability, high-consequence events, tornado hazards can result in catastrophic physical damage to buildings and distributed infrastructure and with subsequent socio-economic losses over (e.g., Lombardo et al. 2015, Prevatt et al. 2012, Wang et al. 2018). Previous studies have focused on the infrastructure damage (e.g., buildings and lifeline systems), economic losses, and household disruption impacted by tornado hazards (e.g., Roueche and Prevatt 2013, Pilkington et al. 2020, Wang et al. 2021b, Wang et al. 2022a, Wang et al. 2022b, Wang et al. 2022c). Businesses located in commercial properties within a community are also severely impacted by tornadoes, resulting in significant business interruption and disruption (e.g., Masoomi and van de Lindt 2018, Smith and Sutter 2013). For example, following the 2011 Joplin tornado, more than 500 businesses were destroyed and had to close their doors, at least temporarily, resulting in loss of sales, loss of customers, and lost employee income. Less than four months after the tornado, it was reported that 69% of the damaged businesses reopened or were open at a temporary location or were rebuilding. Some large corporations such as Walgreens, Home Depot, Walmart, and Chick-fil-A were rebuilding within eight months (Smith and Sutter 2013).

Therefore, it is critical to be able to model the business recovery process in a broader community-level resilience model to enable community planning for resilience including decision-support for policy makers. Commercial building recovery is the key factor for business owners to re-open their businesses following a hazard event, which in turn will influence decision-makers during recovery. This illustrative example is provided to demonstrate implementation of the commercial building recovery model for a community impacted by a simulated tornado scenario. This illustrative example aims to determine the statistics of the recovery time needed for each commercial building to be fully restored and the mean recovery time with uncertainties for commercial buildings tracked through a time-stepping community-level recovery algorithm. The city of Joplin, located in southwest Missouri, was selected based on past work with this community as a testbed. Joplin is a typical small to medium size community in the Midwest of the United States, and used in this illustrative example.

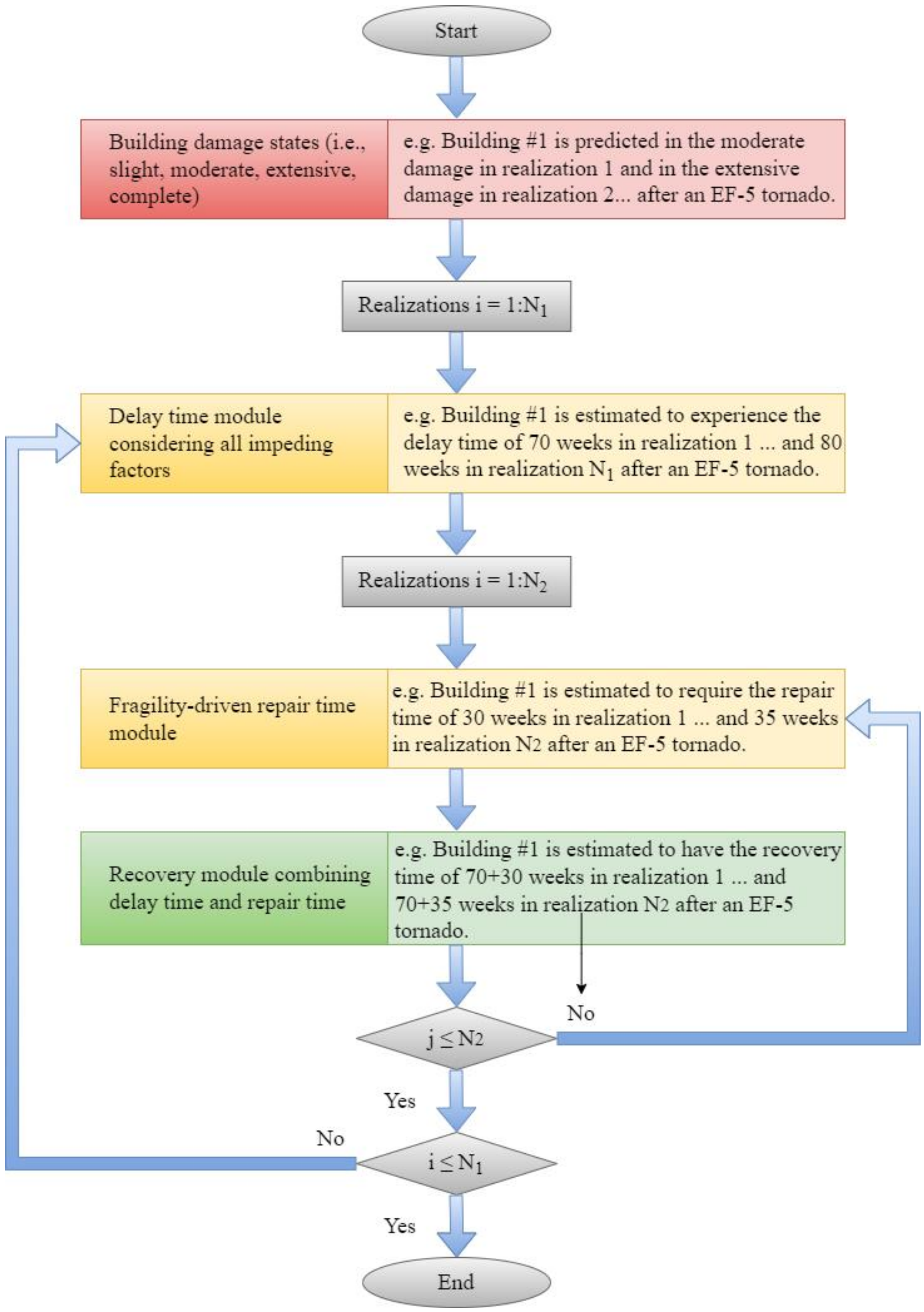

Figure 6-2. A detailed illustration of the multi-layer MCS implemented to integrate the delay module and repair module for commercial buildings

An idealized EF5 tornado (McDonald and Mehta 2004) was used in this chapter to directly impact the built environment in Joplin. The simulated direction and length of the tornado were designed to impact as many community buildings as possible for illustrative purposes. The width of the idealized tornado was the mean EF5 width of historical tornados reported from 1973 to 2011

(Standohar-Alfano and van de Lindt 2015). Figure 6-3 shows the overlay of the built environment of commercial buildings and the tornado simulation. As expected, most commercial buildings are located along several main streets in the community. Table 6-9 illustrates the different types of commercial buildings and the number of commercial buildings falling within the simulated tornado path. Building damage results need to be determined preliminary to then apply the new commercial building recovery model as mentioned earlier. Combining the building damage model, fragility functions, and hazard model, the probability of buildings exceeding each damage states is then determined (Wang and van de Lindt 2022). MCS generated sufficient randomized samples and determined the damage states for each commercial building within each MCS realization. Table 6-10 presents typical building-level hazard exposure and damage results, where each building is tracked using a globally unique identifier (GUID). The limit state (LS) probability at different levels (i.e., LS1-LS3) presented in Table 6-10 are the probabilities shown in the fragility curves at different damage levels at a specified intensity measure in terms of a 3-sec gust wind speed.

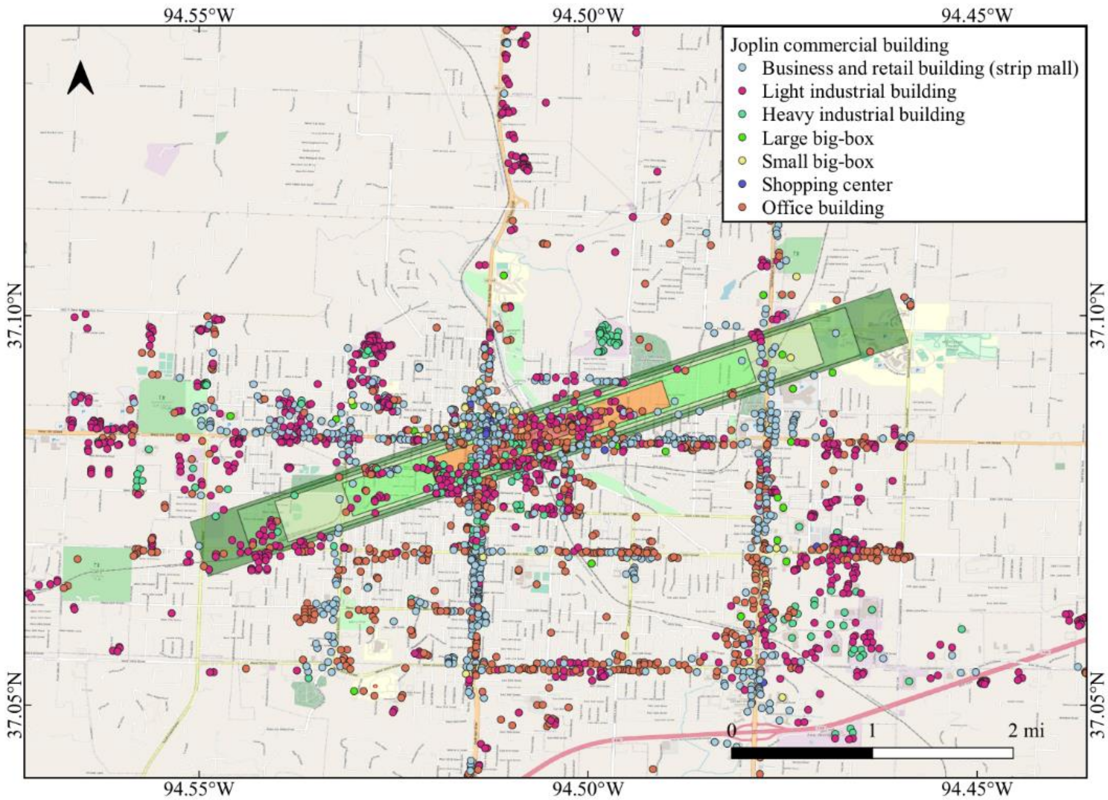

Figure 6-3. The overlay of the built environment for commercial buildings and simulated EF5 tornado

Table 6-9. Commercial buildings falling within the simulated tornado path

Archetypes	Building description	Joplin builidngs	Buildings fallen within the tornado path						
			EF0	EF1	EF2	EF3	EF4	EF5	Total
T6	Business and retail building (strip mall)	736	15	21	20	21	29	4	110
T7	Light industrial building	963	26	36	20	34	42	20	178
T8	Heavy industrial building	155	3	5	5	3	13	7	36
T15	Large big-box	21	0	0	1	0	0	0	1
T16	Small big-box	30	0	0	1	1	0	0	2
T18	Shopping center	10	1	1	2	0	0	0	4
T19	Office building	701	8	17	19	16	28	23	111
In total		2,616	53	80	68	75	112	54	442

Table 6-10. Typical building-level hazard exposure and damage results

Index	GUIDs	Archetypes	Hazard exposure	Wind speed (m/s)	Limit states			MCS samples	
					LS1	LS2	LS3	Sample1	…
1	GUID1	T7	EF0	36.95	0.20	0.04	0.01	DS1	…
2	GUID2	T18	EF1	39.50	0.63	0.02	0.01	DS1	…
3	GUID3	T15	EF2	59.21	0.99	0.69	0.08	DS3	…
4	GUID4	T16	EF3	61.24	1.00	0.58	0.15	DS2	…
5	GUID5	T6	EF4	85.38	1.00	1.00	0.96	DS4	…
6	GUID6	T19	EF5	102.81	1.00	1.00	0.99	DS4	…
…	…	…	…	…	…	…	…	…	…

After applying the commercial building recovery model described in this chapter, Figure 6-4 shows the histograms of delay time (N_1=100) and recovery time (N= N_1× N_2=100×100=10000) from MCS for a typical commercial building in this chapter, which appears to fit a lognormal distribution well. For a typical building within the EF3 region of the EF5 path, the mean delay time and mean recovery time is 69 weeks and 92 weeks, respectively. Figure 6-5 illustrates the average delay and recovery time with uncertainties for all commercial buildings within the tornado path, grouped by different tornado intensity regions. Overall, the average recovery time for commercial buildings within the regions from EF0 to EF5 is 16.2 weeks, 50.1 weeks, 82.0 weeks, 100.3 weeks, 104.5 weeks, and 106.8 weeks. It can be observed that only commercial buildings within the EF0 and EF1 regions can realistically recover in approximately one year. Since the delay time for all the impeding factors presented in this chapter directly rely on building-specific conditions impacted by tornado hazard, buildings within the EF0 region have a high possibility of slight damage, but buildings within the EF3 region or higher are commonly damaged to a complete level. Therefore, the uncertainties of delay time for buildings within EF1 and EF2 regions are relatively higher than those within other regions. Building recovery time has a full uncertainty propagation throughout the multi-layer MCS realizations, aggregated by the combination of delay time and repair time. Therefore, as expected, building recovery time has a higher uncertainty than building delay time. The average delay and recovery time for buildings in the EF3 region or higher do not significantly differ, while the uncertainties of delay and recovery time for buildings in the EF3 region are slightly higher than those in the EF4 and EF5 regions. The delay time and recovery time of buildings presented in Figure 6-4 are color-coded by EF region. The recovery process can be shortened through mitigation strategies applied to buildings, such as the component-level improvement (e.g., connections) for buildings in EF0 and EF1 regions, the system-level improvement (e.g., shear walls) for buildings in EF2 and EF3 regions, and providing alternate approaches (e.g., safe rooms) for buildings in EF4 and EF5 regions (van de Lindt et al. 2013).

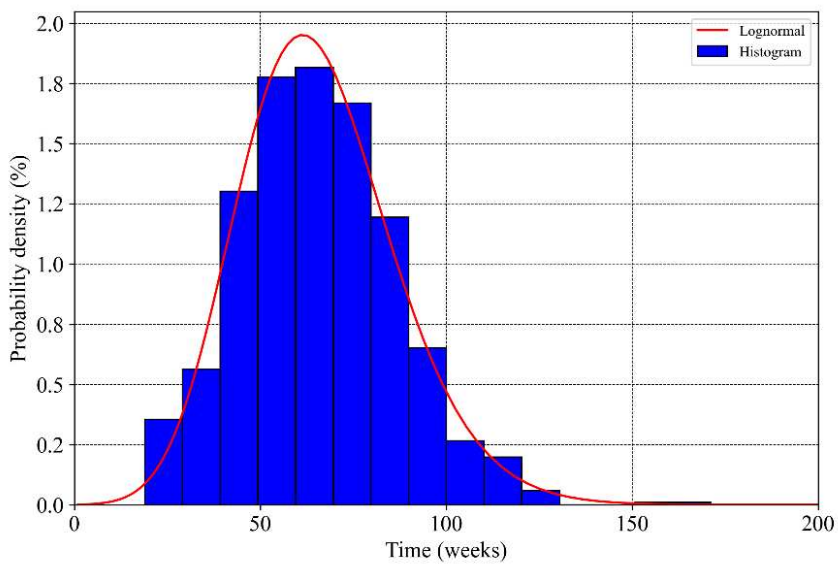

(a)

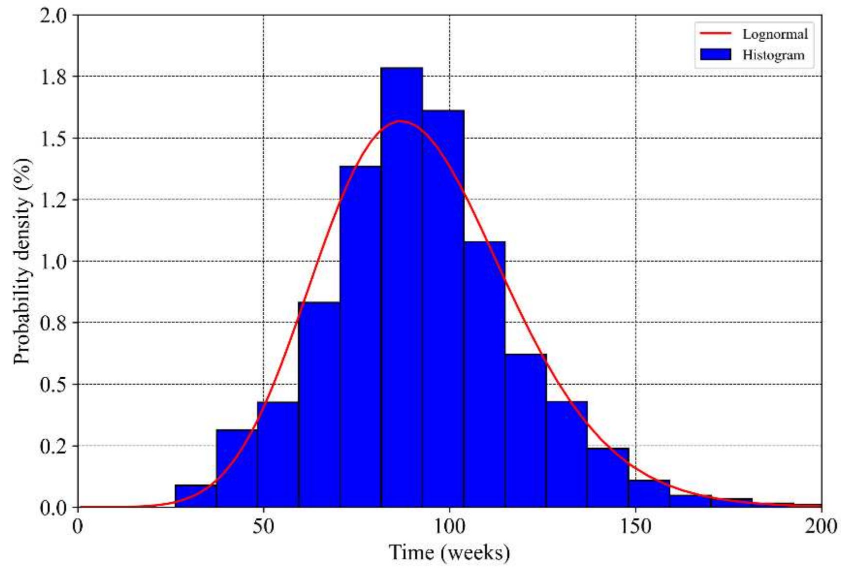

(b)

Figure 6-4. A typical building in the EF3 region over MCS realizations: (a) delay time; (b) recovery time

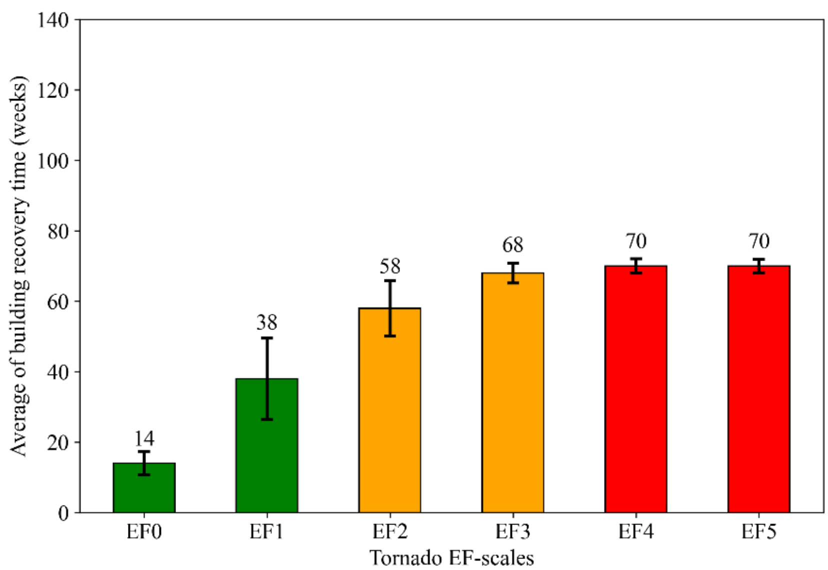

(a)

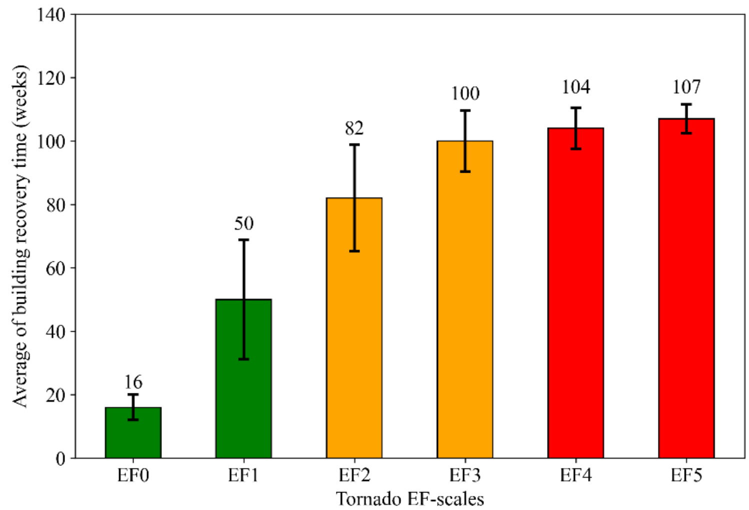

(b)

Figure 6-5. Commercial buildings within the tornado pathway: (a) average of delay time; (b) average of recovery time

In order to track the time-stepping commercial building trajectory over the entire community, This chapter still uses the concept of the binary commercial building recovery performance indicator, the time by quarters, and the calculated recovery time of buildings as thresholds, recall Equation (5.6). The time-stepping commercial building performance recovery probability and the average of the percentage of buildings fully recovered are determined, respectively, recall Equation (5.7) and Equation (5.8). Figure 6-6 shows the building post-disaster recovery performance probability at a community level over time. As expected, the recovery performance probability for most commercial buildings in the EF0 and EF1 regions varies from 0.8 to 1.0 one year after the tornado, and those in the EF3 region or higher are still in the recovery process at two years, which generally match the analytical results of recovery time needed for buildings in each EF region shown in Figure 6-4. Table 6-11 presents the average percentage for different buildings fully recovered at the short-term, intermediate, and long-term phases (NIST 2020) after the tornado, as an essential resilience recovery metric from the perspective of physical service stability. The recovery process of different buildings depends on building damage states based on their locations with tornado intensities, financial resources available to business owners, and other impeding factors resulting in delay before repair initiation. Overall, in this illustrative example, the community begins to have a small number of buildings fully recovered at the intermediate phase, and more than half of buildings complete the recovery process around two years in the long-term phase.

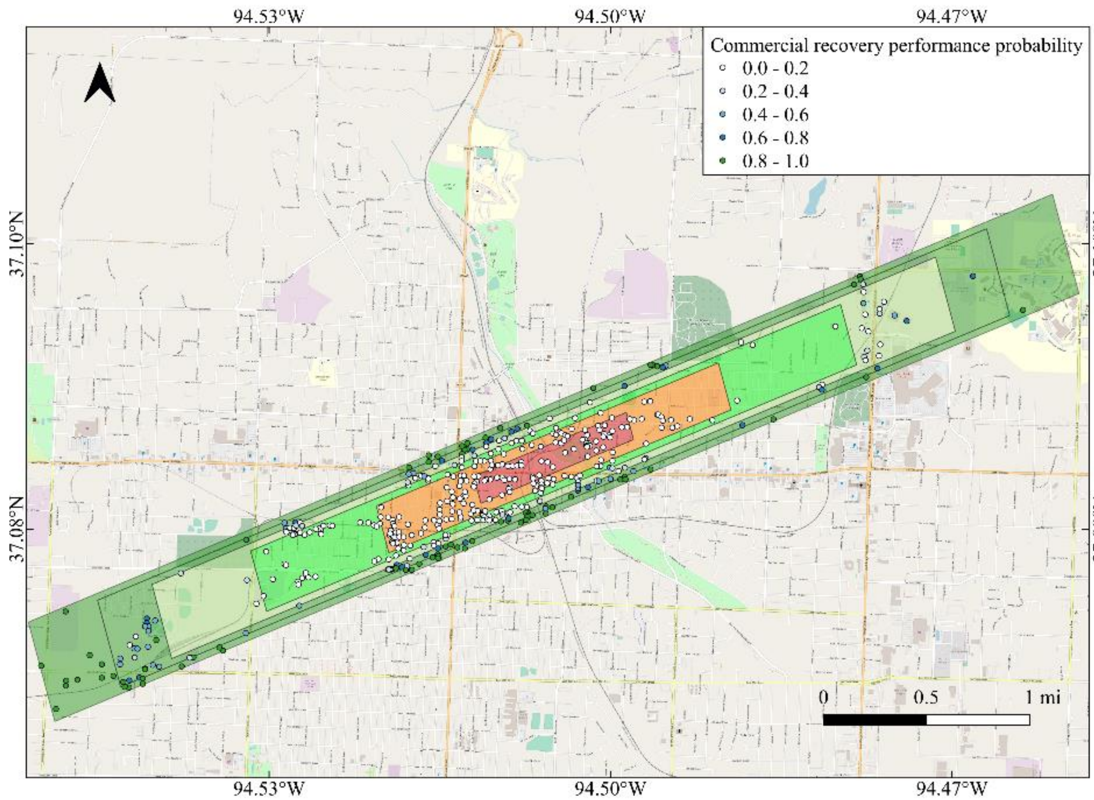

(a)

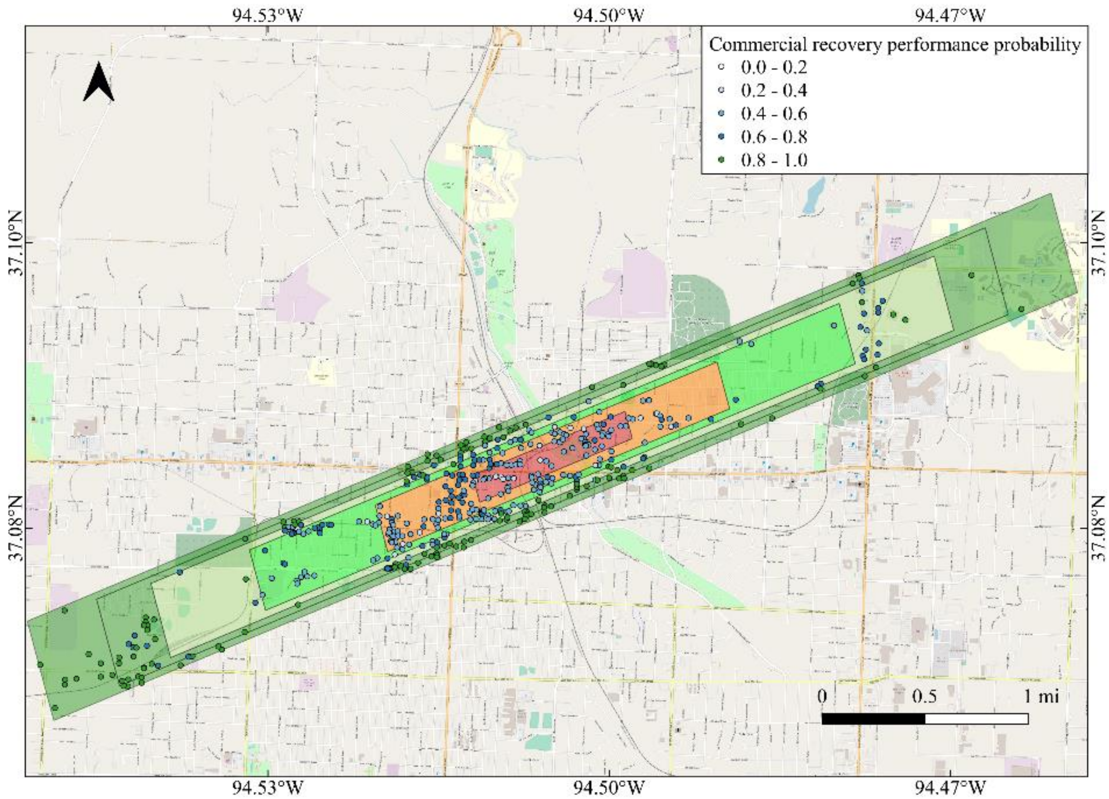
94.53°W
94.50°W
94.47°W
Commercial recovery performance probability
0.0 - 0.2
0.2 - 0.4
0.4 - 0.6
0.6 - 0.8
0.8 - 1.0
37.10°N
37.08°N
0
0.5
1 mi

(b)

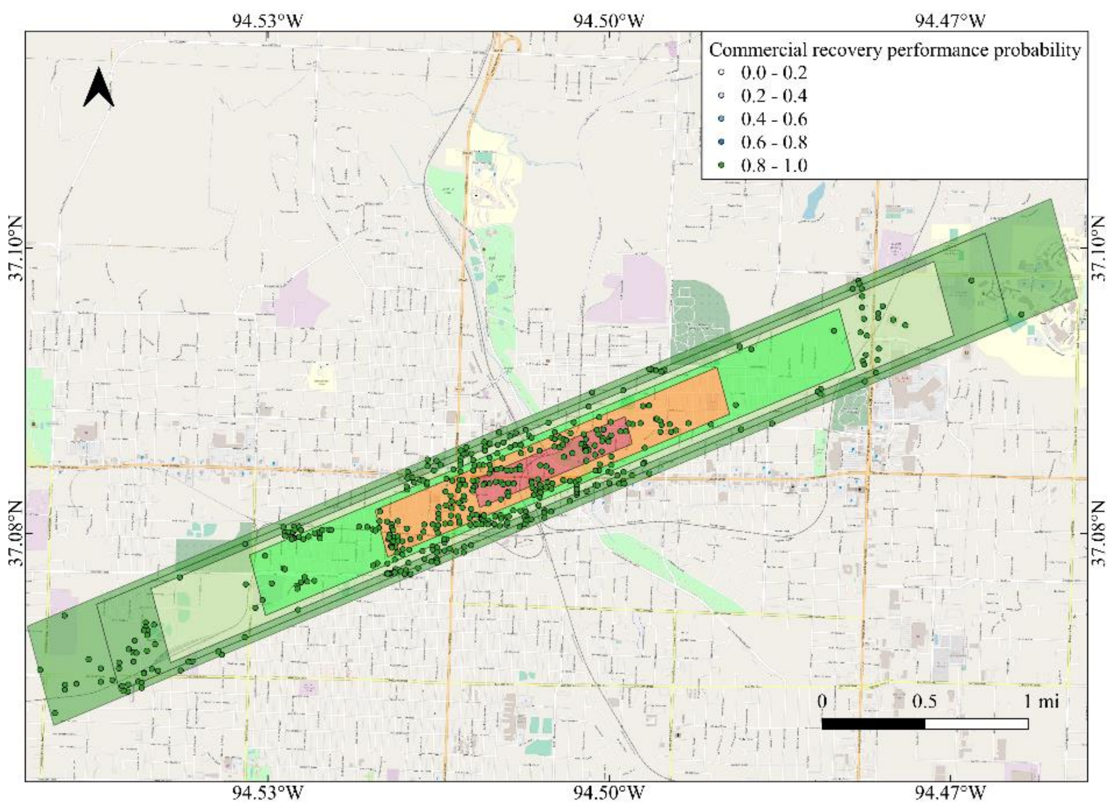
94.53°W
94.50°W
94.47°W
Commercial recovery performance probability
0.0 - 0.2
0.2 - 0.4
0.4 - 0.6
0.6 - 0.8
0.8 - 1.0
37.10°N
37.08°N
0
0.5
1 mi

(c)

Figure 6-6. Time-stepping recovery probability for buildings in the tornado pathway: (a) time = 1 year; (b) time = 2 years; (c) time = 3 years

Table 6-11. The percentage of buildings fully recovered in the tornado pathway (mean values)

Buildings	Design hazard performance								
	Phase 1: Short-term			Phase 2: Intermediate			Phase 3: Long-term		
	Days			Weeks			Months		
	0	1-3	3-7	1-4	4-8	8-12	3-12	12-24	24+
Business and retail building (strip mall)	0%	0%	0%	0%	2.2%	8.3%	34.9%	80.6%	100%
Light industrial building	0%	0%	0%	0%	2.8%	10.4%	25.8%	61.6%	100%
Heavy industrial building	0%	0%	0%	0%	1.2%	4.4%	27.5%	64.1%	100%
Large big-box	0%	0%	0%	0%	0%	0%	42.8%	89.1%	100%
Small big-box	0%	0%	0%	0%	0%	0%	38.9%	80.3%	100%
Shopping center	0%	0%	0%	0%	2.8%	14.7%	53.9%	87.8%	100%
Office building	0%	0%	0%	0%	1.7%	5.7%	25.7%	71.9%	100%

6.4 Summary and Conclusions

Commercial properties/businesses in a hazard-affected area can have a substantial impact on the overall community recovery. Therefore, business recovery is one of the more critical requirements serving as a necessary (although not sufficient) condition to improve resilience. In this chapter, a probabilistic commercial building recovery model was proposed to track the recovery trajectory for commercial buildings over time following a hazard event and measure typical recovery resilience metrics. Based on the work presented herein, the following conclusions can be drawn:

- A resilience resource portfolio available to business owners was developed based on real-world available project survey data collected following Hurricane Ike in 2008 from the associated statistical analysis. The three significant funding resources are personal savings/business revenue, commercial property insurance, and government grants/others. Business owners must choose a single or multiple financial methodologies above to support their post-disaster events depending on the specific conditions of their commercial buildings.

- The average recovery time for commercial buildings in the tornado example in this chapter varies from as little as averaging 16 weeks in very lightly damaged regions (DS0 and DS1) to as much as an average of 107 weeks at the centerline of the tornado path. The uncertainties in recovery time for buildings in the EF1 and EF2 wind regions are higher than those in other tornado regions.
- The recovery process for different commercial building types depends on building damage affected by hazard events, financial resources available to business owners, and other impeding factors. Overall, very few commercial buildings are fully recovered within a year of the hazard event, and, in general, more than 50% are fully restored after approximately two years.

It is worth noting that the methodology proposed in this chapter has several limitations and assumptions, which need to be addressed in future studies. First, the methodology assumed business owners would not select a new location to rebuild their commercial buildings but schedule repair of the original buildings no matter how damaged they were. Second, this chapter mainly considers the recovery of physical buildings without considering the complex personal decision-making processes of business owners, managers, and commercial landlords. For example, business owners are also often residents of the community, homeowners, heads-of-household. If their residential buildings were damaged, they may have dislocated or even outmigrated from the community, which would impede or eliminate their commercial building recovery plan. Lastly, the proposed methodology incorporating real-world funding resource data to estimate the financial delay is based on past statistics but needs empirical field study data related to commercial building recovery and business re-opening for validation.

In summary, the resilience-based methodology presented in this chapter can quantitatively incorporate a resilience resource portfolio into the probabilistic community resilience model and help the community understand and guide the recovery process for commercial buildings. Such a methodology, even with some assumptions and limitations, will be beneficial for business recovery modeling since no model at the building-level currently exists.

CHAPTER 7 PHYSICAL-SOCIAL INTERDEPENDENT RECOVERY

7.1 Introduction

Comprehensive multi-disciplinary community resilience assessment has emerged over the last decade and requires modeling complex interactions over physical infrastructure and social systems to support planning and decisions. Comprehensive community resilience models that fuse disciplines have examined the natural hazard-induced damage to physical infrastructure with propagation to economic losses and population instability. However, most community recovery models thus far were designed to examine the recovery of a single system or rely on a host of assumptions due to a dearth of available data. In this chapter, a methodology to examine physical-social interdependent community recovery is proposed; specifically the process of modeling dislocated households and the damaged residential buildings needing repair. The methodology integrates building damage approach, household allocation, population dislocation, and residential building recovery with an existing household recovery approach developed in previous studies. This chapter aims to comprehensively examine household recovery processes for four cases: Case 1: the household[1] has permanent housing[2] and the residential buildings[3]; Case 2: has permanent housing but without residential buildings; Case 3: has residential buildings but without permanent housing; Case 4: has neither permanent housing nor residential buildings.

---

[1] A household refers to one person or a group of people who dwell under the same roof and compose a family in this chapter.
[2] Permanent housing means housing without a designated length of stay, and includes both permanent supportive housing and rapid rehousing in this chapter.
[3] A residential building refers to a building containing one or more residential dwellings used or occupied, or intended to be used or occupied, for residential purposes in this chapter.

The novelty of this chapter is (1) to develop a methodology, for the first time, to examine the interdependent community recovery process across physical infrastructure and social systems; (2) to examine the integrated recovery process of residential buildings and the household in that building for the community impacted by. The methodology is demonstrated for the city of Joplin, Missouri, impacted by the 2011 Joplin tornado. This chapter specifically focuses on a multi-disciplinary community resilience assessment but with an emphasis on the recovery process, expanding the scope of comprehensive community assessment models to potentially provide decision-support to community leaders, stakeholders, and researchers. The ability to quantify interdependent community recovery across physical and social science models can help communities plan more realistically for their recovery, and maintain social stability following natural hazard events. This chapter follows the methodology presented in Wang and van de Lindt (2023).

7.2 Physical-Social Interdependent Recovery Model

Figure 7-1 shows a simplified flowchart representing an overview of the physical-social interdependent recovery proposed in this chapter. Specifically, social recovery refers to dislocated households re-accessing their permanent housing/dwelling, and physical recovery refers to their residential buildings being fully recovered after the damage and becoming fully operational and functional. The entire process starts from the building damage prediction. Buildings can be damaged immediately after a hazard, particularly tornadoes. Subsequently, many households must temporarily move out of their dwelling, often staying in the emergency shelters for approximately two weeks or more depending on the intensity of the hazard. Over time following a disaster, residential buildings are repaired or new buildings are constructed and ultimately households move to their permanent housing. MCS is a technique that enables the analyst to generate sufficient randomized samples and predict the probability of different outcomes. Within each of the chained analyses mentioned earlier, MCS is widely applied to ensure propagation of uncertainty.

7.2.1 Building Damage Prediction

Fragility functions (*D_Fr*) are developed which represent the probability of physical infrastructure exceeding a damage state under a given intensity measure from a natural hazard. Readers are referred to Chapter 3 for more details about developing wind-induced fragility functions using structural reliability analysis. Equation (7.1) below presents the probability of (P_{damage}) each building (k) exceeding a prescribed damage state (i) at a specific intensity measure (e.g., 3-second gust wind speed, peak ground acceleration, and flood depth) from a natural hazard (e.g., wind, earthquake, and flood) (Wang et al. 2022). For woodframe residential buildings subject to tornado hazards as an example, four damage states (i.e., slight, moderate, extensive, complete) are defined with each represented by different damage descriptions made up of specified conditions for structural components such as roof-to-wall connections and non-structural components such as windows and doors (Masoomi et al. 2018). For example, when residential buildings have a roof covering failure exceeding 15% and less than 50% by area, this represents a particular damage state defined generally as

$$P^{k}_{Damage,i} = D\_Fr^{k}_{DSi}(IM = x) \tag{7.1}$$

7.2.2 Household Dislocation Prediction

The approach to predicting household dislocation in this chapter is consistent with those explained in sections 2.2.4 in Chapter 2 and 3.3.3 in Chapter 3. For each MCS realization, each household (h) allocated to each building (k) is predicted to dislocate ($I^{k,h}_{dis} = 1$) if a random value, R, between

0 and 1, is less than the calculated dislocation probability, as illustrated in Equation (7.2). The dislocated households will be used as an input for being integrated into the household recovery prediction, which will be introduced later to estimate whether they will return or find a new place to live permanently after the damage from a natural hazard.

$$I_{dis}^{k,h} = \begin{cases} 0 & R > P_{dis,m}^{k,h} \\ 1 & R \leq P_{dis,m}^{k,h} \end{cases} \tag{7.2}$$

7.2.3 Residential Building Recovery Prediction

The residential building recovery approach predicts the time required for residential buildings damaged in any damage state to fully recovered due to natural hazard events. Wang and van de Lindt (2021) defined the residential building recovery process as a two-stage process: Stage 1 is downtime due to delays including impeding factors and stage 2 is repair (see Equation (7.3)). Several impeding factors, including post-event inspection (T_{INSP}), engineering mobilization (T_{ENGM}), procuring funding (T_{FINA}), contractor mobilization (T_{CONM}), and construction permitting (T_{PERM}) jointly result in the phase 1, the delay time, which occurs for residential buildings before initiating the repair scheduled by building owners, as suggested by the REDi framework (Almufti and Willford 2013). The delay time was estimated for earthquake events based on the REDi framework and then expanded to other hazard events (Wang and van de Lindt 2021). Equation (7.4) presents the approach to assembling all the impeding factors that occur in different delay phases, which is consistent with the equation in Chapter 5. The repair model was developed based on the repair estimates explained in the FEMA P-58 methodology and assembled from component levels to building levels (Koliou and van de Lindt (2020). The repair time is determined by fragility functions (*R_Fr*) for damaged residential buildings in different damage states, as illustrated in Equation (7.5). Please refer to Wang et al. (2023) for a detailed illustration of integrating delay time (T_{Delay}) and repair time (T_{Repair}) to recovery time ($T_{B\_Recovery}$) using the concept of multi-layer MCS.

$$T^k_{B\_Recovery} = T^k_{Delay} + T^k_{Repair} \tag{7.3}$$

$$T^k_{Delay} = T^k_{INSP} + max\{T^k_{ENGM} + T^k_{FINA} + T^k_{CONM}\} + T^k_{PERM} \tag{7.4}$$

$$T^k_{Repair} = R\_Fr^k(DS = i) \tag{7.5}$$

7.2.4 Household Recovery Prediction

The household recovery prediction in this chapter describes a long-term complex process for households after being disrupted by a natural hazard and consists of four stages: emergency shelter, temporary shelter, temporary housing, and permanent housing (Bolin and Stanford 1998, Badeaux 2018). Sutley and Hamideh (2020) comprehensively detailed the four stages above to model household recovery as stages 1 to 4 and proposed a household recovery failure as a fifth possible stage. They used a Markov chain model to predict the sequence and timing of a household going through recovery to reach either permanent housing or household recovery failure, i.e. resulting in houselessness. This chapter modified this model slightly and implemented it to predict the household recovery process.

The Sutley and Hamideh model (2020) starts with the determination of the social vulnerability scores of each household. Social vulnerability scores are modeled in a nonnegative number varying from 0 to 1, where 0 and 1 represent the lowest and highest possible social vulnerability, respectively. Rosenheim (2021) allocated the household income to each housing unit based on race, ethnicity, and household size at the census block level and income distributions at the census tract level. The household income information is then predicted, which is felt to represent typical sociodemographic characteristics in real-world communities, to group the social vulnerability zones (z), for each household (h). For each social vulnerability zone, a threshold ($R_{threshold}$) is defined to represent the percentage of most households living in this zone with a lower bound ($R_{b,lower}$) and an upper bound ($R_{b,upper}$). The lower and upper bounds are used to calculate a range of social vulnerability scores (SV), when a random number (R) between 0 and 1 is less than this threshold. Another lower bound ($R_{a,lower}$) and upper bound ($R_{a,upper}$) are also defined to represent the remaining households assigned to a broader range of social vulnerability scores to reflect a small number of exceptional cases that exist in reality. The social vulnerability score of each household can be determined using Equation (7.6) below, which is estimated to fit a uniform distribution.

$$SV_z^h = \begin{cases} F_z^h\left(s; R_{b,lower}^z, R_{b,upper}^z\right) & R < R_{threshold}^{h,z}, s\epsilon[R_{b,lower}^z, R_{b,upper}^z] \\ F_z^h\left(s; R_{a,lower}^z, R_{a,upper}^z\right) & R \geq R_{threshold}^{h,z}, s\epsilon[R_{a,lower}^z, R_{a,upper}^z] \end{cases} \tag{7.6}$$

The transition probability matrix (TRM), as illustrated in Equation (7.7), is the core of predicting the social vulnerability-driven household recovery process, $S(t)$. Sutley and Hamideh (2020) proposed the relationships between stage transition probability and social vulnerability based on extensive interviews, household surveys, and past literature (van de Lindt et al. 2020). The nonnegative elements in the transition probability matrix, $p_{i,j}(t)$, defined in Equation (7.8), describe the probability of a household transitioning to state S_q given its current state is S_p.

$$TRM(SV_z^h) = \begin{bmatrix} p_{1,1}(\mathrm{SV} = SV_z^h) & p_{1,2}(SV = SV_z^h) & p_{1,3}(\mathrm{SV} = SV_z^h) & p_{1,4}(\mathrm{SV} = SV_z^h) \\ p_{2,1}(\mathrm{SV} = SV_z^h) & p_{2,2}(\mathrm{SV} = SV_z^h) & p_{2,3}(\mathrm{SV} = SV_z^h) & p_{2,4}(\mathrm{SV} = SV_z^h) \\ p_{3,1}(\mathrm{SV} = SV_z^h) & p_{3,2}(\mathrm{SV} = SV_z^h) & p_{3,3}(\mathrm{SV} = SV_z^h) & p_{3,4}(\mathrm{SV} = SV_z^h) \\ 0 & 0 & 0 & 1 \end{bmatrix} \tag{7.7}$$

$$p_{p,q}(t+1) = P[S(t+1) = S_q | S(t) = S_p] \tag{7.8}$$

The initial ($t = t_0$) stage probability vector, $\pi(t_0) = [\pi_1(t_0); \pi_2(t_0); \pi_3(t_0)]$, where $\sum_{j=1}^{3} \pi_j(t_0) = 1$, is defined due to the joint effect of building damage, utility disruption, and social vulnerability to help determine the initial stage, $S(t_0)$, for each household following the hazard event (Lin and Wang 2017, Sutley and Hamideh 2020). It is worth noting that only the predicted household dislocation is required to estimate their initial stage to track each household recovery process using the Markov chain, as shown in Equation (7.9). For other households still residing in their original residence, this prediction assumes these households have their permanent housing already and do not enter the analysis. At any given time throughout the recovery process, the household can remain in its current state or transition to a higher/lower state in each time step (a time step equates to one month) until permanent housing or failure is reached, depending on its current state and its social vulnerability score, as shown in Equation (7.10). For more details about the cases resulting in household recovery failure (Stage 5), please refer to Sutley and Hamideh (2020).

$$S^h(t_0) = \begin{cases} 1 & I_{dis}^{k,h} = 1 \; and \; R < \pi_1(t_0) \\ 2 & I_{dis}^{k,h} = 1 \; and \; \pi_1(t_0) \le R < \sum_{n=1}^{2} \pi_n(t_0) \\ 3 & I_{dis}^{k,h} = 1 \; and \; \sum_{n=1}^{2} \pi_n(t_0) \le R < 1 \\ 4 & I_{dis}^{k,h} = 0 \end{cases} \tag{7.9}$$

$$S^h(t+1) = \begin{cases} 1 & R < p_{S^h(t),1}(\mathrm{SV} = SV_z^h) \\ 2 & p_{S^h(t),1}(\mathrm{SV} = SV_z^h) \le R < \sum_{n=1}^{2} p_{S^h(t),n}(\mathrm{SV} = SV_z^h) \\ 3 & \sum_{n=1}^{2} p_{S^h(t),n}(\mathrm{SV} = SV_z^h) \le R < \sum_{n=1}^{3} p_{S^h(t),n}(\mathrm{SV} = SV_z^h) \\ 4 & \sum_{n=1}^{3} p_{S^h(t),n}(\mathrm{SV} = SV_z^h) \le R < 1 \\ 5 & Any \; Markov \; chain \; regressive \; steps \; occur \end{cases} \tag{7.10}$$

The time needed for the entire household recovery process ($T_{H\_Recovery}$) is defined whenever the Markov stage of each household moves to permanent housing (Stage 4) for the first time, as illustrated in Equation (7.11). Afterward, this household's stage is stable and equal to 4 in each following time step. The time required for household recovery of each household is compared with that for their residential building recovery, recall Equation (7.5), to explore the physical-social interdependent recovery relationship.

$$T^h_{H\_Recovery} = T(S^h(t) = 4) \tag{7.11}$$

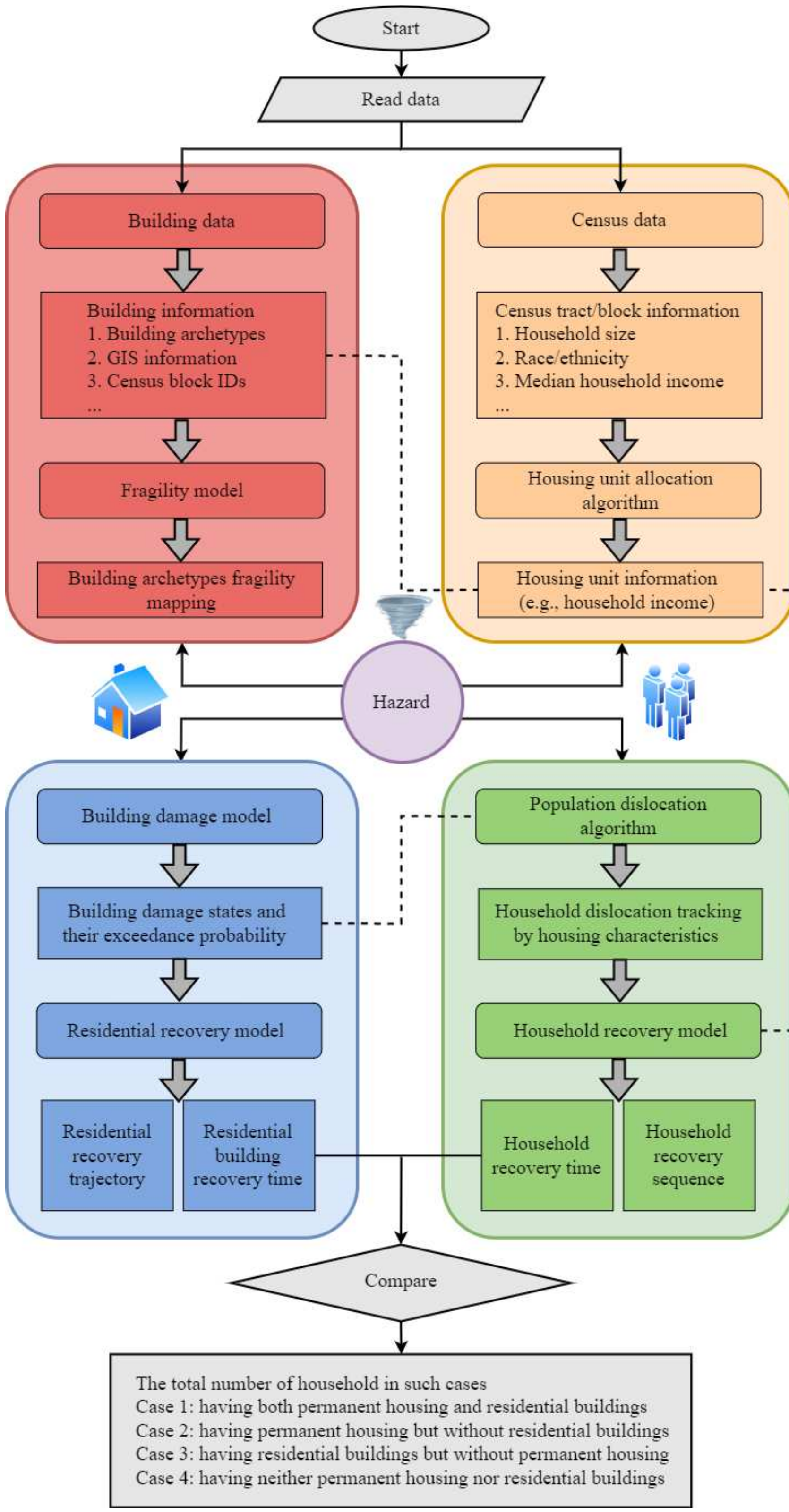

Figure 7-1. A simplified flowchart of the proposed physical-household interdependent recovery methodology

7.3 Illustrative Example

Joplin is a small to medium size community in the United States located in Southwest Missouri, spanning across Jasper county and Newton County. Joplin has a total population size of 50,150 and a land area of 92.09 square kilometers (35.56 square miles), as estimated in 2010 (U.S. Census Bureau. 2010). The 2011 Joplin tornado was a devastating Enhanced Fujita 5 (EF5) multiple-vortex tornado that struck on Sunday, May 22, 2011. This single tornado event resulted in 158 deaths and 1,150 injuries and caused damages amounting to US$2.8 billion (2011 dollars), ranked as the deadliest and costliest single tornado in U.S. history. Additionally, the tornado damaged over 7,400 residential buildings, more than 500 businesses, one of the two major hospitals (i.e., St. John's Regional Medical Center), ten public schools, two fire stations, and twenty-eight churches (Kuligowski et al. 2014). After the tornado, between 5,000 and 7,000 households lost their homes and had to dislocate to temporary housing. Some dislocated families rented or bought available apartments or homes in the area, and others stayed with family or friends. FEMA provided approximately 600 temporary housing units, and the Joplin area's private sectors (e.g., national charities, the business community, and volunteers) accommodated about 90 percent of dislocated households (Smith and Sutter 2013). After two years following the tornado, approximately 80% of residential buildings were fully recovered based on spatial video data (Pilkington et al. 2021). As of June 2013, all households had moved out of FEMA temporary housing and into longer-term or permanent housing (Fact Sheet 2021).

Due to the significant housing/infrastructure damage and long-term recovery in Joplin, this was selected as a testbed for this chapter to explore the preparedness, response, and recovery of the community (e.g., Houston et al. 2017, Ellingwood et al. 2017, Veil and Bishop 2014, Pilkington and Mahmoud 2020, Attary et al. 2018, Stone et al. 2021, Wang and van de Lindt 2021, Wang and van de Lindt 2022, Wang et al. 2021). This chapter also used the Joplin testbed as an illustrative example to implement the proposed methodology and explore the physical-social interdependent recovery relationship across coupled engineering and social science disciplines.

The building dataset was developed for Joplin circa 2010 prior to the 2011 tornado, which included building information such as building archetypes, year of construction, footprint areas, as well as demographic information. The synthetic household allocation algorithm allocates household characteristics such as household size, tenure status, race/ethnicity, and household income to each household in each building by de-aggregating from the census block level. Table 7-1 presents the data format of building information and the allocated household characteristics. The hazard for this illustrative example was the 2011 Joplin tornado. The tornado wind speed contour map was determined by estimating the damage indicators (DI) and degree of damage (DOD) for all the damaged buildings in the tornado path (Kuligowski et al. 2014, Wang et al. 2021).

Table 7-1. Data format of the integrated building information and household characteristics

GUID	Building information			HUID	Household characteristics		
	Archetypes	Year of construction	Footprint areas (ft^2)		Tenure status	Race/ Ethnicity	Household Income
GUID1	T1	1895	908	HUID1	Owner	Other race	HH1
GUID2	T1	1930	1069	HUID2	Renter	Hispanic	HH2
GUID3	T1	1993	2229	HUID3	Owner	Black alone	HH3
GUID4	T5	1955	4820	HUID4	Renter	White alone	HH4
GUID5	T5	1977	3515	HUID5	Owner	White alone	HH5
…	…	…	…	…	…	…	…

The analytical results of building damage prediction and household dislocation prediction are two key inputs for the subsequent physical-social interdependent recovery process, which is the objective of this chapter. Functionality of physical infrastructure (e.g., buildings, lifeline systems) due to natural hazard events is widely used by researchers to quantify the resilience index (e.g., Castillo et al. 2022, Ganin et al. 2016, Davis 2021, Koliou and van de Lindt 2020, Enderami et al. 2021), but researchers have not reached a consensus in defining the concept of functionality in multi-disciplinary community resilience studies. In this chapter, a *building* is defined as non-functional whenever the state of the building exceeds the moderate damage level within each MCS realization (Wang et al. 2022) which is, arguably simplified, but can be modified as more is learned about how to operationalize functional recovery and its definition. The number of buildings in this dataset within the simulated tornado path was 7,834, which generally matches the damaged buildings recorded in Kuligowski et al. (2014), with an error of less than 5%. This example focuses on the allocated Joplin households residing in residential buildings within the tornado path to examine the previously described interdependent recovery methodology.

Figure 7-2 shows the heat maps depicting physical-social disruption immediately following the tornado. Figure 7-2(a) illustrates the spatial probability of buildings being non-functional, where the heatmap uses the Viridis as the color ramp, and bright colors such as green refer to the buildings having a higher probability of being non-functional. Figure 7-2(b) presents the variation of household dislocation probability where the red colors in the spectrum refer to the buildings with a higher dislocation probability. It can be observed that the trend for the brighter color areas in the two figures is almost consistent, which verifies that household dislocation is driven by building damage for the Joplin testbed, but not an exact correlation. All other housing characteristics do not immensely impact the household dislocation decisions (recall Equation (7.3)). Figure 7-3 shows the maps of the dislocated households for a typical MCS realization grouped by the household characteristics of tenure status, race/ethnicity, and household income. It is felt that more social-vulnerable groups such as renters and Hispanics are not shown as more likely to dislocate for

Joplin, or the impact of social vulnerability to household dislocation following the tornado is relatively slight.

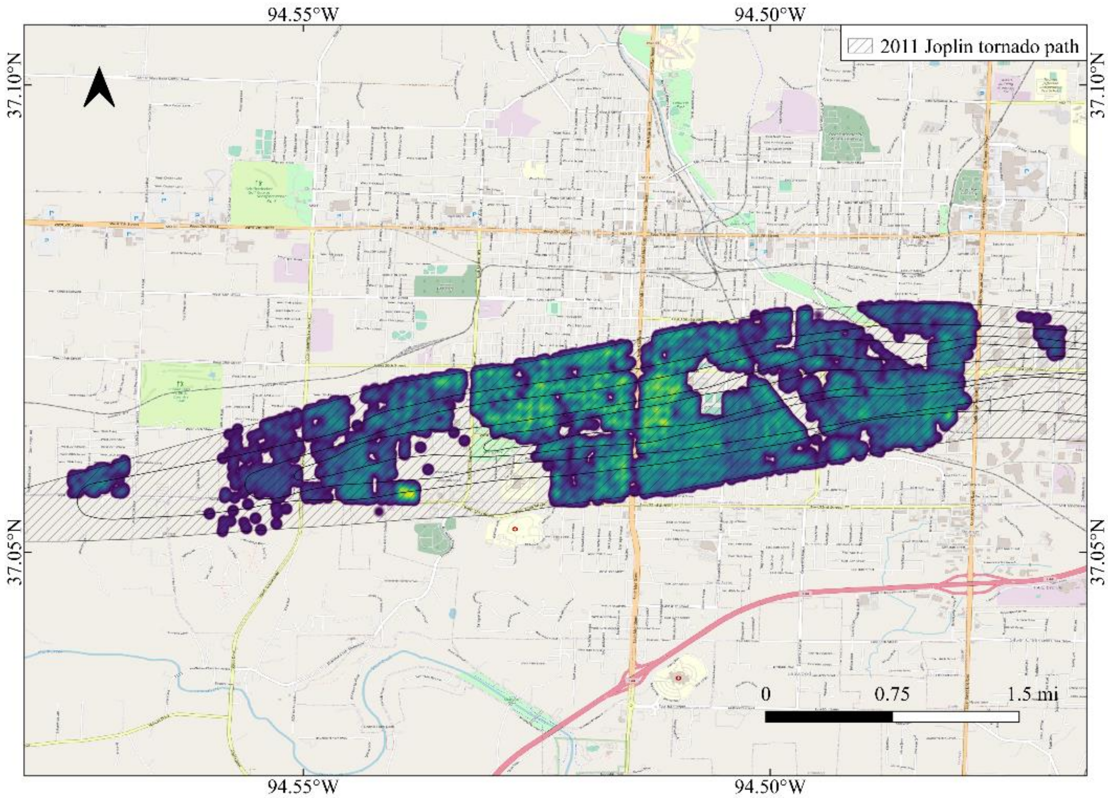

(a)

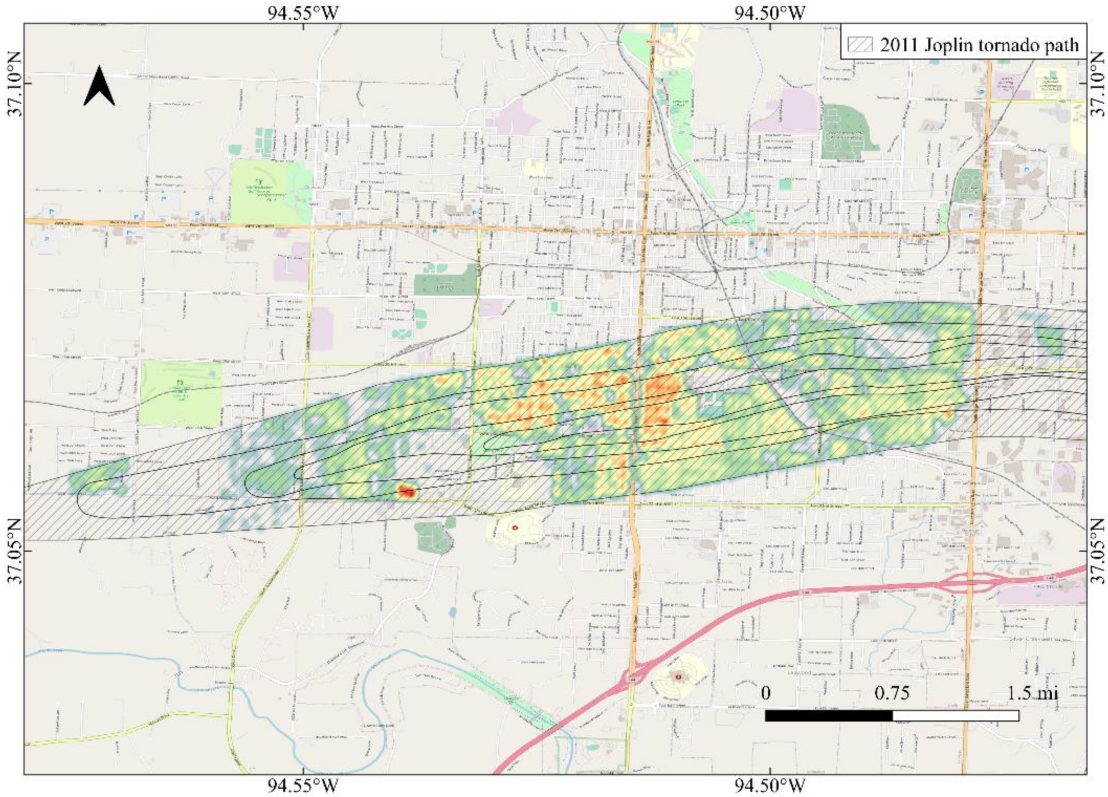

(b)

Figure 7-2. Physical-social disruption immediately following the tornado: (a) building functionality probability; (b) household dislocation probability

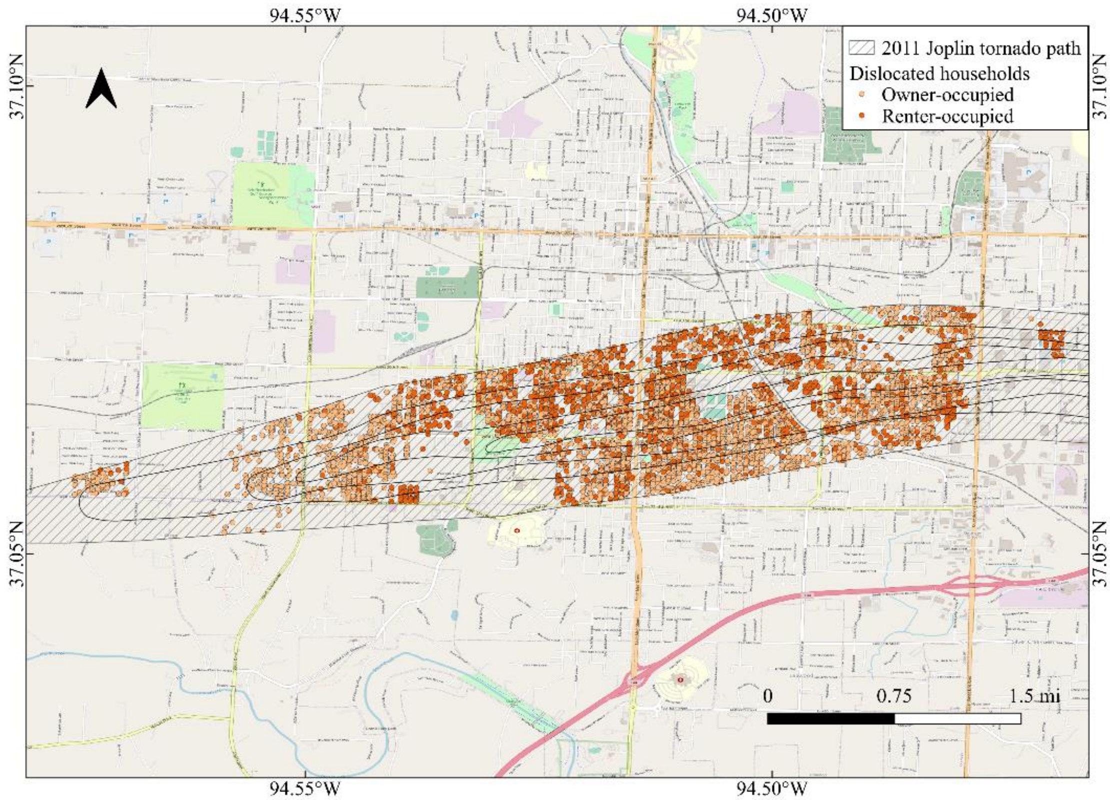
94.55°W
94.50°W
37.10°N
37.05°N
2011 Joplin tornado path
Dislocated households
Owner-occupied
Renter-occupied
0
0.75
1.5 mi

(a)

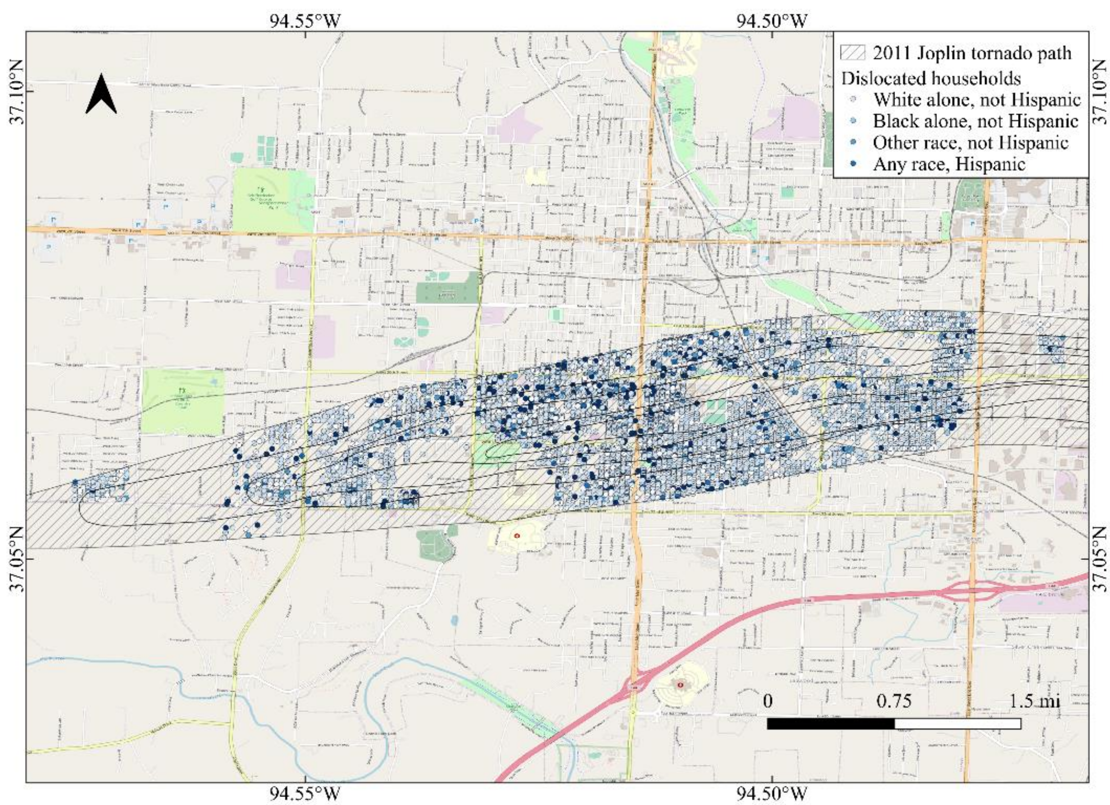
94.55°W
94.50°W
37.10°N
37.05°N
2011 Joplin tornado path
Dislocated households
White alone, not Hispanic
Black alone, not Hispanic
Other race, not Hispanic
Any race, Hispanic
0
0.75
1.5 mi

(b)

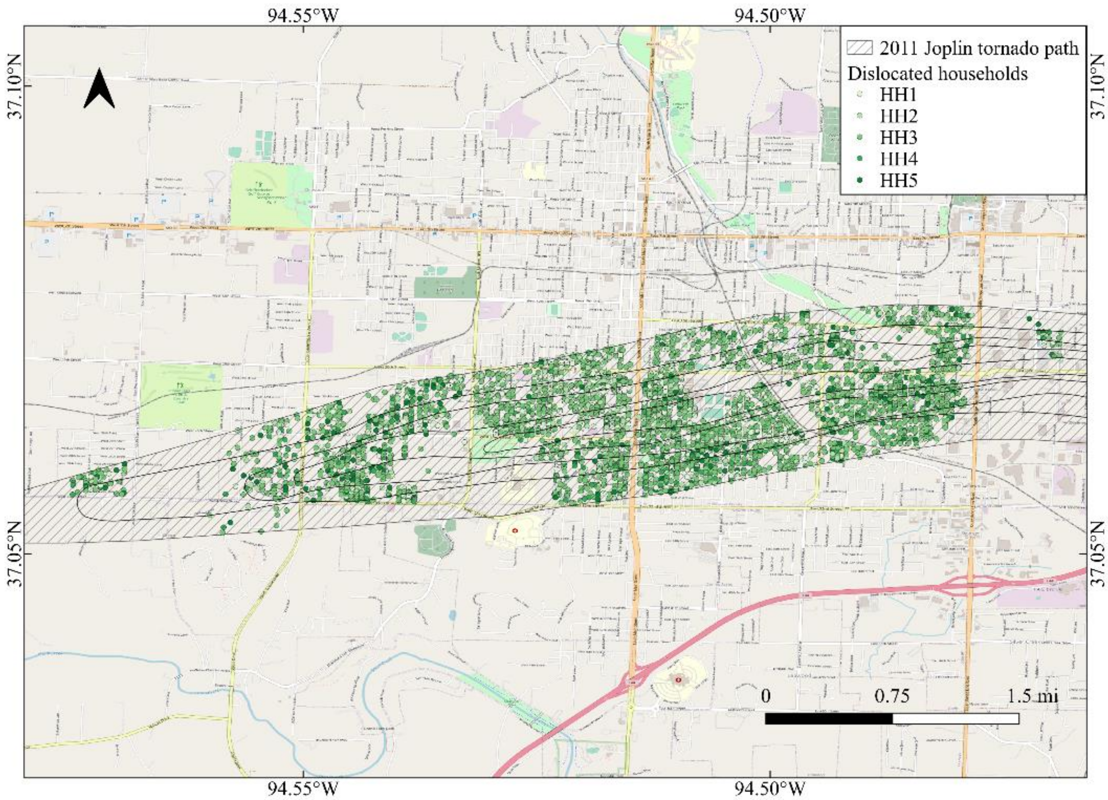

(c)

Figure 7-3. Dislocated households within a typical MCS realization by household characteristics: (a) tenure status; (b) race/ethnicity; (c) household income

Within the tornado path of this illustrative example, there are 7,201 Joplin households residing in 5,327 residential buildings within the community level model that have the possibility of their homes being damaged at different levels (DS's) and potentially dislocate. Table 7-2 indicates the physical damage to buildings and the impacted homes for a typical MCS realization. Around 90% of residential buildings were damaged at a complete level (DS4), and only 3% of residential buildings can keep functional following the tornado. The damageable components for the woodframe residential buildings in this example consists of an asphalt shingle, wood roof sheathing panels nailed every 12 inches (30.5 cm) at the center (field nailing) and every 6 inches (15.2 cm) at the edge (edge nailing), and two toenails used to connect wooden trusses to wall top plates/studs (Wang et al. 2021). Approximately 90% of households experienced the building damage at a complete level. Table 7-3 indicates the household dislocation decisions within a typical MCS realization. Overall, the predicted dislocated households are within the range of the actual number of dislocated households mentioned at the beginning of this section. However, the percentage of dislocated households in different categories grouped by household characteristics (i.e., tenure status, race/ethnicity, and household income herein) does not show a large difference. More specifically, the percentage of dislocated households for more socially-vulnerable groups, including renters, Hispanic, and low-income groups, is relatively higher but not that apparent.

Table 7-2. Physical damage within the tornado path for a typical MCS realization

Building specific conditions	Total buildings	Total households	Dislocated households
Slight	164 (3.0%)	220 (3.1%)	153 (2.7%)
Moderate	183 (3.4%)	228 (3.2%)	144 (2.6%)
Extensive	231 (4.3%)	300 (4.2%)	215 (3.8%)
Complete	4,749 (89.1%)	6,453 (89.6%)	5,087 (90.9%)
In total	5,327 (100%)	7,201 (100%)	5,599 (100%)

Table 7-3. Social disruption within the tornado path for a typical MCS realization

Household characteristics	Dislocated households	Total households
Tenure status		
Owner-occupied	2,645 (75.9%)	3,487 (100%)
Renter-occupied	2,429 (79.6%)	3,052 (100%)
No tenure data	525 (79.3%)	662 (100%)
In total	5,599 (77.8%)	7,201 (100%)
Race/ethnicity		
White alone, not Hispanic	4,572 (77.5%)	5,899 (100%)
Black alone, not Hispanic	113 (76.9%)	147 (100%)
Other race, not Hispanic	253 (77.4%)	327 (100%)
Any race, Hispanic	136 (81.9%)	166 (100%)
No race/ethnicity data	525 (79.3%)	662 (100%)
In total	5,599 (77.8%)	7,201 (100%)
Household income group		
HH1 (less than $15,000)	764 (79.6%)	960 (100%)
HH2 ($15,000-$25,000)	722 (76.7%)	941 (100%)
HH3 ($25,000-$75,000)	2,338 (77.6%)	3,014 (100%)
HH4 ($75,000-$100,000)	343 (77.6%)	442 (100%)
HH5 (more than $100,000)	317 (74.6%)	425 (100%)
No income data	1,115 (78.6%)	1,419 (100%)
In total	5,599 (77.8%)	7,201 (100%)

Following the 2011 Joplin tornado, the local government launched a series of policies to facilitate recovery, including relaxing regulations, hiring extra building inspectors, waiving bidding rules, and resisting the temptation to micromanage (Smith and Sutter 2013). In addition, financial assistance was comprehensively provided from government grants and business donations to help residents overcome the difficulties in finding temporary housing and repairing their buildings, and therefore shorten the recovery process. This example implemented the residential building recovery prediction with these policy decisions incorporated, which have been validated using assessable longitudinal recovery video capture data (Wang and van de Lindt 2021, Pilkington et al. 2021). Figure 7-4 presents the histograms of a typical residential building recovery time in an EF1 and EF2 tornado region over sufficient MCS realizations, where the histograms are normalized and plotted versus a lognormal distribution. The mean recovery time of the two buildings shown is 74 weeks and 83 weeks.

The residential building recovery methodology applied incorporated household income as a socio-demographic indicator to predict the funding options available to households to finance their residential building repairs (Wang and van de Lindt 2021). The recovery time of all residential buildings explored in this example within a typical MCS realization can also fit for a lognormal distribution, as illustrated in Figure 7-5(a). In order to minimize the effect of building damage brought to the community recovery and examine the residential building recovery impacted by household income characteristics, Figure 7-5(b) presents the determined lognormal distributions of all residential building recovery times in the EF2 region grouped by the household income levels. It can be observed that higher household income levels slightly shorten the residential building recovery process, but the effect is not significant. Figure 7-6 shows the mean residential building recovery time over the community. The analytical results indicate that around 82% of residential buildings can be fully recovered two years after the tornado, consistent with the video data (Pilkington et al 2021). More specifically, delay time dominates the residential building recovery process based on the analytical results and accounts for more than 60% of the total time needed for the entire process of residential building recovery.

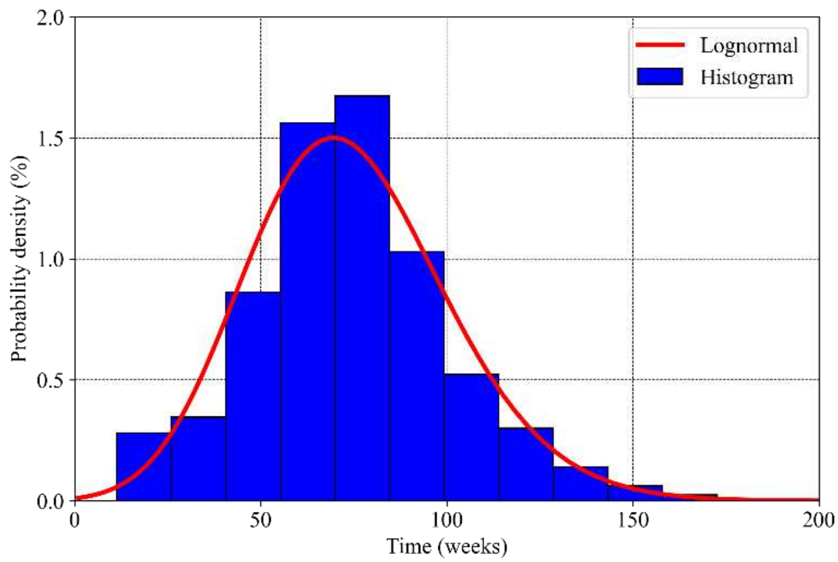

(a)

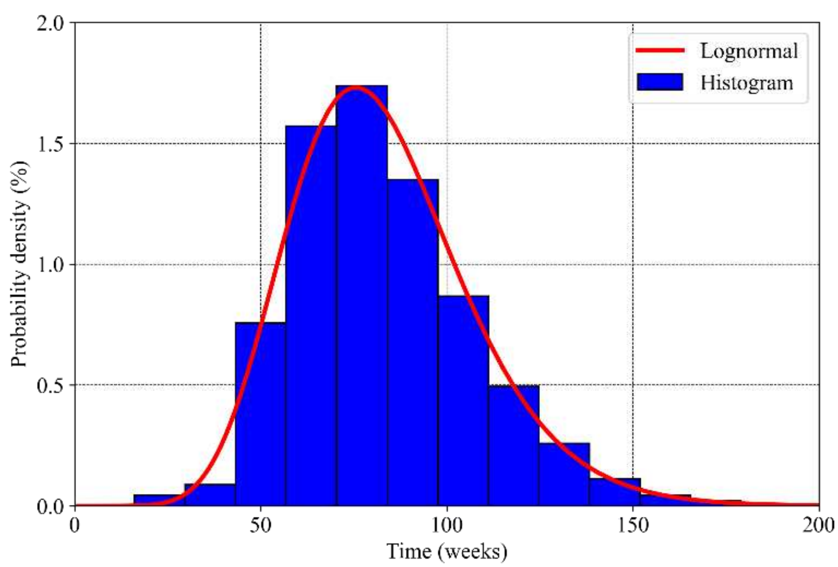

(b)

Figure 7-4. Recovery time of a typical residential building: (a) in the EF1 tornado region; (b) in the EF2 tornado region

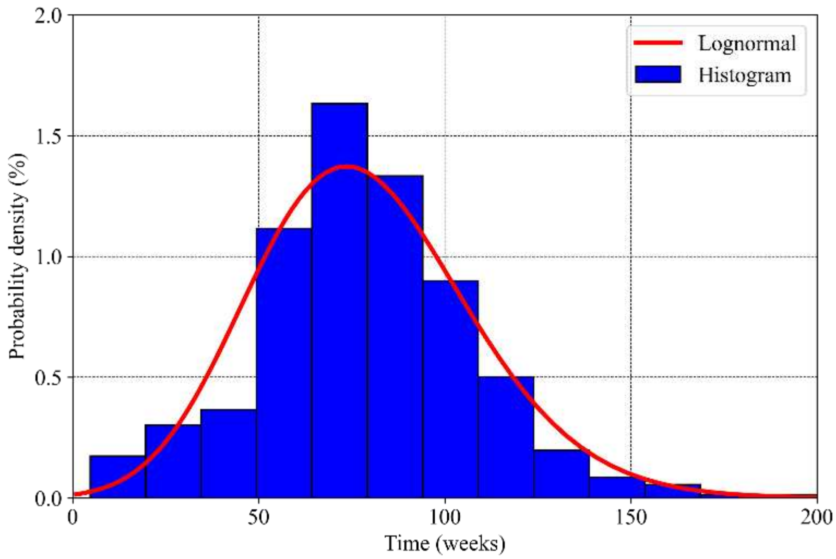

(a)

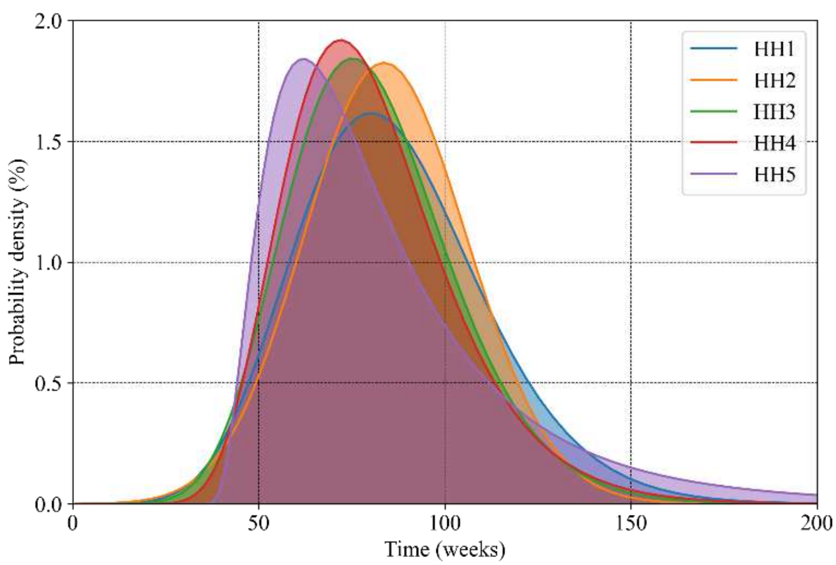

(b)

Figure 7-5. Residential recovery time over the community within a typical MCS realization: (a) histogram and lognormal distribution; (b) grouped by household income for all residential buildings in the EF2 region

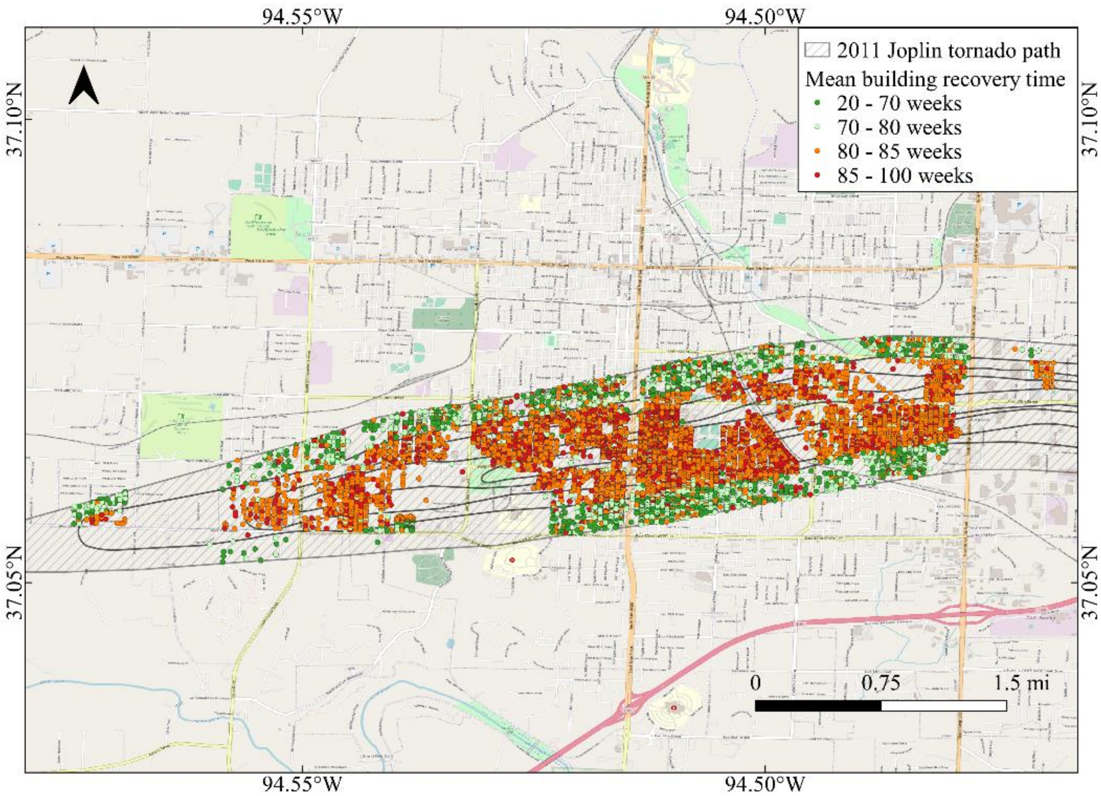

Figure 7-6. Mean building recovery time over the community

The household recovery approach implemented in this example is a social vulnerability-driven approach, and this example modified the social vulnerability assignment approach based on neighborhood zones explained in Sutley and Hamideh (2020). More social-vulnerable groups, such as renters, Hispanics, and lower household income groups, correspond to higher social vulnerability groups. Joplin has a relatively even population distribution, and household characteristics in different neighborhood zones are not significantly different. This example used the allocated household income at a household level to group the social vulnerability zones, building on social vulnerability assignments shown in Table V in Sutley and Hamideh (2020), as indicated in Table 7-4. Two different ranges (percent of households I and percent of households II shown in Table 7-4) were assigned to different proportions of households in each social vulnerability zone. The purpose of this allocation is that a small number of households might be assigned social vulnerability scores in a broader range reflecting the socio-demographic features in real-world communities, recall Equation (7.8). For example, for the highest household income group, HH5, 95% of households were assigned a lower social vulnerability range uniformly distributed from 0.01 to 0.15, and the remaining 5% of households were assigned a more comprehensive social vulnerability range uniformly distributed from 0.1 to 0.9 to represent a small number of exceptional household cases. Figure 7-7 shows the predicted household social vulnerability scores for a typical MCS realization over the community.

Table 7-4. Social vulnerability assignments to Joplin households

Household income group	Percent of households I	Social vulnerability range I	Percent of households II	Social vulnerability range II
HH5	95%	0.01-0.15	5%	0.10-0.90
HH4	85%	0.10-0.50	15%	0.10-0.90
HH3	80%	0.30-0.70	20%	0.10-0.90
HH2	85%	0.50-0.90	15%	0.10-0.90
HH1	95%	0.85-0.99	5%	0.10-0.90

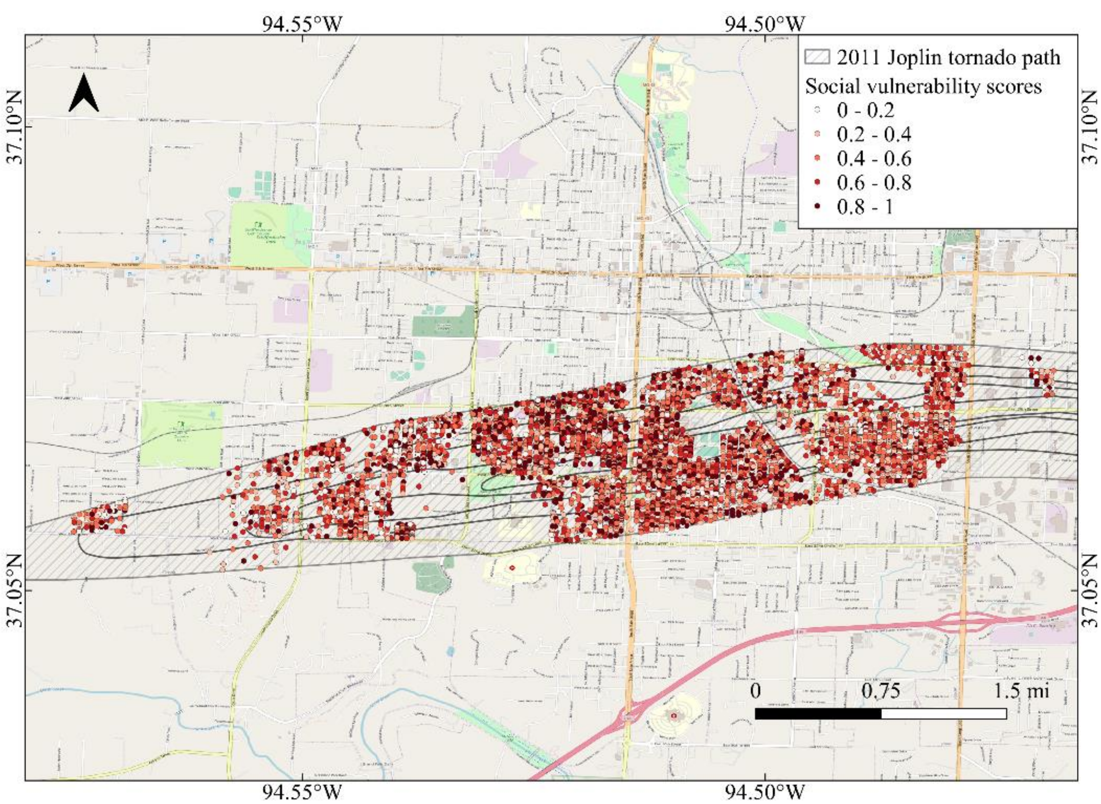

Figure 7-7. Household social vulnerability scores over the community

Figure 7-8 illustrates the predicted household recovery sequences of several households within a typical MCS realization as an example. More specifically, two households shown in Figure 7-8(a) were allocated to the building in the EF1 region shown in Figure 7-4(a), and another two shown in Figure 7-8(b) to the building in the EF2 region shown in Figure 7-4(b). The housing recovery sequences of two example households in the EF1-impacted building differ within MCS realizations, but the mean household recovery time for the two is relatively close, and no recovery failure occurred. One of the households in the EF2-impacted building shown in Figure 7-8(b) was predicted to stay and not dislocate; therefore, the household recovery sequences can be shown as a straight line over time, maintaining the permanent housing status (Stage 4). The other household shown in Figure 7-8(b) reached a household recovery failure in this realization. In this example, the household recovery approach applied predicts the recovery process for 90 months, which can be designed differently for other uses. The household recovery time for the cases reaching a recovery failure was considered 360 weeks to increase the average recovery time of this household significantly to show there is a higher possibility for this household to experience the recovery failure.

In some cases, even though a household was predicted to have permanent housing in the end, the process is relatively challenging, resulting in the household recovery time being relatively more prolonged than in others. The mean household recovery time of two example households in Figure 7-8(a) and the dislocated household in Figure 7-8(b) within MCS realizations is 35, 26, and 214 weeks. Figure 7-9(a) shows the histogram of all household recovery time within a typical MCS realization, which can fit an exponential distribution if exempt from the household recovery failure cases. Figure 7-9(b) presents the exponential distributions of all household recovery time grouped by household income levels in a particular MCS realization. As expected, households in higher income groups reach permanent housing faster than those in lower income groups. The distribution curve for the HH5 group is too sharp, which is not shown in the Figure 7-9(b). Figure 7-10 shows the household recovery time over the community for a typical MCS realization. Most households can assess permanent housing within 70 weeks if generally compared with the mean building recovery time recalling Figure 7-6. More than 10% of households reached recovery failure in this illustrative realization. In addition, it can be observed that the building damage and the tornado regions in different EF scales did not significantly impact the household recovery time.

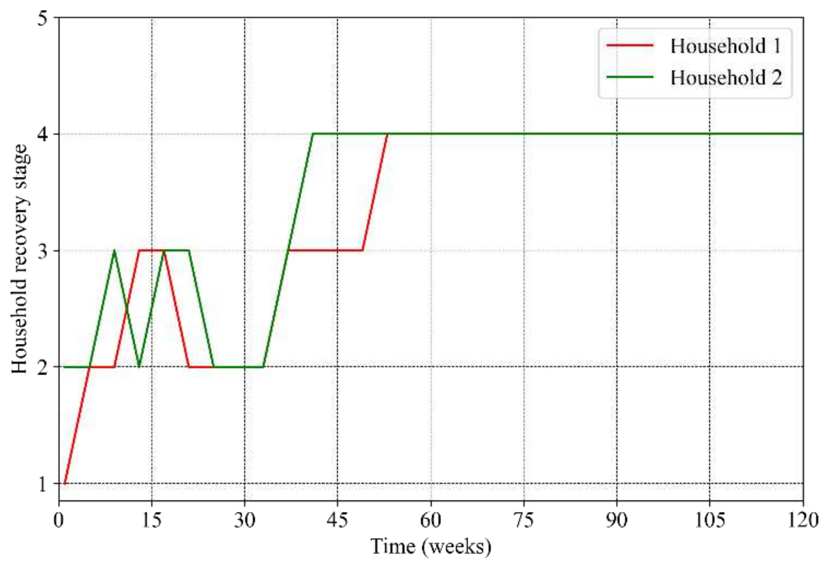

(a)

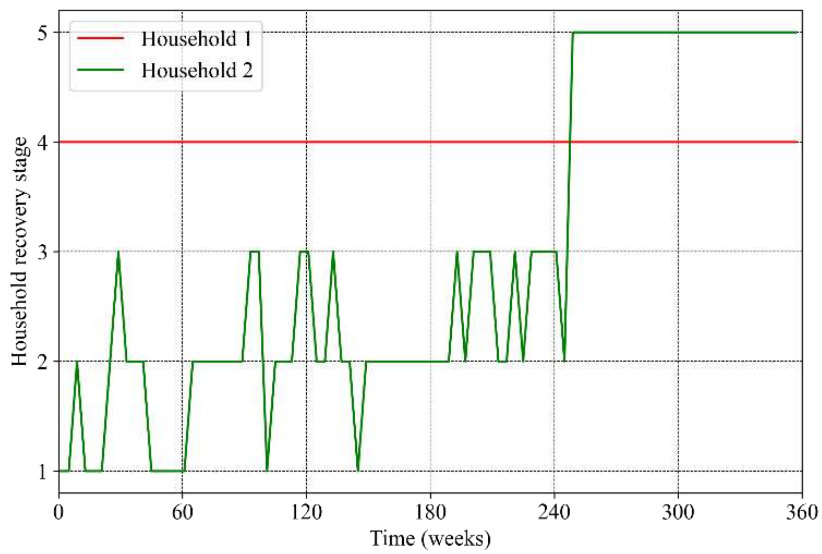

(b)

Figure 7-8. Household recovery sequences for two illustrative example households allocated to a typical residential building: (a) in the EF1 tornado region; and (b) in the EF2 tornado region

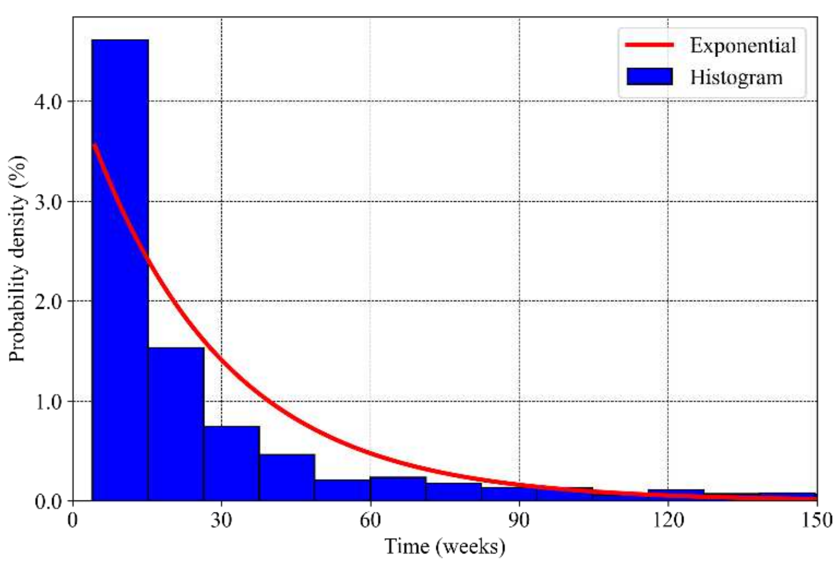

(a)

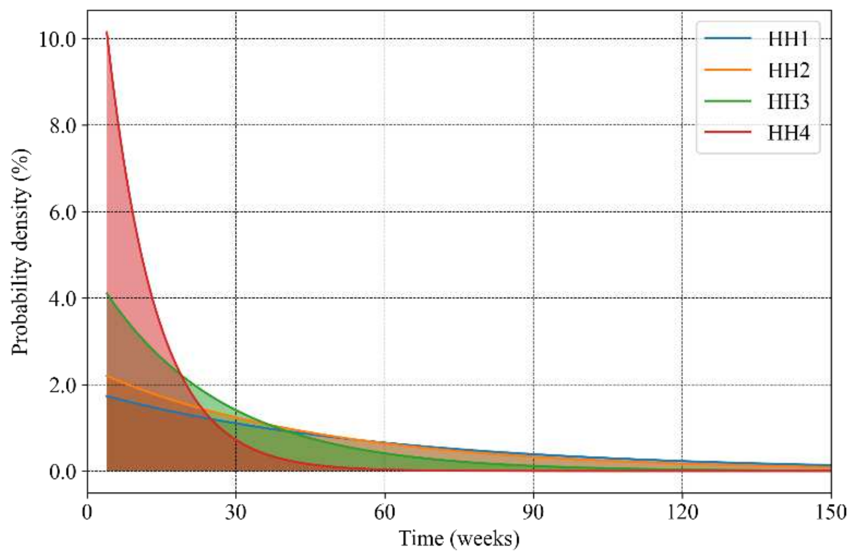

(b)

Figure 7-9. Household recovery time over the community within a typical MCS realization: (a) histogram and exponential distribution; (b) grouped by household income

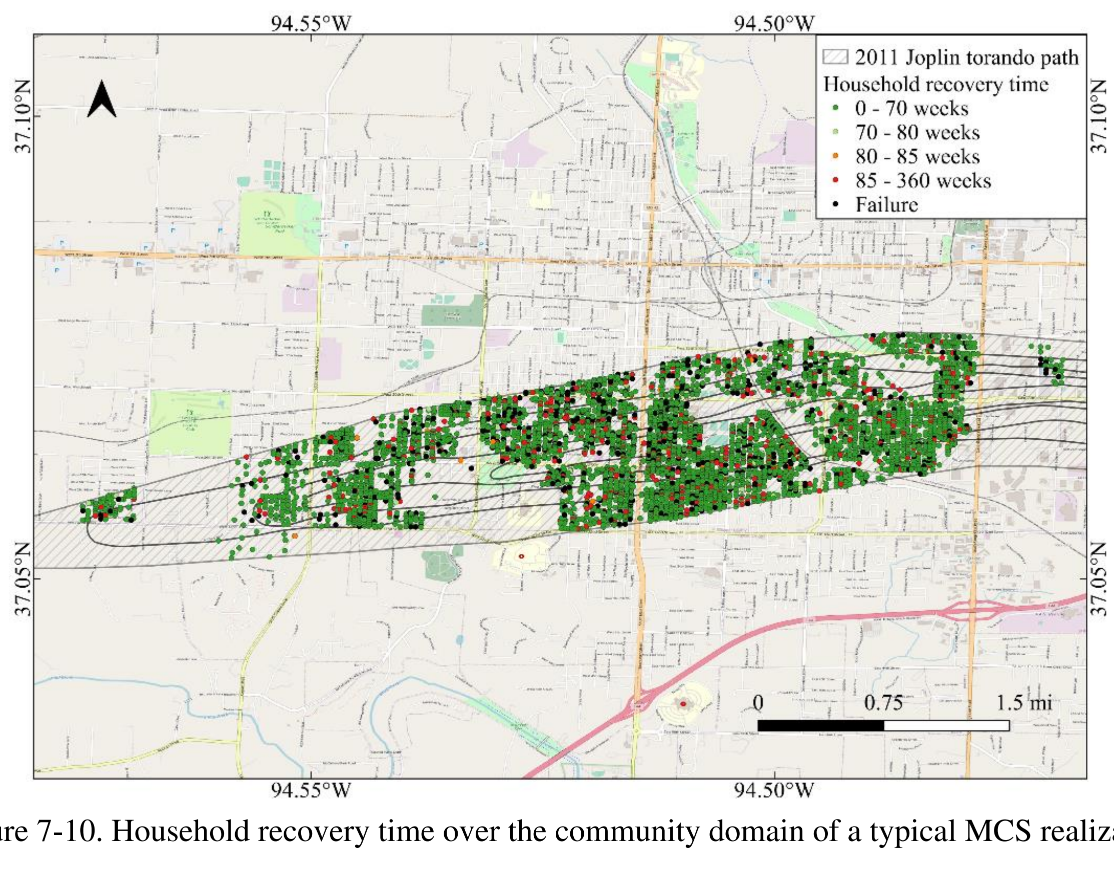

Figure 7-10. Household recovery time over the community domain of a typical MCS realization

Household income information is the key input to group the social vulnerability zones in this example, as mentioned earlier. Due to a small number of data missing related to race and ethnicity of minorities, only around 80% of household income information has been allocated to households. In order to maintain their privacy and keep the income information estimation more accurate, this example did not predict the missing income information for the remaining households. However, it should be noted that the authors can de-aggregate the housing units at the census block level and predict the missing income information based on a Gaussian model (Wang and van de Lindt 2021). Therefore, only dislocated households with the predicted income information have been included in the estimated household recovery process. This example assumes households who decide not to dislocate following the tornado can access their permanent housing directly, no matter whether their residential buildings are damaged.

Around 85% of the households were predicted to experience household recovery, summarized in the following tables to integrate the residential building recovery with the household recovery and explore the physical-social interdependent recovery. Figure 7-11 shows the resulting exponential distribution representative of household recovery and the lognormal distribution representative of residential building recovery within a typical MCS realization. In order to track the building and household recovery performance throughout the community, the average percentage of residential buildings fully recovered and the average percentage of dislocated households moving to permanent housing over time can be determined, where the approach is consistent with that explained in Chapter 5.

Table 7-5 presents the average percentage of fully recovered residential buildings predicted and the average percentage of dislocated households moving to permanent housing over time from the perspective of the community recovery process. The average percentage of residential buildings fully recovered matches the analytical results shown in Figure 5-12 in Chapter 5, which have been validated. Around 80% of households moving into permanent housing after one month following the tornado are because they are not predicted to dislocate. Note that the residential building recovery prediction assumed that no households would out-migrate but rather stay in the community to complete the repairs following a hazard event, which means the actual average percentages of residential buildings fully recovered would be fewer than the percentages shown in Table 7-5. Overall, during the two years after the tornado damage, the housing recovery is faster than the residential building recovery (recall Figure 7-11) and should be further faster if considering the assumption above. After two years, the average percentage of dislocated households moving to permanent housing cannot reach more than 80% because many households experience a recovery failure or are still looking for permanent housing, but the process is struggling.

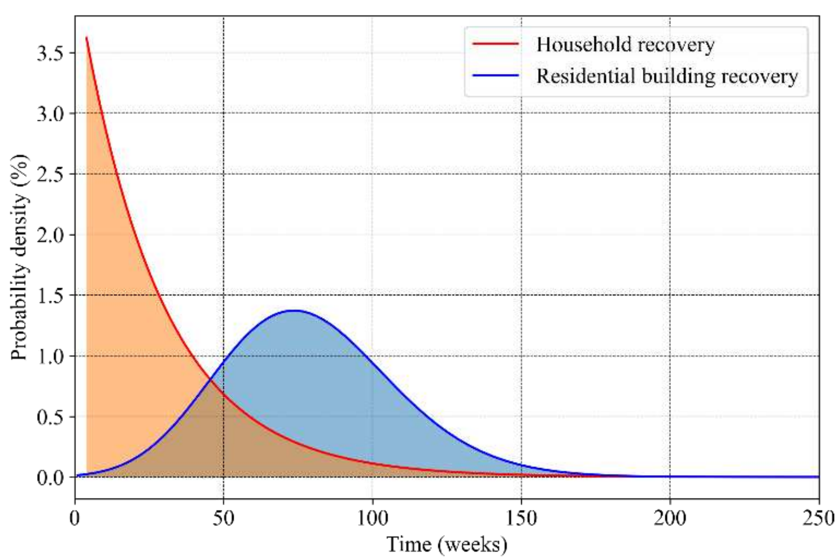

Figure 7-11. Household recovery and residential recovery time over the community for a typical MCS realization

Table 7-5. Physical-social interdependent recovery results emphasizing the community recovery process

Time (months)	Average percentage of residential buildings fully recovered	Average percentage of dislocated households moving into permanent housing	Average percentage of all households moving into permanent housing
1	0 (0%)	418 (9.3%)	2,020 (33.2%)
3	41 (0.1%)	1,337 (29.8%)	2,939 (48.3%)
6	245 (4.6%)	2,168 (48.4%)	3,770 (62.0%)
12	744 (14.0%)	2,808 (62.5%)	4,410 (72.5%)
15	1,527 (28.7%)	2,973 (66.3%)	4,575 (75.2%)
18	2,642 (49.6%)	3,087 (68.9%)	4,689 (77.1%)
21	3,661 (68.7%)	3,180 (71.0%)	4,782 (78.6%)
24	4,387 (82.4%)	3,256 (72.6%)	4,858 (79.8%)
36	5,251 (98.6%)	3,467 (77.4%)	5,069 (83.3%)
In total	5,327 (100%)	4,482 (100%)	6,084 (100%)

Table 7-6 focuses on the recovery process of each household over time using the mean recovery time for each building within MCS realizations. Recall that four cases were proposed to explore the physical-social interdependent recovery relationship in the simplified flowchart shown in Figure 7-1; Figure 7-12 shows the event tree of household options during recovery for different cases. If following all the assumptions involved in the integrated predictions, households are assumed to want/work to return their original residential buildings fully recovered for Case 1. Case 2 refers to households achieving permanent housing, but their residential buildings are still in the repair process, where households have multiple options. For example, the household may dislocate and then return but plan to rebuild/buy another residential building in other areas in the same town. Case 3 occurs relatively low frequency to have their original residential buildings fully recovered but still not access to their permanent housing. It may be because the surrounding business district and K-12 schools need more time to recover, and households feel it is not a perfect time to return. It is assumed that lifeline systems such as electric power, water, and transportation are usually recovered promptly and become operational following the tornado. Households and their residential buildings are still in the recovery process for Case 4, which will typically take more time to reach full recovery.

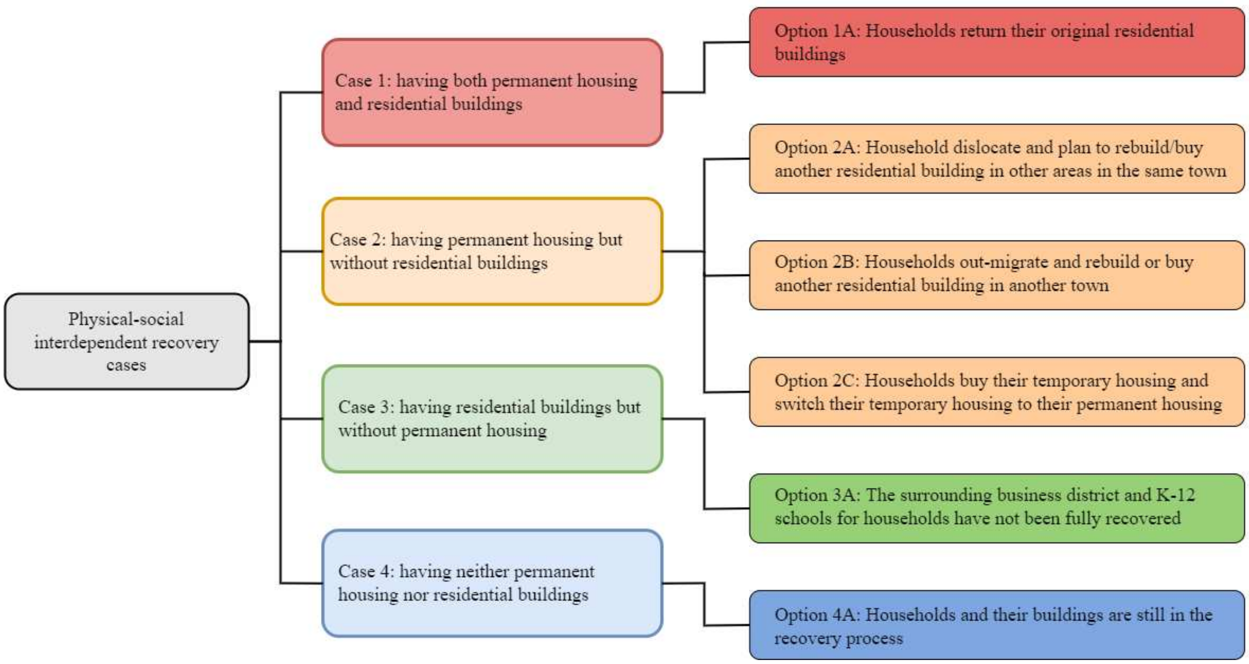

Figure 7-12. The event tree of household options during recovery for different cases

Table 7-6. Physical-social interdependent recovery results emphasizing the recovery process of each household

<table>
<tr><th rowspan="3">Time (months)</th><th colspan="2">Case 1</th><th colspan="2">Case 2</th><th colspan="2">Case 3</th><th colspan="2">Case 4</th></tr>
<tr><th>Building</th><th>Permanent housing</th><th>Building</th><th>Permanent housing</th><th>Building</th><th>Permanent housing</th><th>Building</th><th>Permanent housing</th></tr>
<tr><th>X</th><th>X</th><th></th><th>X</th><th>X</th><th></th><th></th><th></th></tr>
<tr><td>1</td><td colspan="2">0 (0%)</td><td colspan="2">1,633 (26.8%)</td><td colspan="2">0 (0%)</td><td colspan="2">4,451 (73.2%)</td></tr>
<tr><td>3</td><td colspan="2">0 (0%)</td><td colspan="2">2,430 (39.9%)</td><td colspan="2">0 (0%)</td><td colspan="2">3,654 (60.1%)</td></tr>
<tr><td>6</td><td colspan="2">7 (0.1%)</td><td colspan="2">3,379 (55.5%)</td><td colspan="2">1 (0%)</td><td colspan="2">2,697 (44.3%)</td></tr>
<tr><td>12</td><td colspan="2">59 (1.0%)</td><td colspan="2">4,033 (66.3%)</td><td colspan="2">9 (0.1%)</td><td colspan="2">1,983 (32.6%)</td></tr>
<tr><td>15</td><td colspan="2">385 (6.3%)</td><td colspan="2">3,883 (63.8%)</td><td colspan="2">68 (1.1%)</td><td colspan="2">1,748 (28.7%)</td></tr>
<tr><td>18</td><td colspan="2">887 (14.6%)</td><td colspan="2">3,516 (57.8%)</td><td colspan="2">217 (3.6%)</td><td colspan="2">1,464 (24.1%)</td></tr>
<tr><td>21</td><td colspan="2">3,543 (58.2%)</td><td colspan="2">979 (16.1%)</td><td colspan="2">909 (14.9%)</td><td colspan="2">653 (10.7%)</td></tr>
<tr><td>24</td><td colspan="2">4,622 (76.0%)</td><td colspan="2">3 (0%)</td><td colspan="2">1,453 (23.9%)</td><td colspan="2">6 (0.1%)</td></tr>
<tr><td>36</td><td colspan="2">4,925 (81.0%)</td><td colspan="2">0 (0%)</td><td colspan="2">1,159 (19.0%)</td><td colspan="2">0 (0%)</td></tr>
</table>

7.4 Summary and Conclusions

Hazard events are occurring at higher intensities and frequency due to climate change and other environmental variables stimulate researchers and analysts to expedite the progress to achieve the multi-disciplinary community resilience assessments for decision-making support. With the development and improvement of multi-disciplinary community resilience modeling, the ability to model interdependent recovery across physical infrastructure and social systems is novel and urgently needed. The proposed methodology in this chapter chains the building damage methodology, household allocation prediction, population dislocation prediction, residential building recovery prediction, and household recovery prediction developed in previous studies to explore the physical-social interdependent recovery process, especially for the recovery process of dislocated households and the interdependence with their damaged residential buildings. The illustrative example in this chapter uses the 2011 Joplin tornado as the hazard model, but the proposed methodology can be expanded and widely applied to any communities with different hazard events. The following conclusions can be drawn based on the work presented in this chapter:

- For the illustrative example herein, household dislocation occurs more likely due to damage because households do not have accessible and functional residential buildings. The Joplin population is relatively evenly demographically distributed, and socially vulnerable populations such as renters, Hispanics, and low household income groups are predicted to be slightly more likely to dislocate, but the impacts of household characteristics on household dislocation are slight. This situation may not apply to other communities with different population sizes and household characteristics under different natural hazards.

- Overall, household recovery for households re-accessing their permanent housing is much faster than residential building recovery for repair/rebuild. However, the average percentage of dislocated households moving to permanent housing does not reach more than 80% over a long-time horizon because many households experience a household recovery failure. This chapter also provides reasonable explanations for different cases households experience during the recovery process.
- The allocated household income information, representing typical sociodemographic characteristics in real-world communities, is used to group the households in different social vulnerability levels in this chapter. Households with higher incomes reach permanent housing much faster than those with lower incomes. However, households in higher household income groups slightly shorten the residential building recovery process, but the effect is insignificant even when evaluating households located in the same tornado intensity (EF) region.

It is important to note that all households who received temporary housing assistance provided by FEMA were validated to have moved into permanent housing after more than two years following the tornado, but the number of households in this case only accounts for 10% of all dislocated households. The remaining 90% of dislocated households were accommodated by the private sectors and cannot be as easily tracked. Some of them, especially socially vulnerable populations, may experience household recovery failure, as predicted in the illustrative example. The number/percentage of household recovery failures estimated from the household recovery prediction in this chapter cannot be fully validated using real-world data at this stage. In addition, future studies may improve the residential building recovery prediction by incorporating exceptional cases such as household outmigration, recovery plan terminations, and rebuilding decisions. Addressing the above limitations is not within the scope of this chapter. In summary, quantifying the interdependent community recovery across physical infrastructure and social systems can help the community develop resilience planning, guide community recovery, and maintain population stability following hazard events.

CHAPTER 8 SUMMARY, CONCLUSIONS, AND RECOMMENDATIONS

8.1 Summary, Conclusions, and Contributions

This dissertation proposes a series of multi-disciplinary community resilience assessment models across physical infrastructure systems and socio-economic systems across temporal and spatial scales. This dissertation intends to provide a methodology which can provide key technical information to community leaders and stakeholders of the community-wide impacts of natural hazards from a multi-disciplinary and multi-dimensional perspective to help further develop short-term and long-term policies and strategies to improve community resilience.

The most significant anticipated contribution of this dissertation to the research community is developing and demonstrating methodologies to enable resilience-informed decision-making and policy selection by quantifying the effects of hazard events on building performance and socio-economic resilience metrics over time, i.e. recovery modeling for buildings. The core community resilience metrics defined within different community stability areas, namely population stability, economic stability, physical services stability, and social services stability, are impacted by different designs (either retrofits or design codes) and policies that can further inform design guidelines of building codes and standards and inform decision-making and community resilience planning. The de-aggregation of community resilience goals to individual building performance targets can help accelerate the development of resilience-based building codes and standards that satisfy community-wide resilience goals for the built environment. Summarize below are the more specified contributions and findings from chapters following the dissertation outline presented in Chapter 1.

In Chapter 2, a fully quantitative interacting methodology was developed to examine the effect of a tornado damaging physical infrastructure and the effects on a real community's population and the local economy. The effect of retrofit strategies for tornado loading was examined quantitively in terms of their effects on social science and economic community-level metrics. The more robust retrofit strategy most significantly improved the performance of residential buildings and then reduced the economic losses and population dislocation. Less than 50% of buildings and households were able to receive electric power following the simulated 2011 Joplin tornado, which aligns with real-world data.

In Chapter 3, structural performance goals selected for buildings (or any physical system) was developed based on the ability to achieve social and economic goals at the community scale. Performance targets for individual residential buildings were de-aggregated to determine the percentage of buildings that should be retrofitted. The percent loss of functionality to buildings and the percent of economic loss and household dislocation can be reduced at different levels when different percentages of residential buildings are randomly retrofitted throughout the community. The resilience goals are flexible and can be quantitively adjusted for different levels based on community input and a community's unique needs.

In Chapter 4, new fragility functions for school building archetypes were developed using the latest ASCE structural loading standard, including tornado loads that can be used in community resilience studies. The direct dependency of a core resilience metric were illustrated between social service stability (i.e., the number of children remaining in schools) to be used in community resilience planning and the proposed improving school building designs/building codes. Improving the building performance can help significantly mitigate the damage to school buildings following moderate tornado events and provide communities the evidence to strengthen school designs for new/existing buildings. More importantly, building performance improvement further reduces dislocation and maintains educational continuity, which is essential in providing social service stability.

In Chapter 5, quantitative probabilistic analysis was performed to determine the residential building recovery over the community domain when impacted by policy changes implemented by either federal, state, or local governments. The recovery modeling as a time-stepping algorithm (e.g., monthly, quarterly, yearly) with full propagation of uncertainties was provided, thereby allowing investigation of policy changes at different points during the recovery process. Delay time dominated throughout the recovery modeling process. All the proposed policy cases affected the delay process and shortened the recovery process to different extents. The case involved all the proposed policies and mitigation strategies, enabling the recovery process to occur 2.4 times faster than the base case.

In Chapter 6, a commercial building recovery model was developed with the ability to fully propagate uncertainty for business recovery modeling. Post-disaster funding resources were integrated into quantitative probabilistic analysis for community resilience assessment to track commercial building recovery. The recovery process for different commercial building types depends on building damage affected by hazard events, financial resources available to business owners, and other impeding factors. Overall, very few commercial buildings are fully recovered within a year of the hazard event, and, in general, more than 50% are fully restored after approximately two years.

In Chapter 7, a methodology was developed to examine the interdependent community recovery process across physical infrastructure and social systems. The integrated recovery process of residential buildings and the household in that building for the community was examined.

Household recovery for households re-accessing their permanent housing is much faster than residential building recovery for repair. Households with higher incomes reach permanent housing relatively faster than those with lower incomes. However, many households experience a household recovery failure.

8.2 Recommendations

Each chapter, from Chapter 2 to Chapter 7, proposes some limitations at the end of each chapter that can be addressed to respond to the specific research questions and improve the related community resilience models. These limitations are not reiterated herein for brevity, and this chapter mainly emphasizes the recommendations of proposed major new directions based on the completed work and the entire framework shown in Figure 1-1. Recall Figure 1-1 presented at the beginning of the dissertation, the conceptual description of the framework, and many more cross-cutting and cutting-edge studies can be performed to perfect and complete the proposed framework to improve multi-disciplinary and multi-dimensional community resilience and support decision-support. Below are some of the recommendations for future studies. Each task below corresponds to the specific steps shown in the framework in Figure 1-1.

<u>Task 1</u>: Cost-optimal retrofit analysis (1a, 1b, 1c, 2a, 2b, 2c, 3a, 3b, 3c, 3d, 3e, 8a, 8b, 8c):

- Calculate retrofit costs of three residential building retrofit strategies and develop multiple objective functions to reduce indirect socio-economic losses and improve building performance.
- Allocate optimal residential building retrofits (e.g., retrofit level, retrofit spatial distribution) based on the economic, social, and physical infrastructure constraints and multiple community objectives. Multiple solution details under varying assumptions and

resources support in-depth analysis. For example, optimal allocation of limited resources will vary with the change of the defined multiple objectives.

Task 2: Physical-economic interdependent recovery (1a, 1b, 1c, 2a, 2b, 2c, 3a, 3b, 3c, 3e, 4a)

- Chain the building recovery model with the dynamic CGE model (Attary et al. 2020), and record economic community stability metrics with new capital, labor and government investments incorporated over time.
- Explore the business recovery model based on the presented commercial building recovery model and the considerations of the recovery of labor, customer, and the market.

Task 3: Illustrate decision-support using the resilience-informed approach developed

- Integrate the resilience-informed methodologies into the IN-CORE computational environment and demonstrate how decision support can be provided to our community engagement partners, stakeholders, and policymakers via the IN-CORE visualization dashboard.

REFERENCES

Abiassi, J.J., 1981. *The strength of weathered window glass using surface characteristics* (Doctoral dissertation).

ACI Committee, 2019. Building code requirements for structural concrete (ACI 318-19) and commentary. American Concrete Institute.

Aids, J., 2002a. FM global property loss prevention data sheets 1—28.

Aids, J., 2002b. FM global property loss prevention data sheets 1—49.

Aghababaei, M. and Koliou, M., 2022. An agent-based modeling approach for community resilience assessment accounting for system interdependencies: Application on education system. *Engineering Structures*, *255*, p.113889.

Aghababaei, M., Koliou, M., Pilkington, S., Mahmoud, H., van de Lindt, J.W., Curtis, A., Smith, S., Ajayakumar, J. and Watson, M., 2020. Validation of time-dependent repair recovery of the building stock following the 2011 Joplin Tornado. *Natural Hazards Review*, *21*(4), p.04020038.

Aghababaei, M., Koliou, M., Watson, M. and Xiao, Y., 2021. Quantifying post-disaster business recovery through Bayesian methods. *Structure and Infrastructure Engineering*, *17*(6), pp.838-856.

Aldrich, D.P. and Meyer, M.A., 2015. Social capital and community resilience. *American behavioral scientist*, *59*(2), pp.254-269.

Alesch, D.J., Holly, J.N., Mittler, E. and Nagy, R., 2001. Organizations at risk: What happens when small businesses and not-for-profits encounter natural disasters.

Alexander, D.E., 2013. Resilience and disaster risk reduction: an etymological journey. *Natural hazards and earth system sciences*, *13*(11), pp.2707-2716.

Al-Menyawi, Y.M., 2001. *Concrete block masonry construction to resist severe winds*. Texas Tech University.

Almufti, I. and Willford, M., REDi TM Rating System: Resilience-based earthquake design initiative for the next generation of buildings (2013).

Ameri, M.R. and van de Lindt, J.W., 2019. Seismic performance and recovery modeling of natural gas networks at the community level using building demand. *Journal of Performance of Constructed Facilities*, *33*(4), p.04019043.

"American Housing Survey (AHS) - AHS Table Creator." *United States Census Bureau*, https://www.census.gov/programs-surveys/ahs/data/interactive/ahstablecreator.html?s_areas=00000&s_year=2019&s_tablename=TABLE8A&s_bygroup1=1&s_bygroup2=1&s_filtergroup1=1&s_filtergroup2=1.

American Society for Testing and Materials, 2003. *Standard practice for determining load resistance of glass in buildings*. ASTM International.

American Society of Civil Engineers, 2016. Minimum design loads for buildings and other structures: ASCE/SEI 7-16. American Society of Civil Engineers.

American Society of Civil Engineers, 2021. Minimum design loads for buildings and other structures: ASCE/SEI 7-22. American Society of Civil Engineers.

Amini, M.O. and van de Lindt, J.W., 2014. Quantitative insight into rational tornado design wind speeds for residential wood-frame structures using fragility approach. *Journal of Structural Engineering*, *140*(7), p.04014033.

Aryana, S.A., 2006. *Statistical analysis of compressive strength of clay brick masonry prisms*. The University of Texas at Arlington.

Attary, N., Cutler, H., Shields, M. and van de Lindt, J.W., 2020. The economic effects of financial relief delays following a natural disaster. *Economic Systems Research*, *32*(3), pp.351-377.

Attary, N., van de Lindt, J.W., Mahmoud, H. and Smith, S., 2019. Hindcasting community-level damage to the interdependent buildings and electric power network after the 2011 Joplin, Missouri, Tornado. *Natural Hazards Review*, *20*(1), p.04018027.

Attary, N., van de Lindt, J.W., Mahmoud, H., Smith, S., Navarro, C.M., Kim, Y.W. and Lee, J.S., 2018. Hindcasting community-level building damage for the 2011 Joplin EF5 tornado. *Natural Hazards*, *93*(3), pp.1295-1316.

Badeaux, L.L., 2018. *Measuring Sustainability and Resilience Qualities across Post-Disaster Temporary Housing* (Doctoral dissertation, University of Kansas).

Ballard, C.L., Shoven, J.B. and Whalley, J., 1985. General equilibrium computations of the marginal welfare costs of taxes in the United States. *The American Economic Review*, *75*(1), pp.128-138.

Ballard, K.E., 1993. *The impact of disaster on a school district: The Oologah tornado*. Oklahoma State University.

Berd, A., Watson, M., 2020. Follow the Money: Using Content Analysis to Understand Disaster Spending. DesignSafe-CI. https://doi.org/10.17603/ds2-2na8-am90.

Berkes, F. and Ross, H., 2013. Community resilience: toward an integrated approach. *Society & natural resources*, *26*(1), pp.5-20.

Binder, S.B., Barile, J.P., Baker, C.K. and Kulp, B., 2019. Home buyouts and household recovery: neighborhood differences three years after Hurricane Sandy. *Environmental Hazards*, *18*(2), pp.127-145.

Bocchini, P. and Frangopol, D.M., 2011. A stochastic computational framework for the joint transportation network fragility analysis and traffic flow distribution under extreme events. *Probabilistic Engineering Mechanics*, *26*(2), pp.182-193.

Bocchini, P., Frangopol, D.M., Ummenhofer, T. and Zinke, T., 2014. Resilience and sustainability of civil infrastructure: Toward a unified approach. *Journal of Infrastructure Systems*, *20*(2), p.04014004.

Bolin, R. and Stanford, L., 1998. The Northridge earthquake: community-based approaches to unmet recovery needs. *Disasters*, *22*(1), pp.21-38.

Bonstrom, H. and Corotis, R.B., 2016. First-order reliability approach to quantify and improve building portfolio resilience. *Journal of Structural Engineering*, *142*(8), p.C4014001.

Bournonville, M., Dahnke, J. and Darwin, D., 2004. *Statistical analysis of the mechanical properties and weight of reinforcing bars*. University of Kansas Center for Research, Inc..

Bruneau, M., Chang, S.E., Eguchi, R.T., Lee, G.C., O'Rourke, T.D., Reinhorn, A.M., Shinozuka, M., Tierney, K., Wallace, W.A. and Von Winterfeldt, D., 2003. A framework to quantitatively assess and enhance the seismic resilience of communities. *Earthquake spectra*, *19*(4), pp.733-752.

Burfisher, M.E., 2017. *Introduction to computable general equilibrium models*. Cambridge University Press.

Burton, C.G., 2015. A validation of metrics for community resilience to natural hazards and disasters using the recovery from Hurricane Katrina as a case study. *Annals of the Association of American Geographers*, *105*(1), pp.67-86.

Burton, H., Kang, H., Miles, S., Nejat, A. and Yi, Z., 2019. A framework and case study for integrating household decision-making into post-earthquake recovery models. *International Journal of Disaster Risk Reduction*, *37*, p.101167.

Burton, H.V., Deierlein, G., Lallemant, D. and Lin, T., 2016. Framework for incorporating probabilistic building performance in the assessment of community seismic resilience. *Journal of Structural Engineering*.

Capacci, L., Biondini, F. and Frangopol, D.M., 2022. Resilience of aging structures and infrastructure systems with emphasis on seismic resilience of bridges and road networks. *Resilient Cities and Structures*, *1*(2), pp.23-41.

Capacci, L., Biondini, F., Titi, A., Bittencourt, T.N., Frangopol, D.M. and Beck, A., 2016. Seismic resilience of aging bridges and transportation networks. In *Maintenance, monitoring, safety, risk and resilience of bridges and bridge networks* (pp. 336-336). CRC Press.

Carvalho, L.S., Meier, S. and Wang, S.W., 2016. Poverty and economic decision-making: Evidence from changes in financial resources at payday. *American economic review*, *106*(2), pp.260-84.

Castillo, J.G.S., Bruneau, M. and Elhami-Khorasani, N., 2022. Functionality measures for quantification of building seismic resilience index. *Engineering Structures*, *253*, p.113800.

Chang, S.E. and Shinozuka, M., 2004. Measuring improvements in the disaster resilience of communities. *Earthquake spectra*, *20*(3), pp.739-755.

Changnon, S.A., 2009. Tornado losses in the United States. *Natural hazards review*, *10*(4), pp.145-150.

Chell, M.A., 1992. Economic development administration revolving loan funds. *Economic Development Review*, 10(2), 31. https://www.proquest.com/docview/230091190/fulltextPDF/C50FC8A6A1B549EBPQ/1?accountid=10223

Chester, M.V., Underwood, B.S. and Samaras, C., 2020. Keeping infrastructure reliable under climate uncertainty. *Nature Climate Change*, *10*(6), pp.488-490.

Corey, C.M. and Deitch, E.A., 2011. Factors affecting business recovery immediately after Hurricane Katrina. *Journal of Contingencies and crisis management*, *19*(3), pp.169-181.

Coulbourne, W.L. and Miller, J., 2012. Performance of school buildings in the Joplin, MO, Tornado. In *Structures Congress 2012* (pp. 989-998).

Crawford, P.S., Hainen, A., Awondo, S., Graettinger, A. and Powell, L., 2019. Development and Testing of a Resilience Rapidity Model for Disasters. *Journal of Architectural Engineering*, *25*(2), p.04019013.

Cremen, G., Seville, E. and Baker, J.W., 2020. Modeling post-earthquake business recovery time: An analytical framework. *International Journal of Disaster Risk Reduction*, *42*, p.101328.

Croll, Maxime, 2021. Home Insurance Facts and Statistics: Coverage & Claims. ValuePenguin. ValuePenguin, March 15, 2021. https://www.valuepenguin.com/home-insurance-statistics.

Cui, X., 2007. *Reliability of masonry anchorage*. University of Louisville.

Cutler, H. and Davies, S., 2010. The economic consequences of productivity changes: A computable general equilibrium (CGE) analysis. *Regional Studies*, *44*(10), pp.1415-1426.

Cutler, H., Shields, M. and Davies, S., 2018. Can state tax policy increase economic activity and reduce inequality?. *Growth and Change*, *49*(1), pp.142-164.

Cutler, H., Shields, M., Tavani, D. and Zahran, S., 2016. Integrating engineering outputs from natural disaster models into a dynamic spatial computable general equilibrium model of Centerville. *Sustainable and Resilient Infrastructure*, *1*(3-4), pp.169-187.

Cutter, S.L., Ash, K.D. and Emrich, C.T., 2014. The geographies of community disaster resilience. *Global environmental change*, *29*, pp.65-77.

Dahlhamer, J.M. and Tierney, K.J., 1998. Rebounding from disruptive events: business recovery following the Northridge earthquake. *Sociological spectrum*, *18*(2), pp.121-141.

Dalgliesh, W.A. and Taylor, D.A., 1990. The strength and testing of window glass. *Canadian Journal of Civil Engineering*, *17*(5), pp.752-762.

Davis, C.A., 2021. Understanding functionality and operability for infrastructure system resilience. *Natural Hazards Review*, *22*(1), p.06020005.

De Iuliis, M., Kammouh, O., Cimellaro, G.P. and Tesfamariam, S., 2019. Downtime estimation of building structures using fuzzy logic. *International journal of disaster risk reduction*, *34*, pp.196-208.

Dietch, E.A. and Corey, C.M., 2011. Predicting long-term business recovery four years after Hurricane Katrina. *Management Research Review*, *34*(3), pp.311-324.

Dong, Y. and Frangopol, D.M., 2017. Probabilistic assessment of an interdependent healthcare–bridge network system under seismic hazard. *Structure and Infrastructure Engineering*, *13*(1), pp.160-170.

Dong, Y. and Frangopol, D.M., 2015. Risk and resilience assessment of bridges under mainshock and aftershocks incorporating uncertainties. *Engineering Structures*, *83*, pp.198-208.

Doorn, N., Gardoni, P. and Murphy, C., 2019. A multidisciplinary definition and evaluation of resilience: The role of social justice in defining resilience. *Sustainable and Resilient Infrastructure*, *4*(3), pp.112-123.

Dorosh, P. and Thurlow, J., 2014. Can cities or towns drive African development? Economywide analysis for Ethiopia and Uganda. *World Development*, *63*, pp.113-123.

Drennan, L., McGowan, J. and Tiernan, A., 2016. Integrating recovery within a resilience framework: Empirical insights and policy implications from regional Australia. *Politics and Governance*, *4*(4), pp.74-86.

Ellingwood, B.R., Cutler, H., Gardoni, P., Peacock, W.G., van de Lindt, J.W. and Wang, N., 2016. The centerville virtual community: A fully integrated decision model of interacting physical and social infrastructure systems. *Sustainable and Resilient Infrastructure*, *1*(3-4), pp.95-107.

Ellingwood, B.R., Rosowsky, D.V., Li, Y. and Kim, J.H., 2004. Fragility assessment of light-frame wood construction subjected to wind and earthquake hazards. *Journal of Structural Engineering*, *130*(12), pp.1921-1930.

Ellingwood, B.R., van de Lindt, J.W. and McAllister, T.P., 2019. A fully integrated model of interdependent physical infrastructure and social systems. *The Bridge*, *49*(2).

Ellingwood, B., van de Lindt, J. and McAllister, T.P., 2017, August. The science behind community resilience assessment: An overview of the center for risk-based community resilience planning. In *Proc., 12th Int. Conf. on Structural Safety and Reliability* (pp. 2937-2946).

Ellingwood, B.R., Wang, N., Harris, J.R. and McAllister, T.P., 2017. The role of performance-based engineering in achieving community resilience: a first step. *RESILIENCE*, p.62.

Enderami, S.A., Mazumder, R.K. and Sutley, E.J., 2022. Framework for Incorporating Community Social Vulnerability in the Assessment of Hurricane-Induced Wind Risk to Residential Buildings. *arXiv preprint arXiv:2207.14206*.

Enderami, S.A., Sutley, E.J. and Hofmeyer, S.L., 2021. Defining organizational functionality for evaluation of post-disaster community resilience. *Sustainable and Resilient Infrastructure*, pp.1-18.

Fact Sheet – City of Joplin, 2021. Joplin, Missouri Hit by EF-5 Tornado on May 22, 2011. https://www.joplinmo.org/DocumentCenter/View/1985/Joplin_Tornado_factsheet?bidId=.

Farokhnia, K., van de Lindt, J.W. and Koliou, M., 2020. Selection of residential building design requirements to achieve community functionality goals under tornado loading. *Practice Periodical on Structural Design and Construction*, *25*(1), p.04019035.

Farrow, C., 2012. Joplin Tornado Relief Efforts Raise $39 Million. Accessed 26 July 2021. https://philanthropynewsdigest.org/news/joplin-tornado-relief-efforts-raise-39-million.

Federal Emergency Management Agency, 2021. Hazus Hurricane Model Technical Manual. Hazus 4.2 Service Pack 3. Washington, DC: Department of Homeland Security.

Federal Emergency Management Agency, 2012. Multi-hazard loss estimation methodology hurricane model technical manual. Hazus-MH 2.1—Technical manual. Washington, DC: Department of Homeland Security.

Federal Emergency Management Agency, 2011. National disaster recovery framework. Washington, DC: Department of Homeland Security; 2009.

Federal Emergency Management Agency, 2012. Seismic performance assessment of buildings (volume 1-Methodology). Washington, DC: Department of Homeland Security.

Federal Emergency Management Agency, 2011. The response to the 2011 Joplin, Missouri, Tornado lessons learned study. Washington, DC: Department of Homeland Security.

Federal Emergency Management Agency, 2009. Tornado protection selecting refuge areas in buildings. FEMA P-431. 2nd ed. Washington, DC: Department of Homeland Security.

Feng, K., Ouyang, M. and Lin, N., 2022. Tropical cyclone-blackout-heatwave compound hazard resilience in a changing climate. *Nature communications*, *13*(1), pp.1-11.

Fereshtehnejad, E., Gidaris, I., Rosenheim, N., Tomiczek, T., Padgett, J.E., Cox, D.T., Van Zandt, S. and Gillis Peacock, W., 2021. Probabilistic risk assessment of coupled natural-physical-social systems: Cascading impact of hurricane-induced damages to civil infrastructure in Galveston, Texas. *Natural Hazards Review*, *22*(3), p.04021013.

Ferrier, Pat. 2021 Fort Collins Launches $1.5M Small Business Recovery Fund with Coronavirus Relief Money. The Coloradoan. Accessed July 26, 2021. https://www.coloradoan.com/story/news/2020/09/08/covid-19-relief-fort-collins-launches-small-business-recovery-fund/5747986002/.

Friedland, C.J. and Levitan, M.L., 2011. Development of a loss-consistent wind and flood damage scale for residential buildings. In *Solutions to coastal disasters 2011* (pp. 666-677).

Ganin, A.A., Massaro, E., Gutfraind, A., Steen, N., Keisler, J.M., Kott, A., Mangoubi, R. and Linkov, I., 2016. Operational resilience: concepts, design and analysis. *Scientific reports*, *6*(1), pp.1-12.

Gavanski, E. and Kopp, G.A., 2011. Examination of load resistance in window glass design. *Journal of architectural engineering*, *17*(1), pp.42-50.

General liability, 2021c. Manufacturing and Mercantile Rental Property Insurance. Accessed July 26, 2021. https://generalliabilityinsure.com/small-business/manufacturing-mercantile-rental-property-insurance.html.

General liability, 2021b. Office Buildings Insurance. Accessed July 26, 2021. https://generalliabilityinsure.com/small-business/office-buildings-insurance.html.

General liability, 2021a. Shopping Center and Strip Mall Insurance. Accessed July 26, 2021. https://generalliabilityinsure.com/small-business/shopping-center-strip-mall-insurance.html.

Ghanbari, M., Arabi, M., Kao, S.C., Obeysekera, J. and Sweet, W., 2021. Climate Change and Changes in Compound Coastal-Riverine Flooding Hazard Along the US Coasts. *Earth's Future*, *9*(5), p.e2021EF002055.

Girard, C. and Peacock, W.G., 1997. Ethnicity and segregation: Post-hurricane relocation. *Hurricane Andrew: Ethnicity, gender and the sociology of disasters*, pp.191-205.

González, A.D., Dueñas-Osorio, L., Sánchez-Silva, M. and Medaglia, A.L., 2016. The interdependent network design problem for optimal infrastructure system restoration. *Computer-Aided Civil and Infrastructure Engineering*, *31*(5), pp.334-350.

Gotham, K.F., 2014. Reinforcing inequalities: The impact of the CDBG program on post-Katrina rebuilding. *Housing Policy Debate*, *24*(1), pp.192-212.

Griego, A.L., Flores, A.B., Collins, T.W. and Grineski, S.E., 2020. Social vulnerability, disaster assistance, and recovery: A population-based study of Hurricane Harvey in Greater Houston, Texas. *International Journal of Disaster Risk Reduction*, *51*, p.101766.

Guidotti, R., Chmielewski, H., Unnikrishnan, V., Gardoni, P., McAllister, T. and van de Lindt, J., 2016. Modeling the resilience of critical infrastructure: The role of network dependencies. *Sustainable and resilient infrastructure*, *1*(3-4), pp.153-168.

Haan Jr, F.L., Balaramudu, V.K. and Sarkar, P.P., 2010. Tornado-induced wind loads on a low-rise building. *Journal of structural engineering*, *136*(1), pp.106-116.

Haan Jr, F.L., Sarkar, P.P. and Gallus, W.A., 2008. Design, construction and performance of a large tornado simulator for wind engineering applications. *Engineering Structures*, *30*(4), pp.1146-1159.

Hamideh, S., Peacock, W. and Van Zandt, S., 2018. Housing recovery after disasters: Primary versus seasonal/vacation housing markets in coastal communities.

Hannum, C., Cutler, H., Iverson, T. and Keyser, D., 2017. Estimating the implied cost of carbon in future scenarios using a CGE model: The Case of Colorado. *Energy Policy*, *102*, pp.500-511.

Hassan, E.M. and Mahmoud, H., 2020. An integrated socio-technical approach for post-earthquake recovery of interdependent healthcare system. *Reliability Engineering & System Safety*, *201*, p.106953.

Hassan, E.M. and Mahmoud, H., 2021. Healthcare and education networks interaction as an indicator of social services stability following natural disasters. *Scientific reports*, *11*(1), pp.1-15.

Hassan, E.M., Mahmoud, H.N. and Ellingwood, B.R., 2020. Resilience of school systems following severe earthquakes. *Earth's future*, *8*(10), p.e2020EF001518.

Hawley, Jimmy, 2020. Can Impact Windows Break? Understanding Hurricane Glass Strength. Impact Windows Naples, Hurricane Shutters Fort Myers, Cape Coral Glass Repair, November 5, 2020. https://www.storm-solutions.net/blog/can-impact-windows-break-understanding-hurricane-glass-strength.

He, X. and Cha, E.J., 2018. Modeling the damage and recovery of interdependent critical infrastructure systems from natural hazards. *Reliability engineering & System safety*, *177*, pp.162-175.

Hirayama, Y., 2000. Collapse and reconstruction: Housing recovery policy in Kobe after the Hanshin Great Earthquake. *Housing Studies*, *15*(1), pp.111-128.

Holling, C.S., 1973. Resilience and stability of ecological systems. *Annual review of ecology and systematics*, pp.1-23.

Hou, G. and Chen, S., 2020. Probabilistic modeling of disrupted infrastructures due to fallen trees subjected to extreme winds in urban community. *Natural Hazards*, *102*(3), pp.1323-1350.

Hou, G., Chen, S. and Han, Y., 2019. Traffic performance assessment methodology of degraded roadway links following hazards. *Journal of Aerospace Engineering*, *32*(5), p.04019055.

Houston, J.B., Spialek, M.L., First, J., Stevens, J. and First, N.L., 2017. Individual perceptions of community resilience following the 2011 Joplin tornado. *Journal of Contingencies and Crisis Management*, *25*(4), pp.354-363.

Huang, H., Zhang, D. and Huang, Z., 2022. Resilience of city underground infrastructure under multi-hazards impact: From structural level to network level. *Resilient Cities and Structures*, *1*(2), pp.76-86.

Ingram, J.C., Franco, G., Rumbaitis-del Rio, C. and Khazai, B., 2006. Post-disaster recovery dilemmas: challenges in balancing short-term and long-term needs for vulnerability reduction. *Environmental science & policy*, *9*(7-8), pp.607-613.

Jain, A., Bhusar, A.A., Roueche, D.B. and Prevatt, D.O., 2020. Engineering-based tornado damage assessment: numerical tool for assessing tornado vulnerability of residential structures. *Frontiers in Built Environment*, *6*, p.89.

Joshi, A. and Aoki, M., 2014. The role of social capital and public policy in disaster recovery: A case study of Tamil Nadu State, India. *International Journal of Disaster Risk Reduction*, *7*, pp.100-108.

Kameshwar, S., Cox, D.T., Barbosa, A.R., Farokhnia, K., Park, H., Alam, M.S. and van de Lindt, J.W., 2019. Probabilistic decision-support framework for community resilience: Incorporating multi-hazards, infrastructure interdependencies, and resilience goals in a Bayesian network. *Reliability Engineering & System Safety*, *191*, p.106568.

Karamouz, M., Rasoulnia, E., Olyaei, M.A. and Zahmatkesh, Z., 2018. Prioritizing investments in improving flood resilience and reliability of wastewater treatment infrastructure. *Journal of Infrastructure Systems*, *24*(4), p.04018021.

Kennedynews@joplinglobe.com, Wally, 2021. Insurance Payout from Tornado to Be Largest in State History. *Joplin Globe*, 26 July 2011, www.joplinglobe.com/news/local_news/insurance-payout-from-tornado-to-be-largest-in-state-history/article_3556cdc9-5f09-53f9-875f-9f65bbe76d88.html.

Khan, M.A.U. and Sayem, M.A., 2013. Understanding recovery of small enterprises from natural disaster. *Environmental Hazards*, *12*(3-4), pp.218-239.

Kikitsu, H. and Sarkar, P.P., 2015. Building damage, wind speed estimation, and post disaster recovery in an EF5 Tornado. *Natural Hazards Review*, *16*(2), p.04014019.

Kim, H. and Marcouiller, D.W., 2016. Natural disaster response, community resilience, and economic capacity: A case study of coastal Florida. *Society & Natural Resources*, *29*(8), pp.981-997.

Kim, J.H. and Sutley, E.J., 2021. Implementation of social equity metrics in an engineering-based framework for distributing disaster resources. *International Journal of Disaster Risk Reduction*, *64*, p.102485.

Kim, Y.S. and Bennett, R.M., 2002. Flexural tension in unreinforced masonry: Evaluation of current specifications. *TMS J*, *201*, pp.23-30.

Koliou, M. and van de Lindt, J.W., 2020. Development of building restoration functions for use in community recovery planning to tornadoes. *Natural Hazards Review*, *21*(2), p.04020004.

Koliou, M., Masoomi, H. and van de Lindt, J.W., 2017. Performance assessment of tilt-up big-box buildings subjected to extreme hazards: Tornadoes and earthquakes. *Journal of Performance of Constructed Facilities*, *31*(5), p.04017060.

Koliou, M., van de Lindt, J.W., McAllister, T.P., Ellingwood, B.R., Dillard, M. and Cutler, H., 2020. State of the research in community resilience: Progress and challenges. *Sustainable and resilient infrastructure*, *5*(3), pp.131-151.

Kopp, G.A. and Wu, C.H., 2020. A framework to compare wind loads on low-rise buildings in tornadoes and atmospheric boundary layers. *Journal of Wind Engineering and Industrial Aerodynamics*, *204*, p.104269.

Krause, Eleanor, and Richard V. Reeves, 2017. Hurricanes hit the poor the hardest. *Social Mobility Memos (blog), September* 18.

Kuligowski, E.D., Lombardo, F.T., Phan, L., Levitan, M.L. and Jorgensen, D.P., 2014. Final report, National Institute of Standards and Technology (NIST) technical investigation of the May 22, 2011, tornado in Joplin, Missouri.

Landry, C.E., Anderson, S., Krasovskaia, E. and Turner, D., 2021. Willingness to Pay for Multi-peril Hazard Insurance. *Land Economics*, *97*(4), pp.797-818.

Lee, J., 2019. Business recovery from hurricane Harvey. *International journal of disaster risk reduction*, *34*, pp.305-315.

Levitan, Marc, Bruce R. Ellingwood, Peter Vickery, Yue Li, Therese McAllister, 2021 Reliability/Return Period Analysis for Tornado Loads in ASCE 7-22.

Li, Y. and Ellingwood, B.R., 2006. Hurricane damage to residential construction in the US: Importance of uncertainty modeling in risk assessment. *Engineering structures*, *28*(7), pp.1009-1018.

Li, Y., Dong, Y., Frangopol, D.M. and Gautam, D., 2020. Long-term resilience and loss assessment of highway bridges under multiple natural hazards. *Structure and Infrastructure Engineering*, *16*(4), pp.626-641.

Li, Y., van de Lindt, J.W., Dao, T., Bjarnadottir, S. and Ahuja, A., 2012. Loss analysis for combined wind and surge in hurricanes. *Natural hazards review*, *13*(1), pp.1-10.

Lin, P. and Wang, N., 2017. Stochastic post-disaster functionality recovery of community building portfolios I: Modeling. *Structural Safety*, *69*, pp.96-105.

Lin, P. and Wang, N., 2017. Stochastic post-disaster functionality recovery of community building portfolios II: Application. *Structural Safety*, *69*, pp.106-117.

Lin, P., Rosenheim, N.P., Wang, N. and Peacock, W.G., 2019. A Stochastic Approach to Model Household Re-occupancy in A Community Following A Natural Hazard.

Lin, Y.S., Peacock, W.G., Lu, J.C., Zhang, Y. and Center, R., 2008. Household dislocation algorithm 3: A logistic regression approach. *Hazard Reduction and Recovery Center, Texas A&M University. HRRC Reports*, pp.08-05.

Lindell, M.K. and Prater, C.S., 2003. Assessing community impacts of natural disasters. *Natural hazards review*, *4*(4), pp.176-185.

Lindsay, B.R., 2010. SBA Disaster Loan Program: Overview and Possible Issues for Congress.

Lofgren, H., Harris, R.L. and Robinson, S., 2002. *A standard computable general equilibrium (CGE) model in GAMS* (Vol. 5). Intl Food Policy Res Inst.

Lombardo, F.T., Roueche, D.B. and Prevatt, D.O., 2015. Comparison of two methods of near-surface wind speed estimation in the 22 May, 2011 Joplin, Missouri Tornado. *Journal of Wind Engineering and Industrial Aerodynamics*, *138*, pp.87-97.

Ma, Liyang, Paolo Bocchini, and Vasileios Christou. "Fragility models of electrical conductors in power transmission networks subjected to hurricanes." *Structural Safety* 82 (2020): 101890.

Marshall, M.I. and Schrank, H.L., 2014. Small business disaster recovery: a research framework. *Natural Hazards*, *72*(2), pp.597-616.

Masoomi, H., Ameri, M.R. and van de Lindt, J.W., 2018. Wind performance enhancement strategies for residential wood-frame buildings. *Journal of Performance of Constructed Facilities*, *32*(3), p.04018024.

Masoomi, H. and van de Lindt, J.W., 2019. Community-resilience-based design of the built environment. *ASCE-ASME Journal of Risk and Uncertainty in Engineering Systems, Part A: Civil Engineering*, *5*(1), p.04018044.

Masoomi, H. and van de Lindt, J.W., 2018. Fatality and injury prediction model for tornadoes. *Natural Hazards Review*, *19*(3), p.04018009.

Masoomi, H. and van de Lindt, J.W., 2018. Restoration and functionality assessment of a community subjected to tornado hazard. *Structure and Infrastructure Engineering*, *14*(3), pp.275-291.

Masoomi, H. and van de Lindt, J.W., 2017. Tornado community-level spatial damage prediction including pressure deficit modeling. *Sustainable and Resilient Infrastructure*, *2*(4), pp.179-193.

Masoomi, H. and van de Lindt, J.W., 2016. Tornado fragility and risk assessment of an archetype masonry school building. *Engineering Structures*, *128*, pp.26-43.

Masoomi, H., van de Lindt, J.W. and Peek, L., 2018. Quantifying socioeconomic impact of a tornado by estimating population outmigration as a resilience metric at the community level. *Journal of structural engineering (New York, NY)*, *144*(5).

McAllister, T., 2016. Research needs for developing a risk-informed methodology for community resilience. *Journal of Structural Engineering*, *142*(8), p.C4015008.

McAllister, T. and McAllister, T., 2013. *Developing guidelines and standards for disaster resilience of the built environment: A research needs assessment* (pp. 1-142). Gaithersburg, MD: US Department of Commerce, National Institute of Standards and Technology.

McDonald, J.R., and Kishor C.M., 2004. *A Recommendation for an ENHANCED FUJITA SCALE (EF-Scale)*, https://www.spc.noaa.gov/faq/tornado/ef-ttu.pdf.

McDonald, T.M., Florax, R. and Marshal, M.I., 2014. *Informal and formal financial resources and small business resilience to disasters* (No. 329-2016-12746).

Meerow, S., Pajouhesh, P. and Miller, T.R., 2019. Social equity in urban resilience planning. *Local Environment*, *24*(9), pp.793-808.

Memari, M., Attary, N., Masoomi, H., Mahmoud, H., van de Lindt, J.W., Pilkington, S.F. and Ameri, M.R., 2018. Minimal building fragility portfolio for damage assessment of communities subjected to tornadoes. *Journal of Structural Engineering*, *144*(7), p.04018072.

Mieler, M., Stojadinovic, B., Budnitz, R., Comerio, M. and Mahin, S., 2015. A framework for linking community-resilience goals to specific performance targets for the built environment. *Earthquake Spectra*, *31*(3), pp.1267-1283.

Minor, J.E. and Norville, H.S., 1998. A simple window glass design chart. *Journal of Wind Engineering and Industrial Aerodynamics*, *77*, pp.197-204.

Morrish, S.C. and Jones, R., 2020. Post-disaster business recovery: An entrepreneurial marketing perspective. *Journal of Business Research*, *113*, pp.83-92.

Narendra, T., 2010. Design of reinforced masonry structures.

National Institute of Standards and Technology. 2020. *Community resilience planning guide for buildings and infrastructure systems: a playbook*.

National Institute of Standards and Technology. 2015. *Community resilience planning guide for buildings and infrastructure systems, volume i*. No. Special Publication (NIST SP)-1190v1.

National Institute of Standards and Technology. 2015. *Community Resilience Planning Guide for* Buildings *and Infrastructure Systems, Volume II*. No. Special Publication (NIST SP)-1190.

National Oceanic and Atmospheric Administration. 2020. “Weather Related Fatality and Injury Statistics” Accessed August 2020. https://www.weather.gov/hazstat/

Niemiec, S.S. and Brown, T.D., 1988. Care and maintenance of wood shingle and shake roofs.

Nofal, O.M. and van de Lindt, J.W., 2020. Minimal building flood fragility and loss function portfolio for resilience analysis at the community level. *Water*, *12*(8), p.2277.

Nofal, O.M., van De Lindt, J.W., Do, T.Q., Yan, G., Hamideh, S., Cox, D.T. and Dietrich, J.C., 2021. Methodology for regional multihazard hurricane damage and risk assessment. *Journal of Structural Engineering*, *147*(11), p.04021185.

Nozhati, S., Sarkale, Y., Chong, E.K. and Ellingwood, B.R., 2020. Optimal stochastic dynamic scheduling for managing community recovery from natural hazards. *Reliability Engineering & System Safety*, *193*, p.106627.

Oregon Seismic Safety Policy Advisory Commission (OSSPAC), 2013. The Oregon Resilience Plan: reducing risk and improving recovery for the next Cascadia earthquake and tsunami. *Portland, Oregon*. https://www.oregon.gov/oem/documents/oregon_resilience_plan_final.pdf

Orhan, E., 2016. Lessons learned from businesses to ensure community level recovery in a Postdisaster period: case from Adapazari, Turkey. *Natural Hazards Review*, *17*(1), p.05015002.

Ouyang, M. and Duenas-Osorio, L., 2014. Multi-dimensional hurricane resilience assessment of electric power systems. *Structural Safety*, *48*, pp.15-24.

Ouyang, M. and Wang, Z., 2015. Resilience assessment of interdependent infrastructure systems: With a focus on joint restoration modeling and analysis. *Reliability Engineering & System Safety*, *141*, pp.74-82.

Pang, Y. and Wang, X., 2021. Cloud-IDA-MSA conversion of fragility curves for efficient and high-fidelity resilience assessment. *Journal of Structural Engineering*, *147*(5), p.04021049.

Pant, S. and Cha, E.J., 2019. Wind and rainfall loss assessment for residential buildings under climate-dependent hurricane scenarios. *Structure and Infrastructure Engineering*, *15*(6), pp.771-782.

Peacock, W.G., Gladwin, H. and Morrow, B.H., 2012. *Hurricane Andrew: Ethnicity, gender and the sociology of disasters*. Routledge.

Pilkington, S.F., 2019. *Integration of graphical, physics-based, and machine learning methods for assessment of impact and recovery of the built environment from wind hazards* (Doctoral dissertation, Colorado State University).

Pilkington, S.F. and Mahmoud, H.N., 2020. Interpreting the socio-technical interactions within a wind damage–artificial neural network model for community resilience. *Royal Society open science*, *7*(11), p.200922.

Pilkington, S.F., Curtis, A., Mahmoud, H., van de Lindt, J., Smith, S. and Ajayakumar, J., 2021. Preliminary Documented Recovery Patterns and Observations from Video Cataloged Data of the 2011 Joplin, Missouri, Tornado. *Natural Hazards Review*, *22*(1), p.05020015.

Pilkington, S.F., Mahmoud, H., van de Lindt, J.W., Koliou, M. and Smith, S., 2020. Hindcasting loss and evaluating implications of track location for the 2011 Joplin, Missouri Tornado. *ASCE-ASME Journal of Risk and Uncertainty in Engineering Systems, Part B: Mechanical Engineering*, *6*(2), p.020902.

Poland C, 2009. The resilient city: defining what San Francisco needs from its seismic mitigation polices. San Francisco Planning and Urban Research Association report, San Francisco, CA, USA. https://www.spur.org/sites/default/files/2020-03/SPUR_Defining_Resilience.pdf

Potter, Brian. "Every Building in America - an Analysis of the US Building Stock." *Every Building in America - an Analysis of the US Building Stock*, Construction Physics, 2 Nov. 2020, https://constructionphysics.substack.com/p/every-building-in-america-an-analysis#:~:text=Using%20the%20sources%20above%2C%20we,containing%2040%20million%20housing%20units.

PPD-8, 2011. Presidential Policy Directive, PPD-8 – National Preparedness, The White House, March 30, 2011, http://www.dhs.gov/presidential-policy-directive-8-national-preparedness.

PPD-21, 2013. Presidential Policy Directive/PPD-21, The White House, February 12, 2013, http://www.whitehouse.gov/the-press-office/2013/02/12/presidential-policy-directive-riticalinfrastructure-security-and-resil.

Precast/Prestressed Concrete Institute, 1971. PCI design handbook: precast and prestressed concrete, 1st ed., Chicago, IL.

Precast/Prestressed Concrete Institute, 2017. PCI design handbook: precast and prestressed concrete, 8th ed., Chicago, IL.

Prevatt, D.O., Coulbourne, W., Graettinger, A.J., Pei, S., Gupta, R. and Grau, D., 2012, October. Joplin, Missouri, tornado of May 22, 2011: Structural damage survey and case for tornado-resilient building codes. American Society of Civil Engineers.

Prevatt, D.O., McBride, K.E., Roueche, D.B. and Masters, F.J., 2014. Wind uplift capacity of foam-retrofitted roof sheathing panels subjected to rainwater intrusion. *Journal of Architectural Engineering*, *20*(4), p.B4014001.

Prevatt, D.O., Roueche, D.B., Van De Lindt, J.W., Pei, S., Dao, T., Coulbourne, W., Graettinger, A.J., Gupta, R. and Grau, D., 2012. Building damage observations and EF classifications from the Tuscaloosa, AL, and Joplin, MO, tornadoes. In *Structures Congress 2012* (pp. 999-1010).

Ramachandran, V., Long, S.K., Shoberg, T., Corns, S. and Carlo, H.J., 2015. Framework for modeling urban restoration resilience time in the aftermath of an extreme event. *Natural Hazards Review*, *16*(4), p.04015005.

Ravid, S.A., John, K., Gill, B.S. and Choi, J.J., 2021. Polls, Politics and Disaster Relief: Evidence from Federal SBA Loan Programs. *NYU Stern School of Business Forthcoming*.

Richmond, J.L., 2019. *The Relationship Between Policy and Disaster Economic Recovery: A Case Study of the 2011 Joplin, Missouri Tornado* (Doctoral dissertation, Northeastern University).

Robinson, S., 1991. Macroeconomics, financial variables, and computable general equilibrium models. *World development*, *19*(11), pp.1509-1525.

Roohi, M., van de Lindt, J.W., Rosenheim, N., Hu, Y. and Cutler, H., 2020. Implication of building inventory accuracy on physical and socio-economic resilience metrics for informed decision-making in natural hazards. *Structure and infrastructure engineering*, *17*(4), pp.534-554.

Rose, A. and Guha, G.S., 2004. Computable general equilibrium modeling of electric utility lifeline losses from earthquakes. In *Modeling spatial and economic impacts of disasters* (pp. 119-141). Springer, Berlin, Heidelberg.

Rose, A. and Liao, S.Y., 2005. Modeling regional economic resilience to disasters: A computable general equilibrium analysis of water service disruptions. *Journal of regional science*, *45*(1), pp.75-112.

Rosenheim, N., 2020. Detailed Household and Housing Unit Characteristics: Alpha Release of Housing Unit Inventories.

Rosenheim, N., 2021. Detailed Household and Housing Unit Characteristics: Data and Replication Code.

Rosenheim, N., Guidotti, R., Gardoni, P. and Peacock, W.G., 2021. Integration of detailed household and housing unit characteristic data with critical infrastructure for post-hazard resilience modeling. *Sustainable and Resilient Infrastructure*, *6*(6), pp.385-401.

Roueche, D.B. and Prevatt, D.O., 2013. Residential damage patterns following the 2011 Tuscaloosa, AL and Joplin, MO tornadoes. *J. Disaster Res*, *8*(6), pp.1061-1067.

Roueche, D.B., Lombardo, F.T. and Prevatt, D.O., 2015. Development of empirically-based fragilities of residential damage in the 2011 Joplin, Missouri tornado.

Roueche, D.B., Lombardo, F.T. and Prevatt, D.O., 2017. Empirical approach to evaluating the tornado fragility of residential structures. *Journal of Structural Engineering*, *143*(9), p.04017123.

Roueche, D.B., Prevatt, D.O. and Haan, F.L., 2020. Tornado-induced and straight-line wind loads on a low-rise building with consideration of internal pressure. *Frontiers in built environment*, *6*, p.18.

Sabareesh, G.R., Matsui, M. and Tamura, Y., 2019. Vulnerability of roof and building walls under a translating tornado like vortex. *Frontiers in built environment*, *5*, p.53.

Salignac, F., Marjolin, A., Reeve, R. and Muir, K., 2019. Conceptualizing and measuring financial resilience: A multidimensional framework. *Social Indicators Research*, *145*(1), pp.17-38.

Sanderson, D., Cox, D., Barbosa, A.R. and Bolte, J., 2022. Modeling regional and local resilience of infrastructure networks following disruptions from natural hazards. *Journal of Infrastructure Systems*, *28*(3), p.04022021.

Sanderson, D., Kameshwar, S., Rosenheim, N. and Cox, D., 2021. Deaggregation of multi-hazard damages, losses, risks, and connectivity: an application to the joint seismic-tsunami hazard at Seaside, Oregon. *Natural Hazards*, *109*(2), pp.1821-1847.

Sapat, A. and Esnard, A.M., 2016. *Coming home after disaster: Multiple dimensions of housing recovery*. Routledge.

Schultz, M.T. and Smith, E.R., 2016. Assessing the resilience of coastal systems: A probabilistic approach. *Journal of Coastal Research*, *32*(5), pp.1032-1050.

Schwarm, W. and Cutler, H., 2003. Building small city and town SAMs and CGE models. *Review of Urban & Regional Development Studies*, *15*(2), pp.132-147.

Sediek, O.A., El-Tawil, S. and McCormick, J., 2022. Modeling interdependencies between the building portfolio, transportation network, and healthcare system in community resilience. *Natural Hazards Review*, *23*(1), p.04021060.

Sharma, N. and Gardoni, P., 2022. Mathematical modeling of interdependent infrastructure: An object-oriented approach for generalized network-system analysis. *Reliability Engineering & System Safety*, *217*, p.108042.

Simmons, K.M., Sutter, D. and Pielke, R., 2013. Normalized tornado damage in the United States: 1950–2011. *Environmental Hazards*, *12*(2), pp.132-147.

Smith, A.M., Pósfai, M., Rohden, M., González, A.D., Dueñas-Osorio, L. and D'Souza, R.M., 2019. Competitive percolation strategies for network recovery. *Scientific reports*, *9*(1), pp.1-12.

Smith, D.J. and Sutter, D., 2013. Response and recovery after the Joplin tornado: Lessons applied and lessons learned. *The Independent Review*, *18*(2), pp.165-188.

Standohar-Alfano, C.D. and van de Lindt, J.W., 2015. Empirically based probabilistic tornado hazard analysis of the United States using 1973–2011 data. *Natural Hazards Review*, *16*(1), p.04014013.

Stevenson, J.R., Brown, C., Seville, E. and Vargo, J., 2018. Business recovery: An assessment framework. *Disasters*, *42*(3), pp.519-540.

Stone, N.J., Yan, G., Nah, F.F.H., Sabharwal, C., Angle, K., Hatch III, F.G.E., Runnels, S., Brown, V., Schoor, G.M. and Engelbrecht, C., 2021. Virtual reality for hazard mitigation and community resilience: An interdisciplinary collaboration with community engagement to enhance risk awareness. *AIS Transactions on Human-Computer Interaction*, *13*(2), pp.130-144.

Suckling, P.W. and Ashley, W.S., 2006. Spatial and temporal characteristics of tornado path direction. *The Professional Geographer*, *58*(1), pp.20-38.

Sutley, E.J. and Hamideh, S., 2020. Postdisaster housing stages: a markov chain approach to model sequences and duration based on social vulnerability. *Risk Analysis*, *40*(12), pp.2675-2695.

Sun, W., Bocchini, P. and Davison, B.D., 2020. Resilience metrics and measurement methods for transportation infrastructure: The state of the art. *Sustainable and Resilient Infrastructure*, *5*(3), pp.168-199.

Sun, W., Bocchini, P. and Davison, B.D., 2020. Model for estimating the impact of interdependencies on system recovery. *Journal of Infrastructure Systems*, *26*(3), p.04020031.

Sutley, E.J. and Hamideh, S., 2018. An interdisciplinary system dynamics model for post-disaster housing recovery. *Sustainable and Resilient Infrastructure*, *3*(3), pp.109-127.

Taylor, J.E., Yúnez-Naude, A. and Dyer, G., 1999. Agricultural price policy, employment, and migration in a diversified rural economy: A village-town CGE analysis from Mexico. *American Journal of Agricultural Economics*, *81*(3), pp.653-662.

Thomson, K.J. and Psaltopoulos, D., 2007. *General equilibrium analysis of the spatial impacts of rural policy* (No. 688-2016-47153).

TMS 402/602-16, 2016. Building Code Requirements and Specification for Masonry Structures (formerly designated as the ''MSJC" (Masonry Standards Joint Committee) and TMS 402/ACI 530/ASCE 5 and TMS 602/ACI 530.1/ASCE 6).

Tomar, A., Burton, H.V., Mosleh, A. and Yun Lee, J., 2020. Hindcasting the Functional Loss and Restoration of the Napa Water System Following the 2014 Earthquake Using Discrete-Event Simulation. *Journal of Infrastructure Systems*, *26*(4), p.04020035.

Tornados, Floods and without Home Insurance as Reported by AP. *Insurance Agency Plano TX*, 2014. www.tristarins.com/tornados-floods-and-without-home-insurance-as-reported-by-ap/.

Torres, A.P., Marshall, M.I. and Sydnor, S., 2019. Does social capital pay off? The case of small business resilience after Hurricane Katrina. *Journal of Contingencies and Crisis Management*, *27*(2), pp.168-181.

Turner, K., Ha, S.J., Hewings, G.J., Mcgregor, P. and Swales, K., 2012. Econometric estimation of Armington import elasticities for a regional CGE model of the Illinois economy. *Economic Systems Research*, *24*(1), pp.1-19.

Unnikrishnan, V.U. and van de Lindt, J.W., 2016. Probabilistic framework for performance assessment of electrical power networks to tornadoes. *Sustainable and Resilient Infrastructure*, *1*(3-4), pp.137-152.

U.S. Census Bureau. 2010. "." Accessed August 19, 2022. https://www.census.gov/quickfacts/joplincitymissouri

U.S. Census Bureau. 2019. Table DP05: ACS demographic and housing estimates. Accessed February 20, 2022. https://data.census.gov/cedsci/table?q=kids&tid=ACSDP5Y2019.DP05.

U.S. Census Bureau. 2010a. Table H5: Vacancy status Universe: Vacant housing units, 2010 census summary file 1. Accessed August 25, 2020. https://data.census.gov/cedsci/table?q=h5&g=1600000US2937592&tid=DECENNIALSF12010.H5

U.S. Census Bureau. 2010b. Table H11: Total population in occupied housing units by Tenure Universe: Population in occupied housing units, 2010 census summary file 1. Accessed August 25, 2020. https://data.census.gov/cedsci/table?q=h11&g=1600000US2937592&tid=DECENNIALSF12010.H11

U.S. Census Bureau. 2010d. Table H12: Average household size of occupied housing units by tenure, 2010 census summary file 1. Accessed August 25, 2020. https://data.census.gov/cedsci/table?q=h12&g=0400000US29_1600000US2937592&tid=DECENNIALSF12010.H12

U.S. Census Bureau. 2010c. Table H16: Tenure by Household Size, 2010 census summary file 1. Accessed August 25, 2020.

https://data.census.gov/cedsci/table?q=h16&g=1600000US2937592&tid=DECENNIALSF12010.H16

U.S. Economic Development Administration, 2021. Revolving Loan Fund Program. Accessed August 25, 2021. https://www.eda.gov/rlf/.

U.S. Small Business Administration, 2021b. Economic Injury Disaster Loans. Accessed August 25, 2021. https://www.sba.gov/funding-programs/disaster-assistance/economic-injury-disaster-loans.

U.S. Small Business Administration, 2021a. Physical Damage Loans. Accessed August 25, 2021. https://www.sba.gov/funding-programs/disaster-assistance/physical-damage-loans.

van de Lindt, J.W., Ellingwood, B.R., Cutler, H., Gardoni, P., Lee, J.S., Cox, D. and Peacock, W.G., 2019, June. The structure of the interconnected networked community resilience modeling environment (IN-CORE). In *Proc., 2nd Int. Conf. on Natural Hazards and Infrastructure* (pp. 23-26).

van de Lindt, J.W., Peacock, W.G., Mitrani-Reiser, J., Rosenheim, N., Deniz, D., Dillard, M., Tomiczek, T., Koliou, M., Graettinger, A., Crawford, P.S. and Harrison, K., 2020. Community resilience-focused technical investigation of the 2016 Lumberton, North Carolina, flood: An interdisciplinary approach. *Natural Hazards Review*, *21*(3), p.04020029. Vaughan, E.J. and Vaughan, T., 2007. *Fundamentals of risk and insurance*. John Wiley & Sons.

van de Lindt, J.W., Pei, S., Dao, T., Graettinger, A., Prevatt, D.O., Gupta, R. and Coulbourne, W., 2013. A dual-objective-based tornado design philosophy. *Journal of Structural Engineering*, *139*(2).

Van Zandt, S., Peacock, W.G., Henry, D.W., Grover, H., Highfield, W.E. and Brody, S.D., 2012. Mapping social vulnerability to enhance housing and neighborhood resilience. *Housing Policy Debate*, *22*(1), pp.29-55.

Veil, S.R. and Bishop, B.W., 2014. Opportunities and challenges for public libraries to enhance community resilience. *Risk analysis*, *34*(4), pp.721-734.

Vickery, P.J., Skerlj, P.F., Lin, J., Twisdale Jr, L.A., Young, M.A. and Lavelle, F.M., 2006. HAZUS-MH hurricane model methodology. II: Damage and loss estimation. *Natural Hazards Review*, *7*(2), pp.94-103.

Wang, J., Cao, S., Pang, W. and Cao, J., 2018. Experimental study on tornado-induced wind pressures on a cubic building with openings. *Journal of Structural Engineering*, *144*(2), p.04017206.

Wang, W.L. and van de Lindt, J.W., 2021. Quantitative modeling of residential building disaster recovery and effects of pre-and post-event policies. *International Journal of Disaster Risk Reduction*, *59*, p.102259.

Wang, W.L. and van de Lindt, J.W., 2022. Quantifying the effect of improved school and residential building codes for tornadoes in community resilience. *Resilient Cities and Structures*, *1*(1), pp.65-79.

Wang, W.L., van de Lindt, J.W. and Rosenheim, N., 2022a. Method to Plan for Population Dislocation Based on Damage Prediction and Household Characteristics Following a Tornado. In *14th Americas Conference on Wind Engineering* (ACWE 2022).

Wang, W.L., van de Lindt, J.W., Cutler, H., Hartman, B., Rosenheim, N., Kruse, J.L. and Lee, J.S., 2022b. Integration of physical infrastructure and socio-economic systems for comprehensive uncertainty propagation in community resilience models. In *International Conference on Structural Safety & Reliability*. ICOSSAR.

Wang, W.L., van de Lindt, J.W., Cutler, H., Rosenheim, N., Koliou, M., Lee, J.S. and Calderon, D., 2021a. Community resilience assessment of an EF-5 tornado using the IN-CORE modeling environment. In *Life-Cycle Civil Engineering: Innovation, Theory and Practice* (pp. 394-398). CRC Press.

Wang, W.L., van de Lindt, J.W., Hartman, B., Cutler, H., Kruse, J.L., McAllister, T.P. and Hamideh, S., 2022c. Determination of individual building performance targets to achieve community-level social and economic resilience metrics. *Journal of Structural Engineering*, *148*(5), p.04022045.

Wang, W.L., van de Lindt, J.W., Rosenheim, N., Cutler, H., Hartman, B., Sung Lee, J. and Calderon, D., 2021b. Effect of residential building wind retrofits on social and economic community-level resilience metrics. *Journal of Infrastructure Systems*, *27*(4), p.04021034.

Wang, W.L., Watson, M., van de Lindt, J.W., and Xiao Y., 2023. Commercial building recovery methodology for use in community resilience modeling. *Natural Hazards Review (under review)*

Wang, X., Mazumder, R.K., Salarieh, B., Salman, A.M., Shafieezadeh, A. and Li, Y., 2022. Machine Learning for Risk and Resilience Assessment in Structural Engineering: Progress and Future Trends. *Journal of Structural Engineering*, *148*(8), p.03122003.

Wang, Y., Wang, N., Lin, P., Ellingwood, B., Mahmoud, H. and Maloney, T., 2018. De-aggregation of community resilience goals to obtain minimum performance objectives for buildings under tornado hazards. *Structural Safety*, *70*, pp.82-92.

Wang, Z. and Jia, G., 2020. Efficient sample-based approach for effective seismic risk mitigation of transportation networks. *Sustainable and Resilient Infrastructure*, *5*(6), pp.349-364.

Wasileski, G., Rodríguez, H. and Diaz, W., 2011. Business closure and relocation: a comparative analysis of the Loma Prieta earthquake and Hurricane Andrew. *Disasters*, *35*(1), pp.102-129.

Watson, M., 2014. Business Recovery Financing: Galveston, TX after Hurricane Ike. [Unpublished master's professional paper]. Texas A&M University.

Watson, M., 2022. Disaster Assistance Winners and Losers: Do Small Businesses Benefit?. *Journal of the American Planning Association*, *88*(3), pp.305-318.

Watson, M., Alaffa, S., Farquhar, A., Li, P., Rahmadina, I., Southerland, C., Stephens, B., 2020b. Federal Disaster Spending: Trends and Observations Between 2010-2019. DesignSafe-CI. https://doi.org/10.17603/ds2-pmds-kk73.

Watson, M., Thornton, P.H. and Xiao, Y., 2019, July. Time will tell: Sequencing institutional logics to aid business recovery after natural disasters. In *Academy of Management Proceedings* (Vol. 2019, No. 1, p. 11188). Briarcliff Manor, NY 10510: Academy of Management.

Watson, M., Xiao, Y., Helgeson, J. and Dillard, M., 2020. Importance of households in business disaster recovery. *Natural Hazards Review*, *21*(4), p.05020008.

Weaver, K.M. and Vozikis, G.S., 2010. The Economic Impacts of a Hurricane Disaster Bridge Loan Program in Southern Louisiana: The Aftermath of Hurricanes Katrina and Rita. *The Journal of Applied Business and Economics*, *10*(4), p.63.

Wei, D., Chen, Z. and Rose, A., 2020. Evaluating the role of resilience in reducing economic losses from disasters: A multi-regional analysis of a seaport disruption. *Papers in Regional Science*, *99*(6), pp.1691-1722.

Xiao, Y. and Peacock, W.G., 2014. Do hazard mitigation and preparedness reduce physical damage to businesses in disasters? Critical role of business disaster planning. *Natural Hazards Review*, *15*(3), p.04014007.

Xiao, Y. and Van Zandt, S., 2012. Building community resiliency: Spatial links between household and business post-disaster return. *Urban Studies*, *49*(11), pp.2523-2542.

Yang, L., Kajitani, Y., Tatano, H. and Jiang, X., 2016. A methodology for estimating business interruption loss caused by flood disasters: insights from business surveys after Tokai Heavy Rain in Japan. *Natural Hazards*, *84*(1), pp.411-430.

Yanweerasak, T., Pansuk, W., Akiyama, M. and Frangopol, D.M., 2018. Life-cycle reliability assessment of reinforced concrete bridges under multiple hazards. *Structure and Infrastructure Engineering*, *14*(7), pp.1011-1024.

Zhang, W., Wang, N. and Nicholson, C., 2017. Resilience-based post-disaster recovery strategies for road-bridge networks. *Structure and Infrastructure Engineering*, *13*(11), pp.1404-1413.

Zhang, Y. and Peacock, W.G., 2009. Planning for housing recovery? Lessons learned from Hurricane Andrew. *Journal of the American Planning Association*, *76*(1), pp.5-24.

Zhang, Y., Lindell, M.K. and Prater, C.S., 2009. Vulnerability of community businesses to environmental disasters. *Disasters*, *33*(1), pp.38-57.

Zhang, Y., Yang, N. and Lall, U., 2016. Modeling and simulation of the vulnerability of interdependent power-water infrastructure networks to cascading failures. *Journal of Systems Science and Systems Engineering*, *25*(1), pp.102-118.

Zou, Q. and Chen, S., 2019. Enhancing resilience of interdependent traffic-electric power system. *Reliability Engineering & System Safety*, *191*, p.106557.

Zou, Q. and Chen, S., 2020. Resilience modeling of interdependent traffic-electric power system subject to hurricanes. *Journal of Infrastructure Systems*, *26*(1), p.04019034.

VITA

Education

Ph.D. Structural Engineering, Colorado State University, Fort Collins, CO, 2022
Advisor: Dr. John W. van de Lindt

M.S. Structural Engineering, University of Colorado Denver, Denver, CO, 2015
Advisor: Dr. Chengyu Li

M.S. Structural Engineering, Jilin University, Changchun, Jilin, China, 2015
Advisor: Dr. Hanbing Liu

B.S. Civil Engineering, Jilin University, Changchun, Jilin, China, 2012

Publications

This dissertation is developed based on Wanting (Lisa) Wang's journal papers/conference proceedings, which have already been published or are currently under review, during her graduate study at Colorado State University starting from August 2019, listed below.

Wang, W.L., and van de Lindt, J.W., 2023. Physical-Social Interdependent Recovery Methodology for Community Resilience Modeling. *(to be submitted)*

Wang, W.L., Watson, M., van de Lindt, J.W., and Xiao Y., 2023. Commercial building recovery methodology for use in community resilience modeling. *Natural Hazards Review (under review)*

Wang, W.L. and van de Lindt, J.W., 2022. Quantifying the effect of improved school and residential building codes for tornadoes in community resilience. *Resilient Cities and Structures*, *1*(1), pp.65-79.

Wang, W.L., van de Lindt, J.W. and Rosenheim, N., 2022a. Method to Plan for Population Dislocation Based on Damage Prediction and Household Characteristics Following a Tornado. In *14th Americas Conference on Wind Engineering* (ACWE 2022).

Wang, W.L., van de Lindt, J.W., Cutler, H., Hartman, B., Rosenheim, N., Kruse, J.L. and Lee, J.S., 2022b. Integration of physical infrastructure and socio-economic systems for comprehensive uncertainty propagation in community resilience models. In *International Conference on Structural Safety & Reliability*. ICOSSAR.

Wang, W.L., van de Lindt, J.W., Hartman, B., Cutler, H., Kruse, J.L., McAllister, T.P. and Hamideh, S., 2022c. Determination of individual building performance targets to achieve

community-level social and economic resilience metrics. *Journal of Structural Engineering*, *148*(5), p.04022045.

Wang, W.L. and van de Lindt, J.W., 2021. Quantitative modeling of residential building disaster recovery and effects of pre-and post-event policies. *International Journal of Disaster Risk Reduction*, *59*, p.102259.

Wang, W.L., van de Lindt, J.W., Cutler, H., Rosenheim, N., Koliou, M., Lee, J.S. and Calderon, D., 2021a. Community resilience assessment of an EF-5 tornado using the IN-CORE modeling environment. In *Life-Cycle Civil Engineering: Innovation, Theory and Practice* (pp. 394-398). CRC Press.

Wang, W.L., van de Lindt, J.W., Rosenheim, N., Cutler, H., Hartman, B., Sung Lee, J. and Calderon, D., 2021b. Effect of residential building wind retrofits on social and economic community-level resilience metrics. *Journal of Infrastructure Systems*, *27*(4), p.04021034.